NORTHROP TECHNICAL REPORT

EFFECTS OF MATERIALS AND PROCESSES DEFECTS ON THE COMPRESSION PROPERTIES OF ADVANCED COMPOSITES

CONTRACT N00019-80-C-0490
CONTRACT N00019-80-C-0484

FINAL TECHNICAL REPORT

R. L. Ramkumar
G. C. Grimes
D. F. Adams
E. G. Dusablon

May 1982

Prepared for:

19951228 070

DEPARTMENT OF THE NAVY
NAVAL AIR SYSTEMS COMMAND
WASHINGTON, D.C. 20361

DEPARTMENT OF DEFENSE
PLASTICS TECHNICAL EVALUATION CENTER
ARRADCOM, DOVER, N. J. 07801

by

Northrop Corporation
Aircraft Division
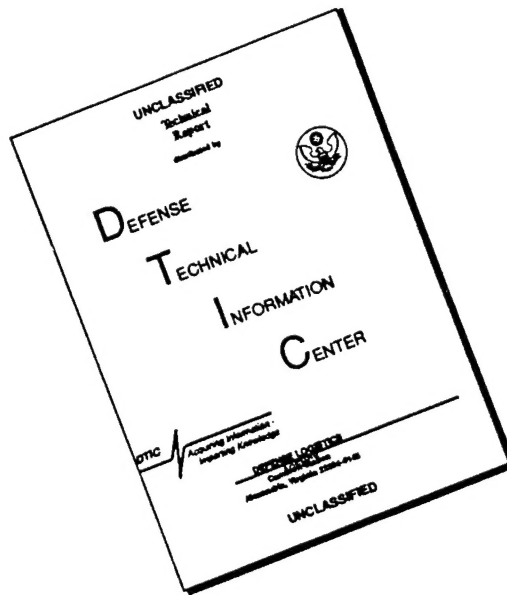One Northrop Avenue
Hawthorne, California 90250

and

University of Wyoming
Composite Materials Research Group
Mechanical Engineering Department
Laramie, Wyoming 82071

DISCLAIMER NOTICE

2   OF   4
--   ***DTIC DOES NOT HAVE THIS ITEM***
-- 1 - AD NUMBER: D436127
-- 5 - CORPORATE AUTHOR: NORTHROP CORP HAWTHORNE CA AIRCRAFT DIV
-- 6 - UNCLASSIFIED TITLE: EFFECTS OF MATERIALS AND PROCESSES DEFECTS
--   ON THE COMPRESSION PROPERTIES OF ADVANCED COMPOSITES.
-- 9 - DESCRIPTIVE NOTE: FINAL REPT., 29 SEP 80 - 26 FEB 82,
--10 - PERSONAL AUTHORS: RAMKUMAR,R. L. ;GRIMES,G. C. ;ADAMS,D. F. ;
--   DUSABLON,E. G. ;
--11 - REPORT DATE: MAY , 1982
--12 - PAGINATION: 168P
--14 - REPORT NUMBER: NOR-82-103
--15 - CONTRACT NUMBER: N00019-80-C-0490, N00019-80-C-0484
--20 - REPORT CLASSIFICATION: UNCLASSIFIED
--22 - LIMITATIONS (ALPHA):   APPROVED FOR PUBLIC RELEASE; DISTRIBUTION
--   UNLIMITED. AVAILABILITY: DEPARTMENT OF THE NAVY, NAVAL AIR SYSTEMS
--   COMMAND (AIR5304-C), WASHINGTON, D. C. 20361.
--33 - LIMITATION CODES: 1 24

REPORT DOCUMENTATION PAGE		READ INSTRUCTIONS BEFORE COMPLETING FORM
1. REPORT NUMBER	2. GOVT ACCESSION NO.	3. RECIPIENT'S CATALOG NUMBER
4. TITLE *(and Subtitle)* Effects of Materials and Processes Defects on the Compression Properties of Advanced Composites		5. TYPE OF REPORT & PERIOD COVERED Final Report 29 Sep 1980 to 26 Feb 1982
		6. PERFORMING ORG. REPORT NUMBER NOR 82-103
7. AUTHOR(s) R. L. Ramkumar (Northrop Corporation) G. C. Grimes (Northrop Corporation) D. F. Adams (University of Wyoming) E. G. Dusablon (Northrop Corporation)		8. CONTRACT OR GRANT NUMBER(s) N00019-80-C-0490 (Northrop) N00019-80-C-0484 (University of Wyoming)
9. PERFORMING ORGANIZATION NAME AND ADDRESS Northrop Corporation University of Wyoming Aircraft Division College of Engineering One Northrop Avenue University Station, Box 3295 Hawthorne, CA 90250 Laramie, Wyoming 82071		10. PROGRAM ELEMENT, PROJECT, TASK AREA & WORK UNIT NUMBERS
11. CONTROLLING OFFICE NAME AND ADDRESS Department of the Navy Naval Air Systems Command (AIR5304-C) Washington, D.C. 20361		12. REPORT DATE May 1982
		13. NUMBER OF PAGES 168
14. MONITORING AGENCY NAME & ADDRESS*(if different from Controlling Office)*		15. SECURITY CLASS. *(of this report)* Unclassified
		15a. DECLASSIFICATION/DOWNGRADING SCHEDULE

16. DISTRIBUTION STATEMENT *(of this Report)*

Approved for public release, distribution unlimited.

17. DISTRIBUTION STATEMENT *(of the abstract entered in Block 20, if different from Report)*

DTIC QUALITY INSPECTED 2

18. SUPPLEMENTARY NOTES

19. KEY WORDS *(Continue on reverse side if necessary and identify by block number)*

Graphite/epoxy composites; porosity; delamination; ply drop-off analysis; compression loading; static and fatigue; moisture effects; elevated temperature wet conditions; chemical and image analyses; photomicrographs; SEM.

20. ABSTRACT *(Continue on reverse side if necessary and identify by block number)*

An experimental program was conducted to quantify the severity of materials-related or process-induced defects in AS/3501-6 graphite/epoxy laminates. Porosity was studied as the primary defect and an investigation of the effect of imbedded delaminations was also carried out. Test laminates had $[0]_{24T}$, $[90]_{24T}$, $[\pm 45]_{6S}$ and $[(\pm 45)_5/0_{16}/90_4]_c$ layups. The 30-ply laminate had a layup similar to a typical vertical stabilizer skin layup. Program laminates were cured under

DD $_{1\ \text{JAN }73}^{\text{FORM}}$ 1473   EDITION OF 1 NOV 65 IS OBSOLETE

vacuum plus 15 psi conditions to introduce a fairly severe level of uniform porosity (1.5% to 2% by chemical analysis). Porous test specimens were subjected to static compression and constant amplitude (R=10) compression fatigue loading. Test conditions were chosen to be room temperature, dry (RTD), room temperature, wet (RTW) and elevated temperature, wet (218FW) conditions. Wet specimens were preconditioned to absorb approximately 1% moisture by weight prior to being tested. Generated data from porous specimens were compared with available data on non-porous specimens with the same layups to quantify the effect of porosity. A limited number of non-porous 30-ply specimens, containing a 1.27 cm long delamination at the midplane, were also subjected to static compression and compression fatigue (R=10) tests, and the results compared with available defect-free specimen test data.

Significant reductions (19% to 39%) in the static compressive strengths and failure strains were caused by the induced uniform porosity and the imbedded delaminations. RTD, RTW and 218FW test conditions induced approximately the same strength losses in the porous laminates. The presence of moisture in porous laminates induced significant reductions (as high as 50%) in the proportional limit stress and strain values. Poisson's ratio and modulus of elasticity were relatively unaffected by defects and environment, except in the $[90]_{24T}$ specimens. Empirical relationships were developed to relate the percentage loss in the static compressive strength to the void content in porous laminates.

Compression fatigue (R=10) test data, obtained in the form of S-N curves, were used to identify threshold strain levels (TSLs). TSL is the maximum strain amplitude at which 1.25 million cycles of fatigue loading (R=10) are sustained without failure. The TSLs of defective laminates were compared with available TSLs for defect-free laminates to quantify the effect of the induced defect on compression fatigue behavior. Imbedded delaminations had no deleterious effects, whereas induced uniform porosity caused significant reductions in the TSLs of the test laminates (40% in $[0]_{24T}$, 29% in $[90]_{24T}$, 33% in $[\pm 45]_{6s}$, and 6% to 10% in the 30-ply laminates).

A three-dimensional finite element analysis was also carried out to investigate the effects of temperature and moisture on the compression behavior of the 30-ply laminate in the presence of ply drop-offs. The analysis was performed on laminates with no drop-offs, 0° ply drop-offs and 45° ply drop-offs, which were tested in an earlier program. Analytical predictions verified the general experimental observation that the considered ply drop-offs do not significantly influence the compressive strength of the 30-ply laminate. The more significant effects of hygrothermal environments and interlaminar stresses along the free edges were quantified. The analysis possesses the potential to consider the combined influences of ply drop-offs, loaded or unloaded holes, and manufacturing defects such as porosity in general laminates.

PREFACE

This report was prepared by the Northrop Corporation under Contract N00019-80-C-0490 and includes an input from the University of Wyoming, Laramie, Wyoming under Contract N00019-80-C-0484. The contracts were administered by the Naval Air Systems Command with Mr. Maxwell Stander as the Program Monitor.

The experimental design, materials and processing, fabrication, testing, and data/analysis (Contract N00019-80-C-0490) were conducted at Northrop under the direction of Dr. R. L. Ramkumar and Mr. Glenn C. Grimes. Mr. Grimes served as the Program Manager during the first three quarters of the program, and was assisted by Mr. E. G. Dusablon at that time. Dr. Ramkumar served as the Program Manager during the last quarter (test phase) of the program period. Dr. Ramkumar, Mr. Grimes, and Mr. Dusablon reported to Dr. Ralph Verette, Manager of the Structural Mechanics Research Department.

Test laminate layup and cure, specimen machining, quality control testing, and Celanese compression testing were accomplished in the Materials Research Laboratory under the supervision of Dr. S. McGovern and Mr. B. J. Mays. The remaining tests were carried out at the Engineering Test Laboratory under the supervision of Mr. T. R. Miller, with guidance from Mr. D. Atmur.

Stress and failure analyses of ply drop-off test specimens were performed at the University of Wyoming under the direction of Dr. D. F. Adams, Program Manager for Contract N00019-80-C-0484. He was assisted by Mr. B. A. Coulter, Staff Engineer, and Mr. D. A. Briggs, Research Assistant.

Ms. Beverly Parish typed the manuscript and Ms. Rocio Cordero provided assistance with illustrations.

TABLE OF CONTENTS

TABLE OF CONTENTS (CONCLUDED)

LIST OF ILLUSTRATIONS

LIST OF ILLUSTRATIONS (CONTINUED)

LIST OF ILLUSTRATIONS (CONTINUED)

LIST OF ILLUSTRATIONS (CONCLUDED)

LIST OF TABLES

SECTION 1

INTRODUCTION

The increasing application of advanced composite materials in primary
and secondary aircraft structural components has spurred a need to establish,
and periodically assess, acceptance criteria for production components built
out of these new materials. In order to establish appropriate acceptance
criteria, the effect of materials-, process-, or service-induced defects
on the mechanical response of laminated aircraft structural components
must be quantified. The results must relate the size of a flaw, as
measured through routine quality control procedures, to the corresponding
degradation in mechanical properties that influence design criteria. An
examination of these defect-degradation relationships, and a knowledge
of acceptable property degradation levels, will establish critical defect
levels above which components will be rejected from use in production aircraft
or require repair.

This report discusses a program that attempts to quantify the severity
of materials-related or process-induced defects in AS/3501-6 graphite/epoxy
laminates. Emphasis is laid on porosity as the primary defect under study,
though a limited number of tests on specimens with imbedded delaminations
was also carried out. The primary laminate under study is a 30-ply lami-
nate with a layup similar to a highly-loaded portion of the F/A-18A
vertical stabilizer skin. Grimes and Adams (Ref. 1) have generated the
basic properties under compressive loading situations, for defect-free
AS/3501-6 laminates including some basic laminates ($[0]_{24T}$, $[90]_{24T}$ and
$[\pm 45]_{6s}$), and the 30-ply, $[(\pm 45)_5/0_{16}/90_4]_c$ laminate. The program discussed
in this report adopts the above-mentioned AS/3501-6 laminates for a test
program that aims at quantifying the effect of materials- and process-induced
defects.

At the initiation of the program, a preliminary study was conducted
to simulate the various plausible situations under which porosity can be
introduced in a laminate during material handling and processing. Results

1

from this study were used to introduce uniform porosity levels in test laminates. In a limited number of 30-ply specimens, delaminations were introduced at midplane, during layup, using Teflon inclusions. Defective laminates were subsequently subjected to static and cyclic compressive loading, and the results compared with those in Reference 1, to assess the effect of materials-related or process-induced defects on the structural response of AS/3501-6 laminates. Prior to drawing comparisons, differences in the fiber volume percentages of compared laminates were appropriately accounted for. Static compression test results quantified the effect of porosity and delaminations on the ultimate and proportional limit values of stress and strain, Poisson's ratio and the modulus of elasticity. Constant amplitude, compression fatigue (R=10) test results quantified the effect of porosity on the threshold strain level at which 1.25×10^6 cycles of loading can be sustained without failure. Failed test specimens were analyzed at the University of Wyoming to observe failure surfaces, to predict the sequence of these failures, and to correlate predictions with test results.

It must be noted here, that the laminates tested in this program deliberately contained a high level of porosity, approximately twice as severe as the worst situation realized thus far in the production of the F/A-18A vertical stabilizer. Presented results should, therefore, be evaluated with this in mind.

2

SECTION 2

DETAILS OF THE EXPERIMENTAL PROGRAM

2.1 SUMMARY

Uniform porosity was identified as the predominant materials-related or process-induced defect in AS/3501-6 graphite/epoxy test laminates. On a limited scale, the effect of an imbedded delamination on the compression behavior of a chosen AS/3501-6 laminate was also studied. Table 1 lists the various tests conducted under the program. Static compression and compression fatigue (R=10) tests were carried out on basic laminates - $[0]_{24T}$, $[90]_{24T}$ and $[\pm 45]_{6S}$ - with uniform porosity, under room temperature dry (RTD) and room temperature wet (RTW) conditions. Fatigue tests were limited to RTW conditions, and the moisture content in the specimens was monitored to be approximately 1% by weight. Static compression and compression fatigue (R=10) tests were then conducted on a porous, 30-ply, $[(\pm 45)_5/0_{16}/90_4]_c$ laminate with a layup similar to that of a portion of the F/A-18A vertical stabilizer skin. These tests were conducted under RTD, RTW and 218FW conditions. Finally, static compression and compression fatigue (R=10) tests under RTD conditions were also carried out on non-porous, $[(\pm 45)_5/0_{16}/90_4]_c$ specimens with imbedded, 0.5 inch long delaminations between plies 15 and 16. The delamination in these specimens were located at mid-length and extended across the entire width.

Details pertaining to the introduction of uniform porosity in the test laminates, and the execution of the various tests in Table 1, are presented in the following sub-sections.

2.2 TEST MATERIAL EVALUATION

Test laminates were fabricated from AS/3501-6 graphite/epoxy prepreg. Table 2 presents acceptance test results on three rolls of material used in the fabrication of the program test laminates. Quality control (QC) and process specifications for the test program are presented in Appendix A. It is seen that material acceptance test results meet the QC requirements

3

TABLE 1.   STATIC COMPRESSION AND COMPRESSION FATIGUE PROGRAM TEST MATRIX

Test Series	Laminate	Layup	Type of M&P Defect+	Type of Loading	Test Conditions	Test Fixture*	No. of Replicates
I	A	$[0]_{24T}$	UP	Static	RTD	Celanese	4
II	A			Static	RTW	Atmur	4
III	A			C-C Fat.	RTW	Atmur	8
IV	A	$[90]_{24T}$	UP	Static	RTD	ETL	4
V	A			Static	RTW	Atmur	4
VI	A			C-C Fat.	RTW	Atmur	8
VII	B	$[\underline{+45}]_{6s}$	UP	Static	RTD	ETL	4
VIII	B			Static	RTW	Atmur	4
IX	B			C-C Fat.	RTW	Atmur	8
X	C	**	UP	Static	RTD	ETL	4
XI	C			Static	RTW		4
XII	C			Static	218FW		4
XIII	C			C-C Fat.	RTD	Atmur	8
XIV	C			C-C Fat.	RTW		8
XV	C			C-C Fat.	218FW		8
XVI	D	**	DL	Static	RTD	ETL	4
XVII	D			C-C Fat.	RTD	Atmur	8
						Total	96

*See Appendix B for fixture details.

**Actual 30-ply lamination sequence is $\left[\overline{+45}/0/90/0_3/90/0_3/\overline{+45}/0/\underline{+45}\right]_s$. It is abbreviated in the report to $\left[(\underline{+45})_5/0_{16}/90_4\right]_c$.

+UP→uniform porosity;   DL→delamination between plies 15 and 16.

TABLE 2. AS/3501-6 GRAPHITE/EPOXY AVERAGE ACCEPTANCE TEST RESULTS

	PREPREG MATERIAL IDENTIFICATION				PREPREG TEST RESULTS					CURED [0]$_{16}$ LAMINATE TEST RESULTS							
LOT NO.	SPOOL NO.	MFG. DATE	TEST DATE	MATERIAL FORM	% R.C. BY WT	% FLOW	GEL TIME, MIN.	% VOLATILES	ACL NO.	% R.C. BY WT	SPECIFIC GRAVITY	% FIBER VOLUME	% VOID VOLUME	90° TENSION STRESS, KSI	4 PT. FLEXURE KSI	FLEXURE MODULUS, 10^6 PSI	S/D
1699	15D	9/30/80	2/81	12 IN. W. TAPE	38.62	18.91	13.0	0.0087	4458	29.12	1.6207	63.79	0.30	10.74	250.9	19.9	32:1
1699	16B	→	2/81	12 IN. W. TAPE	40.60	14.63	14.5	0.0086	4459	28.94	1.6236	64.09	0.39	10.49	269.7	20.9	→
1699	15B		1/81	12 IN. W. TAPE	38.74	17.60	16.0	0.0099	4460	28.96	1.6323	64.42	0.94	9.98	252.9	19.9	
				MEAN	39.32	17.05	14.5	0.0091		29.01	1.6255	64.10	0.54	10.40	257.8	20.2	___

Note: Fiber S.G. = 1.80
Matrix S.G. = 1.26

Legend: R.C. = resin content
P T. = point
S/D = span-to-depth ratio
ksi = 1000 psi
psi = pounds/in^2

listed in Appendix A.

2.3 POROSITY EVALUATION STUDY

This sub-section has to be prefaced by the statement that the quantification of the level of porosity in a laminate is nebulous, and very much dependent on the employed evaluation technique (see Ref. 2). In this study, a chemical analysis technique (using acid digestion) and an image analysis of cross-sectional photomicrographs under a scanning electron microscope (SEM) were employed to quantify the porosity content in the test laminates. Void contents measured by the chemical analysis technique are very sensitive to the assumed fiber and matrix density values (see Ref. 2). Computation of porosity levels via SEM image analysis is restricted to the observed laminate cross-section, and an average of many examinations is mandatory for a reliable laminate void content measurement. Image analysis void content measurements were observed, in this study, to be approximately 1% in excess of chemical analysis measurements. Ultrasonic through transmisssion records and x-radiographs were obtained to nondestructively observe the extent of porosity in the test laminates. The program goal was to introduce uniform porosity in the test laminates, amounting to 3 ± 2% via chemical analysis, or 4 ± 2% via SEM image analysis.

An initial porosity evaluation study was conducted using "over-aged" material (Batch A) and fresh material (Batch B). The "over-aged" material had exceeded the maximum allowable time for being out of the freezer at room temperature. Three laminates of different configurations were fabricated using Batch A material, and four laminates were built out of Batch B material (see Table 3). Batch A laminates (Nos. 1, 2 and 3 in Table 3) were not debulked during layup, and were cured under vacuum pressure only. Physical properties of these laminates are listed in Table 3. X-radiographs indicated severe porosity levels in all three laminates, and void contents ranging from 1.83% to 5.27% were measured via chemical analysis.

Laminates identified as ACL-4410, -4411, - 4412 and -4416 in Table 3 were made from fresh material (Batch B) and all of them had the configuration of Laminate No. 2. Laminate ACL-4410 was not debulked and was cured under vacuum pressure only, similar to laminate No's. 1, 2, and 3.

6

TABLE 3. INITIAL POROSITY EVALUATION.

LAMINATE NUMBER AND DESCRIPTION	CURE METHOD *	LAMINATE THICKNESS, INCHES	RESIN CONTENT % BY WEIGHT	FIBER VOLUME %	SPECIFIC GRAVITY	% VOID VOLUME (CHEM. ANAL.)	X-RAY RESULTS	% VOID VOLUME (SEM IMAGE ANAL.)	PLY THICKNESS INCHES	COMMENTS
No. 1 $(0/\pm45/90)_{4s}$ Prepreg Batch A	vacuum only	.190	34.15	56.40	1.54	1.83	heavy porosity	–	.0059	1
No. 2 $(0_3/\pm45/0_2/90)_{2s}$ Prepreg Batch A	vacuum only	.198	36.55	51.98	1.47	5.27	heavy porosity	–	.0062	
No. 3 $(0)_{32}$ Prepreg Batch A	vacuum only	.198	33.60	56.68	1.54	2.36	heavy porosity	–	.0062	
ACL 4410 $(0_3/\pm45/0_2/90)_{2s}$ Prepreg Batch B	vacuum only	.189	31.40	56.23	1.47	7.04	heavy porosity	8.63	.0059	2
ACL 4411 $(0_3/\pm45/0_2/90)_{2s}$ Prepreg Batch B	vacuum bag leak	.154	24.33	69.37	1.65	0	–	0.90	.0048	
ACL 4412 $(0_3/\pm45/0_2/90)_{2s}$ Prepreg Batch B	no vent/pressure	.157	24.82	68.84	1.65	0	–	0	.0049	
ACL 4416 $(0_3/\pm45/0_2/90)_{2s}$ Prepreg Batch B	moist pre-preg	.150	23.90	69.42	1.64	0	–	1.05	.0047	

[1] Over-age (out-time exceeds specification requirements) material.
[2] Fresh material
*Time-temperature portion of cure cycle was per Process Instruction Sheet No. 1 (See Appendix A)

Laminate ACL-4410 has a somewhat higher level of porosity than laminate No. 2, and both the laminates contained heavy porosity as seen through X-radiographs. Laminate ACL-4410 also had selected cross-section photomicrographs subjected to SEM Image Analysis, giving a void volume percentage of 8.63%, a larger value than that yielded by the chemical analysis technique (7.04%). Laminate ACL-4411 used the standard cure cycle (see Appendix A), but with the vacuum bag made to develop a leak during initial heat-up and dwell. The computed void content was low-0% by chemical analysis and 0.90% by image analysis. Laminate ACL-4412 used the standard cure cycle except that, when the vacuum was turned off, the bag was not vented to the atmosphere. The physical properties of ACL-4412 are similar to those of ACL-4411. Void content is zero by both methods. Prior to laying up laminate 4416, the prepreg was hung in a 90^0F temperature humidity chamber (95% RH) for 72 hours. The standard cure cycle was used. Void content was 0% by chemical analysis and 1.05% by image analysis.

Subsequent to the initial study (Table 3), a second porosity evaluation study was conducted using fresh AS/3501-6 material. One control laminate and five others were fabricated as listed in Table 4. Laminate ACL-4446 was the void-free, $[0_3/\pm45/0_2/90]_{2s}$ control laminate. A 50x photomicrograph of laminate 4446 (Fig. 1) verifies that it has negligible porosity. The remaining five laminates were fabricated using vacuum plus different cure pressures (0, 15 and 30 psi). From the results presented in Table 4, it is seen that laminate void content increases as the cure pressure decreases. Void content measurements by the Image Analysis technique are again significantly higher than chemical analysis measurements, as seen in the initial evaluation study. Void contents for the three laminates of the second porosity evaluation study (Table 4), fabricated using vacuum plus 15 psi cure pressure, ranged from 0% to 1.9% by chemical analysis and from 2.70% to 6.08% by Image Analysis. A photomicrograph of a section of one of these porous laminates is shown in Figure 2. Based on the results of Table 4, vacuum plus 15 psi cure pressure was selected for making program laminates with uniform porosity.

TABLE 4. SECOND POROSITY EVALUATION

LAMINATE NUMBER AND DESCRIPTION	CURE METHOD	LAMINATE THICKNESS, IN.	RESIN CONTENT BY WT, %	FIBER VOLUME, %	SPECIFIC GRAVITY	CHEMICAL % VOID VOL.	X-RAY RESULTS POROSITY	PHOTO METHOD* % VOID VOL.	PLY THICKNESS, IN.	SHORT BEAM SHEAR, KSI	LONGITUDINAL COMPRESSION ULTIMATE STRENGTH, KSI	ULTIMATE STRAIN μ-IN/IN	MOD.OF ELAS., 10^6 PSI	PREPREG ROLL/SPOOL
1. ACL-4446														
a) $[0_3/\pm45/0_2/90]_{2S}$	Control	0.160	26.42	67.60	1.6538	0	None	0	0.00500	-	-97.7	-8988	11.7	1699/15D
b) $[0]_{15T}$	Control	0.072	21.77	73.79	1.6979	0	None	0	0.00480	10,229	-	-	-	" "
2. ACL-4447														
a) $[0_3/\pm45/0_2/90]_{2S}$	Vacuum only	0.175	28.09	63.06	1.5781	1.8		3.92	0.00547	-	-98.7	-8866	11.3	1699/15D
b) $[0]_{15T}$	"	0.077	25.30	67.36	1.6230	0.1		-	0.00513	9,030	-	-	-	" "
3. ACL-4448														
a) $[0_3/\pm45/0_2/90]_{2S}$	Vacuum +15 psi	0.178	28.61	62.41	1.5735	1.9		2.86	0.00556	-	-107.0	-9615	11.4	1699/15D
b) $[0]_{15T}$	"	0.075	23.68	67.77	1.5983	1.6		-	0.00500	7,577	-	-	-	" "
4. ACL-4449														
a) $[0_3/\pm45/0_2/90]_{2S}$	Vacuum +30 psi	0.173	29.19	62.20	1.5810	1.2		2.14	0.00541	-	-116.7	-12074	10.4	1699/15D
b) $[0]_{15T}$	"	0.074	23.99	67.54	1.5994	1.2		-	0.00493	10,249	-	-	-	" "
5. ACL-4462-1														
a) $[0_3/\pm45/0_2/90]_{2S}$	Vacuum +15 psi	0.155	28.96	61.96	1.5700	0		2.70	0.00484		-91.4	-7357	10.9	1699/16B
6. ACL-4462-2														
$[0_3/\pm45/0_2/90]_{2S}$	Vacuum +15 psi	0.175	28.83	64.78	1.6384	1.3		6.08	0.00547	-	-100.4	-8693	11.7	1699/16B

*Using Image Analysis

▼Time-temperature portion of cure cycle was per Process Instruction Sheet M & P-D No. 1
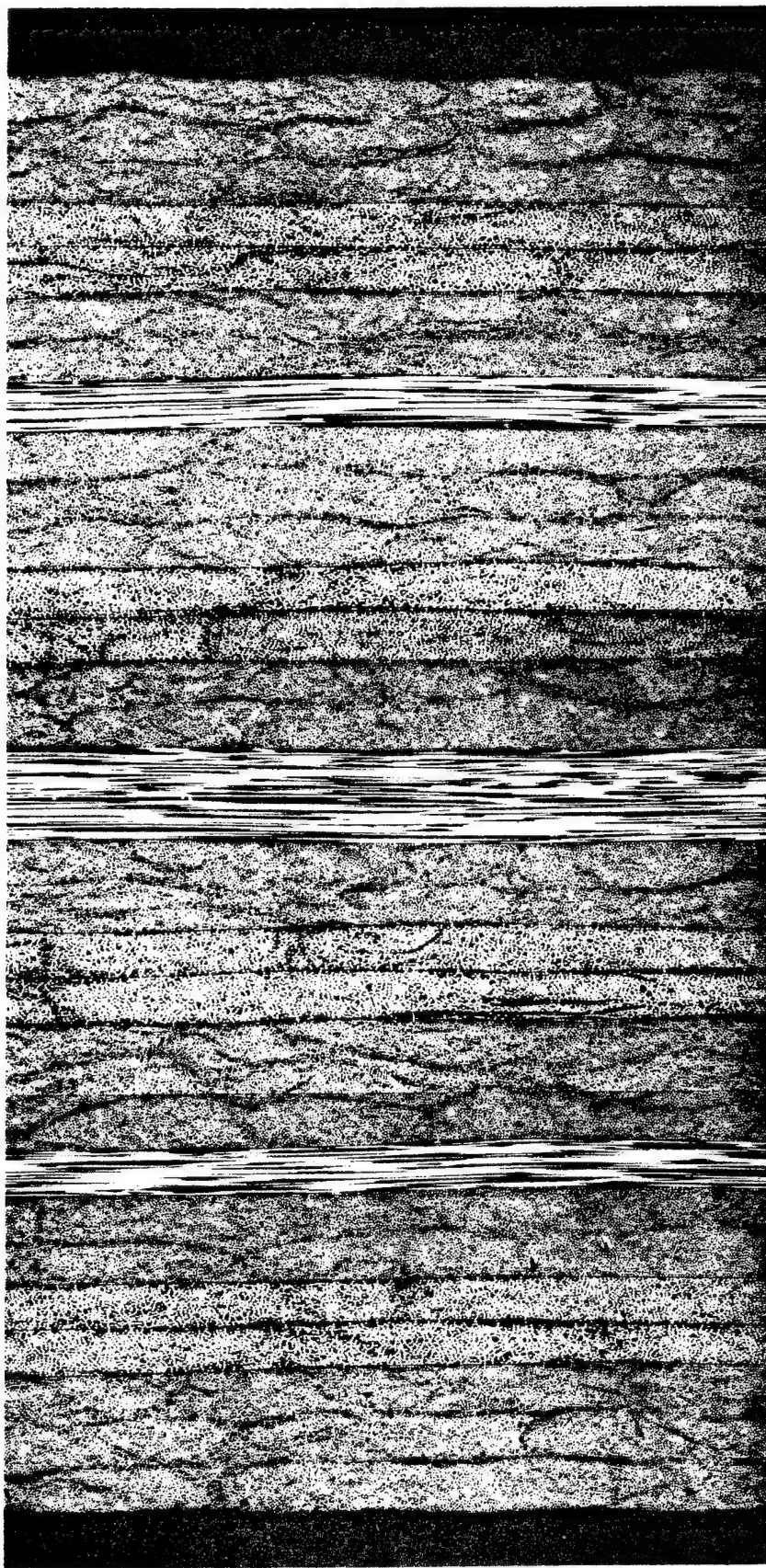
Figure 1. Photomicrograph of an ACL-4446 Cross-Section.
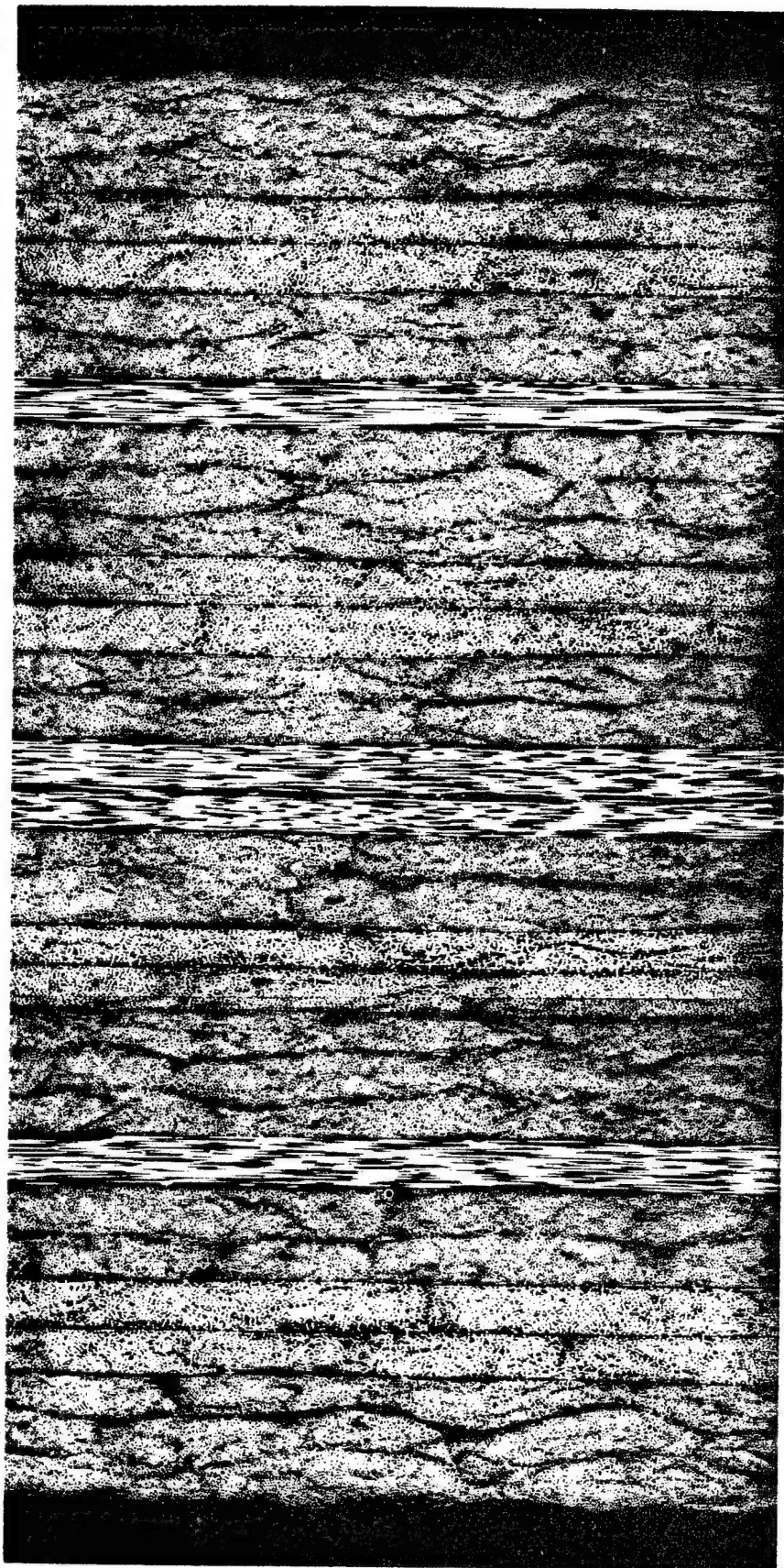
Figure 2.   Photomicrograph of an ACL-4462-1 Cross Section.

2.4   FABRICATION AND EVALUATION OF PROGRAM TEST LAMINATES

In compliance with the program requirements listed in Table 1, four laminates – three with uniform porosity and a non-porous laminate with an imbedded delamination – were fabricated according to process instructions detailed in Appendix A and the drawings in Appendix B (see Table 5). Laminates A, B and C were porous and had configurations of $[0]_{24T}$, $[\pm 45]_{6s}$ and $[(\pm 45)_5/0_{16}/90_4]_c$, respectively.   Laminate D was identical to laminate C in configuration, non-porous, and contained 0.5 inch long Teflon inclusions (imbedded delaminations) between plies 15 and 16.

Fabricated test panels were subjected to nondestructive inspection to observe the presence of induced defects.   Initial ultrasonic C-scan records of the porous laminates (A, B and C) were obtained using a 27-ply defect standard panel.   As expected, the C-scan printouts were blank, indicating a porous laminate.   A second setting was then achieved by using lead tapes on the back surface of the laminate and adjusting the instrumentation until a signal was transmitted through the laminate.   This required power 100 times in excess of that normally used and yielded a C-scan pattern of the relative areal gross density of porosity in the laminate.   Figure 3 shows a sample comparison of the C-scan records corresponding to the two settings.   An ultrasonic C-scan record of laminate D reveals the built-in delaminations, and shows that the laminate is defect-free otherwise (Fig. 4).

The void contents and other physical properties of laminates A, B, C and D were obtained through specimens identified in the fabrication drawings (see Appendix B).   Enlarged (50x) cross-section photomicrographs of laminate cross-sections were obtained, showing intentionally induced porosity and delamination defects.   The locations of these particular specimens in each laminate are shown in the fabrication drawings in Appendix B.   Four specimens from each laminate were examined, and longitudinal (parallel to the 0^0 laminate axis) and transverse (perpendicular to the 0^0 laminate axis) cross-sections of each specimen were photomicrographed. An SEM Image Analysis of the photomicrographs yielded the void volumes of the corresponding cross-sections.   The average Image Analysis void volume of each specimen's longitudinal and transverse cross-sections, abbreviated as IAVV, was recorded.   Figure 5 presents sample photomicrographs

TABLE 5. SUMMARY OF MATERIAL AND PROCESS PARAMETERS FOR PROGRAM LAMINATES

PROCESSING DETAILS	ACL-4464 LAMINATE A	ACL-4465 LAMINATE B	ACL-4466 LAMINATE C	ACL-4472 LAMINATE D
1. Prepreg Lot/Spool	1699/16B	1699/16B	1699/16D	1699/16D
2. Debulking	No	No	No	Yes
3. No. of Bleeder Plies (120 glass)	6	6	7	7
4. Actual Vacuum Level, psig	*	*	*	*
5. Actual Positive Pressure, psig	*	*	*	*
6. Actual Heat-up Rate (RT to Dwell Temp)	4.4°F/min.	***	1.7°F/min. ⊕	4.1°F/min.
7. Actual Time @ Dwell Temp., Min. @ °F	60 min. @ 235°F ± 5°F	***	35 min. @ 235°F ±5°F ⊛	60 min. @ 235°F ± 5°F
8. Actual Heat-up Rate to Cure Temp.	1.7°F/min.	***	2.6°F/min.	4.6°F/min.
9. Actual Time @ Cure Temp, min. @ °F	90 min. @ 345°F ± 5°F **	***	120 min. @ 345°F ± 5°F	120 min. @ 345°F ± 5°F
10. Actual Cool Down Time to Temp Under Pressure, min. to °F	30 min. to 185°F (5.3°F/min.)	***	38 min. to 172°F (4.5°F/min.)	23 min. to 100°F (11°F/min.)
11. Actual Postcure Time and Temp, Hrs & °F	8 Hrs @ 355°F ± 5°F	8 Hrs @ 355°F ± 5°F	8 Hrs @ 352°F ± 3°F	8 Hrs @ 352°F ± 3°F

⊛ plus 25 min. @ from 229°F to 235°F
⊕ 2.8°F/min. from RT to 229°F
** plus 30 min. @ from 336°F to 345°F
Note: Cure temp data on Laminates A and C are based on avg of two (top and bottom) thermocouples and that of Laminate C are based on a top thermocouple, only.

*Laminate fab. work order lists pressure at full vacuum and 15 psi
***Laminate fab work order lists 1) heat up to 240°F and hold for 60 min., 2) heat up to 350°F and hold for 120 min., and 3) cool down to 150°F under pressure
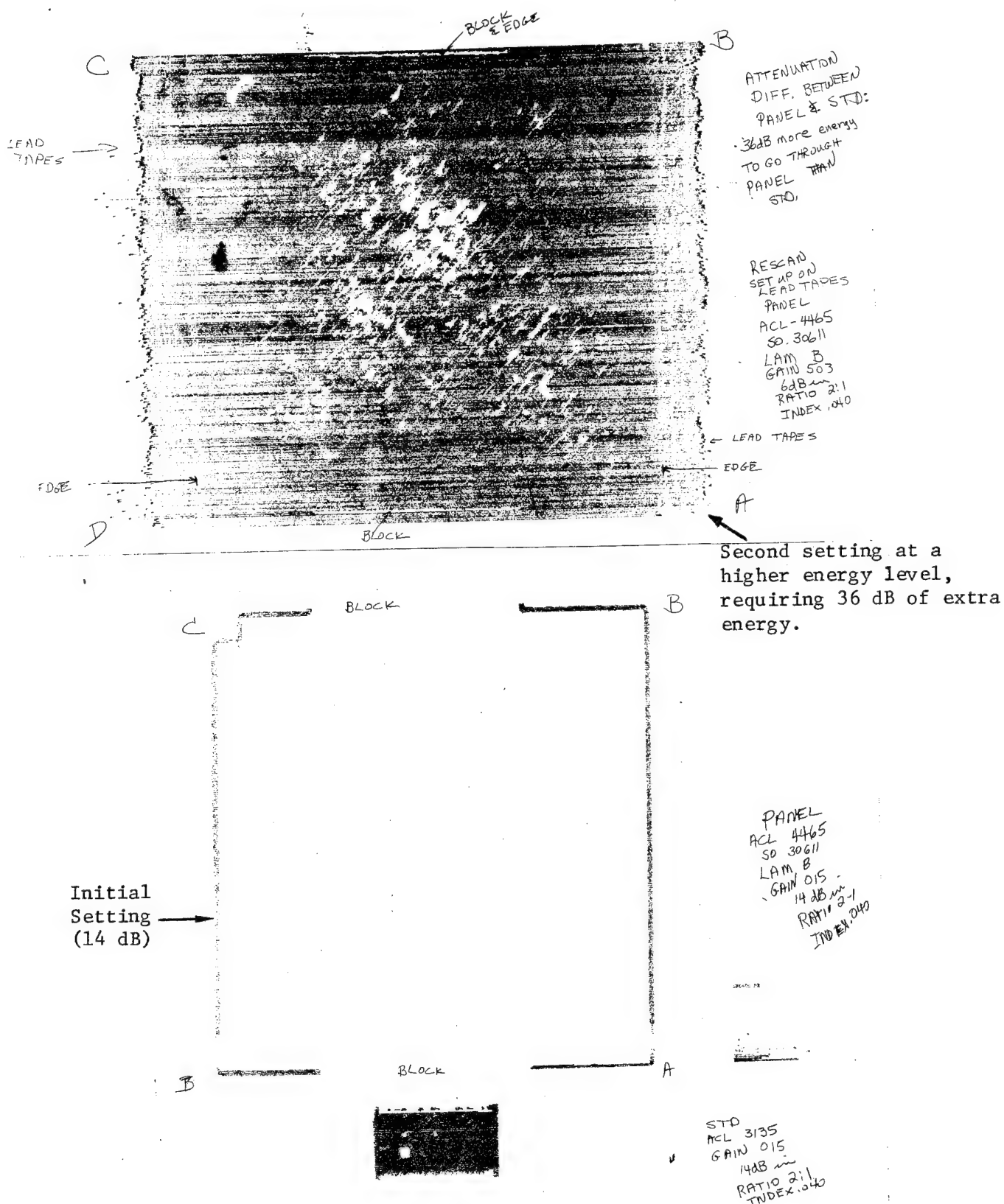
Figure 3. Ultrasonic C-Scan Records of Porous Laminate B at Two Instrumentation Settings.

14
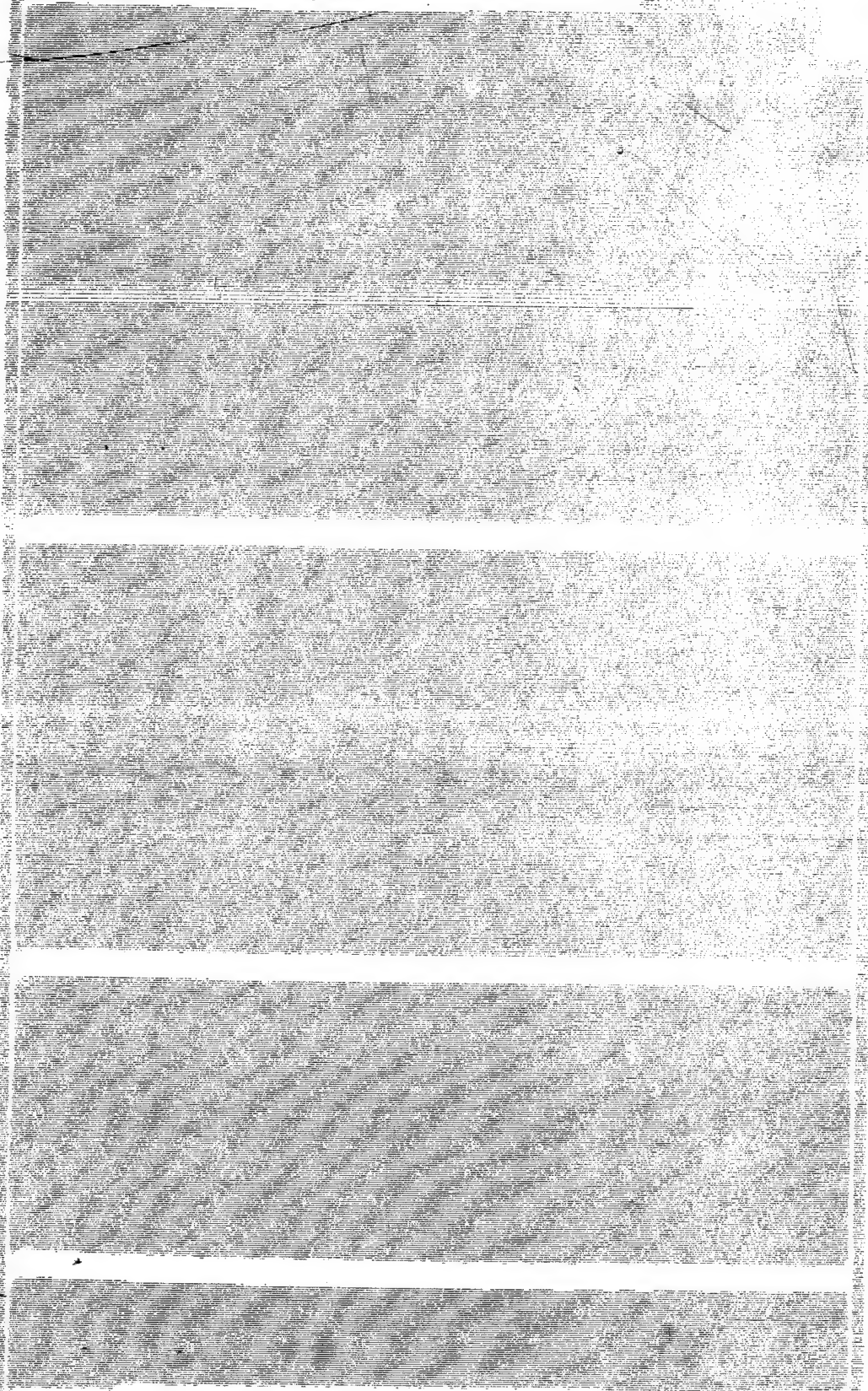
Figure 4. Ultrasonic C-Scan Record of Non-Porous Laminate D, Showing Imbedded Delamination Locations.

15
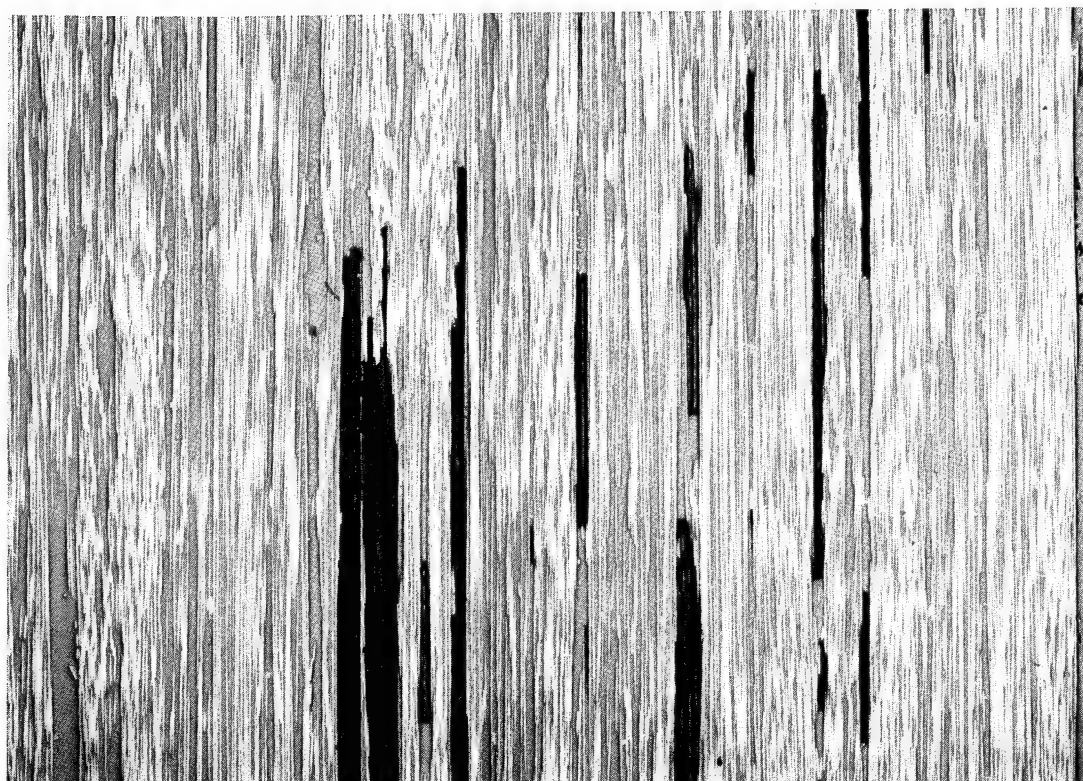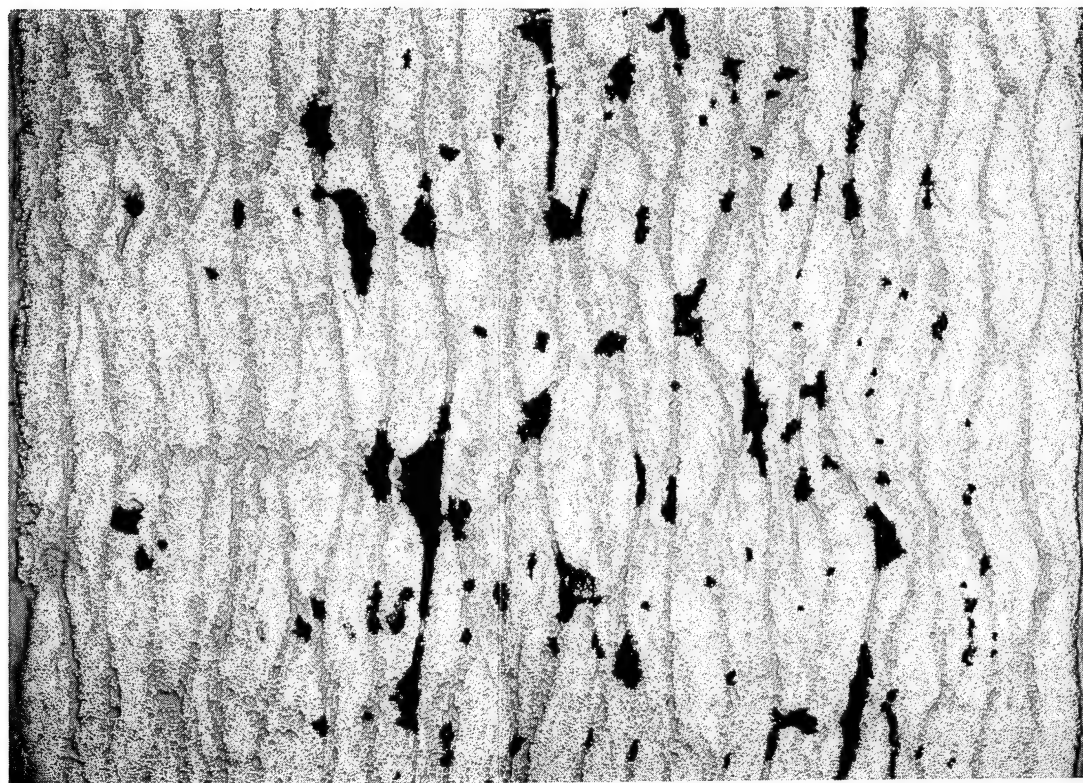
Specimen A-81T

Specimen A-81L

Figure 5. Photomicrograph (~40 X) of the Longitudinal (L) and Transverse (T) Cross-
Sections of Specimen A-81; IAVV = 3.90%.

16

of a Laminate A specimen. The remaining three sets of photomicrographs for laminate A, and similar records for laminates B, C and D are presented in Appendix B. The average of the four sets of data yielded the void volume as measured via an SEM image analysis technique. The porosity level in Laminate A ranged from 1.05% to 5.70% with a mean value of 3.06%. The porosity content of Laminate B ranged from 2.10% to 2.60% with a mean value of 2.31%. The Image Analysis void volume measurements for laminate C ranged from 2.70% to 3.35%, with a mean value of 3.05%. Image analysis of Laminate D specimens measured an average porosity level of < 0.06%, which is essentially a "non-porous" value. In a similar manner, void volumes were also measured using a chemical analysis. This involved acid digestion of sample specimens from the program laminates, and computations based on assumed fiber and matrix density values (Ref. 2). As mentioned in subsection 2.3, a considerable difference was observed in the void content values computed by the two techniques. Nevertheless, a look at the photomicrographs of the corner specimens and the ultrasonic C-scans of each of the program laminates ascertains the fact that some level of uniformity does exist in the induced porosity. How uniform the porosity in each laminate is, when viewed in a three-dimensional manner, is difficult to establish without sacrificing test specimens. The fiber volume percentage, resin content and specific gravity of each of the four program laminates were also determined using standard procedures (Refs. 1 and 3).

A summary of the average physical properties is presented in Table 6. The goal of obtaining a uniform porosity level of 3 ± 2%, by chemical analysis, was achieved in laminates A, B and C. It is also seen, in Table 6, that the void content of the non-porous laminate D was measured to be 0%. Differences in the physical properties, other than void content, of the test laminates may be explained by reviewing the material and process parameters in Table 5. Two contributing factors of significance are: (1) the material batch variability, and (2) the heat-up rates from room temperature to dwell temperature, and from dwell temperature to cure temperature.

The differences in the physical properties of the various test laminates will undoubtedly affect the interpretation of their relative mechanical

17

TABLE 6. PHYSICAL PROPERTIES OF TEST LAMINATES

Laminate	Configuration	Defect Type *	% Voids Chemical Analysis	% Voids Image Analysis	Fiber Volume %	Resin Content (% by wt.)	Specific Gravity
A	$[0]_{24T}$	UP	2.12	3.06	57.23	33.21	1.5423
B	$[\pm 45]_{6S}$	UP	1.49	2.31	58.47	32.40	1.5570
C	$[(\pm 45)_5/0_{16}/90_4]_c$	UP	1.61	3.05	60.29	30.67	1.5653
D	$[(\pm 45)_5/0_{16}/90_4]_c$	DL	0	< .06	61.40	31.10	1.6047

*UP denotes uniform porosity.

DL denotes an imbedded delamination.

18

responses. But, of all the properties listed in Table 6, laminate mechanical response is expected to be affected significantly only by the void content and the fiber volume percentage. Further, the void volume effect is expected to be more significant than the fiber volume effect on the mechanical properties of the test laminates.

2.5 QUALITY CONTROL (QC) TESTS ON PROGRAM LAMINATES

2.5.1 QC Flexure Tests

Longitudinal and transverse flexure tests were conducted on laminate A specimens per ASTM standards spelled out in D-790. A four point beam test, with quarter point loading, was carried out. A nominal beam width of 0.5 inch was used. Span-to-depth ratios of 32:1 for longitudinal flexure tests, and 25:1 for transverse flexure tests were selected. Four tests were conducted for each case. Longitudinal flexure tests on laminate A specimens yielded an average failure load of 480 lbs, a mean ultimate stress value of 167.58 ksi, an average modulus of 17.38×10^6 psi, and a mean beam failure deflection value of 0.324 in. Transverse flexure tests on laminate A specimens yielded an average failure load of 37 lbs, a mean ultimate stress value of 9.98 ksi, an average modulus of 1.36×10^6 psi, and a mean beam failure deflection value of 0.146 inch. Comparing these results with those in Table 2, it is seen that the longitudinal flexural strength of porous laminate A specimens is 73% of the value corresponding to non-porous $[0]_{16T}$ specimens, after fiber volume differences are accounted for. Longitudinal modulus of porous laminate A specimens is 96% of the value corresponding to non-porous $[0]_{16T}$ specimens. Similar reductions are expected in the transverse flexure properties, but these data were not generated on non-porous specimens to form a basis for comparison.

2.5.2 QC Static Compression Tests

Porous laminate C specimens were subjected to transverse static compression tests under room temperature, dry (RTD) conditions. Test specimens were 3 in. long and 2 in. wide, and were supported laterally in an ETL test fixture (see Appendix B). Three tests were conducted. The average transverse compression strength was measured to be -54.2 ksi, which is in excess of the requirements (-40 ksi) spelled out in the Q.C.

19

instruction sheet (see Appendix A). But the porous strength of -54.2 ksi
is only 64% of the nonporous strength, reported in Reference 3, after fiber
volume differences are accounted for.

2.5.3 QC Static Tension Tests

Quality Control (QC) static tension tests were carried out, per ASTM
D-3039 standards, on specimens from laminates A, B, C and D, under RTD
conditions. The results are presented in Table 7. A comparison of these
results for porous laminates with corresponding results for non-porous
laminates, presented in References 1 and 3, enables one to assess the effect
of porosity on static tension response. But, prior to drawing comparisons,
the effect of the differences in the fiber volume percentages on mechan-
ical response has to be considered for the compared laminates. This is
done by establishing criteria, presented in Table 8, based on a comparison
of available data in the literature and intuition. The criteria in
Table 8 are valid both for tensile and compressive mechanical property
dependence on fiber volume percentage. The degradation in the
static tension test data due only to porosity effects is listed in Table
9. Fiber volume differences between compared laminates have been accounted
for, per Table 8, in the results of Table 9. A comparison between non-
porous laminate C tension data (Ref. 3) and tension data for laminate D
(non-porous, laminate C layup, but including an imbedded delamination
at midplane) is also included in Table 9.

A review of the results in Table 9 indicates a 21% reduction in the
tensile strength of $[0]_{24T}$ and $[90]_{24T}$ specimens due to 2.12% voids
as measured by chemical analysis. It must be noted, though, that hydraulic
grips seemed to have applied excess pressure in the tab region in both
test cases causing failure under the bevelled region of the tabs. The
measured ultimate strengths of these porous specimens are therefore
suspected to be lower than actual. Consequently the 21% reduction in
the tensile strengths is believed to be an overestimation, particularly
so for the $[0]_{24T}$ layup. The tensile modulus of $[0]_{24T}$ specimens was un-
affected by porosity, while an 8% reduction was observed in the modulus
of $[90]_{24T}$ specimens.

TABLE 7. Q.C. STATIC TENSILE DATA ON LAMINATES A, B, C AND D UNDER RTD CONDITIONS

Laminate	Load Dirn.	Specimen	Nominal Width (In.)	Thickness (In.)	Ultimate Stress (Ksi)	Ultimate Strain (µin/in)	Prop. Limit Stress (Ksi)	Prop. Limit Strain (µin/in)	Poisson's Ratio	Modulus of Elasticity (10⁶ PSI)
A $\rightarrow$	0° $\rightarrow$	4464-33	0.500	0.124	162.945	8,882			0.3185	17.93
		4464-34		0.135	182.525	9,518			0.3326	18.11
		4464-35		0.143	166.712	9,266			0.3290	16.73
		Mean $\rightarrow$			170.727	9,222			0.3267	17.59
A $\rightarrow$	90° $\rightarrow$	4464-36	1.000	0.143	5.534	4,181			0.0118	1.20
		4464-37		0.142	5.690	4,512			0.0225	1.27
		4464-38		0.143	5.220	4,166			0.0247	1.22
		Mean $\rightarrow$			5.481	4,286			0.0197	1.23
B $\rightarrow$	0° $\rightarrow$	4465-17	1.000	0.136	25.935	18,658	10.000	4,049	0.6737	2.47
		4465-18		0.136	26.222	17,101	9.265	3,457	0.6723	2.68
		4465-19		0.134	26.395	17,341	10.000	3,817	0.6944	2.62
		Mean $\rightarrow$			26.184	17,700	9.755	3,774	0.6801	2.59
C $\rightarrow$	0° $\rightarrow$	4466-37	1.000	0.180	121.723	11,323			0.3505	10.49
		4466-38		0.180	121.587	11,075			0.3458	10.44
		4466-39		0.183	112.386	10,608			0.3218	10.16
		Mean $\rightarrow$			118.565	11,002			0.3424	10.36
C $\rightarrow$	90° $\rightarrow$	4466-40	1.000	0.180	43.153	10,815	16.667	3,840	0.1445	4.34
		4466-41		0.178	38.697	9,380	15.385	3,374	0.1418	4.56
		4466-42		0.176	42.468	10,710	18.000	3,986	0.1323	4.52
		Mean $\rightarrow$			41.439	10,302	16.684	3,733	0.1395	4.47
D $\rightarrow$	90° $\rightarrow$	4472-13	1.000	0.176	37.863	8,148	28.214⊖	6,100⊖	0.1548	4.65
		4472-14		0.174	38.913	8,290	28.072⊖	5,891⊖	0.1500	4.60
		4472-15		0.172	39.422	9,000	26.868⊖	5,890⊖	0.1493	4.50
		Mean $\rightarrow$			38.729	8,479	27.718	5,960	0.1514	4.58

⊖Values represent start of micromechanical damage as observed on stress-strain curve; however, the slope doesn't change above this point so it's not a proportional limit.

21

TABLE 8. EFFECT OF FIBER VOLUME PERCENTAGE (FVP)
ON THE MECHANICAL PROPERTIES OF TEST LAMINATES

Property	Effect of Fiber Volume Percentage (FVP) on the Mechanical Properties of the Following Laminates*			
	$[0]_{nt}$	$[90]_{nt}$	$[\pm45]_{ns}$	$[(\pm45)_5/0_{16}/90_4]_c$
Ultimate Strength	Varies directly with FVP	Not sensitive to FVP	Varies directly with FVP	varies directly with FVP
Ultimate Strain	Not sensitive to FVP	Not sensitive to FVP	Not sensitive to FVP	Not sensitive to FVP
Prop. Limit Stress	Varies directly with FVP	Not sensitive to FVP	Varies directly with FVP	Varies directly with FVP
Prop. Limit Strain	Varies directly with FVP	Not sensitive to FVP	Varies directly with FVP	Varies directly with FVP
Poisson's Ratio	Not sensitive to FVP	Not sensitive to FVP	Varies inversely with FVP	Not sensitive to FVP
Modulus of Elasticity	Varies directly with FVP	Varies directly with FVP	Varies directly with FVP	Varies directly with FVP

*The above deductions are valid for both tensile and compressive properties.

TABLE 9. COMPARISON OF RTD STATIC TENSION DATA ON DEFECTIVE AND DEFECT-FREE LAMINATES

Laminate	Load Direction	(Property of Defective Laminate/Property of Defect-Free Laminate) x100* For						
		Ultimate Stress	Ultimate Strain	Prop. Limit Stress	Prop. Limit Strain	Poisson's Ratio	Modulus of Elasticity	Fiber Vol. %
A	0°	79.3	75.6	--	--	116.4	102.0	91.57
A	90°	79.4	89.9	--	--	--	92.0	91.57
B	0° or 90°	110.9	98.1	128.0	120.8	98.7	104.4	101.63
C	0°	101.4	110.0	--	--	98.6	89.3	110.64
C	90°	90.7	95.6	71.1	71.0	94.6	92.0	110.64
D	90°	83.2	78.7	116.0	111.2	102.0	92.5	112.74

*Properties were corrected for fiber volume differences, per Table 8, before comparisons were made. Defect-free laminate data were obtained from References 1 and 3.

A porosity level of 1.49% (chemical analysis) has insignificant effects on the tensile strength and modulus of $[\pm 45]_{6S}$ specimens.

A porosity level of 1.61% (chemical analysis) has negligible effects on the tensile strength of $[(\pm 45)_5/0_{16}/90_4]_C$ specimens, but a 11% drop in the modulus of elasticity is noted. Transverse tensile tests on laminate C specimens, though, indicated a 9% loss in the strength, an 8% loss in the modulus of elasticity, and a 29% loss in the proportional limit stress value. The measurable losses in the transverse tensile tests are believed to be due to the large fraction of 90^0 fiber orientation under this loading situation.

The tensile strength and modulus of non-porous laminate D specimens suffered 17% and 8% losses, respectively, in comparison to non-porous laminate C specimens. The losses are attributed to the presence of imbedded delaminations in laminate D specimens.

2.6 DETAILS PERTAINING TO PROGRAM TEST MATRIX

After the completion of material evaluation, porosity investigation, fabrication and inspection of program laminates, and quality control tests, the program test matrix presented in Table 1 was executed. A summary of the tests is outlined in sub-section 2.1. The various test variables are discussed below.

2.6.1 Test Fixtures and Test Specimens

Static compression tests on $[0]_{24T}$ specimens were conducted in a Celanese test fixture (see Appendix B). The specimens were 5.5 in. long, 0.25 in. wide, and had a test length between tabs of 0.5 in. Static compression tests on $[90]_{24T}$ specimens and specimens from laminates B, C and D were conducted in an ETL test fixture (see Appendix B). These specimens were 3 in. long and 2 in. wide, and were supported laterally by the test fixture for stability under compressive loading. All the compression fatigue tests were conducted at R=10 and $\omega \approx$ 10 Hertz in an Atmur test fixture (see Appendix B). Fatigue test specimens were 8 in. long, 2 in. wide, and had a 3.5 in. long test section between tabs that was laterally supported during fatigue (see Figure 6).
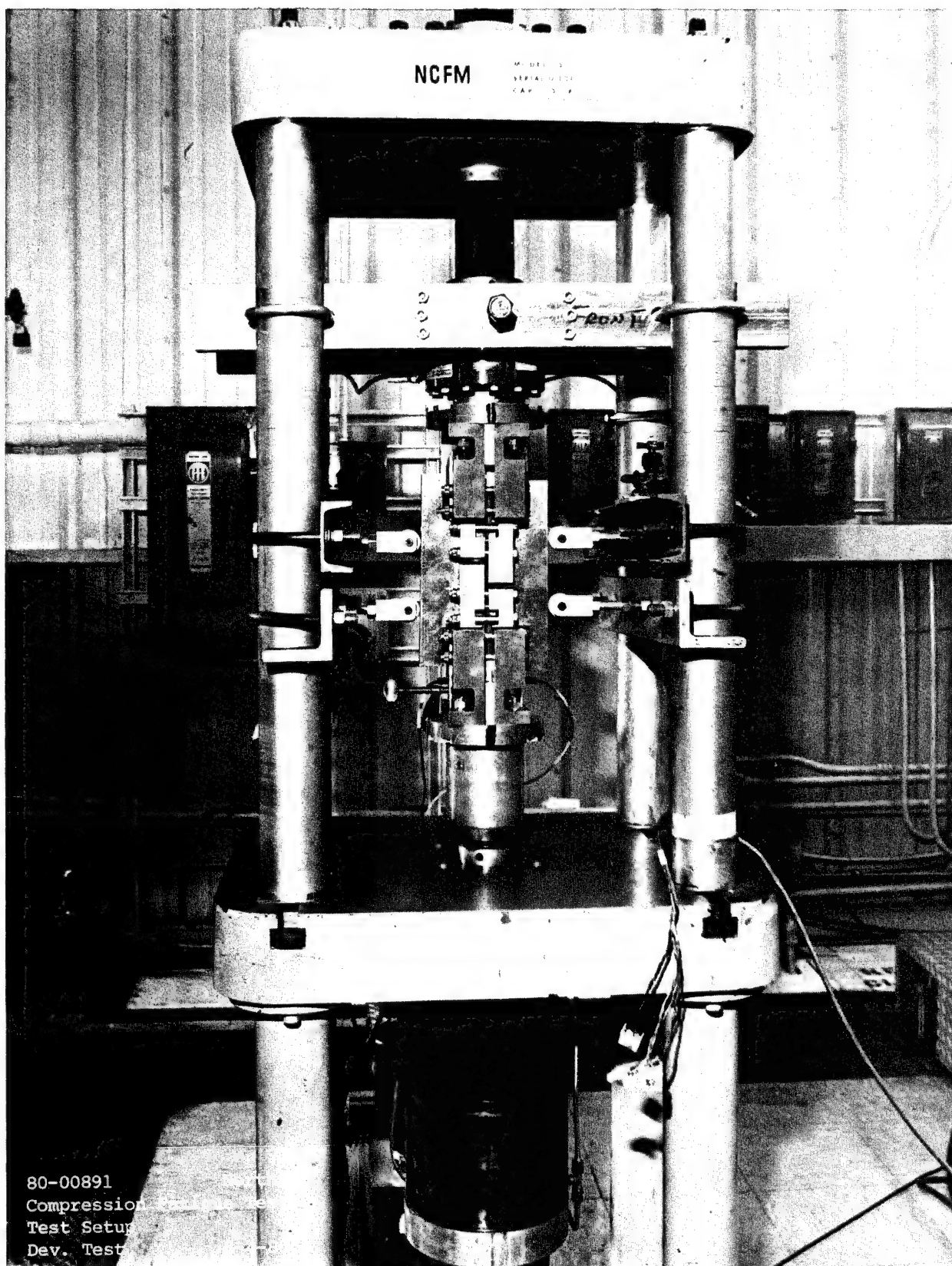
Figure 6. Overall View of Compression Fatigue Test Setup.

It must be noted that the platen side supports used in the ETL and Atmur test fixtures have a retarding effect on the growth of delaminations, if any. This is especially important in the interpretation of results corresponding to laminate D specimens. But, since the imbedded delaminations in laminate D specimens are at the midplane between plies 15 and 16, the out-of-plane deflection associated with the post-buckling deformation in these specimens is expected to be very small (see Ref. 5). In Reference 1, the lateral constraint effect on the static compression data on $[\pm 45]_{6S}$ laminates is discussed. Nevertheless, the ETL and Atmur test methods are employed in this program to be consistent with the methods used in References 1 and 3, which provide the data base for quantifying the effects of porosity and delaminations.

2.6.2 Static and Fatigue Test Procedures

Static and residual strength tests were conducted at a loading rate of 10,000 lbs/min. Back-to-back strain gages (350 ohm resistance type), wtih a biaxial gage on one surface, were used to monitor strain data. Constant amplitude, compression-compression fatigue tests were conducted at R=10 and $\omega \approx 10$ Hertz. R is the algebraic ratio of the minimum cyclic load to the maximum cyclic load. All the fatigue test specimens were loaded statically at the initiation of the test to set the load amplitude corresponding to a desired strain level. Back-to-back axial strain gages were bonded to the specimens for this purpose. If the specimens survived 1.25×10^6 cycles of the imposed fatigue loading without failure (referred to as run-out) they were subsequently subjected to residual static compression strength tests. The ratio of the minimum cyclic strain value to the static failure strain value (S) was varied to induce fatigue failures at cycles (N_f) ranging from a few thousands to below 1.25×10^6 cycles. Threshold strain levels - the maximum absolute cyclic strain values at which fatigue failures are not induced for 1.25×10^6 cycles were established from the resulting test data.

2.6.3 Moisture Conditioning For RTW and 218FW Tests

In an attempt to achieve a moisture content of 1% by weight in some of the test specimens (see Table 1) the exposures used in the previous studies

26

(Refs. 1 and 3) were adopted. The 24-ply specimens (laminates A and B) were thus exposed for 40 days to a 170F, 95% RH environment, followed by 24 days of exposure to a 170F, 80% RH environment. The 30-ply specimens (laminate C) were exposed for 63 days to a 170F, 95% RH environment, followed by 36 days of exposure to a 170F, 80% RH environment. The results are listed along with the mechanical properties in Section 3. It is noted here that the absorbed moisture contents were 0.75, 0.54 and 0.70% for laminates A, B and C - considerably lower than the desired 1% value. An explanation for this result is based on an observation made during the RTD test phase of the program on some moisture control specimens. Monitoring of the traveler control specimens, from fabrication until the RTD tests were completed, revealed a 0.11% moisture gain in the non-porous delaminated laminate D specimens, a 0.25% to 0.28% moisture gain in specimens from the porous laminates A and B, and a 0.35% moisture gain the porous laminate C specimens. Moisture absorbed from in situ laboratory conditions (RTD) increases in quantity when microvoids (porosity) are present in the specimens. Likewise, the presence of porosity may also dry out the moisture faster when secondary conditioning (at 170^0F and 80% RH) is imposed on the specimens. This is believed to be the reason for moisture contents much lower than the desired 1% value in the program laminates (see Table 11, Section 3).

2.6.4 Test Data Evaluation

Data generated from the static compression tests of Table 1 were compared with the data from References 1 and 3 to quantify the effects of induced defects (porosity and delamination). Fiber volume differences between laminates were accounted for, per Table 8, prior to making comparisons. Results are presented in section 3 in the form of percentages of the mechanical properties of defect-free laminates retained by defective laminates (with porosity or imbedded delaminations). Compression fatigue test results were cast in the form of modified S-N curves, incorporating residual strength data, if any. From the modified S-N curves, threshold strain levels for defective laminates were obtained, and these values were compared with corresponding values for defect-free laminates (Ref. 1) to quantify the effects of porosity and delamination on the compression fatigue behavior of the test laminates. Failed specimens were also observed for failure surfaces, and analyzed, to predict failure histories.

27

SECTION 3

DISCUSSION OF RESULTS

3.1 STATIC COMPRESSION TEST RESULTS

Results from static compression tests on laminates A, B, C and D, under RTD conditions, are presented in Table 10. Similar results on laminates A and B under RTW conditons, and on laminate C under RTW and 218FW conditions, are presented in Table 11. A comparison of these results with the data generated in References 1 and 3 for defect-free laminates of the same configurations is presented in Table 12. Compared mechanical properties include the stresses and strains at the proportional limit and at failure, Poisson's ratio, and the longitudinal modulus of elasticity. All the mechanical properties were corrected for fiber volume differences between compared laminates, per Table 8, before the results in Table 12 were computed. It is important to note that the gross failure modes in the defective laminates (see Appendix C) were observed to be the same as those seen in the defect-free laminates of References 1 and 3. Differences in the failure surfaces at the micromechanical level will be discussed in Section 4. The choice of the same material, laminate configurations, test methods and test environment, coupled with the observation of similar gross failure modes, justifies the interpretation of the results in Table 12 as being representative of the quantitative effects of induced defects (porosity and delamination) on the static compression properties of test laminates. A reduction in a defect-free laminate property of 10% or over is considered significant in making the following observations.

The effect of a uniform porosity of 2.12% by chemical analysis, or 3.06% by SEM image analysis, on the static compression properties of $[0]_{24T}$ specimens is considered first. Under RTD conditions, a 38.5% reduction in the ultimate strength and a 48.7% reduction in the failure strain were recorded. Poisson's ratio and modulus suffered insignificant losses. Similar results were realized under RTW conditions, with nearly identical reductions in the compressive strength (38%) and the failure strain (48%).

TABLE 10. STATIC COMPRESSION PROPERTIES OF LAMINATES A, B, C AND D UNDER RTD CONDITIONS

Test Series	Laminate	Loading Direction	Specimen ID	Width (in.)	Thickness (in)	Ultimate		Prop. Limit		ν	E (Msi)
						Stress (ksi)	Strain (μin/in.)	Stress (ksi)	Strain (μin/in.)		
I	A	0°	4464-2	.250	.142	-121.4	-8157			.31	15.58
			4464-3	.250	.141	-126.7	-8501			.32	15.91
			4464-4	.249	.143	-101.3	-7059			.30	15.36
			4464-5	.250	.143	-107.7	-7377			.31	15.56
			Mean →			-114.2	-7774	--	--	.31	15.60
IV	A	90°	4464-9	1.989	.1285	-27.39	-21,557	-11.74	-7983	.019	1.46
			4464-10	1.989	.1389	-22.40	-19,697	-9.05	-6828	.019	1.33
			4464-11	1.989	.1384	-22.38	-19,217	-8.17	-6183	.019	1.32
			4464-12	1.989	.1394	-22.50	-17,874	-8.65	-6288	.020	1.39
			Mean →			-23.67	-19,586	-9.40	-6821	.019	1.38
VII	B	0° or 90°	4465-1	1.989	.1307	-37.69 / -30.77	-23,947	-11.54	-5098	.75	2.26
			4465-2	1.989	.1334	-39.02 / -30.15	-24,212	-11.32	-4944	.76	2.29
			4465-3	1.989	.1356	-37.82 / -29.66	-23,026	-11.12	-4805	.79	2.32
			4465-4	1.989	.1375	-34.15 / -29.25	-24,133	-10.97	-4892	.78	2.24
			Mean →		See Note	-37.17 / -29.96	-23,830	-11.24	-4935	.77	2.28
X	C	0°	4466-1	1.990	.1563	-91.64	-9255	-48.23	-4599	.35	10.49
			4466-2	1.990	.1708	-96.79	-10304	-44.14	-4360	.36	10.19
			4466-3	1.990	.1744	-89.89	-9719	-50.43	-5107	.34	9.88
			4466-4	1.990	.1756	-82.43	-8875	-35.78	-3650	.36	9.80
			Mean →			-90.19	-9538	-44.65	-4429	.35	10.09
XVI	D	0°	4472-1	1.989	.1628	-98.52	-9850	-60.22	-5655	.36	10.65
			4472-2	1.989	.1683	-99.16	-10025	-59.76	-5719	.38	10.45
			4472-3	1.989	.1686	-101.07	-10350	-59.64	-5763	.38	10.35
			4472-4	1.989	.1696	-94.28	-9450	-59.29	-5704	.38	10.40
			Mean →			-98.26	-9919	-59.73	-5710	.37	10.46

Note: The upper value is the measured strength, and the lower value is the modified strength (see text for explanation).

29

TABLE 11. STATIC COMPRESSION PROPERTIES OF LAMINATES A, B AND C UNDER RTW AND 218FW CONDITIONS

Test Series	Laminate	Load Dirn.	Test Condition	Moisture Content (% by Wt.)	Specimen	Width (in.)	Thickness (in.)	Ultimate Stress (ksi)	Ultimate Strain (μin/in)	Prop. Limit Stress (ksi)	Prop. Limit Strain (μin/in)	ν	E (Msi)
II	A	0°	RTW	0.75	4464-6	.251	.140	-93.70	-6144			.34	15.66
					4464-7	.251	.145	-91.68	-6216			.33	15.74
					4464-8	.252	.143	-91.64	-5934			.32	15.84
					Mean →			-92.34	-6098			.33	15.75
V	A	90°	RTW	0.75	4464-13	1.989	.140	-20.18	-16800	-9.69	-7400	.017	1.31
					4464-14	1.989	.140	-20.36	-17600	-9.34	-7200	.019	1.30
					4464-15	1.989	.138	-21.86	-18600	-11.29	-8600	.016	1.31
					4464-16	1.989	.140	-20.65	-17950	--	--	--	--
					Mean →			-20.76	-17738	-10.11	-7733	.017	1.31
VIII	B	90°	RTW	0.54	4465-5	1.989	.1374	-31.10 / -25.98	-18700	-8.42	-3300	.69	2.55
					4465-6	1.989	.1373	-32.95 / -26.00	-19400	-8.06	-3300	.73	2.44
					4465-7	1.989	.1364	-35.02 / -26.17	-19500	-6.82	-2700	.72	2.53
					4465-8	1.989	.1335	-36.35 / -26.40	-19700	-6.97	-2700	.73	2.58
					Mean →		See Note	-33.86 / -26.14	-19325	-7.57	-3000	.72	2.53
XI	C	0°	RTW	0.70	4466-5	1.989	.1758	-78.64	-8208	--	--	--	--
					4466-6	1.989	.1738	-84.18	-9400	-30.08	-2900	.30	10.37
					4466-7	1.989	.1717	-87.85	-9152	-24.01	-2200	.30	10.91
					4466-8	1.989	.1738	-88.23	-9100	-23.43	-2150	.30	10.90
					Mean →			-84.73	-8965	-25.84	-2417	.30	10.73
XII	C	0°	218FW	0.70	4466-9	1.989	.1758	-64.34	-6401	-24.02	-2100	.29	11.44
					4466-10	1.989	.1780	-63.56	-6300	-23.74	-2100	.28	11.30
					4466-11	1.989	.1768	-63.97	-5900	--	--	--	--
					4466-12	1.989	.1709	-63.55	-6250	-22.65	-2000	.32	11.33
					Mean →			-63.86	-6213	-23.47	-2067	.30	11.36

Note: The upper value is the measured strength, and the lower value is the modified strength (see text for explanation).

30

TABLE 12. COMPARISON OF STATIC COMPRESSION DATA ON DEFECTIVE AND DEFECT-FREE LAMINATES

Laminate	Load Direction	Test Condition+	(Property of Defective Laminate/Property of Defect-Free Laminate) x 100 * For						
			Ultimate Stress	Ultimate Strain	Prop. Limit Stress	Prop. Limit Strain	Poisson's Ratio	Modulus of Elasticity	Fiber Volume Fraction
A	0°	RTD	61.5	51.3	--	--	91.2	106.9	91.57
A	0°	RTW	62.0	52.0	--	--	98.5	106.8	91.57
A	90°	RTD	63.2	64.6	61.4	72.4	79.2	88.6	91.57
A	90	RTW	71.8	58.0	62.4	61.8	130.8	112.6	91.57
B	0° or 90°	RTD	86.1	77.6	98.6	99.8	103.9	94.7	101.63
B	0° or 90°	RTW	83.9	69.4	65.3	62.1	102.1	101.6	101.63
C	0°	RTD	78.6	80.7	84.1	86.9	108.3	88.8	109.28
C	0°	RTW	80.8	85.6	54.9	53.5	94.9	97.9	109.28
C	0°	218FW	77.0	74.1	63.7	47.8	123.0	100.2	109.28
D	0°	RTD	84.1	83.9	110.5	110.0	114.5	90.4	111.29

* Properties were corrected for fiber volume differences, per Table 8 , before comparisons were made. Defect-free laminate data were generated in References 1 and 3.

+ Wet specimens contained approximately 1% of moisture by weight
RTD—room temperature dry; RTW—room temperature wet; 218FW—218F wet.

The effect of the same amount of porosity (2.12% by chemical analysis or 3.06% by SEM image analysis) on $[90]_{24T}$ compression properties is considered next. Under RTD conditions, significant losses in the ultimate strength (36.8%), failure strain (35.4%), proportional limit stress (38.6%) and strain (27.6%), Poisson's ratio (20.8%) and modulus of elasticity (11.4%) were recorded. Comparable reductions in the ultimate strength (28.2%), failure strain (42%), and proportional limit stress (37.6%) and strain (28.2%) were recorded under RTW conditions, too. But the Poisson's ratio and modulus of elasticity increased in value somewhat, probably within the range of experimental variation.

The effect of a uniform porosity of 1.49% by chemical anlaysis, or 2.31% by SEM image analysis, on the compression properties of $[\pm45]_{6S}$ specimens is also quantified in Table 12. The stress-strain behavior of these specimens is highly nonlinear (see Ref. 1), and their failure strain values are very high (see Tables 10 and 11). The platen side supports in the ETL test fixture also constrain the specimens in a beneficial manner when the applied strain is large, resulting in high ultimate strength values (see Ref. 1). The introduction of the added platen constraint is identified in the nonlinear stress-strain curves by locating the strain level at which the apparent modulus suddenly starts to increase. And, a more realistic strength value is obtained by assuming the modulus at the inflection point to remain unchanged to the failure strain value (see Ref. 1). The measured and the modified strength values are listed in Tables 10 and 11. A comparison between defective and defect-free strengths is based on the more realistic modified strength values rather than the measured strengths. Under RTD conditions, the porous $[\pm45]_{6s}$ specimens exhibited significant losses in the ultimate strength (13.9%) and failure strain (22.4%) values (Table 12). Other properties were relatively unaffected. Under RTW conditions, significant reductions were recorded in the ultimate strength (16.6%), failure strain (30.6%), and proportional limit stress (34.7%) and strain (37.9%) values.

Porous $[(\pm45)_5/0_{16}/90_4]_c$ specimens, containing a uniform porosity of 1.61% by chemical analysis, or 3.05% by image analysis, were also subjected to static compression. Significant reductions in the ultimate strength (21.4, 19.2 and 23%), failure strain (19.3, 14.4 and 25.9%), and proportional

32

limit stress (15.9, 45.1 and 36.3%) and strain (13.1, 46.5 and 52.2%) values
were recorded under RTD, RTW and 218FW conditions, respectively. In compari-
son to RTD conditions, lower reductions in the strength and failure strain
values were recorded under RTW conditions, and larger reductions under
218FW conditions. But, the proportional limit stress and strain values
suffered large reductions under RTW conditions, too. The combination of
porosity and moisture is believed to be the cause for large reductions in the
proportional limit stress and strain values. Insignificant changes in the
Poisson's ratio and modulus of elasticity were recorded under all three
environments, with the exception of a 11.2% reduction in the modulus under
RTD conditions.

Non-porous, $[(\pm 45)_5/0_{16}/90_4]_c$ specimens, containing a 1/2 in.-long
delamination at midplane (between plies 15 and 16), exhibited significant
reductions in the compression strength (15.9%) and failure strain (16.1%)
values under RTD conditions. These reductions, attributable solely to the
early precipitation of failure by the catastrophic growth of the imbedded
delamination, may be lower in magnitude than what would be realized if the
platen constraints were removed.

In summary, induced defects (porosity and delamination) caused signifi-
cant reductions in the static compressive strength and failure strain
values of program test laminates under the environmental conditions (RTD,
RTW and 218FW) considered. The combination of moisture and porosity induced
very significant reductions in the proportional limit stress and strain
values. Poisson's ratio and modulus of elasticity were relatively unaffected
by defects and environment, except in the case of $[90]_{24T}$ specimens under
RTD conditions. It must be borne in mind that the large strength reductions
in Table 12 are associated with porosity levels very much in excess of
of what is normally observed to exist in production aircraft components
(Ref. 2).

3.2 AN INITIAL PREDICTION OF THE EFFECT OF POROSITY ON
     THE STATIC COMPRESSIVE STRENGTH

The degradation in the static compressive strength of program laminates
with induced porosity level (Table 12) is plotted in Figure 7. Data corres-
ponding to RTD and RTW conditions seem to follow bilinear variations as
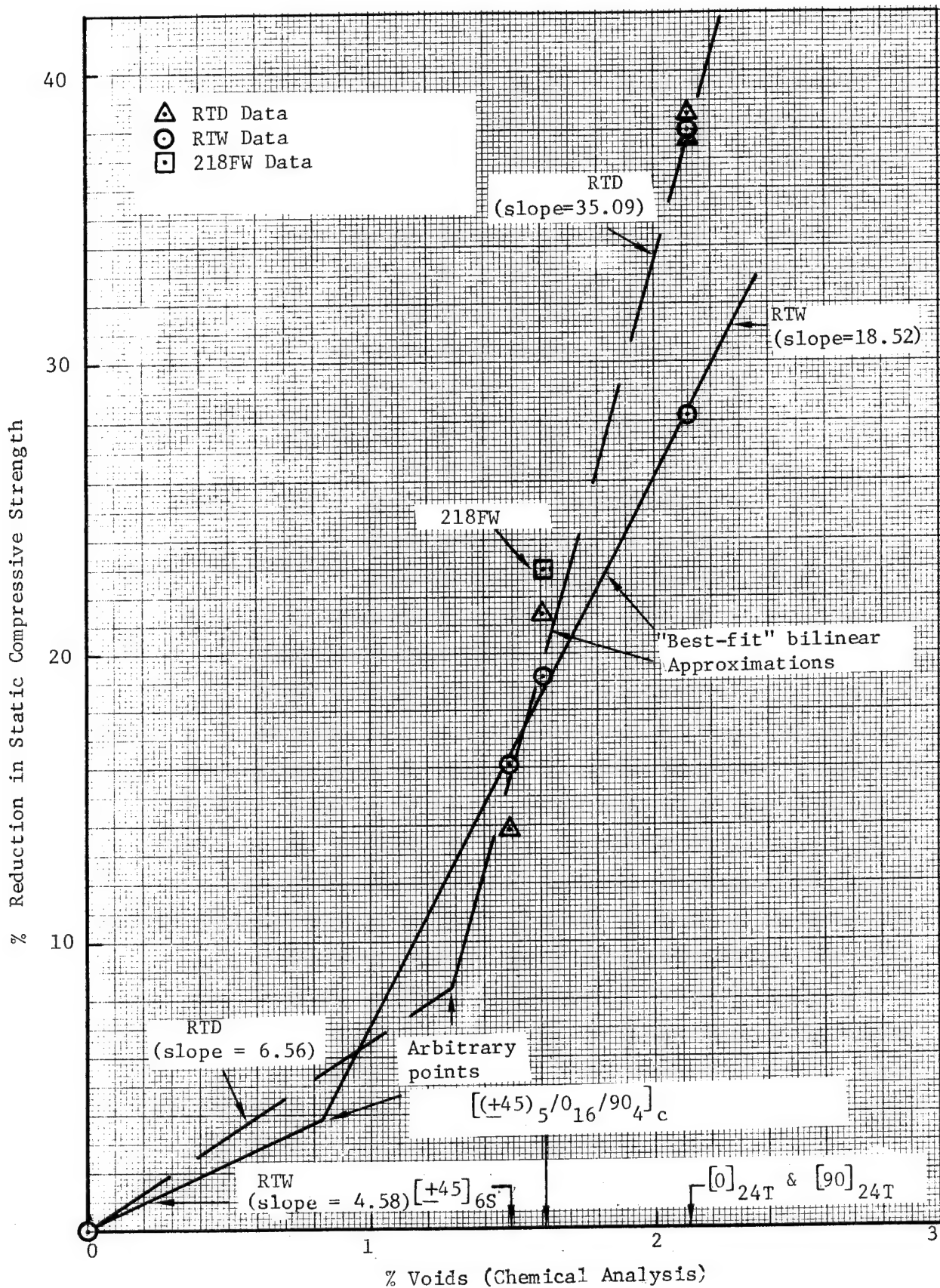
Figure 7.   Effect of Porosity Content on the Static Compressive
Strength of AS/3501-6 Laminates

shown in the figure, probably conservative in the lower void content range. Based on this assumption, the following empirical relationships are proposed for AS/3501-6 graphite/epoxy laminates:

Under RTD Conditions,

$$\% \Delta\sigma^{ult} = 6.56 \times \% \text{ Voids} \qquad \text{for} \quad 0 < \% \text{ Voids} < 1.28$$

$$= 8.4 + 35.09 \times \% \text{ Voids} \qquad \text{for} \quad \% \text{ Voids} > 1.28$$

Under RTW Conditions,

$$\% \Delta\sigma^{ult} = 4.58 \times \% \text{ Voids} \qquad \text{for} \quad 0 < \% \text{ Voids} < 0.83$$

$$= 3.8 + 18.52 \times \% \text{ Voids} \qquad \text{for} \quad \% \text{ Voids} > 0.83$$

In the above equations, $\% \Delta\sigma^{ult}$ is the percentage reduction in the static compressive strength and, % Voids is the void content percentage measured via chemical analysis.

The above empirical equations are independent of the laminate configuration, and assume bilinearity inflection points that are arbitrary choices. Additional data in the porosity range $0 < \%$ Voids < 1.4 must be generated to establish the void volume percentage at which an increase in the strength degradation rate occurs. It is believed that for void contents approximately below 1%, strength degradation rates are reduced drastically, and for void contents approximately below 0.1%, there will be negligible strength reductions.

3.3 COMPRESSION FATIGUE TEST RESULTS

Constant amplitude, compression fatigue ($R=10$, $\omega=10$ Hertz) test results were generated in the form of curves relating minimum cyclic strain values to the numbers of cycles to failure. These results are presented in Figures 8 to 14, and are slight modifications of S-N curves. The normalization of the minimum cyclic strain value with respect to the static failure strain value, to yield an S value, is not adopted in the presented figures. Alongside each modified S-N curve for a defective laminate, the threshold strain level for an identical defect-free laminate (from Ref. 1) is also marked. Threshold strain level is defined here as the absolute maximum cyclic strain amplitude at which the specimen will suffer no failure for 1.25×10^6 cycles. It is the asymptotic strain value corresponding to 1.25×10^6 cycles in the modified S-N curve.

35
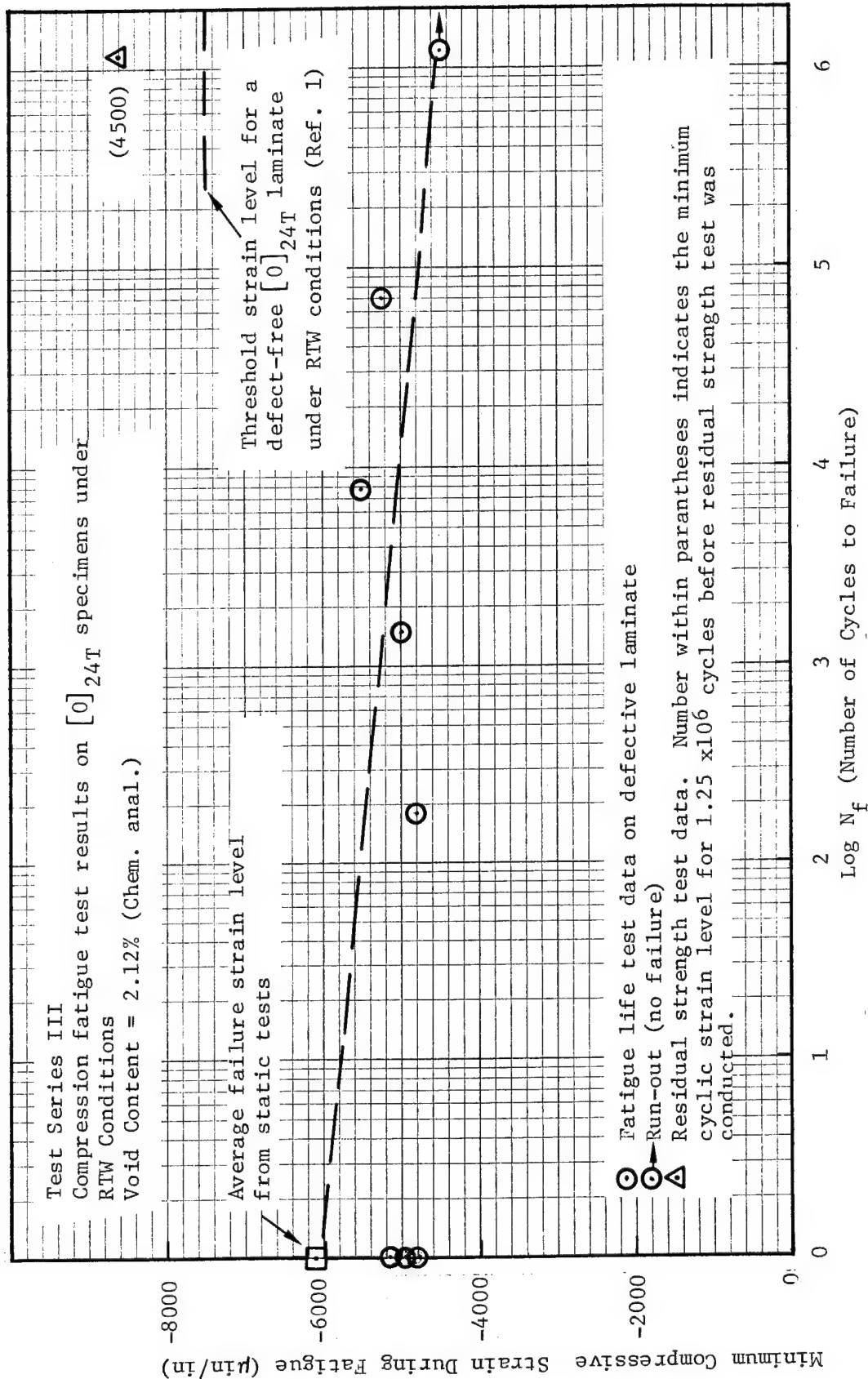
Figure 8. Compression Fatigue Test Results on $[0]_{24T}$ AS/3501-6 Specimens, With 2.12% Voids, Under RTW Conditions.

36
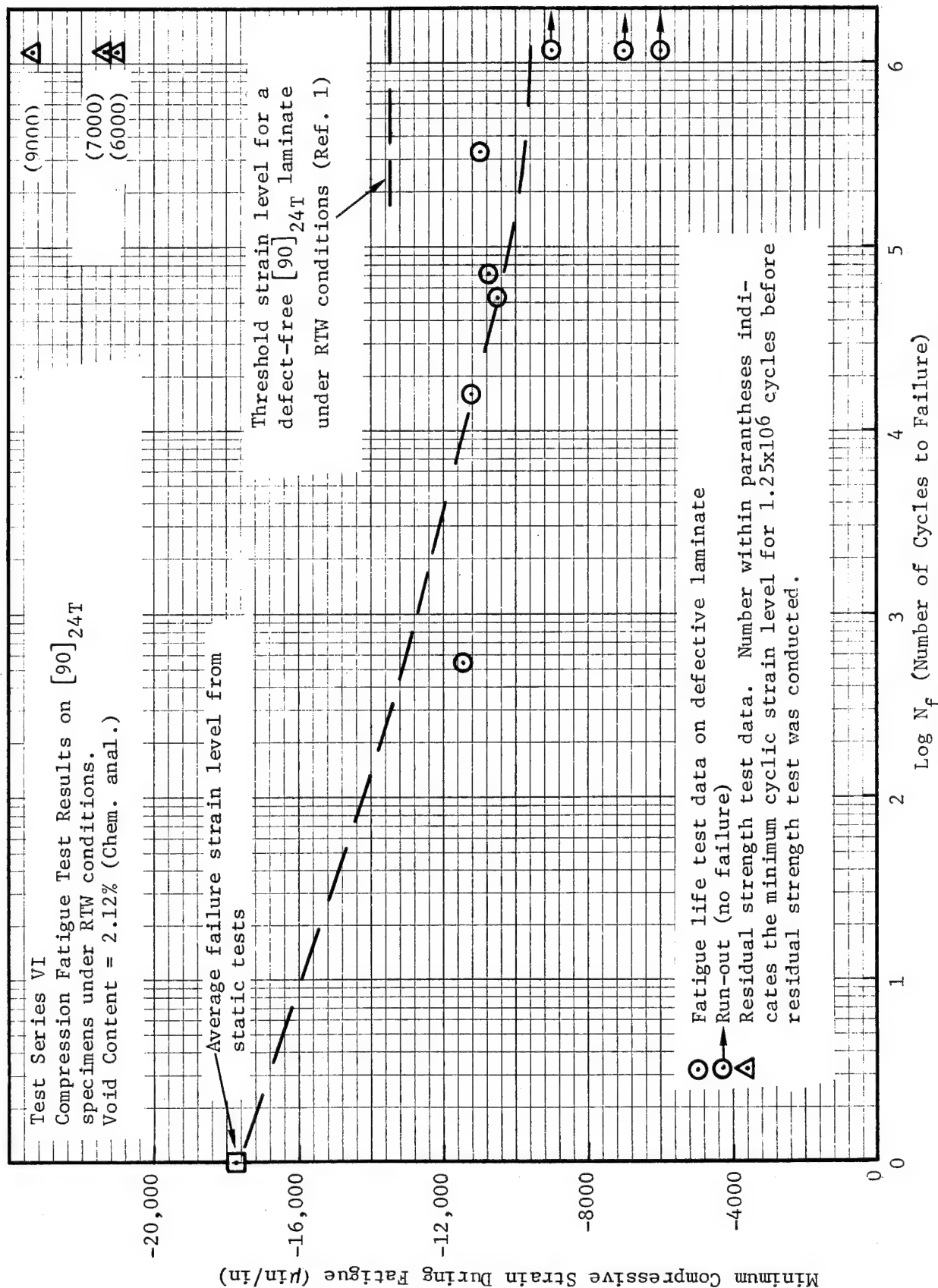
Figure 9. Compression Fatigue Test Results on $[90]_{24T}$ AS/3501-6 Specimens, With 2.12% Voids, Under RTW Conditions.

37
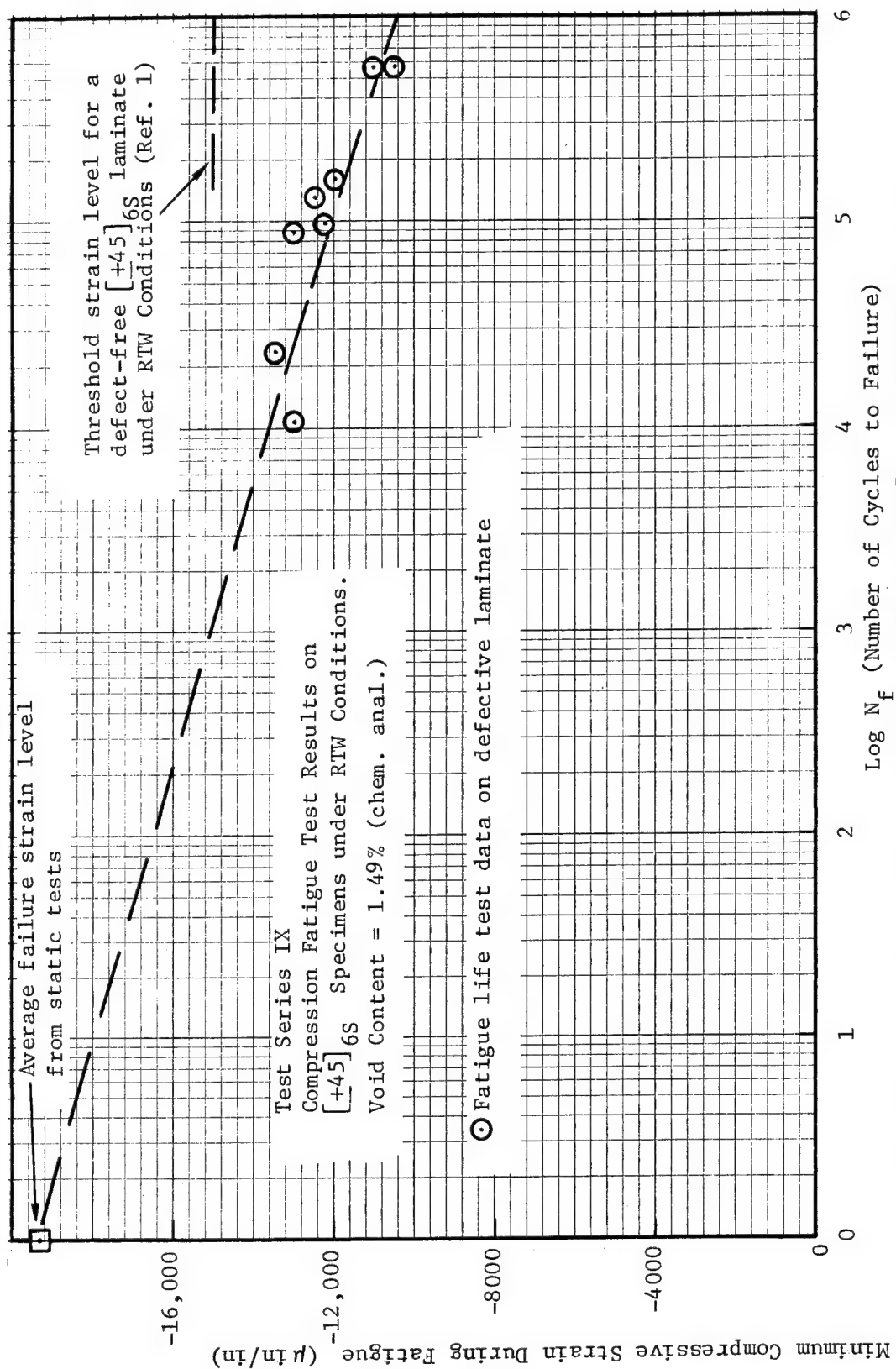
Figure 10. Compression Fatigue Test Results on $[\pm45]_{6S}$ AS/3501-6 Specimens, With 1.49% Voids, Under RTW Conditions.
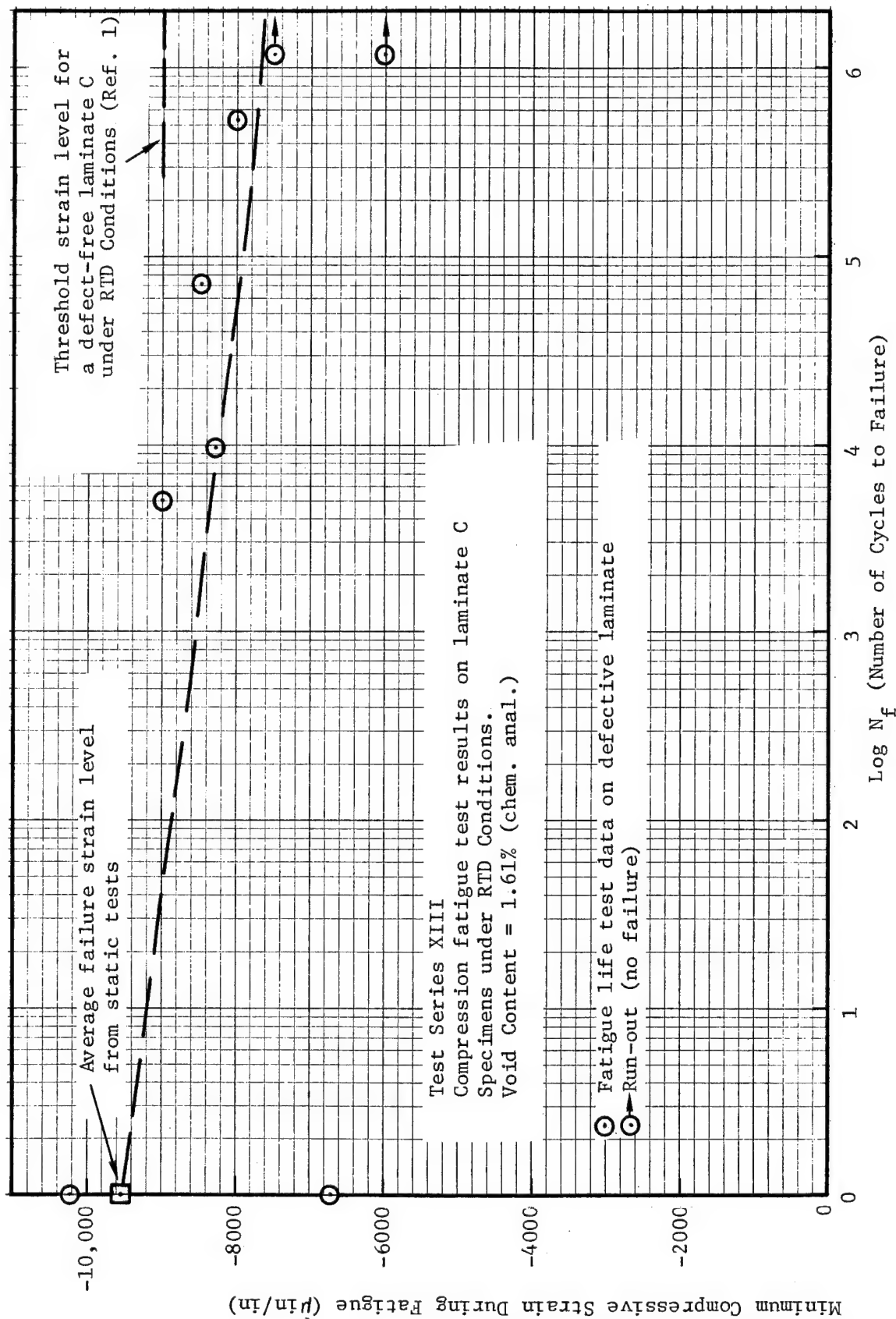
Figure 11. Compression Fatigue Test Results on $[(\pm 45)_5/0_{16}/90_4]_c$ AS/3501-6 Specimens, With 1.61% Voids, Under RTD Conditions.

39
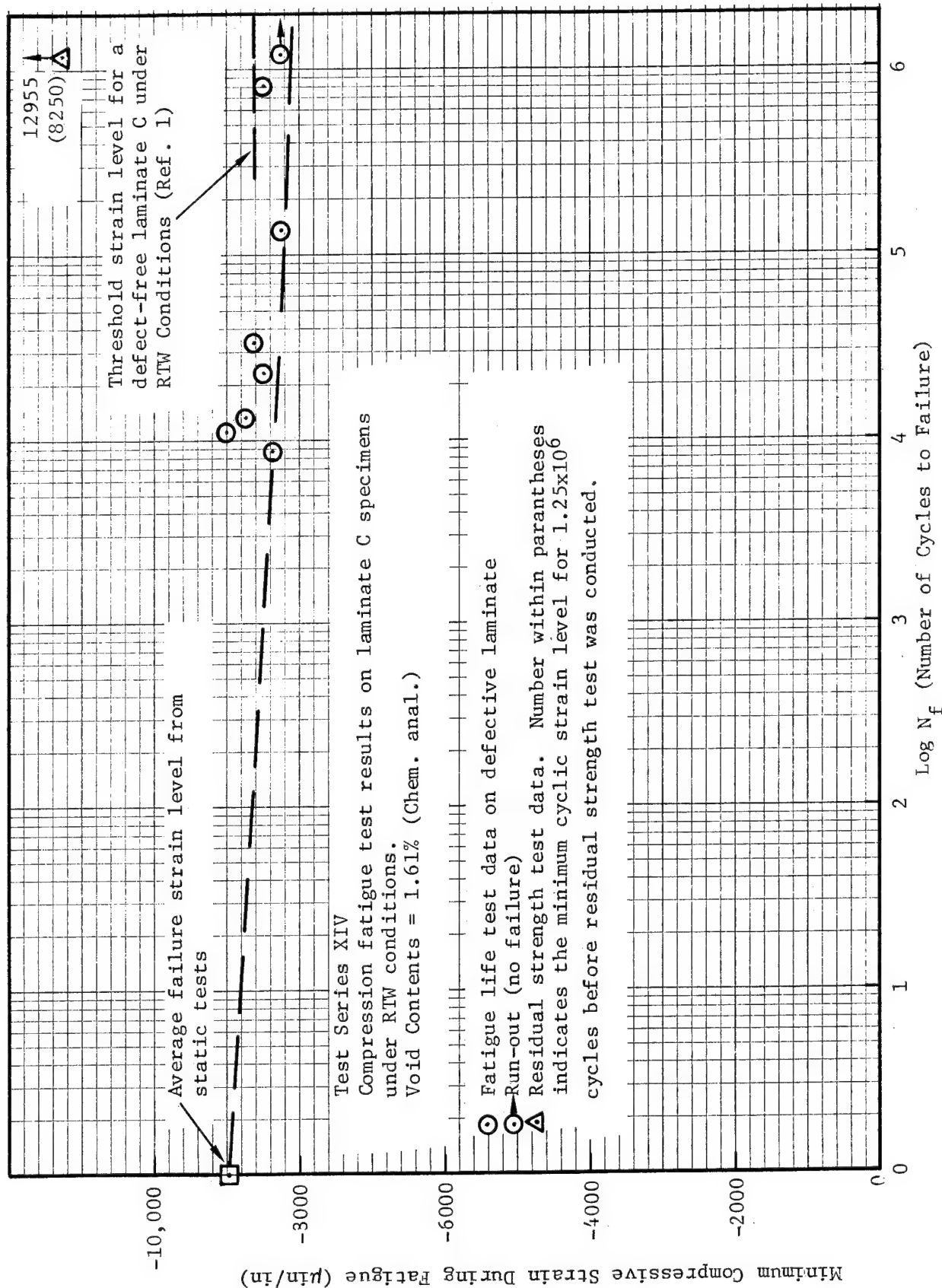
Figure 12. Compression Fatigue Test Results on $[(\underline{+}45)_5/0_{16}/90_4]_c$ AS/3501-6 Specimens, With 1.61% Voids, Under RTW Conditions.
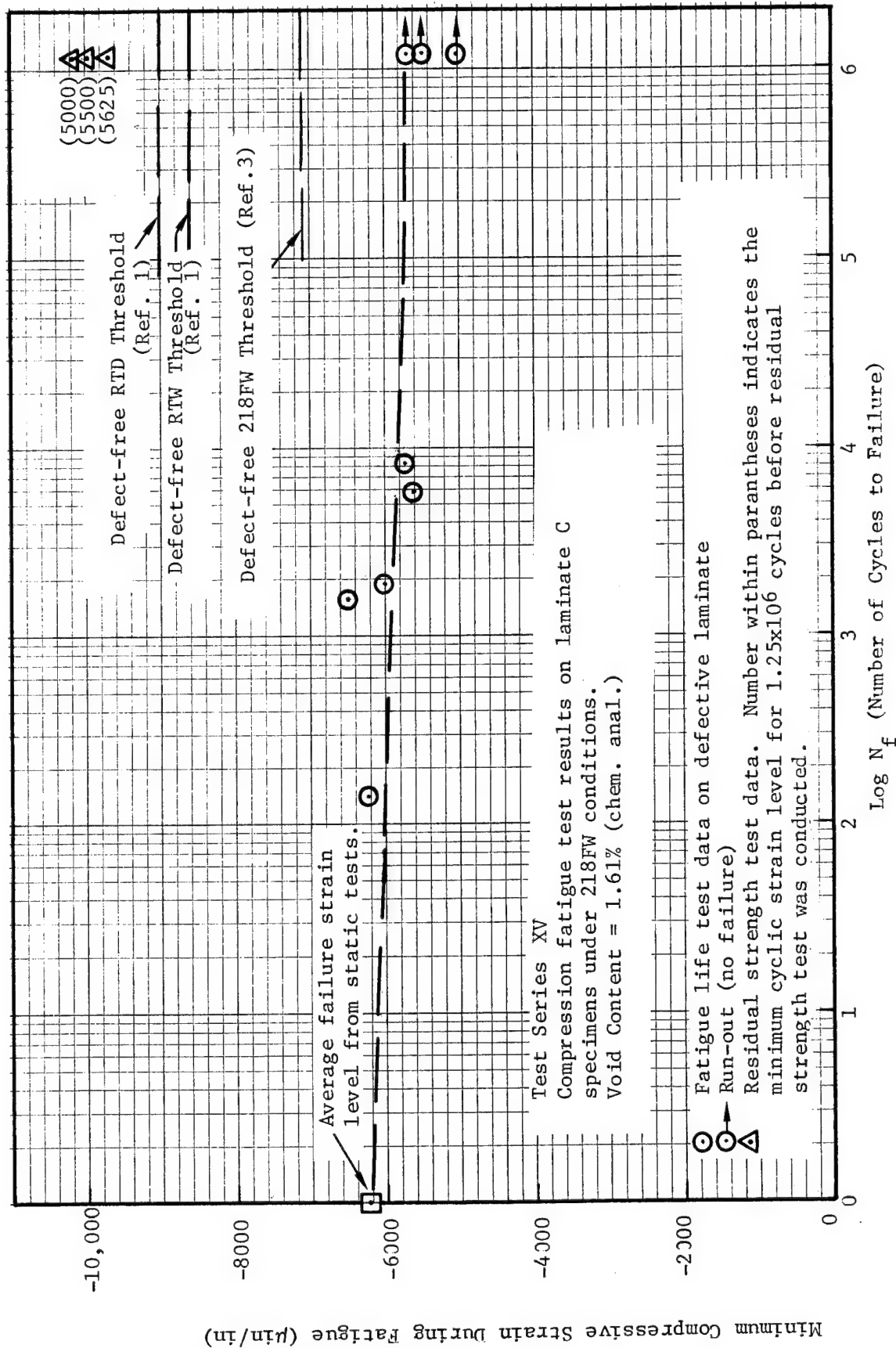
Figure 13. Compression Fatigue Test Results on $\left[(\pm 45)_5/0_{16}/90_4\right]_c$ AS/3501-6 Specimens, With 1.61% Voids, Under 218FW Conditions.
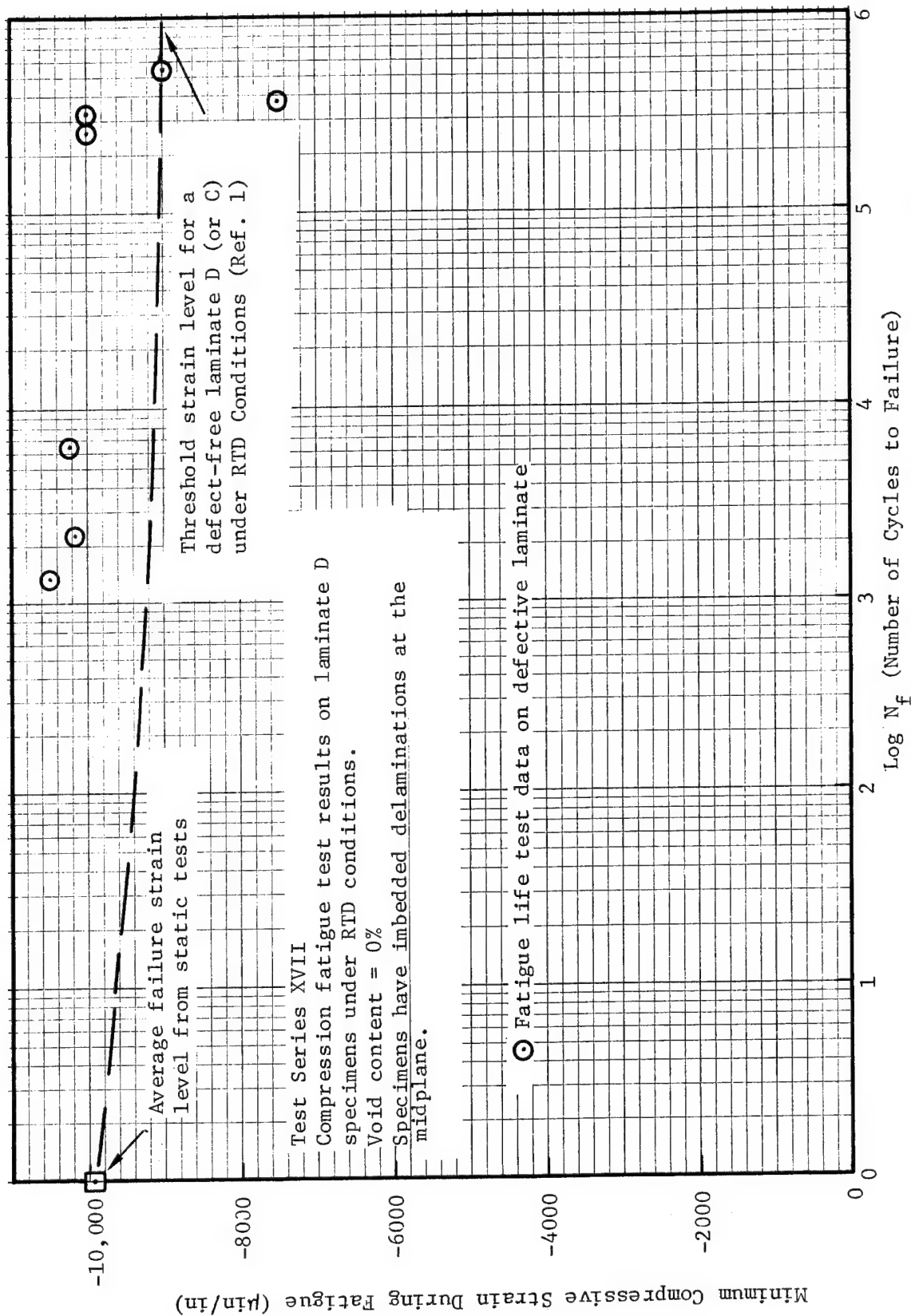
Figure 14. Compression Fatigue Test Results on $[(\pm 45)_5/0_{16}/90_4]_c$ AS/3501-6 Specimens, With Imbedded Delaminations And No Voids, Under RTD Conditions.

42

Compression fatigue test results on porous $[0]_{24T}$ specimens, under RTW conditions, are presented in Figure 8. A considerable amount of scatter is noticeable in the test data. Three specimens failed in a static mode while strain levels lower than the static failure value were being introduced to initiate the fatigue tests. One specimen, which ran-out at a strain amplitude of -4500 μin/in, exhibited a very high static failure strain value during residual strength testing. Variations in the porosity levels with the planform locations in laminate A, however small, are believed to be the predominant cause for this scatter. In comparison with the results for nonporous $[0]_{24T}$ laminates (from Ref. 1), a 40% reduction in the threshold strain level was induced by 2.12% of porosity (by chemical analysis).

Compression fatigue tests on porous $[90]_{24T}$ specimens, under RTW conditions, yielded the results presented in Figure 9. The scatter in the data is acceptable. Again, specimens that ran-out exhibited failure strains, during residual strength testing, that were in excess of the static failure value. Compared to the results in Reference 1, for defect-free $[90]_{24T}$ specimens, a 28.9% reduction in the threshold strain level was induced by 2.12% voids (by chemical analysis).

RTW compression fatigue test results on porous $[\pm45]_{6S}$ specimens are presented in Figure 10. Minimal scatter is observed in the test data. Compared to the defect-free specimen test results (Ref. 1), a 33.3% reduction in the threshold strain level was induced by 1.49% voids (by chemical analysis).

Compression fatigue test results on porous laminate C specimens, under RTD, RTW and 218FW conditions, are presented in Figures 11, 12 and 13, respectively. One RTD specimen failed during load introduction, at the initiation of the fatigue test (Fig. 11). An RTW specimen that ran-out at a strain amplitude of -8250 μin/in, yielded a failure strain value, during residual strength testing, that was considerably larger than the mean static failure strain level. Three 218FW specimens ran-out at strain amplitudes of -5000, -5500 and -5625 μin/in, and also exhibited failure strains, during residual strength testing, that were much larger than the static failure strain

43

value. Compression fatigue test data on defect-free laminate C specimens, under RTD and RTW conditions are presented in Reference 1. A comparison of Figures 11 and 12 with the data in Reference 1 indicates reductions in the threshold strain values of 15.6% under RTD conditions and 5.8% under RTW conditions, due to a porosity level of 1.61% (by chemical analysis). Reference data on defect-free laminate C specimens subjected to compression fatigue loading under 218FW conditions are presented in Reference 3. Comparing these results with Figure 13, a 19.7% reduction in the threshold strain level is measured under 218FW conditions.

RTD compression fatigue test results on nonporous laminate D specimens, with imbedded 0.5 in. long delaminations at midplane, are presented in Figure 14. Considerable scatter in the test data is noticeable. Many specimens survived a cyclic strain amplitude in excess of the static failure value, for thousands of fatigue cycles, without failure. A comparison with compression fatigue test data on defect-free laminate D (which is the same as defect-free laminate C) specimens, from Reference 1, indicates a negligible change in the threshold strain level.

A summary of the effects of induced porosity and delamination defects on the compression fatigue behavior of AS/3501-6 test laminates, under various environmental conditions, is presented in Table 13. The effects are quantified as percentage reductions in threshold strain levels due to the induced defects. The defect content, test environment, threshold strain levels for defect-free and defective comparison laminates, and the percentage reduction in the threshold strain for each test case are listed in Table 13. Very significant effects were realized in $[0]_{24T}$, $[90]_{24T}$ and $[\pm 45]_{6S}$ specimens under RTW conditions, due to induced porosity. A moderate effect was recorded during RTD tests on porous $[(\pm 45)_5/0_{16}/90_4]_c$ specimens, a small effect during RTW tests, and a considerable effect under 218FW conditions. The threshold strain level values were 7600, 8100 and 5700 μin/in for porous laminate C specimens under RTD, RTW and 218FW conditions, respectively, while the corresponding values for defect-free laminate C specimens under RTD, RTW and 218FW conditions were 9000, 8600 and 7100, μin/in, respectively. The threshold strain was lowered by the presence of porosity, to a large extent, under 218FW conditions. And, the largest reduction in the

TABLE 13. EFFECTS OF MATERIALS AND PROCESSES DEFECTS ON THE
COMPRESSION FATIGUE BEHAVIOR OF PROGRAM LAMINATES

Laminate	% Void Content by Chemical Analysis	Load Direction	Test Condition+	Threshold Strain Level* of		% Reduction in Threshold strain level under comp-comp. fatigue
				Defective Laminate (μin/in)	Defect-Free Laminate (Refs. 1, 3) (μin/in)	
A	2.12	0°	RTW	4,500	7,500	40.0
A	2.12	90°	RTW	9,600	13,500	28.9
B	1.49	0° or 90°	RTW	10,000	15,000	33.3
C	1.61	0°	RTD	7,600	9,000	15.6
C	1.61	0°	RTW	8,100	8,600	5.8
C	1.61	0°	218FW	5,700	7,100	19.7
D	0++	0°	RTD	9,000	9,000	0

*Threshold strain level is defined as the maximum compressive strain amplitude imposed during the constant amplitude fatigue test (R = 10) at which the specimen will complete 1.25×10^6 cycles without failure.

+ RTD, RTW, 218FW denote room temperature dry, room temperature wet, and 218F wet conditions, respectively.

++ This laminate has an imbedded delamination.

45

threshold strain value was also recorded under 218FW conditions (19.7%).
The imbedded delaminations in laminate D specimens had no measurable effect
on the threshold strain level. It is believed that this is possibly due
to the midplane location, and the size, of the imbedded delamination. A more
detailed study, like the one in Reference 5, will shed additional light on
the effect of imbedded delaminations on the compression fatigue behavior
of laminate C.

SECTION 4

PLY DROP-OFF ANALYSIS

4.1 SCOPE OF WORK

As in the work of the previous two years [1,3], emphasis during the present third-year program has been on the analysis of static test data. As stated in Reference [3], a three-dimensional approach is needed for the analysis of ply drop-offs because of complex stress states around the drop-off itself, and interlaminar shear and edge effects on the whole laminate. The University of Wyoming's three-dimensional finite element analysis program was completed shortly before the second-year report was published. This analysis tool was utilized in the present report.

The plain, 0° drop-off, and 45° drop-off laminates tested by Northrop in the previous year [3] were analysed under room-temperature dry (RTD), elevated-temperature wet (ETW), and elevated-temperature dry (ETD) environmental conditions. Various resin pocket sizes for the ply drop-off cases were considered as well. Although the present analysis program has a nonlinear (plastic) analysis capability, such an analysis was not performed. Also, the assumed yield criterion given in Section 4.3 of this report has not been experimentally verified or disproved to date. Thus, the accuracy of analysis results based on this criterion is not well defined.

Although the 3-D analysis program is a powerful tool, it is as yet not capable of performing crack propagation analysis. Consequently, the results given indicate only where first failure occurs, and not how failure progresses. A three-dimensional crack propagation capability will be added in the future to the existing program.

4.2 PHOTOGRAPHS OF PLY DROP-OFFS

The details of the ply drop-offs are presented in the second-year report [3], but are repeated here in Figures 15 and 16 for clarity. Regions between dashed lines define where the photographs presented in subsequent figures were taken.

After much experimentation with a variety of techniques, it was determined that conventional low magnification photography through a Zeiss Universal microscope, using Poloraoid Type 55 film, is the most suitable. A large number of photographs of failed specimens were taken, seven of which are

47

Region photographed

1	−45		−45	1
2	+45		+45	2
3	0		0	3
4	90		90	4
5	0		0	5
6	0		0	6
7	0		0	7
8	90		90	8
9	0	End of Ply		
10	0		0	9
11	0		0	10
12	−45		−45	11
13	+45		+45	12
14	0		0	13
15	+45		+45	14
16	−45		−45	15
17	0		0	16
18	+45		+45	17
19	−45		−45	18
20	0		0	19
21	0		0	20
22	0	End of Ply		
23	90		90	21
24	0		0	22
25	0		0	23
26	0		0	24
27	90		90	25
28	0		0	26
29	+45		+45	27
30	−45		−45	28

Upper Region

Lower Region
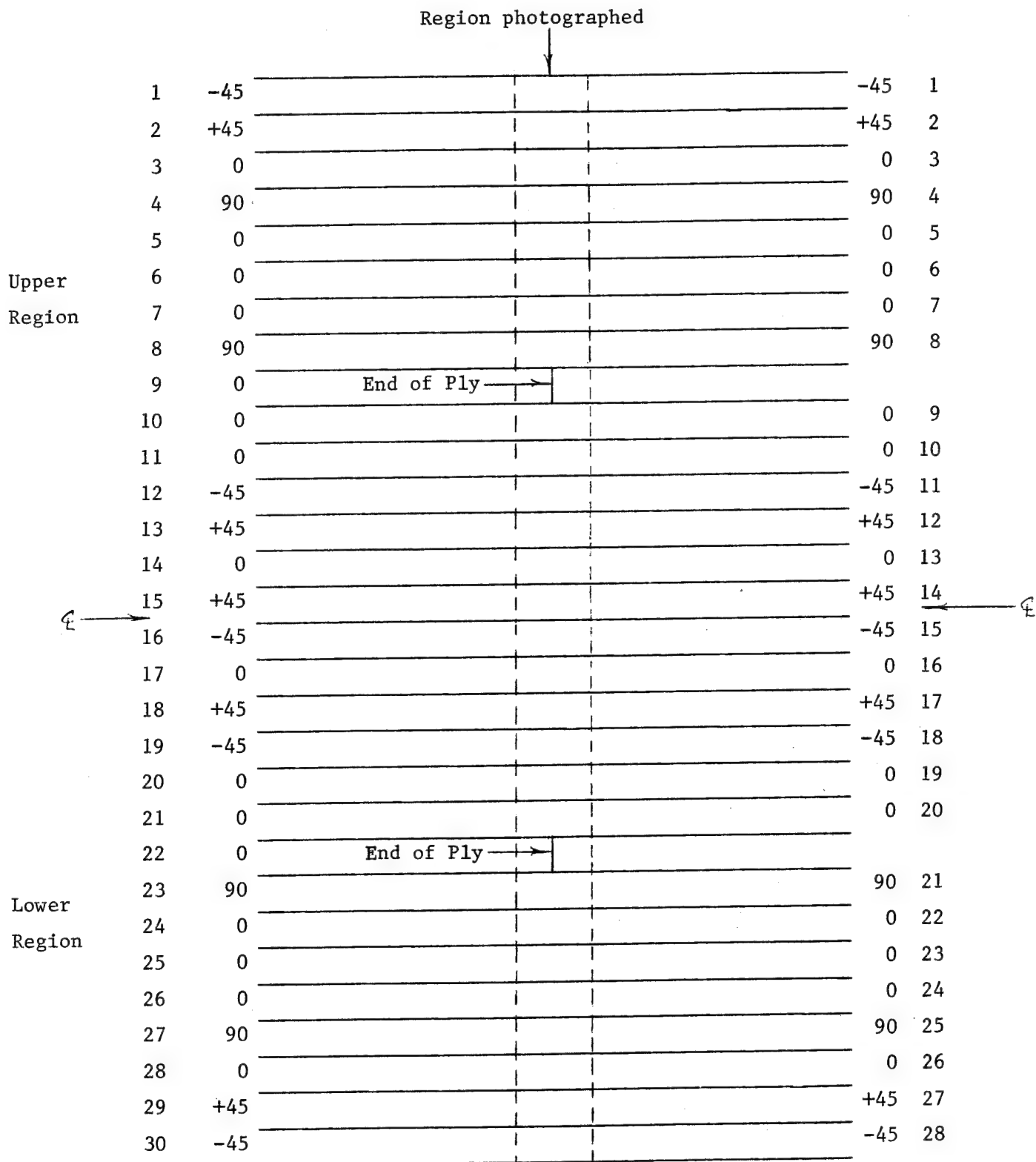
Figure 15.   Details of 0° Ply Drop-off.
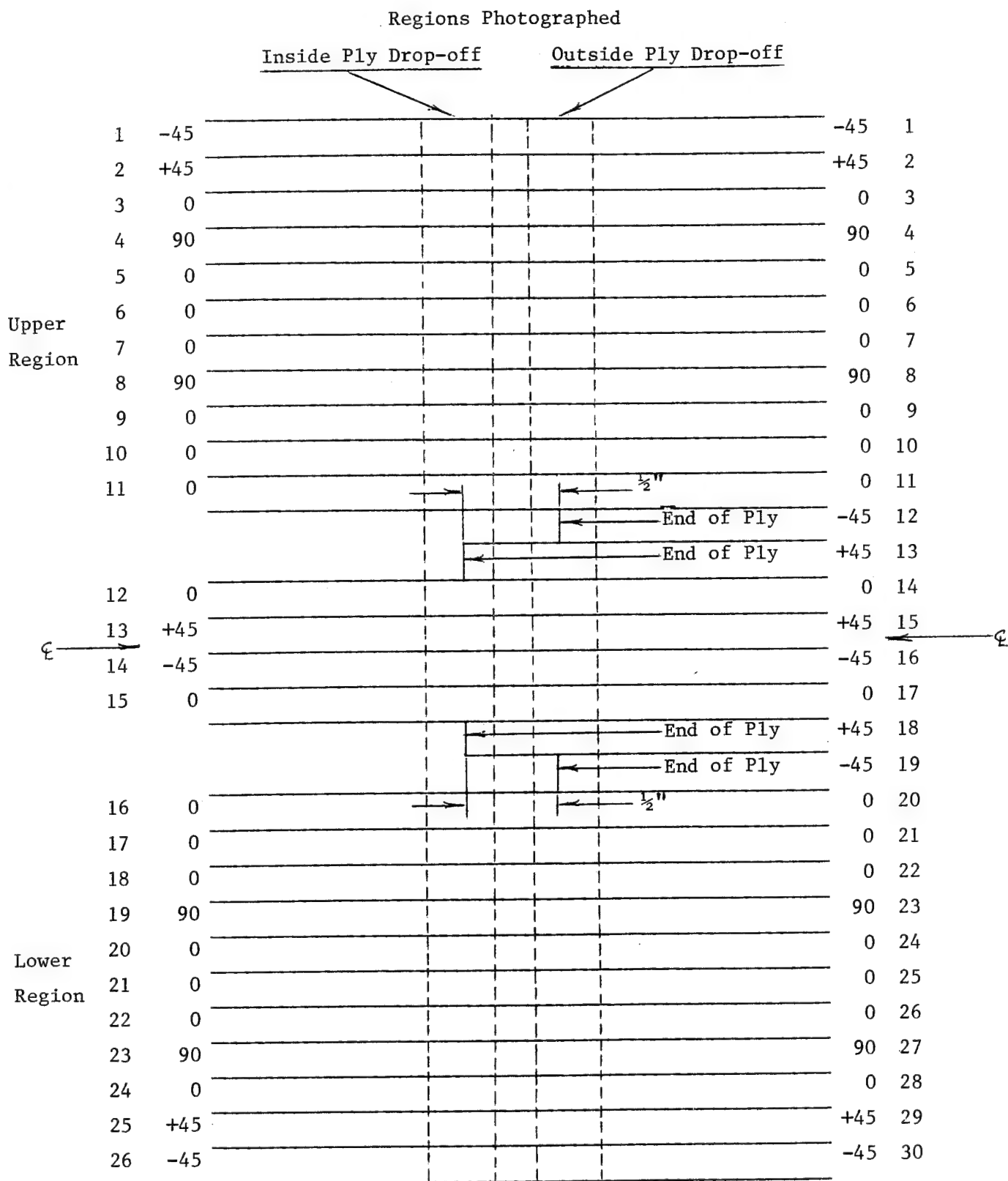
Figure 16. Details of 45° Ply Drop-off.

shown in Figures 17 through 23. In all photographs the orientation of the fibers in the various plies is clearly seen. Figures 17, 18 and 19 indicate 0° ply drop-offs. The abrupt end of the fibers is apparent, as is the distortion of the adjacent 90° plies to fill the gaps created. The spaces at the immediate end of the terminated plies are resin pockets, not voids. As can be seen, these resin pockets are not large. Figure 19 shows the smallest resin pocket. For comparison purposes in the subsequent analysis, however, the terms "small resin pocket" and "large resin pocket" will be used to distinguish relative resin pocket sizes for a given drop-off case, and not to indicate absolute resin pocket sizes.

Figures 20 and 21 are photographs of the inside ply drop-offs for the 45° drop-off case. These are typical photographs, the matrix pockets extending further out than those for the 0° drop-off case. This is due to the fact that the 45° inside plies cannot deform as easily to fill the gaps as can the 90° plies in the 0° drop-off case.

Figures 22 and 23 are photographs of the outside ply drop-offs for the 45° drop-off case. These show the resin pockets as extending quite far away from the drop-offs. In this case, 0° plies border the dropped ply, and since these plies are most resistant to transverse deformation, long, tapered resin pockets result.

The resin pocket geometries observed in these photographs were the basis for the sizes of those modeled in the three-dimensional finite element analysis.

4.3 THREE-DIMENSIONAL FINITE ELEMENT ANALYSIS CAPABILITIES

Descriptions of the capabilities of the University of Wyoming's 3-D finite element program were given in the second-year report [3], but are repeated in part here for clarity. The unique features of the program include a full three-dimensional analysis for orthotropic materials, nonlinear elastoplastic analysis, temperature- and moisture-dependent material properties, and completely general mechanical loadings combined with arbitrary thermal and moisture exposure histories. Eight-node isoparametric elements are used, and a frontal solution technique, rather then a band algorithm, is used to solve the stiffness equations. A reduced integration technique is utilized to minimize numerical errors resulting when elements are much longer than they are thick, which occurs in laminate analysis because ply thicknesses are much smaller than laminate widths and

Figure 17. Specimen A-6-1, 0° Ply Drop-offs: Upper Region
Shown (Ply No. 9 Dropped Off).
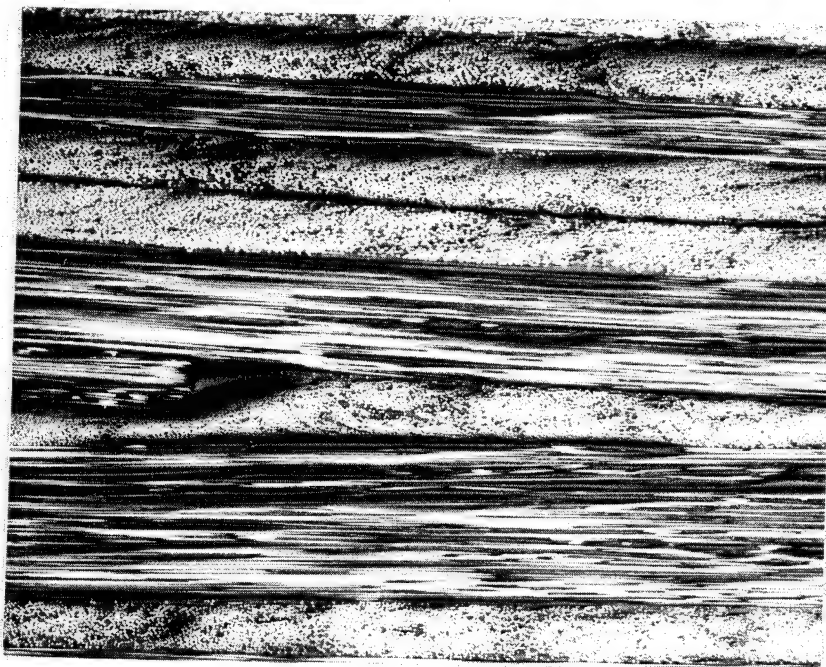
Figure 18. Specimen A-5-24, 0° Ply Drop-offs: Lower Region
Shown (Ply No. 22 Dropped Off).
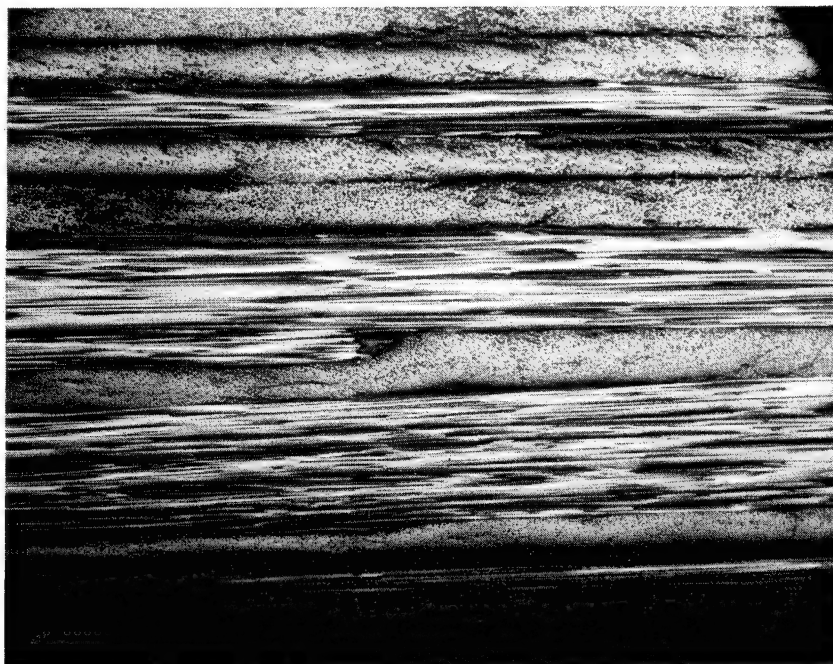
Figure 19.   Specimen B-10-36, 0° Ply Drop-off: Lower Region
Shown (Ply No. 22 Dropped Off).

Figure 20. Specimen A-8-17, ± 45° Ply Drop-offs: Inside +45°
Plies (Ply Nos. 13 and 18) Dropped Off.
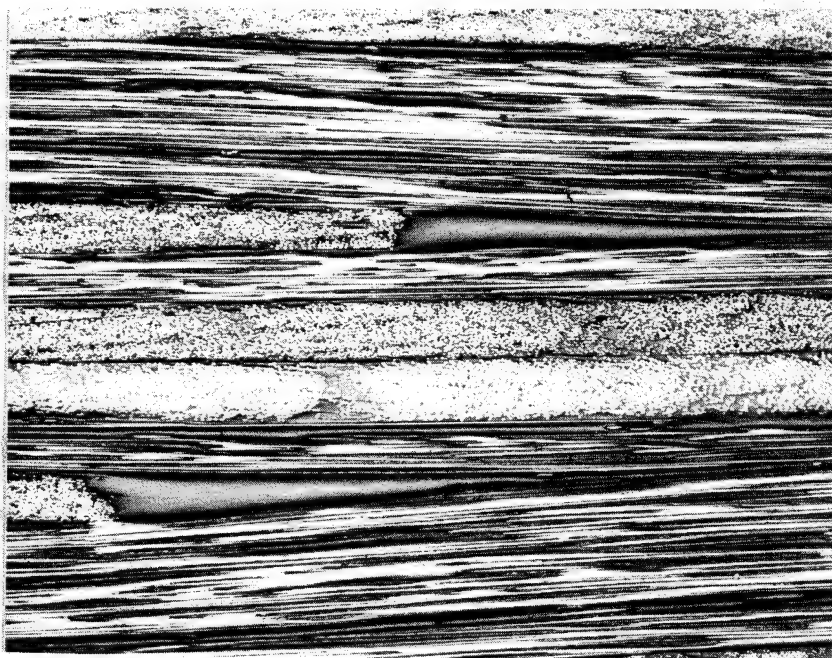
Figure 21. Specimen B-12-26, ± 45° Ply Drop-offs: Inside +45°
Plies (Ply Nos. 13 and 18) Dropped Off.

Figure 22.   Specimen A-8-17, $\pm$45° Ply Drop-offs: Outside
              -45° Plies (Ply Nos. 12 and 19) Dropped Off.
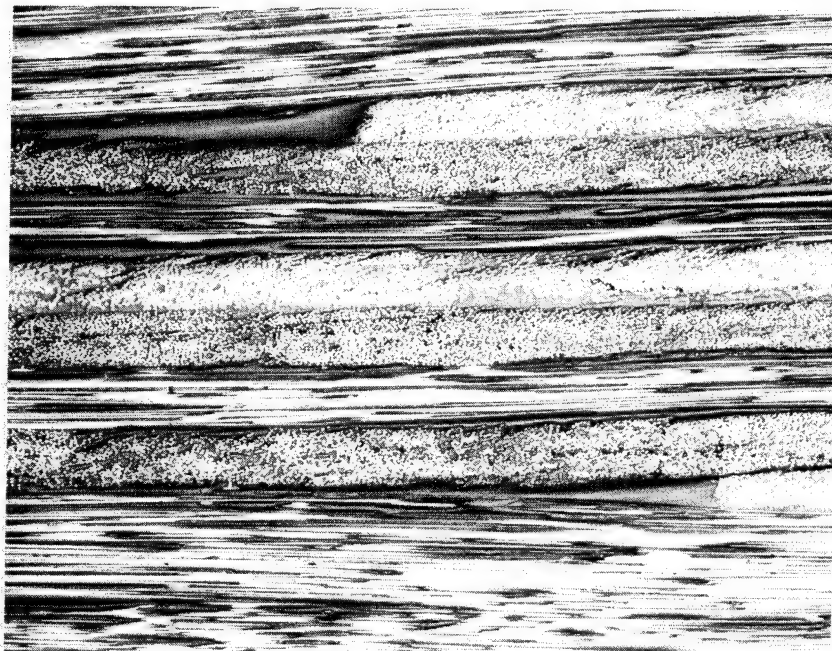
Figure 23.   Specimen B-12-26, $\pm$45° Ply Drop-offs, Outside
              -45° Plies (Ply Nos. 12 and 19) Dropped Off.

lengths. A complete discussion of the above capabilities is given in Reference [6]; a brief summary will be given here.

4.3.1 Hygrothermal Loading with Temperature- and Moisture-Dependent Material Properties

A second-order polynomial in temperature and relative humidity is assumed for each material property. Therefore, a given material property P is given in terms of temperature T and relative humidity M as

$$P(T,M) = C_1 T^2 + C_2 M^2 + C_3 TM + C_4 T + C_5 M + C_6 \qquad (4.1)$$

where the constants C_1 through C_6 are determined from a least-squares algorithm based on experimental data. The program permits mechanical and hygrothermal loading by increments. Therefore, for each hygrothermal load increment, Eq. (4.1) permits the material properties to change with each increment. If the load increments were infinitesimal, the material properties would vary continuously with temperature and moisture changes, which happens in actuality. Obviously, the computer program can handle only finite load increments, rather than infinitesimal ones. Thus, depending on the size of the finite element grid, the limits of available computer time and resource allocation define the number of finite load increments allowed. Clearly however, greater accuracy is obtained when several load increments are used to bring a material from one environmental state to another, and the material properties are allowed to change with each increment, thanwhen a single load increment is used to bring about the change, and the material properties are not allowed to vary. The present program is one of the few available to date that permits such material property variations with temperature and moisture.

A total of 29 material properties are required as input to the program, and are input as the six constants C_i in Eq. (4.1). Table 14 lists the material properties required, where subscript 1 denotes properties in the direction of the fibers, subscript 2 denotes properties transverse to the fibers and in the plane of the ply, and subscript 3 denotes properties transverse to the fibers and normal to the ply. Typically, material properties in the 2 and 3 directions are assumed to be equal, and are entered as such, but this need not be the case; the present program permits modeling of a fully orthotropic material.

TABLE 14. MATERIAL PROPERTIES REQUIRED AS INPUT
TO THE FINITE ELEMENT PROGRAM

Elastic Moduli	Shear Moduli	Poisson's Ratios	Thermal Expansion Coefficients	Moisture Expansion Coefficients
E_{11}	G_{23}	ν_{23}	α_{11}	β_{11}
E_{22}	G_{13}	ν_{13}	α_{22}	β_{22}
E_{33}	G_{12}	ν_{12}	α_{33}	β_{33}

Normal Yield Strengths	Shear Yield Strengths	Normal Ultimate Strengths	Shear Ultimate Strengths	Plastic Flow Parameters
σ_1^y	τ_{23}^y	σ_1^u	τ_{23}^u	σ_o
σ_2^y	τ_{13}^y	σ_2^u	τ_{13}^u	n
σ_3^y	τ_{12}^y	σ_3^u	τ_{12}^u	

56

The program permits the use of up to five different materials in a given analysis; 29 material properties must be defined for each material.

The first 27 material properties of Table 14 are self-explanatory. The remaining two, σ_o and n, are plasticity parameters, as discussed in the next section.

4.3.2 Yield, Plastic Flow, and Failure Criteria

As mentioned in the second-year report [3], the basic limitation of all yield criteria is the lack of experimental evidence to verify them, especially when complex stress states are involved. For lack of a better definition of material response, the following yield criterion due to Hill [7] is assumed:

$$F(\sigma_2-\sigma_3)^2 + G(\sigma_1-\sigma_3)^2 + H(\sigma_1-\sigma_2)^2 + 2L\tau_{23}^2 + 2M\tau_{13}^2 + 2N\tau_{12}^2 = 1 \quad (4.2)$$

where F through N are constants. This criterion 1) does not recognize a Bauschinger effect because there are no linear normal stress terms, 2) does not recognize hydrostatic stress because only differences of normal stresses occur, and 3) reduces to the von Mises distortional energy criterion when applied to an isotropic material.

The stresses in the above equation must be those in the principal directions of orthotropy of the material. If they are not, as in the case where a ply is rotated off-axis from the global coordinate system, such as a 45° ply in the present study, they must be transformed to the principal directions of orthotropy before Eq.(4.2) can be invoked.

The constants in this equation can be determined from the independent application of individual uniaxial normal and shear stresses on the material, and noting that the yield condition is met when yielding occurs for the particular stress acting by itself. After some algebra, the following equations result:

$$F = \frac{1}{2}\left[\frac{1}{(\sigma_2^y)^2} + \frac{1}{(\sigma_3^y)^2} - \frac{1}{(\sigma_1^y)^2}\right]$$

$$G = \frac{1}{2}\left[\frac{1}{(\sigma_1^y)^2} + \frac{1}{(\sigma_3^y)^2} - \frac{1}{(\sigma_2^y)^2}\right] \quad (4.3)$$

$$H = \frac{1}{2}\left[\frac{1}{(\sigma_1^y)^2} + \frac{1}{(\sigma_2^y)^2} - \frac{1}{(\sigma_3^y)^2}\right]$$

$$2L = \frac{1}{(\tau_{23}^y)^2}, \quad 2M = \frac{1}{(\tau_{13}^y)^2}, \quad 2N = \frac{1}{(\tau_{12}^y)^2}$$

Since the individual yield stresses are temperature- and moisture-dependent, so are the constants in the yield criterion.

A single stress, called the equivalent or effective stress, is defined to account for all six stress components (acting in the principal directions of orthotropy) and is given by

$$\sigma_{eff} = \left\{\frac{3}{2}\left(\frac{1}{F+G+H}\right)\right\}^{\frac{1}{2}}[F(\sigma_2-\sigma_3)^2 + G(\sigma_1-\sigma_3)^2 + H(\sigma_1-\sigma_2)^2 + 2L\tau_{23}^2 \qquad (4.4)$$

$$+ 2M\tau_{13}^2 + 2N\tau_{12}^2]^{\frac{1}{2}}$$

Thus, a material has yielded when

$$\sigma_{eff} \geq \left\{\frac{3}{2}\left(\frac{1}{F+G+H}\right)\right\}^{\frac{1}{2}} = \left(\frac{3}{\frac{1}{(\sigma_1^y)^2} + \frac{1}{(\sigma_2^y)^2} + \frac{1}{(\sigma_3^y)^2}}\right) \qquad (4.5)$$

This effective stress is analogous to octahedral stress for isotropic materials. A relationship between effective stress and effective strain is needed to define a complete stress-strain curve for a complex stress state. The Richard-Blacklock equation given in the second-year report [3], and in Reference [6], is well-suited as a fit to uniaxial stress-strain curves for composites, and is given by

$$\sigma = E\varepsilon/[1 + |E\varepsilon/\sigma_o|^n]^{1/n'} \qquad (4.6)$$

where σ_o, n and E are curve-fit parameters, E being the initial slope of the curve. Since an effective stress-effective strain curve has a shape similar to a uniaxial stress-strain curve, an equation similar to Eq. (4.6)

can be assumed for the effective stress-effective strain relation, where $\bar{E}$, $\bar{\sigma}_o$ and $\bar{n}$ are the parameters. The **relationships between** the effective parameters and the uniaxial parameters are as follows:

$$\bar{E} = E_{11}\left[\frac{3}{2}\left(\frac{F+G}{F+G+H}\right)\right]$$

$$\bar{\sigma}_o = \sigma_o\left[\frac{3}{2}\left(\frac{F+G}{F+G+H}\right)\right]^{\frac{1}{2}} \qquad (4.7)$$

$$\bar{n} = n$$

Thus, the only plasticity parameters needed to define the effective stress-effective strain relation in the nonlinear (plastic) range are σ_o and n, as best-fit to a uniaxial stress-strain curve for the composite. These are the remaining two temperature- and moisture-dependent material properties needed as input to the finite element program.

The details of how the plastic, instantaneous stiffness matrix is formed are given fully in Reference [6], and more briefly in the second-year report [3].

The assumption of isotropic hardening given in Reference [6] implies that the failure envelope of a composite will take the same form as Eq. (4.2), except that ultimate strengths replace yield strengths in determining the constants F through N. This failure criterion is used in the present program, for lack of a better one, yet it may not always be valid. Data taken from ultimate strength tests of [± 45] laminates do not validate the predicted strengths of such laminates when a Hill failure envelope is assumed. Nevertheless, this failure criterion was used in the present study, along with a maximum normal stress criterion, and the results compared for each case. Perhaps in future work, a more suitable failure criterion will be found.

4.4 FINITE ELEMENT ANALYSIS OF PLY DROP-OFFS

Preliminary results indicated that stress disturbances near the ply drop-offs die out at very short distances from the drop-offs. Therefore, to concentrate on the drop-off areas themselves, small regions, roughly of the same areas shown in the photographs of Section 4.2 of this report, were modeled. For the 45° drop-off area, only the inside ply drop-offs were modeled.

The laminate lay-ups tested by Northrop in the second-year study [3], and shown again here in Figures 15 and 16, would be symmetrical about the centerline if the 45° plies bordering the centerline were of the same sign. Since all other plies are symmetrical about the centerline, complete symmetry was assumed. The assumption of symmetry about the centerline implies that under symmetrical loading, such as occurs in the uniaxial compression loading studied here, the stress response at any point in the upper section is identical to that of the corresponding point in the lower section. Therefore, only one section need be modeled. The upper section was modeled, and the bottom +45° ply in that section was changed to a -45° ply, to invoke the symmetry condition needed. The results shown in subsequent sections of this report indicate that no element in this bottom ply was critical; therefore, the change in its orientation was assumed not to be critical either.

Figure 24 shows the gross finite element grid used to model the ply drop-offs. Three layers of elements in the specimen width direction were utilized, starting from the edge of the laminate, since this is where the most severe stress state occurs, due to free-edge stress effects. Since the laminate is much wider than it is thick, the assumption of plane strain in the plane of the laminate (i.e., the x-y plane) is valid except near the edge. Therefore, the inside face of Layer 1 was modeled as not warping in the y-direction. The face x=0 was constrained from warping in the x-direction because preliminary results showed that the effect of the ply drop-off did not influence stresses significantly this far back from the drop-off. Finally, the z=0 face was constrained from warping in the z-direction because of the condition of laminate symmetry above and below the x-y plane.

Dimension D_3 in Figure 24 is representative of half the thickness of the laminates shown in Figures 15 and 16. Dimension D_4 reflects the reduced thickness due to the drop-offs, yet does not account for reduction in thickness of a full ply because the photographs indicated that surrounding plies after the drop-off swelled somewhat, thus reducing the discrepancy of thicknesses due to the drop-offs. Dimension D_1 was found to be the smallest one for which ply drop-offs did not influence stresses significantly on the x=0 face. Dimension D_2 was chosen as convenient for the analysis.

In all cases, laminates were loaded by a uniform negative (compressive) displacement in the x-direction, as shown in Figure 24.

60
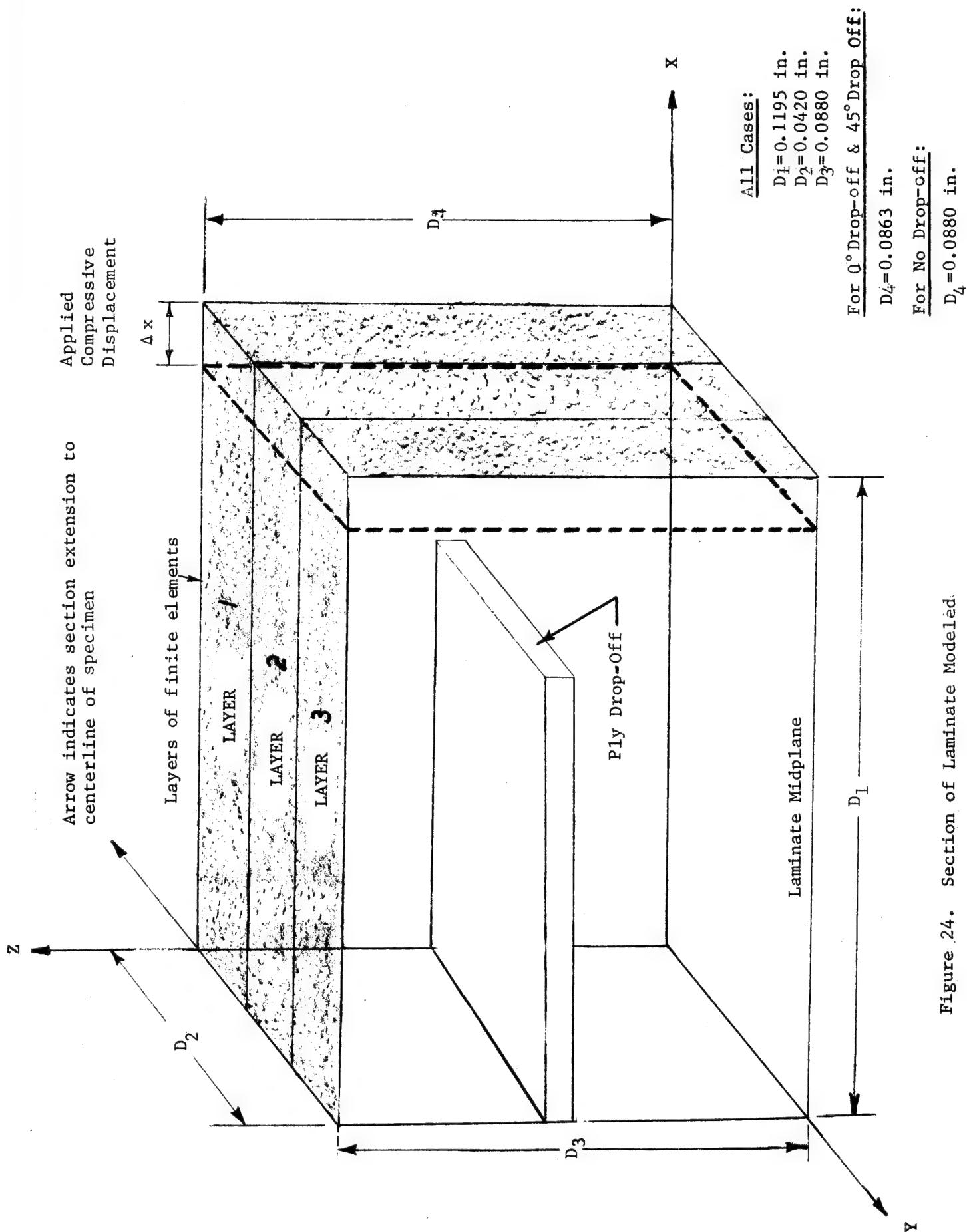
Figure 24. Section of Laminate Modeled

All Cases:
D_1=0.1195 in.
D_2=0.0420 in.
D_3=0.0880 in.

For 0° Drop-off & 45° Drop Off:
D_4=0.0863 in.

For No Drop-off:
D_4=0.0880 in.

Applied
Compressive
Displacement

Arrow indicates section extension to
centerline of specimen

Layers of finite elements

LAYER 1

LAYER 2

LAYER 3

Ply Drop-Off

Laminate Midplane

Δx

D_4

D_2

D_3

D_1

X

Y

Z

4.4.1 Finite Element Grids

All three layers of Figure 24 have the same element grids in the x-z plane, and are, of course, one element thick. Three different grids were chosen, one each for the plain laminate, 0° drop-off laminate, and 45° drop-off laminate. These grids are shown in Figures 25, 26 and 27, respectively. All of the grids are coarse around the edges, and more refined near the drop-off, for obvious reasons. The grid for the plain laminate was chosen to be nearly the same as for the 0° drop-off laminate, for comparison purposes.

Different resin pocket sizes were noted in the photographs, and modeled accordingly. The lightly shaded area of Figure 26 denotes a small resin pocket shown in the photographs for the 0° ply drop-off case (see, for example, Figure 19). The lightly and darkly shaded regions combined denote a large resin pocket. The lightly and darkly shaded regions of Figure 27 denote resin pocket sizes for the 45° drop-off case. As mentioned previously, the terms "small" and "large" resin pocket sizes denote a comparison of resin pocket sizes for a given drop-off case, not between cases, as the resin pocket for the 45° drop-offs were always larger than those for the 0° drop-offs.

Since the program utilizes linear isoparametric elements, the refining of the mesh near the drop-off requires that elements in the transition region be highly skewed, as shown in the figures. However, the reduced integration method utilized in the computer program prevents significant numerical errors from occurring as a result of highly skewed elements.

4.4.2 Material Properties

Material properties needed are for the AS/3501-6 graphite/epoxy composite, and for the 3501-6 epoxy matrix itself. As indicated in Section 4.3.1, 29 material properties are needed for each material, to make use of all features of the finite element program. These properties are not all easily obtained experimentally, and indeed some of them have been estimated, based on elasticity theory, since available experimental results differ, depending on what test method was used.

The values given in Tables 15 and 16 were taken from a variety of sources, including University of Wyoming and Northrop Corporation data. Where disparities arose, elasticity theory was invoked to provide certain values. All values shown are tensile rather than compressive properties, as
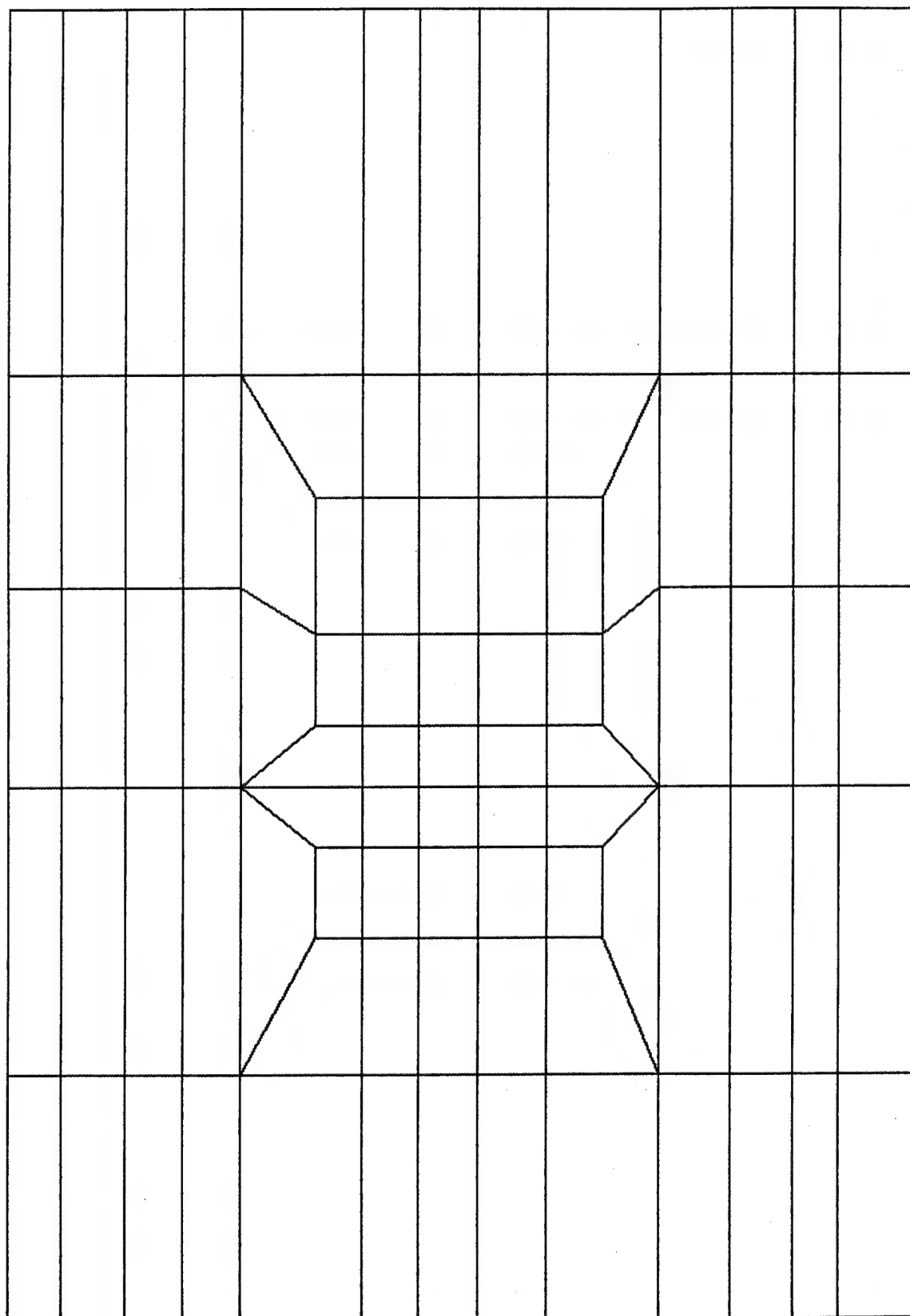
Figure 25. Finite Element Grid For The No Drop-off Case.
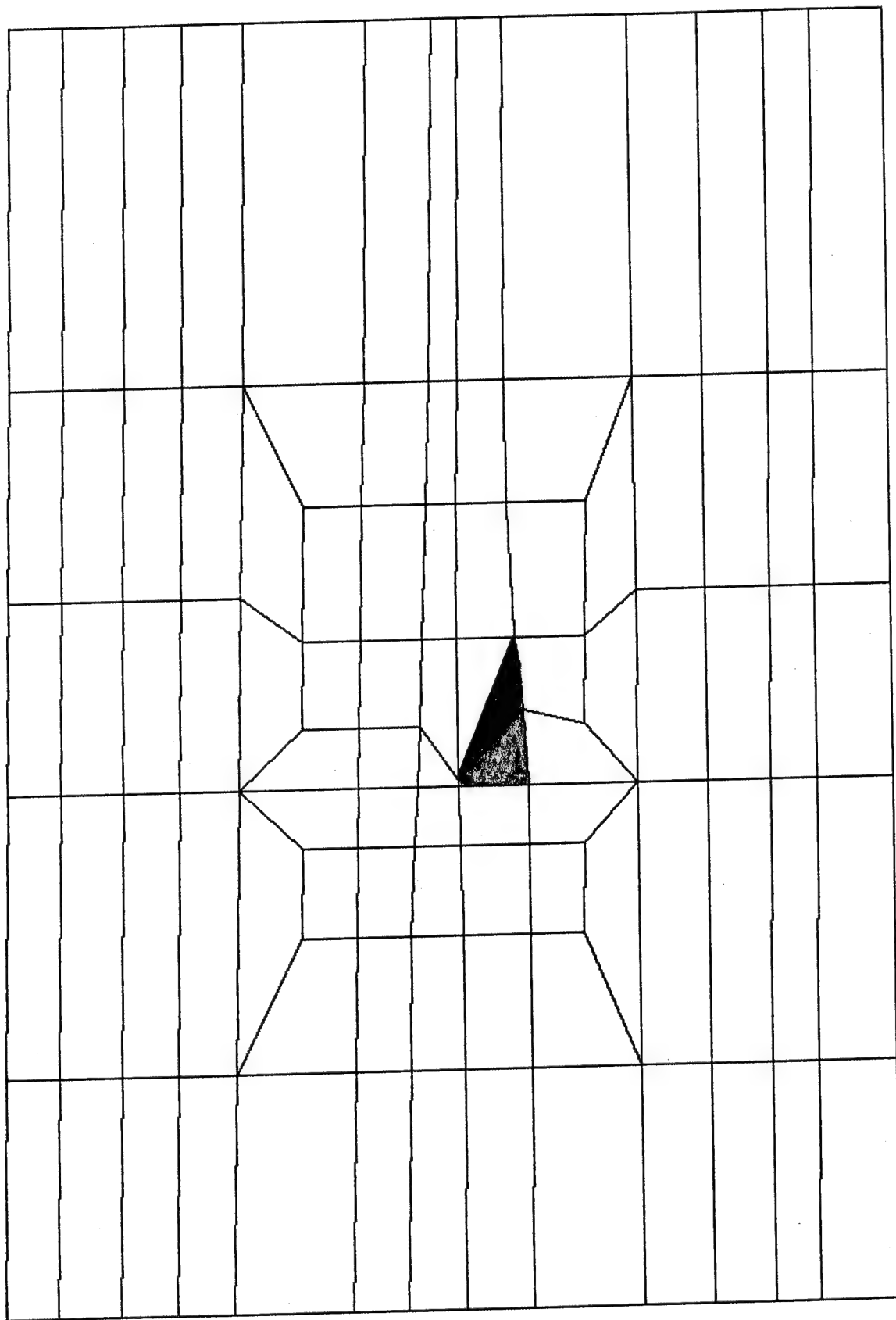
Figure 26. Finite Element Grid For The 0° Drop-off Case.
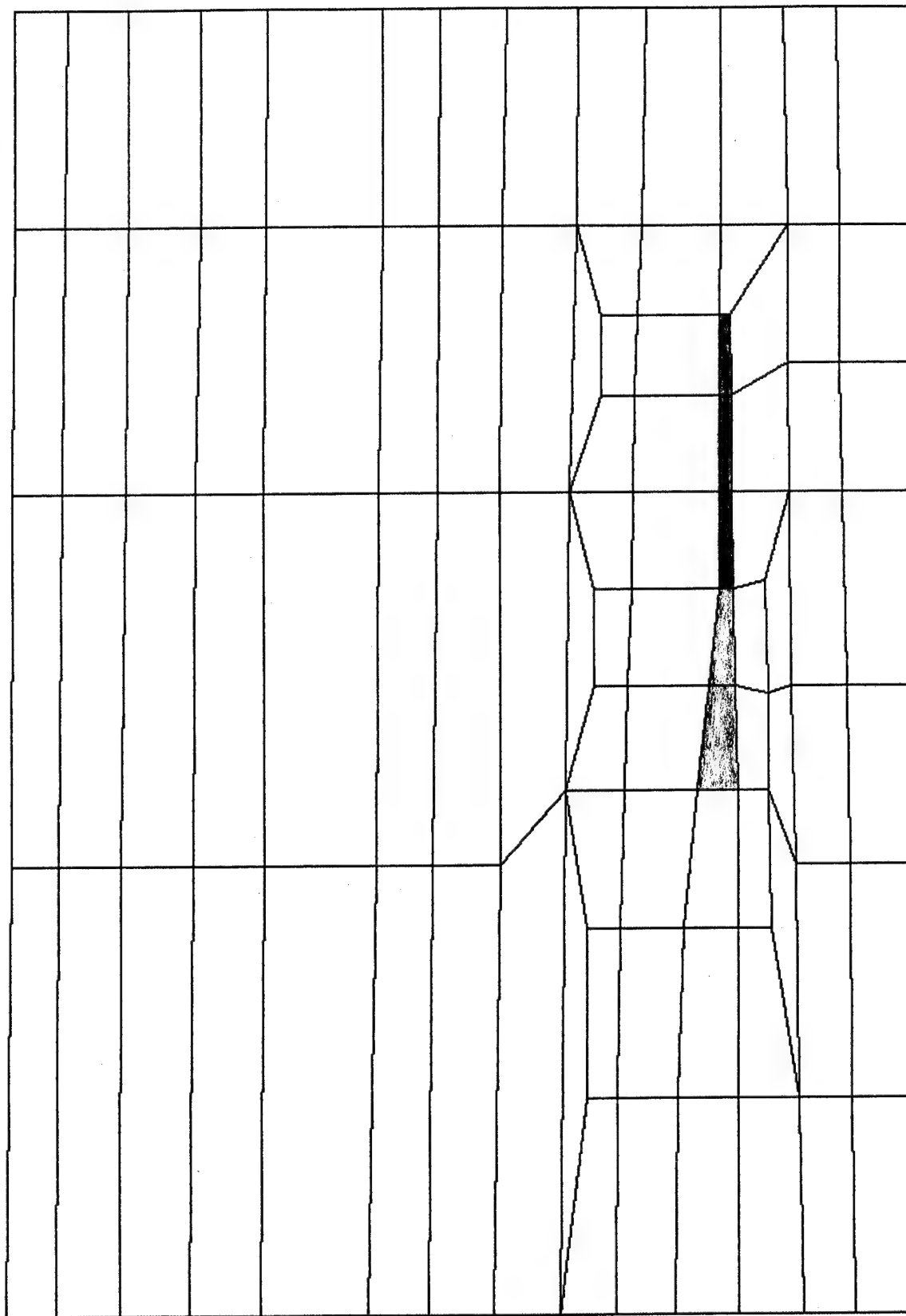
Figure 27. Finite Element Grid For The 45° Drop-off Case

TABLE 15. PROPERTIES OF HERCULES AS/3501-6 UNIDIRECTIONAL GRAPHITE/EPOXY COMPOSITE

Material Property	C_1	C_2	C_3	C_4	C_5	C_6
E_{11} (MPa)	-0.424	-1.357	-1.329	-13.66	8.781	1.301×10^5
E_{22} (MPa)	-0.164	-0.211	-0.133	-10.97	0.121	1.119×10^4
E_{33} (MPa)	-0.164	-0.211	-0.133	-10.97	0.121	1.119×10^4
G_{23} (MPa)	-0.046	-0.095	1.33×10^{-2}	-5.45	-4.035	3.748×10^3
G_{13} (MPa)	-0.086	-0.177	2.50×10^{-2}	-10.23	-7.570	7.031×10^3
G_{12} (MPa)	-0.086	-0.177	2.50×10^{-2}	$-10/23$	-7.570	7.031×10^3
ν_{23}						0.492
ν_{13}						0.308
ν_{12}						0.308
α_{11} (°C^{-1})	-4.908×10^{-9}			2.325×10^{-7}	-1.517×10^{-7}	4.498×10^{-5}
α_{22} (°C^{-1})	3.858×10^{-9}		8.377×10^{-9}	-1.330×10^{-6}	-8.656×10^{-7}	3.266×10^{-3}
α_{33} (°C^{-1})	3.858×10^{-9}		8.377×10^{-9}	-1.330×10^{-6}	-8.656×10^{-7}	3.266×10^{-3}
β_{11} (%M^{-1})	-2.340×10^{-10}			9.662×10^{-9}	-6.897×10^{-9}	4.100×10^{-6}
β_{22} (%M^{-1})	5.135×10^{-7}			-7.004×10^{-4}	-2.759×10^{-5}	1.206×10^{-3}
β_{33} (%M^{-1})	5.135×10^{-7}			-7.004×10^{-4}	-2.759×10^{-5}	1.206×10^{-3}
$\sigma_1 y$ (MPa)	-3.095×10^{-1}	-6.807×10^{-1}	-3.000×10^{-1}	-0.477	-0.068	7.761×10^2
$\sigma_2 y$ (MPa)	-7.211×10^{-2}	-1.276×10^{-1}	1.372×10^{-1}	-0.148	-0.158	5.240×10^1
$\sigma_3 y$ (MPa)	-7.211×10^{-2}	-1.276×10^{-1}	1.372×10^{-1}	-0.148	-0.158	5.240×10^1
$\tau_{23} y$ (MPa)	-3.171×10^{-1}	-6.468×10^{-2}	-9.800×10^{-2}	0.536	0.037	3.070×10^1
$\tau_{13} y$ (MPa)	-3.171×10^{-2}	-6.468×10^{-2}	-9.800×10^{-2}	0.536	0.037	3.070×10^1
$\tau_{12} y$ (MPa)	-3.171×10^{-2}	-6.468×10^{-2}	-9.800×10^{-2}	0.536	0.037	3.070×10^1
$\sigma_1 u$ (MPa)	-5.881×10^{-1}	-0.017	-7.508×10^{-1}	-0.206	0.321	1.467×10^3
$\sigma_2 u$ (MPa)	-5.892×10^{-2}	-1.792×10^{-1}	1.431×10^{-1}	-0.163	-0.189	6.070×10^1
$\sigma_3 u$ (MPa)	-5.892×10^{-2}	-1.792×10^{-1}	1.431×10^{-1}	-0.163	-0.189	6.070×10^1
$\tau_{23} u$ (MPa)	-9.130×10^{-2}	-8.208×10^{-2}	1.431×10^{-1}	-0.141	-0.139	8.730×10^1
$\tau_{13} u$ (MPa)	-9.130×10^{-2}	-8.208×10^{-2}	1.431×10^{-1}	-0.141	-0.139	8.730×10^1
$\tau_{12} u$ (MPa)	-9.130×10^{-2}	-8.208×10^{-2}	1.431×10^{-1}	-0.141	-0.141	8.730×10^1

TABLE 16. PROPERTIES OF HERCULES 3501-6 EPOXY MATRIX

Material Property	C_1	C_2	C_3	C_4	C_5	C_6
E_{11} (MPa)	-8.251×10^{-4}		7.773×10^{-3}	-2.650×10^{1}	-1.085×10^{1}	6.357×10^{3}
E_{22} (MPa)	-8.251×10^{-4}		7.773×10^{-3}	-2.650×10^{1}	-1.085×10^{1}	6.357×10^{3}
E_{33} (MPa)	-8.251×10^{-4}		7.773×10^{-3}	-2.650×10^{1}	-1.085×10^{1}	6.357×10^{3}
G_{23} (MPa)	-3.079×10^{-4}		2.901×10^{-3}	-9.890	-4.047	2.308×10^{3}
G_{13} (MPa)	-3.079×10^{-4}		2.901×10^{-3}	-9.890	-4.047	2.308×10^{3}
G_{12} (MPa)	-3.079×10^{-4}		2.901×10^{-3}	-9.890	-4.047	2.308×10^{3}
ν_{23}						0.340
ν_{13}						0.340
ν_{12}						0.340
α_{11} (°C^{-1})						4.000×10^{-5}
α_{22} (°C^{-1})						4.000×10^{-5}
α_{33} (°C^{-1})						4.000×10^{-5}
β_{11} (%M^{-1})						2.000×10^{-3}
β_{22} (%M^{-1})						2.000×10^{-3}
β_{33} (%M^{-1})						2.000×10^{-3}
σ_1^y (MPa)	9.678×10^{-4}	1.930×10^{-5}	8.553×10^{-4}	-1.141	-1.792×10^{-1}	1.935×10^{2}
σ_2^y (MPa)	9.678×10^{-4}	1.930×10^{-5}	8.553×10^{-4}	-1.141	-1.792×10^{-1}	1.935×10^{2}
σ_3^y (MPa)	9.678×10^{-4}	1.930×10^{-5}	8.553×10^{-4}	-1.141	-1.792×10^{-1}	1.935×10^{2}
τ_{23}^y (MPa)	4.839×10^{-4}	9.648×10^{-6}	4.277×10^{-5}	-0.5706	-8.960×10^{-2}	9.677×10^{1}
τ_{13}^y (MPa)	4.839×10^{-4}	9.648×10^{-6}	4.277×10^{-5}	-0.5706	-8.960×10^{-2}	9.677×10^{1}
τ_{12}^y (MPa)	4.839×10^{-4}	9.648×10^{-6}	4.277×10^{-5}	-0.5706	-8.960×10^{-2}	9.677×10^{1}
σ_1^u (MPa)	9.678×10^{-4}	1.930×10^{-5}	8.554×10^{-4}	-1.141	-1.792×10^{-1}	1.935×10^{2}
σ_2^u (MPa)	9.678×10^{-4}	1.930×10^{-5}	8.554×10^{-4}	-1.141	-1.792×10^{-1}	1.935×10^{2}
σ_3^u (MPa)	9.678×10^{-4}	1.930×10^{-5}	8.554×10^{-4}	-1.141	-1.792×10^{-1}	1.935×10^{2}
τ_{23}^u (MPa)	4.839×10^{-4}	9.648×10^{-6}	4.277×10^{-5}	-0.5706	-8.960×10^{-2}	9.677×10^{1}
τ_{13}^u (MPa)	4.839×10^{-4}	9.648×10^{-6}	4.277×10^{-5}	-0.5706	-8.960×10^{-2}	9.677×10^{1}
τ_{12}^u (MPa)	4.839×10^{-4}	9.648×10^{-6}	4.277×10^{-5}	-0.5706	-8.960×10^{-2}	9.677×10^{1}

these were the most broadly defined properties available. Plasticity parameters σ_o and n were not needed since a plastic analysis was not performed, as discussed in Section 4.1.

Since material properties are a function of temperature and moisture, they are defined by Eq. (4.1) of Section 4.1. Thus, the six constants of this equation are needed to define a material property under a given environmental condition. The values given are for temperature given in degrees centigrade, and moisture given in terms of the corresponding relative humidity.

4.4.3 Method of Presentation

Although the only loading on a laminate was a negative (compressive) normal stress via a uniform compressive displacement, the stress response of each element in the laminate was complex, involving many stress components. It is logical to relate each of these stress components to the ultimate values given in the material properties section. To accomplish this, an arbitrary compressive displacement was placed on the laminate, and the stress components for each element were then divided by their respective ultimate values. The resulting values were very small, as a small arbitrary displacement was employed to produce them. The largest of all these normalized values in all three layers and for all six stresses was then found. Then the actual displacement required to bring this largest normalized stress value up to 1.00 was determined, i.e., the displacement (or corresponding average applied stress) required to bring this critical element to failure.

It was discovered that finding this displacement when the material was allowed to deform plastically before failing would be a very tedious process, involving much computer time and resources. Therefore, in order to provide results for various resin pocket sizes and hygrothermal preconditionings, it was decided that the simplifying assumption of linear elasticity to failure should be employed. Under this assumption, all displacements required to produce first element failure were easily found by direct proportionality in the case of no preconditioning, and by linear proportionality in the case of preconditioning.

From these displacements, corresponding average applied stresses were computed. Results due to these average applied stresses are presented in the form of the element grids presented in Section 4.4.1. For each grid shown, the layer number and particular stress as well as the resin pocket

68

size is denoted. The resin pocket itself is outlined. A number appears in the center of each element, representing the relative size of its actual stress to its corresponding failure stress. The element possessing a 1.00 value is the critical element, and is the first to fail. Unless two or more elements become critical simultaneously, only one plot out of 18 (three layers times six stresses) will possess a critical element.

Certainly not all 18 grids are important, so not all are presented here. However one additional stress, the effective stress, is presented because it represents as a single value the combined effect of all six stress components. The value of this effective stress is calculated from Eqs. (4.4) and (4.3) of Section 4.3.2, except that the ultimate strength quantities replace the yield strengths. The normalization value for effective stress is given by Eq. (4.5) where again, ultimate strength quantities replace yield strengths.

It was found that in some cases effective stress was critical, while in others, one of the six stress components (which always was, not surprisingly, the normal stress in the x-direction) was critical. For this reason, it seemed reasonable to treat effective stress as a separate quantity, and to calculate a separate average applied stress required to produce a first-critical element for effective stress. Therefore, two failure criteria were considered, viz, effective stress, and maximum normal stress. Neither always controlled, indicating that a better failure criterion is needed, which must be verified experimentally.

As a verification of the accuracy of the effective stress failure criterion, experimental data for the ultimate strength in uniaxial tension for 45° plies were employed. If the effective stress failure criterion is valid, then all that would be needed would be to transform the uniaxial stress to the principal directions of orthotropy of the ply, and use these values to compute the effective stress at failure. This was done, and predicted versus actual results differed considerably. Aside from the question of the validity of the effective stress criterion, the question arose as to what stresses to use as ultimate values to normalize the stresses in 45° plies. In view of some experimental tensile data for 45° plies, it was decided to use these values, and to use stress transformations to compute values not available, rather than use the effective stress criterion to predict them. These values are given in Table 17.

69

TABLE 17.   ULTIMATE TENSILE AND SHEAR STRENGTHS FOR 45° PLIES

Ultimate Stresses	RTD	ETW	ETD
$\sigma_x^{\,u}$(MPa)	180.5	135.7	135.6
$\sigma_y^{\,u}$(MPa)	180.5	135.7	135.6
$\sigma_z^{\,u}$(MPa)	57.0	36.0	37.6
$\tau_{yz}^{\,u}$(MPa)	83.9	63.0	63.0
$\tau_{xz}^{\,u}$(MPa)	83.9	63.0	63.0
$\tau_{xy}^{\,u}$(MPa)	94.3	67.9	67.8

Three environmental conditions were considered, viz, room temperature, dry (RTD), elevated temperature, wet (ETW), and elevated temperature, dry (ETD), corresponding to the conditions under which specimens were tested by Northrop in the second-year study [3]. The elevated temperature was 218°F and the wet condition was 1% moisture.

4.4.4 Room Temperature, Dry (RTD) Results

Results for the no drop-off, 0° drop-off, and 45° drop-off cases are presented, with the resin pocket being both large and small in the latter two cases. In all cases the maximum normal stress and effective stress failure criteria are compared. For important stresses, Layers 1 and 3 are compared because, with few exceptions, these layers represent extremes; stress values in Layer 2 always lie between those of Layers 1 and 3.

4.4.4.1 Plain Laminate

Figures 28 and 29 show normalized σ_x stresses in Layers 1 and 3. The first two elements of the upper 90° ply of Layer 3 are critical, with the remaining elements in the 90° plies very nearly critical. This is to be expected since the 90° plies are weakest in the x-direction. Values for the elements of the 90° plies in Layer 1 are high, but not as high as those in Layer 3 because edge effects in Layer 3 shift more of the load toward the edge, i.e. to Layer 3. The required average applied compressive stress to fail the first elements was $\bar{\sigma}_x = -52.7$ ksi.

Although the normalized values of the stresses σ_y, σ_z, τ_{yz}, and τ_{xz} are not critical, they are presented here to show the effects of interlaminar shear and laminate free edges on the stress state within the laminate. For the same applied compressive stress of $\bar{\sigma}_x = -52.7$ ksi, Figures 30 through 33 show the normalized stresses for σ_y, σ_z, τ_{yz}, and τ_{xz}, respectively. In the case of σ_y, values as high as 0.31 occur in the lowest 0° ply in Layer 2. These somewhat high values result because the two oppositely orientated 45° plies bounding the 0° ply tend to shear in opposite directions, producing both σ_x and σ_y stresses in the 0° ply. However, this ply is not very strong in the y-direction; thus, moderate normalized values result. In the case of σ_z, the large difference in Poisson effects for the 0° and 90° plies produced interlaminar normal stresses between these plies. To maintain equilibrium, the values change sign from Layer 1 to Layer 3.

71

PLY

-45	-.74	-.63	-.65	-.66	-.62	-45
45	-.64	-.70	-.71	-.70	-.80	45
0	-.40	-.42	-.43	-.43	-.45	0
90	-.82	-.82	-.83	-.84	-.84	90
0	-.42	-.42 -.43 -.43 -.43 -.43 -.43	-.43	-.43	-.43	0
0	-.43	-.43 -.43 -.43-.43 -.43 -.43 -.43			-.43	0
90	-.86	-.85 -.85 -.85-.85 -.85 -.85 -.85			-.84	90
0	-.43	-.43 -.43 -.43-.43 -.43 -.43 -.42			-.42	0
0	-.44	-.43 -.43 -.45-.43 -.43 -.43 -.42 -.44 -.43 -.42			-.41	0
-45	-.77	-.67	-.66	-.65	-.63	-45
45	-.68	-.72	-.71	-.69	-.71	45
0	-.44	-.43	-.43	-.42	-.42	0
-45	-.71	-.53	-.52	-.51	-.45	-45

Figure 28. Normalized Values for σ_x in Layer $\underline{1}$ for the No Drop-off Case, Under RTD Conditions, where $\overline{\sigma}_x$ = -52.7 ksi.

PLY

-45	-.55	-.59	-.59	-.57	-.61	-45
45	-.65	-.66	-.65	-.64	-.62	45
0	-.46	-.44	-.43	-.42	-.41	0
90	-1.00	-1.00	-.99	-.99	-.99	90
0	-.43	-.43 -.43 -.43-.43 -.43 -.43 -.43			-.43	0
0	-.43	-.43 -.43 -.43-.43 -.43 -.43 -.43			-.43	0
90	-.97	-.98 -.98 -.98-.98 -.98 -.99 -.99			-.99	90
0	-.43	-.42 -.43 -.43-.43 -.43 -.43 -.43			-.43	0
0	-.41	-.42 -.42 -.42-.43 -.43 -.43 -.43 -.41 -.42 -.43			-.44	0
-45	-.57	-.60	-.60	-.62	-.63	-45
45	-.64	-.64	-.64	-.66	-.65	45
0	-.41	-.41	-.42	-.43	-.44	0
-45	-.44	-.52	-.53	-.54	-.57	-45
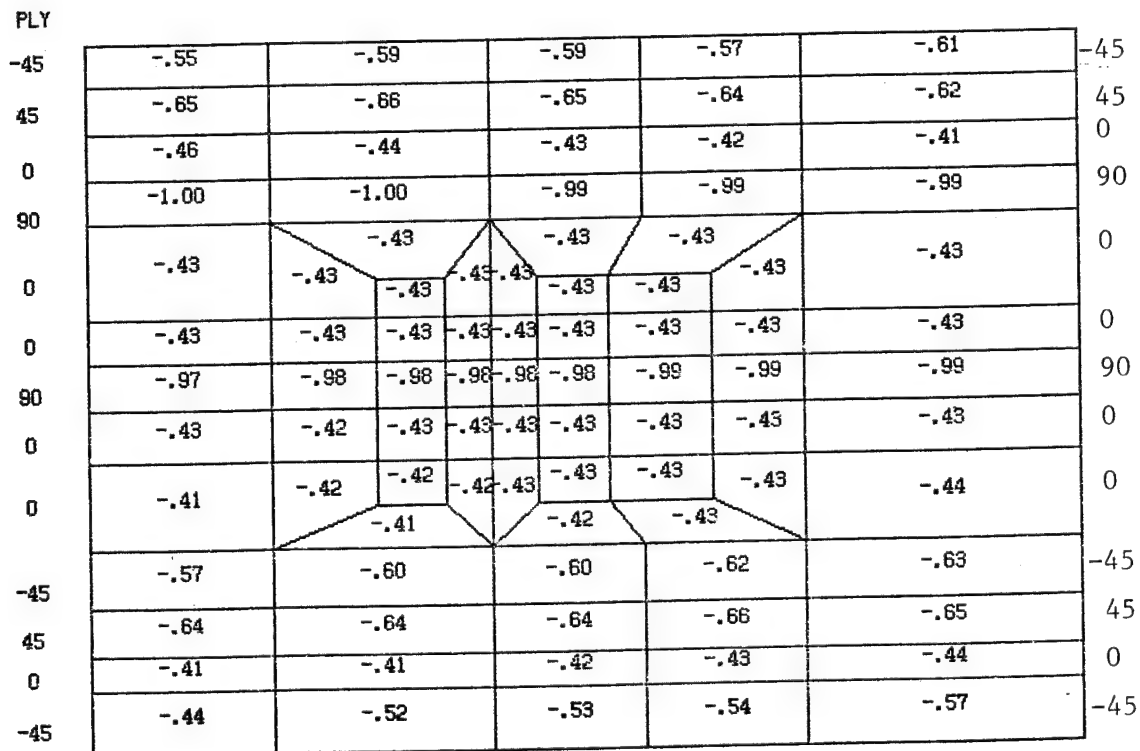
Figure 29. Normalized Values for σ_x in Layer $\underline{3}$ for the No Drop-off Case, Under RTD Conditions, where $\overline{\sigma}_x$ = -52.7 ksi.

Figure 30. (σy in Layer 2)

PLY						PLY
-45	-.06	-.08	-.05	-.06	-.05	-45
45	-.16	-.21	-.19	-.21	-.20	45
0	.01	.01	.01	.01	.00	0
90	.05	.05	.05	.05	.04	90
0	-.18	-.19 / -.18 / -.20	.19 .19 / -.18 / -.20	-.18 / -.20	-.19	0
0	-.20	-.19 / -.19	-.19 -.19 / -.19	-.19 / -.20	-.20	0
90	.03	.03 / .03	.03 .03 / .03	.03 / .03	.03	90
0	-.11	-.10 / -.10	-.10 -.10 / -.11	-.11 / -.11	-.09	0
0	.04	.02 / .00 / .12	.03 .03 / -.00 / .13	-.01 / .02 / .12	.07	0
-45	-.12	-.13	-.10	-.12	-.09	-45
45	-.13	-.15	-.14	-.15	-.12	45
0	.23	.30	.31	.30	.30	0
-45	-.00	-.01	.03	.01	.07	-45

Figure 30.   Normalized Values for σ_y in Layer 2 for the
No Drop-off Case, Under RTD Conditions, where $\bar{\sigma}_x$ = -52.7 ksi.

Figure 31. (σz in Layer 3)

PLY						PLY
-45	.03	-.01	-.02	.00	-.04	-45
45	.05	-.02	-.04	-.04	-.11	45
0	-.05	-.11	-.13	-.14	-.19	0
90	-.16	-.18	-.19	-.20	-.23	90
0	-.15	-.14 / -.16 / -.14	.15 .15 / -.17 / -.14	-.17 / -.16	-.19	0
0	-.14	-.15 / -.15	-.15 -.15 / -.15	-.16 / -.16	-.17	0
90	-.14	-.15 / -.16	-.16 -.16 / -.16	-.16 / -.17	-.18	90
0	-.09	-.10 / -.10	-.10 -.10 / -.11	-.11 / -.12	-.13	0
0	-.02	-.03 / -.03 / .02	-.01 .02 / -.04 / .02	-.04 / -.03 / .01	-.00	0
-45	.07	.08	.07	.07	.08	-45
45	.14	.10	.09	.09	.06	45
0	.10	.07	.07	.07	.05	0
-45	.01	.04	.05	.05	.09	-45

Figure 31.   Normalized Values for σ_z in Layer 3 for the
No Drop-off Case, Under RTD Conditions, where $\bar{\sigma}_x$ = -52.7 ksi.

-45	-.07	-.00	-.01	-.02	.02	-45
45	.04	.09	.07	.06	.10	45
0	.22	.16	.17	.17	.13	0
90	.03	.01	.01	.02	-.00	90
0	-.04 / -.03	-.06 / -.01	-.03 .03	-.06 / -.01	-.06 / -.03	-.04	0
0	.05	.04 .04	.05 .05 .04	.04 .05	.05	0
90	-.02	-.02 -.02	-.01 -.01 -.01	-.01 -.01	-.01	90
0	-.09	-.10 -.10	-.10 -.10 -.10	-.09 -.09	-.10	0
0	-.06 / -.08	-.07 / -.08 .08	-.07 / -.09	-.07 -.06	-.09 / -.08	-.09	0
-45	-.12	-.05	-.06	-.07	-.02	-45
45	-.01	.04	.03	.02	.06	45
0	.12	.03	.05	.07	-.01	0
-45	.05	.01	.01	.03	-.01	-45

Figure 32.   Normalized Values for τ_{yz} in Layer_3 for the
No Drop-off Case, Under RTD Conditions, where $\overline{\sigma}_x$ = -52.7 ksi.

-45	.02	.11	.11	.11	.06	-45
45	.02	.07	.09	.08	.01	45
0	-.04	-.08	-.07	-.08	-.04	0
90	-.01	-.03	-.04	-.03	-.02	90
0	-.00 / -.01	-.01 / -.01	.01 .02	-.02 / -.01	-.02 / -.01	-.01	0
0	.00	-.00 -.01	-.01 -.00 -.01	-.01 -.00	-.00	0
90	.00	-.00 -.00	-.01 -.01 -.01	-.01 -.00	-.00	90
0	.00	-.01 -.02	-.02 -.02 -.02	-.02 -.01	-.00	0
0	-.02 / -.05	-.06 / -.07 .07	-.06 / -.07	-.06 -.06	-.06 / -.08	-.03	0
-45	-.00	.05	.05	.05	.03	-45
45	.02	.02	.02	.03	-.00	45
0	-.08	-.18	-.20	-.20	-.10	0
-45	-.02	-.09	-.10	-.09	-.05	-45

Figure 33.   Normalized Values for τ_{xz} in Layer_3 for the
No Drop-off Case, Under RTD Conditions, where σ_x = -52.7 ksi.

The largest value of -0.23 occurred in Layer 3 (shown in Figure 31), in the last element of the upper 90° ply.

It should be pointed out that the reason for the non-zero values in the top and bottom plies is because these values represent average stresses for the elements, not those on the element surface, which, of course, would be zero since the laminate is not loaded in the z-direction. This same explanation of average element stress applies to all other cases where there is no applied stress.

In the case of τ_{yz} (Figure 32), the largest value of 0.22 occurred in the left element of the upper 0° ply in Layer 3. One would expect negligible τ_{yz} stresses in the third layer since it is closest to an edge, where there are no applied τ_{yz} stresses. However, studies such as Reference [8] show that edge effects can produce shear stresses that reach a peak value near the edge, and then suddenly decline to zero at the edge itself. Since stresses shown for each element represent average stresses throughout that element, they may take into account the sudden peak of shear stress near the edge. Perhaps this is the reason for the unexpected value of 0.22 for normalized τ_{yz} in Figure 32.

In the case of τ_{xz} (Figure 33), the largest value of -0.20 occurred in the lowest 0° ply of the third layer, and is due to the shearing effect of the oppositely-orientated 45° plies bounding this 0° ply.

Figures 34 and 35 show normalized stresses for τ_{xy} in Layers 1 and 3. This shear stress is most significant since it represents direct in-plane shear. As both figures indicate, τ_{xy} values for the 0° and 90° plies are negligible since there is no tendency for in-plane shear in these plies. The shear is as high as 0.79 for the upper right element of the +45° ply of Layer 1, which is in direct interlaminar shear coupling with the -45° ply above. The corresponding value for Layer 3 is 0.46, which is less because Layer 3 is nearest the edge, where apparently there is no peak-and-drop effect. Shear values as high as these increase the effective stress, which is dominated by the high values which already exist for σ_x, effective stress being representative of the effect of all stresses acting at once.

Figures 36 and 37 show normalized effective stresses for Layers 1 and 3. Using the effective stress failure criterion, an average stress of $\overline{\sigma}_x = -39.5$ ksi was applied before an element failed. The critical element was the same one that reached a high τ_{xy} stress in Figure 34. Thus, when this

-.66	-.48	-.51	-.53	-.49
.53	.63	.63	.60	.79
-.05	-.08	-.09	-.08	-.06
-.01	-.02	-.03	-.03	-.02

PLY labels left: -45, 45, 0, 90, 0, 0, 90, 0, 0, -45, 45, 0, -45

Right labels: -45, 45, 0, 90, 0, 0, 90, 0, 0, -45, 45, 0, -45

Figure 34 values (middle region):
- -.00 | -.01 / -.01 / -.00 | -.01 / -.00 | -.01 / -.00 | -.00 / -.00 | -.00
- -.00 | -.00 | -.00 / -.00 / .00 | -.00 | -.00 | -.00 | -.00
- .00 | .00 | .00 / .00 / .00 | .00 | .00 | .00 | .00
- .00 | .00 | .00 / .00 / .00 | .01 | .01 | .00 | .00
- .04 | .04 | .03 / .04 / .04 | .03 | .03 | .04 | .04
- .07 / .08 / .08

-.69	-.52	-.51	-.52	-.50
.56	.64	.63	.60	.65
.00	.01	.01	.01	.00
-.53	-.22	-.22	-.23	-.17

Figure 34. Normalized Values for τ_{xy} in Layer 1 for the No Drop-off Case, Under RTD Conditions, where $\bar{\sigma}_x = -52.7$ ksi.

-.38	-.41	-.39	-.40	-.40
.49	.52	.50	.51	.46
-.07	-.06	-.06	-.06	-.05
-.02	-.02	-.02	-.02	-.02

PLY labels left: -45, 45, 0, 90, 0, 0, 90, 0, 0, -45, 45, 0, -45

Right labels: -45, 45, 0, 90, 0, 0, 90, 0, 0, -45, 45, 0, -45

Figure 35 values (middle region):
- -.01 | .00 / -.01 / -.00 | -.00 / -.01 | -.00 / -.01 | -.01 / -.01 | -.01
- -.00 | -.00 | -.00 / .00 / -.01 | -.00 | -.00 | -.00 | -.00
- .00 | .00 | .00 / .00 / .00 | .00 | .00 | .00 | .00
- .00 | .01 | .00 / -.00 / .00 | .00 | .00 | .00 | .01
- .05 | .03 | .02 / .04 / .03 | .02 | .02 | .04 | .05
- .06 / .06 / .06

-.41	-.46	-.45	-.48	-.47
.56	.56	.54	.58	.55
.01	.02	.02	.02	.03
-.17	-.27	-.25	-.27	-.25

Figure 35. Normalized Values for τ_{xy} in Layer 3 for the No Drop-off Case, Under RTD Conditions, where $\bar{\sigma}_x = -52.7$ ksi.

PLY

-45	.91	.83	.85	.86	.83	-45
45	.81	.89	.90	.90	1.00	45
0	.31	.34	.35	.35	.36	0
90	.58	.57	.58	.59	.59	90
0	.37 / .38	.37 / .38	.38 / .38	.38 / .39	.38 / .39	.39	0
0	.37	.38	.38 / .38	.38 / .38	.38	.38	.38	.39	0
90	.56	.57	.57 / .57	.57 / .57	.57	.57	.57	.58	90
0	.34	.34	.34 / .34	.34 / .34	.34	.34	.34	.34	0
0	.33	.33	.33 / .33	.33 / .32	.32 / .34	.32 / .34	.32 / .33	.31	0
-45	.92	.85	.84	.83	.81	-45
45	.82	.87	.85	.83	.88	45
0	.40	.42	.42	.41	.38	0
-45	.91	.78	.75	.72	.66	-45

Figure 36. Normalized Values for σ_{eff} in Layer 1 for the No Drop-off Case, Under RTD Conditions, where $\bar{\sigma}_x$ = -39.5 ksi.

PLY

-45	.77	.81	.81	.79	.83	-45
45	.89	.85	.83	.83	.78	45
0	.37	.34	.34	.33	.32	0
90	.51	.50	.48	.48	.47	90
0	.32 / .32	.33 / .32	.32 / .32	.32 / .32	.32 / .32	.32	0
0	.32	.32	.32 / .32	.32 / .32	.32	.32	.32	.32	0
90	.50	.50	.50 / .50	.50 / .50	.50	.50	.50	.49	90
0	.33	.33	.33 / .33	.33 / .33	.33	.33	.33	.33	0
0	.32	.33	.33 / .34	.34 / .34	.34 / .35	.34 / .36	.34	.35	0
-45	.81	.83	.84	.86	.88	-45
45	.89	.86	.87	.89	.87	45
0	.33	.38	.39	.39	.38	0
-45	.68	.78	.81	.82	.91	-45

Figure 37. Normalized Values for σ_{eff} in Layer 3 for the No Drop-off Case, Under RTD Conditions, where $\bar{\sigma}_x$ = -39.5 ksi.

77

failure criterion is used, in-plane shear effects can be quite detrimental. Because of in-plane shear, most of the effective stress values for 45° plies are large in both Layers 1 and 3, whereas those for the 0° and 90° plies are smaller.

In conclusion, first-element failure occurs in the 90° plies at an applied stress of $\bar{\sigma}_x$ = -52.7 ksi, if the maximum normal stress failure criterion is used, and in the upper right +45° ply under an applied stress of $\bar{\sigma}_x$ = -39.5 ksi, if the effective stress failure criterion is used.

4.4.4.2 0° Drop-off Laminate

Figures 38 and 39 show normalized σ_x stresses for Layers 1 and 3, respectively, for the small resin pocket case. The critical element occurs immediately above the resin pocket in Layer 3, with the corresponding element in Layer 1 being near critical at -0.95. Since the resin pocket itself is less stiff than the 90° element above it, the latter takes most of the load when the 0° ply drops off. Thus, it is not surprising that these 90° elements become critical. The applied stress required to fail these elements was $\bar{\sigma}_x$ = 20.1 ksi, 60 percent less than that required to fail an element in the no drop-off case.

Figures 40 and 41 show normalized σ_z stresses for Layers 1 and 3, respectively. Although no element is near critical, the element above the resin pocket reaches a value of -0.21 in Layer 1, and -0.31 in Layer 3. These values have a beneficial effect on effective stress because they are of the same sign as the σ_x values, and effective stress recognizes only differences between normal components.

Figures 42 and 43 show normalized τ_{xz} stresses for Layers 1 and 3, respectively. A value of -0.19 occurs in the element above the resin pocket in both layers. This value has a detrimental effect on effective stress, the sign of the shear stress being irrelevant. Values of the other stress components are not presented because their values for the critical element were very small, and did not influence effective stress significantly.

The purpose of presenting values of both σ_z and τ_{xz} here is to show how they influenced effective stress, shown in Figures 44 and 45 for Layers 1 and 3, respectively. The critical element was again the one above the resin pocket, only in this case in Layer 1, although the corresponding element in Layer 3 was near critical at 0.94. The required applied stress to fail this critical element was $\bar{\sigma}_x$ = -32.6 ksi, 50 percent

Figure 38. Normalized Values for σ_x in Layer 1 for the
0° Drop-off Case, Small Resin Pocket, Under RTD Conditions,
where $\bar{\sigma}_x$ = -20.1 ksi.

Figure 39. Normalized Values for σ_x in Layer 3 for the
0° Drop-off Case, Small Resin Pocket, Under RTD Conditions,
where $\bar{\sigma}_x$ = -20.1 ksi.

PLY

-45	-.01	-.00	-.00	-.01	.01	-45
45	-.01	.01	.01	.01	.03	45
0	.01	.02	.02	.02	.04	0
90	.04	.04	.04	.04	.05	90
0	.05	.06 .06 .07	.06 .03 .02 .04	.04 .04	.05 .05	0
0	.05	.06 .09 .07	.02 .01 .04	.04 .04	.04	0
90	.03	.04 .05 .16	.21 .05 .07 .04	.03	.03	90
0	.01	.02 .04 .15	.04 .03 .07	.03	.03	
0	.01	.03 .08	.03 -.05 -.03 .02	.02	.00	0
		.05	-.06 -.01			
-45	.01	-.01	-.04	-.04	-.02	-45
45	-.02	-.02	-.05	-.05	-.02	45
0	-.01	-.02	-.05	-.05	-.03	0
-45	.01	-.01	-.04	-.05	-.04	-45

Figure 40. Normalized Values for σ_z in Layer 1 for the 0° Drop-off Case, Small Resin Pocket, Under RTD Conditions, where $\bar{\sigma}_x = -20.1$ ksi.

PLY

-45	.01	-.01	-.01	.00	-.02	-45
45	.02	-.01	-.02	-.02	-.05	45
0	-.01	-.04	-.05	-.06	-.09	0
90	-.05	-.06	-.08	-.08	-.10	90
0	-.05	-.04 -.05 -.03	-.05 .07 -.08 -.07	-.07 -.07	-.08	0
0	-.04	-.04 -.02 -.04	-.08 -.09 -.07 -.07	-.07	-.09	0
90	-.05	-.06 -.05 .05	-.31 -.05 -.04 -.08		-.10	90
0	-.04	-.05 -.03 .07	-.06 -.06 -.02 -.07		-.09	
0	.00	.00 .04	.01 -.07 -.07 -.03	-.03	-.03	0
		.05	-.05 -.00			
-45	.06	.04	.01	.01	.03	-45
45	.09	.05	.02	.02	.02	45
0	.07	.04	.02	.02	.01	0
-45	.04	.03	.01	.01	.03	-45

Figure 41. Normalized Values for σ_z in Layer 3 for the 0° Drop-off Case, Small Resin Pocket, Under RTD Conditions, where $\bar{\sigma}_x = -20.1$ ksi.

Figure 42. Normalized Values for τ_{xz} — PLY rows (left labels) / right labels

PLY						PLY
-45	-.01	-.04	-.04	-.05	-.02	-45
45	-.01	-.03	-.03	-.03	-.01	45
0	.03	.07	.07	.07	.04	0
90	-.01	-.01	-.01	-.02	-.01	90
0	.01	.02 .03	.04 .04 .03	.03 .02	.01	0
0	.00	.00 -.00 .03 .02	.02 .04	.05	.02	0
90	-.03	-.08 -.14 -.24 .19	-.11 -.03	-.03	-.02	90
0	-.00	.01 .06 .11 .03	.02 -.02	-.05	-.02	0
0	.03	.06 .09 .07 .06 .07	.02 -.00 .08	.00 .05	.00	0
-45	-.01	-.03	-.03	-.02	-.01	-45
45	-.01	-.02	-.02	-.01	-.01	45
0	.03	.08	.09	.08	.04	0
-45	.01	.03	.04	.03	.01	-45

Figure 42. Normalized Values for τ_{xz} in Layer 1 for the 0° Drop-off Case, Small Resin Pocket, Under RTD Conditions, where σ_x = -20.1 ksi.

PLY						PLY
-45	.01	.05	.05	.05	.03	-45
45	.01	.03	.04	.03	.00	45
0	-.00	.01	.01	.00	-.00	0
90	-.02	-.04	-.04	-.05	-.02	90
0	.01	.01 .02 .02	.03 .03 .02 .02	.01 .01	.01	0
0	.00	-.00 -.01 .02 .02	.01 .03	.04	.02	0
90	-.03	-.08 -.15 -.24 .19	-.11 -.04	-.03	-.02	90
0	.00	.01 .04 .10 .02	.01 -.03	-.03	-.02	0
0	.01	.02 .05 .02 .01 .03	-.02 -.04 .02	-.04 -.01	-.02	0
-45	.00	.02	.03	.04	.01	-45
45	.01	.00	.01	.02	.00	45
0	-.03	-.06	-.06	-.06	-.03	0
-45	-.01	-.04	-.04	-.04	-.02	-45

Figure 43. Normalized Values for τ_{xz} in Layer 3 for the 0° Drop-off Case, Small Resin Pocket, Under RTD Conditions, where σ_x = -20.1 ksi.

81

Figure 44.

PLY

						PLY
-45	.72	.69	.73	.78	.78	**-45**
45	.65	.74	.78	.81	.93	**45**
0	.27	.32	.34	.34	.33	**0**
90	.48	.48	.50	.52	.53	**90**
0	.31	.33 / .33 / .35	.34 .34 / .33	.34 / .34	.34	**0**
0	.33	.33 .35	.36 .33 .34	.35 .35	.32	**0**
90	.46	.45 .43	.49 .00 .79	.58 .49	.46	**90**
0	.25	.23 .24	.32 .24 .78	.56 .47	.47	**0**
0	.27	.29 .33	.31 .35 .33	.31 .29	.27	**0**
		.33	.33	.30		
-45	.81	.76	.70	.72	.72	**-45**
45	.73	.76	.72	.71	.76	**45**
0	.34	.37	.39	.39	.34	**0**
-45	.83	.68	.63	.61	.56	**-45**

Figure 44. Normalized Values for σ_{eff} in Layer 1 for the 0° Drop-off Case, Small Resin Pocket, Under RTD Conditions, where $\overline{\sigma}_x = -32.6$ ksi.

PLY

						PLY
-45	.62	.66	.68	.68	.76	**-45**
45	.73	.71	.71	.73	.71	**45**
0	.32	.30	.31	.30	.29	**0**
90	.43	.43	.42	.42	.42	**90**
0	.27	.28 / .28	.28 .23 / .28	.28 / .28	.28	**0**
0	.28	.28 .29	.30 .29 .30	.30 .30	.27	**0**
90	.41	.39 .37	.43 .94 .70	.50 .42	.38	**90**
0	.24	.22 .20	.26 .23 .71	.51 .43	.41	**0**
0	.25	.25 .26	.27 .34 .35	.34 .32	.32	**0**
		.28	.30	.31		
-45	.71	.73	.70	.74	.78	**-45**
45	.80	.75	.73	.75	.74	**45**
0	.28	.31	.32	.32	.33	**0**
-45	.64	.70	.70	.70	.77	**-45**

Figure 45. Normalized Values for σ_{eff} in Layer 3 for the 0° Drop-off Case, Small Resin Pocket, Under RTD Conditions, where $\overline{\sigma}_x = -32.6$ ksi.

above that needed to fail an element if the maximum normal stress failure criterion was used. The reason why the effective stress failure criterion is more favorable this time is because the beneficial effect of σ_x and σ_z being of the same sign was more compensating than the detrimental effect of τ_{xz}, the other stresses being negligible, as already stated.

The element that failed in effective stress for the no drop-off case reached a value of 0.93 in this case, indicating that interlaminar shear is almost as detrimental as the ply drop-off itself for the effective stress failure criterion.

Comparisons will now be made with the large resin pocket case. Figures 46 and 47 show normalized σ_x stresses for Layers 1 and 3, respectively. The critical element again is the one above the resin pocket in Layer 3, with the critical element in Layer 1 reaching 0.98. The applied stress at failure is $\overline{\sigma}_x$ = -18.8 ksi, which is slightly below the value of $\overline{\sigma}_x$ = -20.1 ksi for the small resin pocket case. The reason for this decrease is that the larger resin pocket, being less stiff than the small one, shifts more load to the upper 90° element, causing it to fail at a lower stress level.

The effect that σ_z and τ_{xz} have on effective stress is similar to that for the small resin pocket case, so these stresses are not presented here. Normalized effective stress is shown in Figures 48 and 49. The critical element is again the one above the resin pocket in Layer 1, with the corresponding element in Layer 3 reaching 0.95. The value in the 45° ply that was critical in the no drop-off case was 0.88 in this case, indicating again that, in spite of drop-offs and resin pocket sizes, interlaminar shear is quite detrimental if the effective stress failure criterion is used. The value of applied stress required to produce effective stress failure was -31.0 ksi, slightly below the value of -32.6 ksi for the small resin pocket case. The reason is the same as that given above for the σ_x failure case.

4.4.4.3 45° Drop-off Laminate

Figures 50 and 51 show normalized σ_x stresses for Layers 1 and 3, respectively. The critical elements were in the upper 90° ply of Layer 3, with values in the lower 90° ply nearly critical. Thus, the effect of the drop-off is not severe enough to override the low load-carrying capabilities of the 90° plies, since the load carried by the dropped 45° ply is much less than that carried by the dropped 0° ply of the previous case. Much of the load carried by the dropped ply was shifted to the

83

PLY

-45	-.25	-.23	-.24	-.26	-.25	-45
45	-.22	-.26	-.27	-.27	-.32	45
0	-.14	-.15	-.16	-.16	-.17	0
90	-.29	-.30	-.31	-.32	-.33	90
0	-.15	-.16 -.16 -.16 -.16 -.16 -.16 -.16 -.16			-.16	0
0	-.16 -.16 -.16 -.18 -.16 -.17 -.17 -.16			-.15		0
90	-.30 -.28 -.24 -.15 .96 -.49 -.35 -.31 -.30					90
0	-.14 -.13 -.11 -.09 -.16 -.57 -.33 -.31 -.31					
0	-.15 -.15 -.15 -.15 -.19 .19 -.17 -.16 -.16					0
		-.16 -.16 -.16				
-45	-.26	-.25	-.25	-.25	-.25	-45
45	-.25	-.27	-.26	-.26	-.27	45
0	-.16	-.16	-.16	-.16	-.16	0
-45	-.27	-.20	-.19	-.19	-.17	-45

Figure 46. Normalized Values for σ_x in Layer 1 for the 0° Drop-off Case, Large Resin Pocket, Under RTD Conditions where $\bar{\sigma}_x = -18.8$ ksi.

PLY

-45	-.19	-.21	-.21	-.21	-.24	-45
45	-.23	-.24	-.24	-.25	-.25	45
0	-.17	-.16	-.16	-.16	-.16	0
90	-.36	-.37	-.36	-.38	-.39	90
0	-.16 -.16 -.16 -.16 -.16 -.16 -.16 -.16 -.16			-.16		0
0	-.16 -.16 -.16 -.17 -.17 -.17 -.17 -.16 -.15					0
90	-.34 -.32 -.29 -.20 1.03 -.54 -.41 -.37 -.37					90
0	-.14 -.13 -.11 -.09 -.16 -.61 -.39 -.37 -.37					
0	-.14 -.14 -.14 -.15 -.19 .19 -.17 -.17 -.17					0
		-.15 -.16 -.17				
-45	-.21	-.23	-.22	-.24	-.24	-45
45	-.24	-.24	-.24	-.25	-.24	45
0	-.16	-.15	-.16	-.16	-.16	0
-45	-.17	-.20	-.20	-.20	-.21	-45

Figure 47. Normalized Values for σ_x in Layer 3 for the 0° Drop-off Case, Large Resin Pocket, Under RTD Conditions, where $\bar{\sigma}_x = -18.8$ ksi.

84

PLY

-45	.69	.66	.70	.75	.74	-45
45	.62	.71	.74	.77	.88	45
0	.26	.30	.32	.33	.32	0
90	.46	.46	.47	.49	.50	90
0	.30	.32 .31 .34	.33 .32 .31 .32	.32 .33	.33	0
0	.32	.32 .34 .34	.31 .32 .34 .33		.30	0
90	.44	.43 .41 .47	1.00 .74 .55 .47		.44	90
0	.24	.22 .23 .31	.20 .79 .54 .45		.45	90
0	.26	.27 .31 .30	.33 .31 .29 .27		.26	0
		.31	.31 .29			
-45	.77	.72	.67	.69	.69	-45
45	.70	.72	.69	.68	.72	45
0	.32	.35	.37	.37	.33	0
-45	.79	.65	.60	.58	.54	-45

Figure 48. Normalized Values for σ_{eff} in Layer 1 for the 0° Drop-off Case, Large Resin Pocket, Under RTD Conditions, where $\bar{\sigma}_x = -31.0$ ksi.

PLY

-45	.59	.63	.65	.65	.73	-45
45	.69	.68	.68	.70	.68	45
0	.30	.29	.30	.29	.28	0
90	.41	.41	.41	.41	.40	90
0	.26	.26 .26 .27	.27 .27 .26 .27	.27 .27	.27	0
0	.27	.27 .27 .28	.27 .28 .29 .28		.26	0
90	.39	.37 .35 .41	.95 .66 .48 .41		.36	90
0	.23	.21 .19 .24	.19 .72 .49 .41		.39	0
0	.24	.24 .25 .25	.32 .33 .32 .31		.30	0
		.26	.28 .30			
-45	.68	.70	.67	.71	.74	-45
45	.76	.72	.70	.72	.71	45
0	.27	.30	.31	.31	.31	0
-45	.61	.67	.67	.67	.73	-45

Figure 49. Normalized Values for σ_{eff} in Layer 3 for the 0° Drop-off Case, Large Resin Pocket, Under RTD Conditions, where $\bar{\sigma}_x = -31.0$ ksi.

PLY

-45	-.65	-.63	-.67	-.63	-45
45	-.62	-.68	-.71	-.83	45
0	-.40	-.42	-.44	-.45	0
90	-.82	-.84	-.85	-.86	90
0	-.43	-.43	-.42	-.43	0
0	-.44	-.42	-.42	-.42	0
90	-.87	-.86	-.83	-.87	90
0	-.43	-.43	-.41	-.42	0

Overlain region (Figure 50):
.44 .42 .41
-.45 -.45 -.44 -.42 -.42 -.42 -.41 -.40 -.40 -.40   (0)
-.49 -.46 -.43 -.41 -.37 -.36 -.36 -.39 -.39 -.40   (0)
-.89 -.76 -.64 -.19 .18 .67 .73 .74 .61 -.72   (-45 / 45)
-.73 -.70 -.60 .65 .66 -.60 -.57 -.59
.85 -.63 -.60
-.46 -.45 -.43 -.41 -.41 -.40 -.40   (0)
-.74 -.56 -.53 -.53 -.53 -.49 -.43   (-45)

Figure 50. Normalized Values for σ_x in Layer 1 for the 45°
Drop-off Case, Small Resin Pocket, Under RTD Conditions, where
$\bar{\sigma}_x = -55.0$ ksi.

PLY

-45	-.56	-.59	-.59	-.64	-45
45	-.62	-.63	-.63	-.61	45
0	-.44	-.43	-.42	-.40	0
90	-1.00	-1.00	-.98	-.99	90
0	-.43	-.43	-.43	-.43	0
0	-.44	-.43	-.42	-.42	0
90	-.99	-.98	-.94	-.97	90
0	-.43	-.43	-.42	-.43	0

Overlain region (Figure 51):
.44 .42 .42
-.45 -.44 -.44 -.42 -.43 -.42 -.41 -.40 -.41 -.41   (0)
-.46 -.46 -.45 -.44 -.39 -.37 -.38 -.39 -.39 -.38   (0)
-.67 -.72 -.69 -.20 .15 .56 .64 .67 .51 -.51   (-45 / 45)
-.69 -.68 -.63 .67 .58 -.51 -.58 -.58
.61 -.60 -.59
-.44 -.42 -.42 -.41 -.41 -.41 -.42   (0)
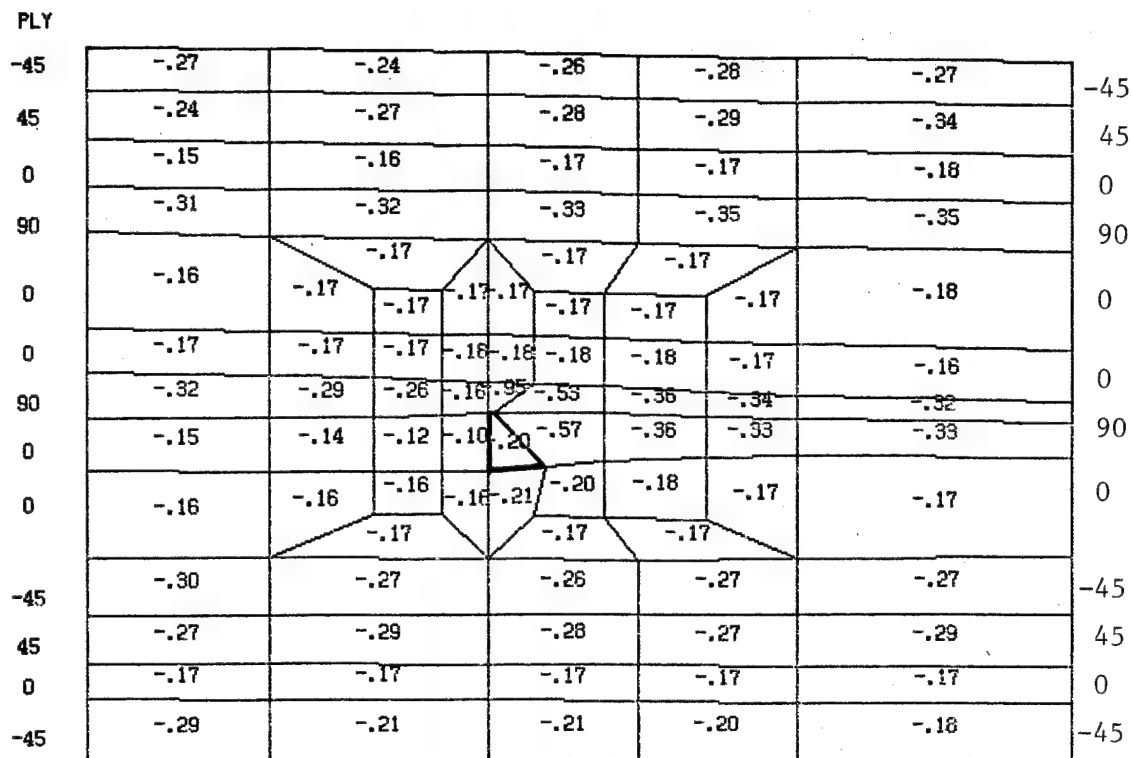-.47 -.54 -.53 -.52 -.53 -.54 -.57   (-45)
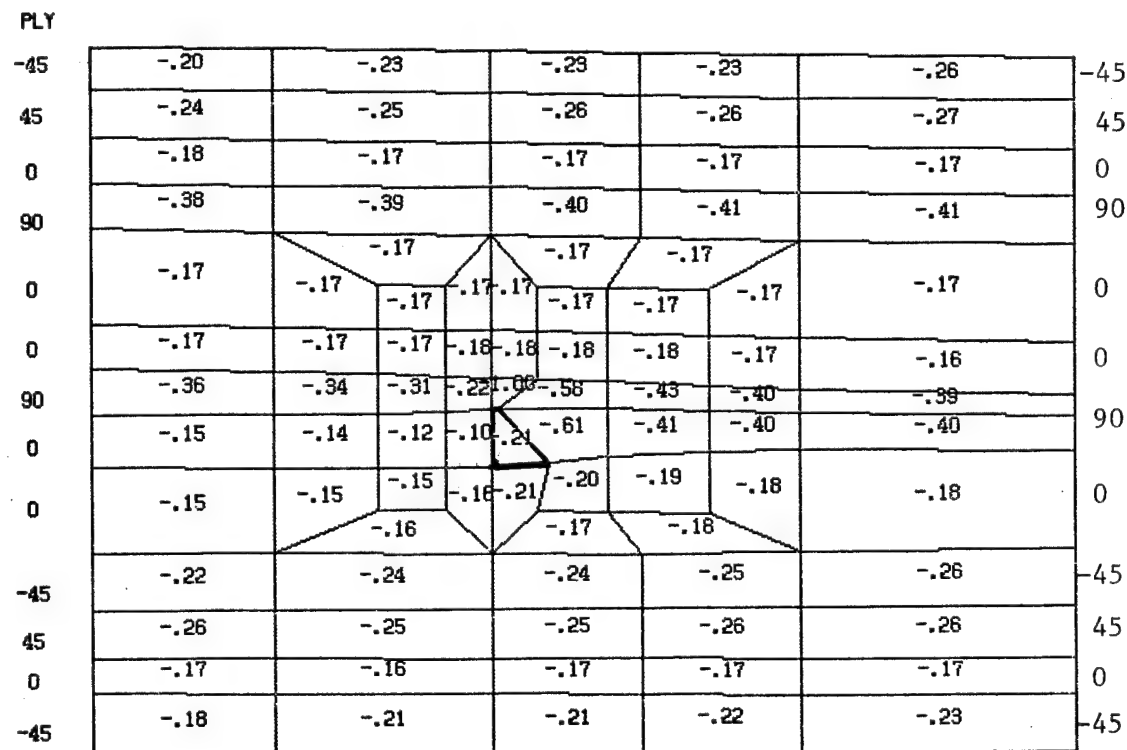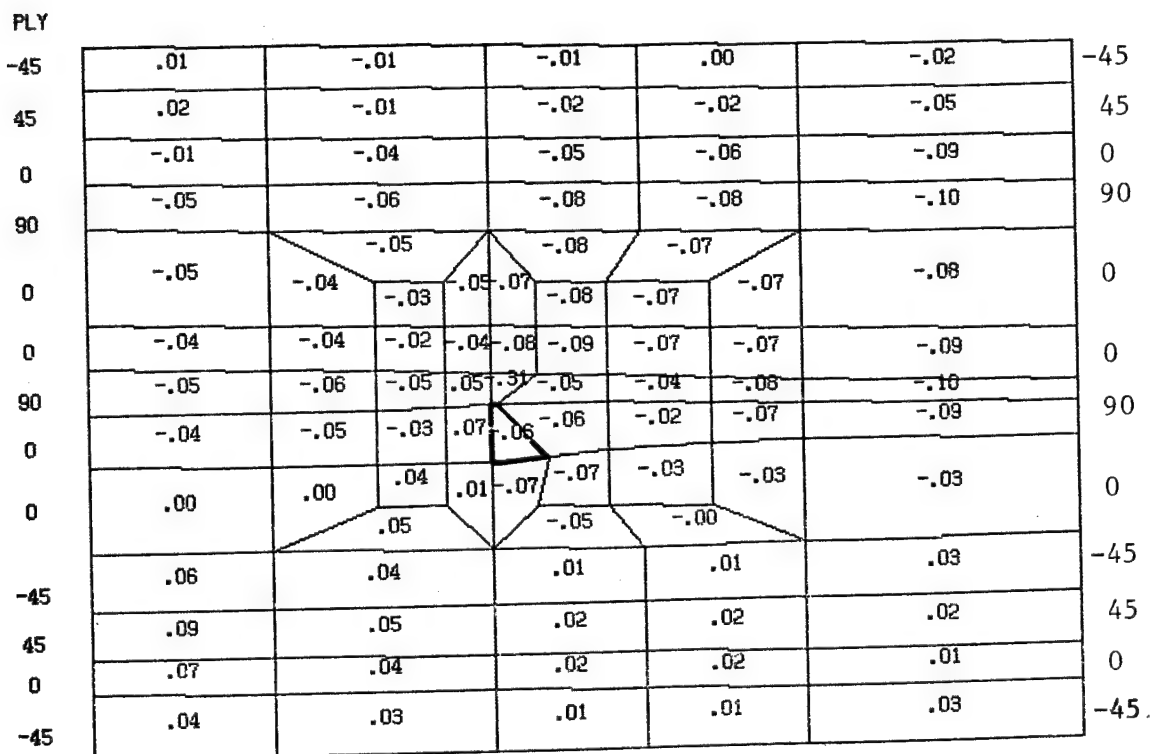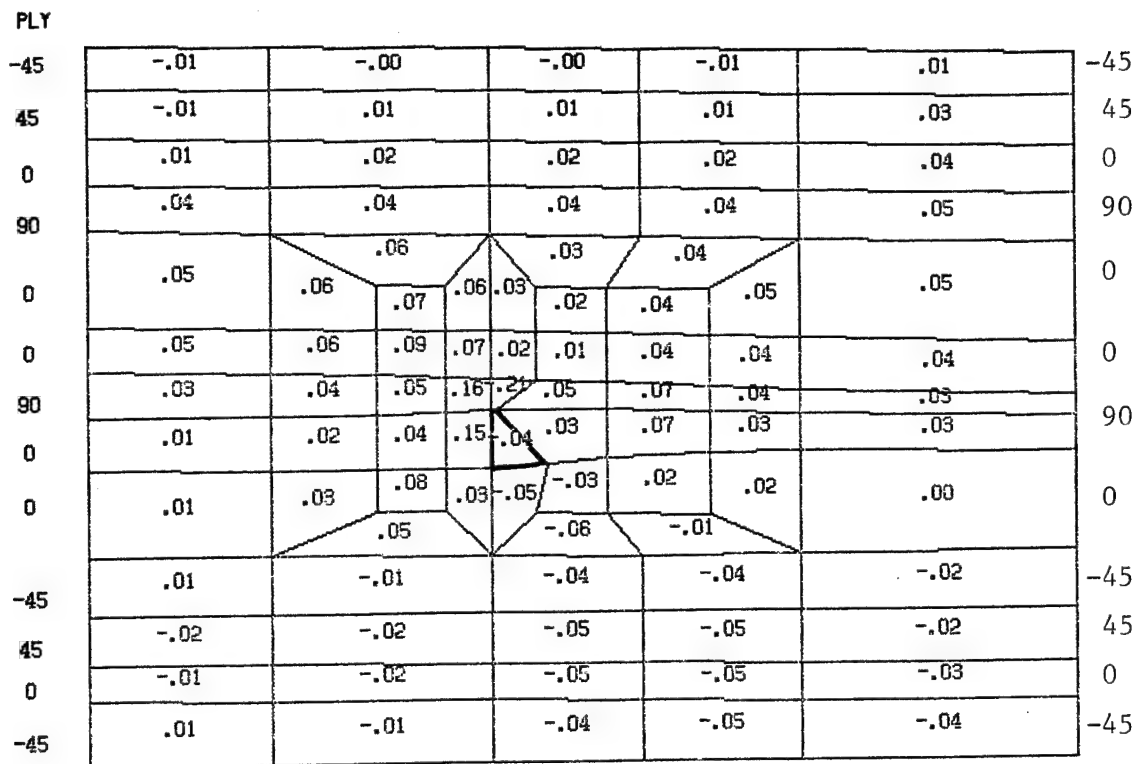
Figure 51. Normalized Values for σ_x in Layer 3 for the 45°
Drop-off Case, Small Resin Pocket, Under RTD Conditions, where
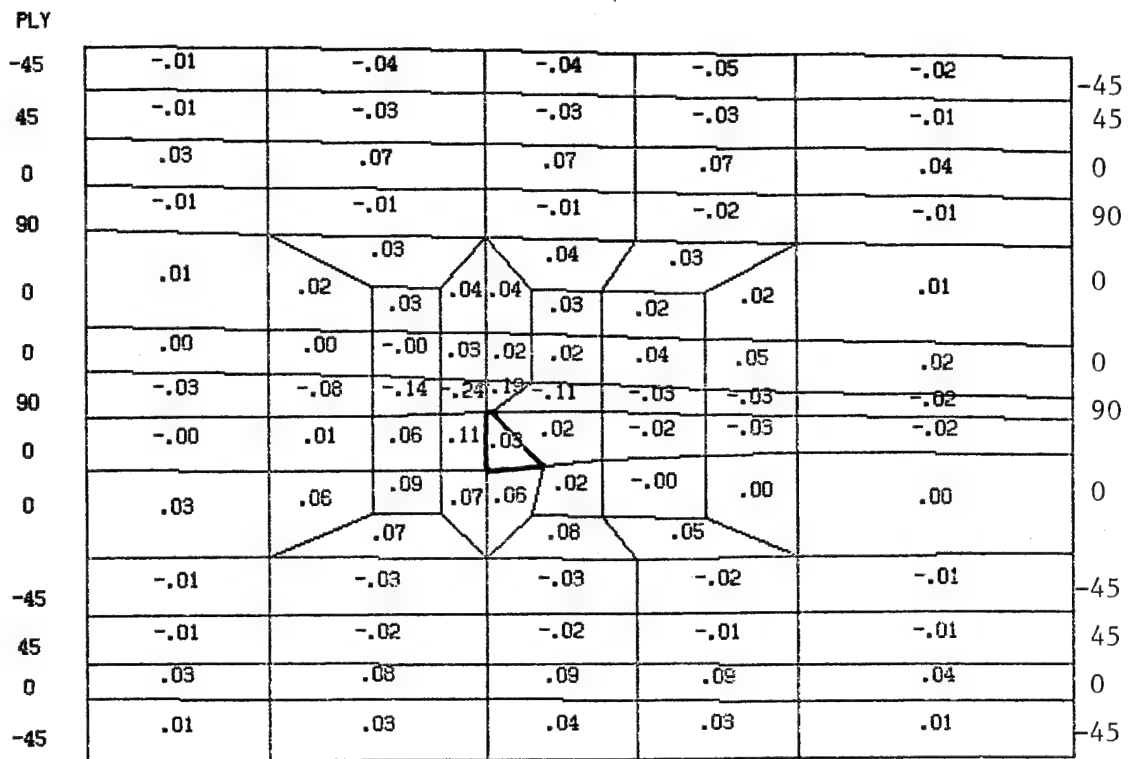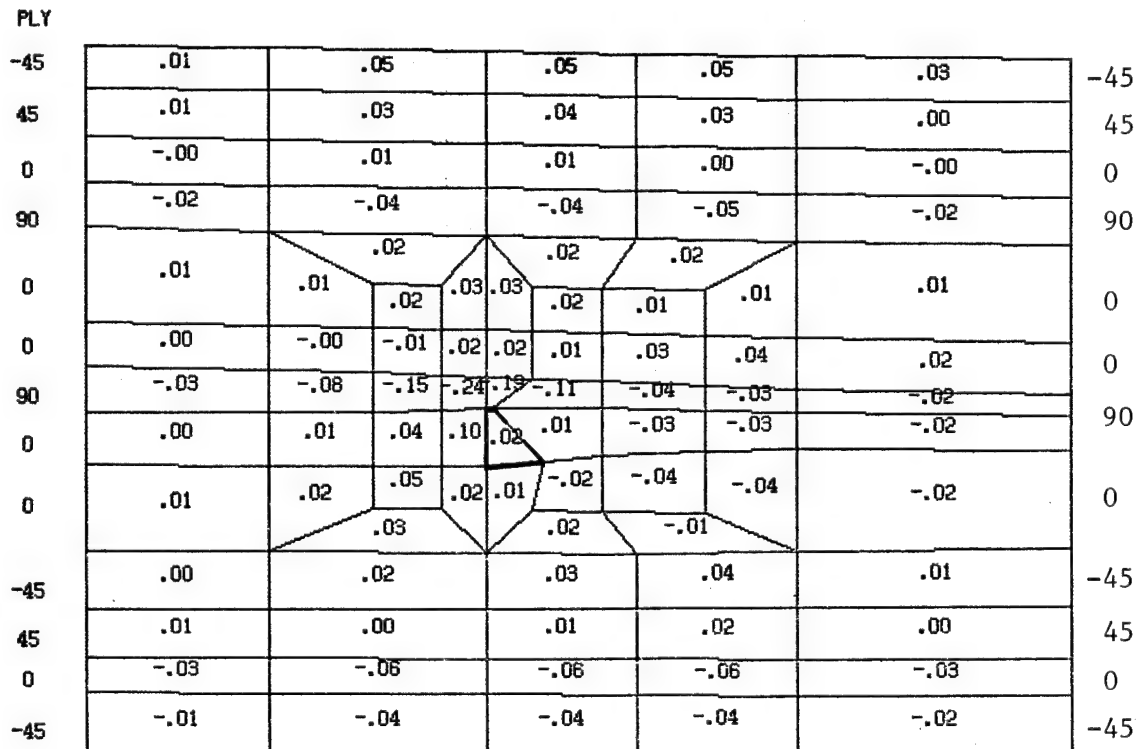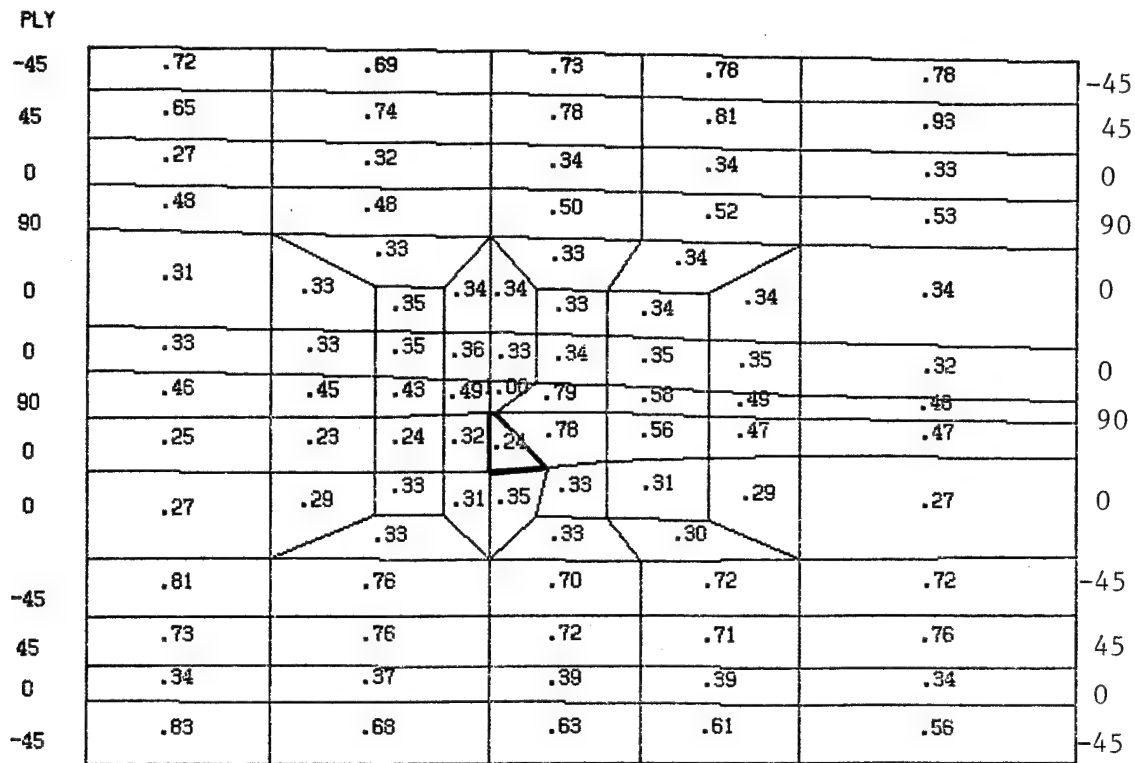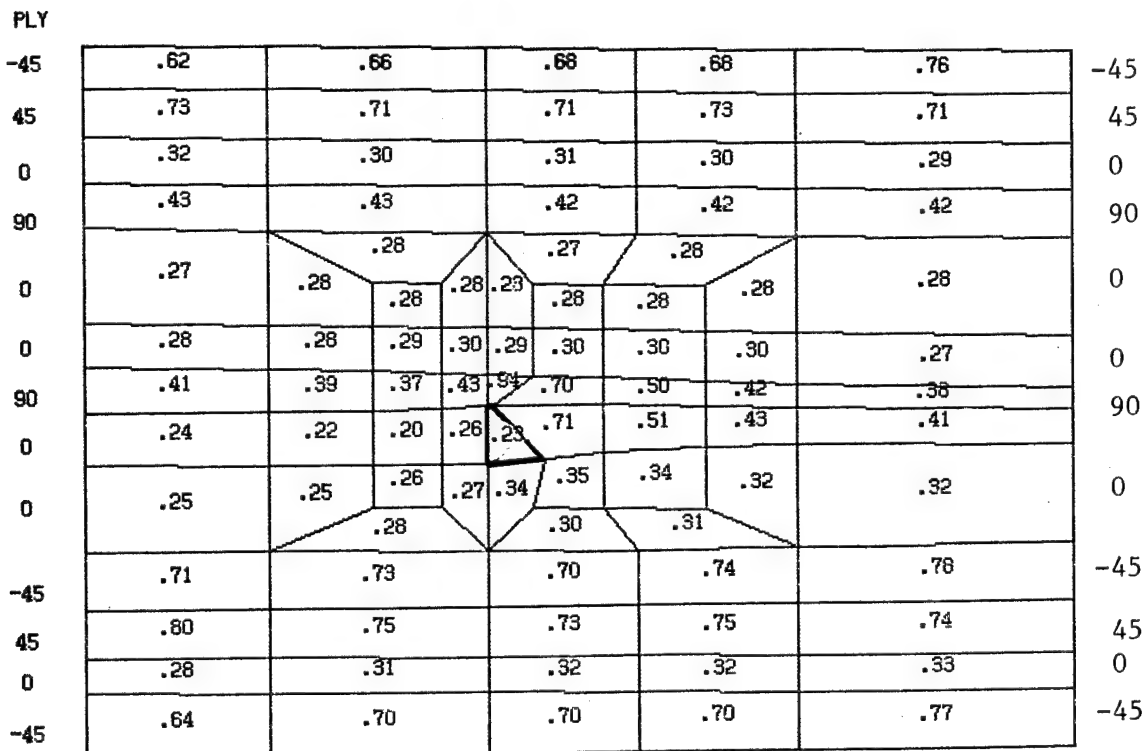$\bar{\sigma}_x = -55.0$ ksi.

leftmost element of this ply, bringing the normalized value of the leftmost element in Layer 1 for that ply up to -0.89, whereas values around the drop-off and resin pocket areas were smaller. The lower values in the resin pocket itself are due to the resin pocket being less stiff than the 45° ply below it. The applied stress at failure is $\overline{\sigma}_x$ = -55.0 ksi, which is larger than that for the no drop-off case (-52.7 ksi), because the dropped ply transfers more load to the 0° ply above it, making the laminate more efficient since 0° plies are the best load carriers.

The only other significant stress was τ_{xy}, shown in Figures 52 and 53. This in-plane shear stress is negligible in the 0° and 90° plies, and quite pronounced in the 45° plies, as expected. The leftmost element in the dropped -45° ply in Layer 1 reached -0.85, with the diagonally opposite element in the upper 45° ply reaching 0.82

Normalized effective stress is shown in Figures 54 and 55 for Layers 1 and 3, respectively. The critical element is the leftmost element of the dropped ply in Layer 1. This results because of the combination of large σ_x and τ_{xy} stresses acting on that element. The high value of 0.97 in the element diagonally opposite the critical element results from the same combination of σ_x and τ_{xy} stresses acting there. The failure stress $\overline{\sigma}_x$ was -38.0 ksi, 30 percent below that required to fail an element if the maximum normal stress failure criterion was used.

Results for the large resin pocket case were almost identical to those for the small resin pocket case, the only difference being smaller values for elements now considered resin pockets, which were formerly +45° elements. Results for σ_x and effective stress are shown in Figures 56 through 59. These figures are nearly identical to those for the small resin pocket case. All critical elements are the same, and the required applied stress to produce them was also the same. Thus, resin pocket size had little influence on the strength of these 45° drop-off laminates.

4.4.5 Results for the Elevated Temperature, Wet (ETW) Case

Assuming a stress-free state at room temperature and no moisture content, a hygrothermal load was applied in five load increments to bring the temperature up to 218°F and moisture up to 1% by weight, to correspond with the conditions under which testing was done at Northrop in the second-year

PLY					PLY
-45	-.55	-.48	-.52	-.46	-45
45	.52	.58	.59	.82	45
0	-.05	-.08	-.07	-.05	0
90	-.01	-.02	-.02	-.01	90
0	-.00	-.00	-.00	-.00	0
0	-.00	-.00	-.00	-.00	0
90	-.00	-.00	-.00	.00	90
0	.00	-.00	-.00	-.00	0

(lower region values)

PLY											PLY
0	.01	.01	.00	-.00	-.00	-.00	-.00	-.00	-.00	-.00	0
0	.05	.05	.04	-.03	-.02	-.01	-.02	-.02	-.04	-.04	0
-45	-.85	-.65	-.48	-.03	.02	-.73	-.81	-.80	.41	.64	45
45	.60	.59	.47	.40	.44	.39	.45	.42	.43		0
0	-.01	.01	.01	.01			.01	.00	-.00		0
-45	-.57	-.26	-.23	-.25			-.26	-.23	-.15		-45

Figure 52. Normalized Values for τ_{xy} in Layer 1 for the 45° Drop-off Case, Small Resin Pocket, Under RTD Conditions, where $\bar{\sigma}_x = -55.0$ ksi.

PLY					PLY
-45	-.40	-.39	-.40	-.39	-45
45	.46	.49	.48	.41	45
0	-.05	-.05	-.05	-.06	0
90	-.01	-.01	-.01	-.01	90
0	-.00	-.00	-.00	-.00	0
0	.00	.00	.00	.00	0
90	.00	.00	.00	.00	90
0	.00	-.01	.00	-.00	0

(lower region values)

PLY											PLY
0	.02	.01	.00	-.02	-.02	-.01	.01	-.00	-.01	-.01	0
0	.07	.05	.03	-.11	-.04	.01	.00	.00	-.05	-.06	0
-45	-.54	-.62	-.58	-.06	.03	-.51	-.64	-.69	.29	.29	45
45	.57	.58	.48	.33	.33	.38	.48	.45			0
0	-.01	.02	.00	.37	.41	.02	.03	.01	.02		0
-45	-.21	-.30	-.28	-.24			-.24	-.29	-.24		-45

Figure 53. Normalized Values for τ_{xy} in Layer 3 for the 45° Drop-off Case, Small Resin Pocket, Under RTD Conditions, where $\bar{\sigma}_x = -55.0$ ksi.

88

-45	.76	.77	.81	.79	-45
45	.74	.82	.86	.97	45
0	.29	.34	.35	.34	0
90	.52	.52	.53	.53	90
0	.36	.36	.36	.36	0
0	.37	.36	.35	.34	0
90	.54	.53	.51	.51	90
0	.32	.32	.31	.31	0

.31 | .31 | .30 | .30
.31 | .32 | .31 | .30 | .30 | .30 | .29 | .28 | .28 | .28
.35 | .38 | .40 | .38 | .32 | .28 | .27 | .28 | .29 | .28
1.00 | .90 | .82 | .18 | .17 | .68 | .73 | .76 | .73 | .79
.84 | .80 | .74 | .84 | .80 | .72 | .70 | .66 | .69 | .73
.37 | .35 | .34 | .32 | .32 | .32 | .31
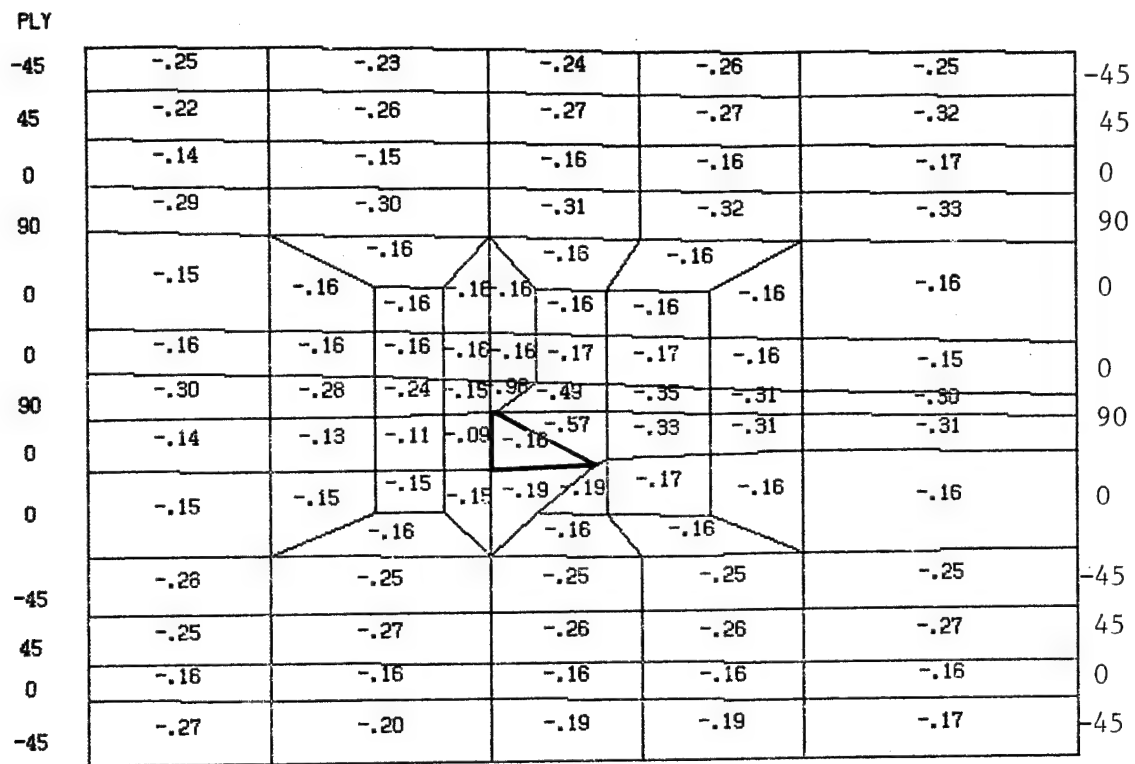.88 | .76 | .72 | .71 | .69 | .63 | .56
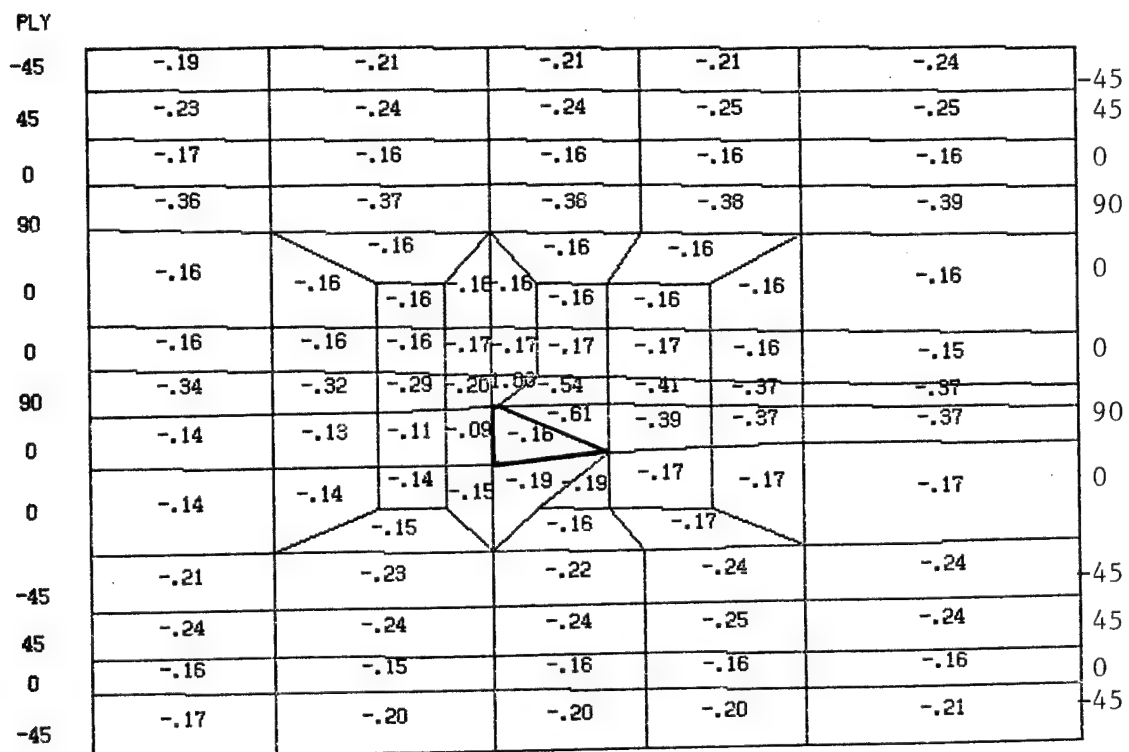
Figure 54. Normalized Values for σ_{eff} in Layer 1 for the 45° Drop-off Case, Small Resin Pocket, Under RTD Conditions, where $\bar{\sigma}_x = -38.0$ ksi.

-45	.70	.74	.74	.80	-45
45	.77	.76	.76	.71	45
0	.32	.31	.31	.29	0
90	.46	.45	.44	.43	90
0	.30	.30	.29	.29	0
0	.31	.30	.29	.29	0
90	.48	.47	.45	.46	90
0	.31	.30	.29	.29	0

.31 | .30 | .29 | .29
.31 | .31 | .31 | .29 | .30 | .30 | .29 | .29 | .28 | .28
.32 | .33 | .35 | .37 | .35 | .31 | .29 | .28 | .28 | .28
.90 | .93 | .94 | .17 | .18 | .65 | .71 | .74 | .66 | .64
.93 | .88 | .85 | .95 | .80 | .78 | .65 | .71 | .71 | .64
.33 | .41 | .45 | .45 | .43 | .39 | .35
.66 | .74 | .74 | .74 | .76 | .77 | .86
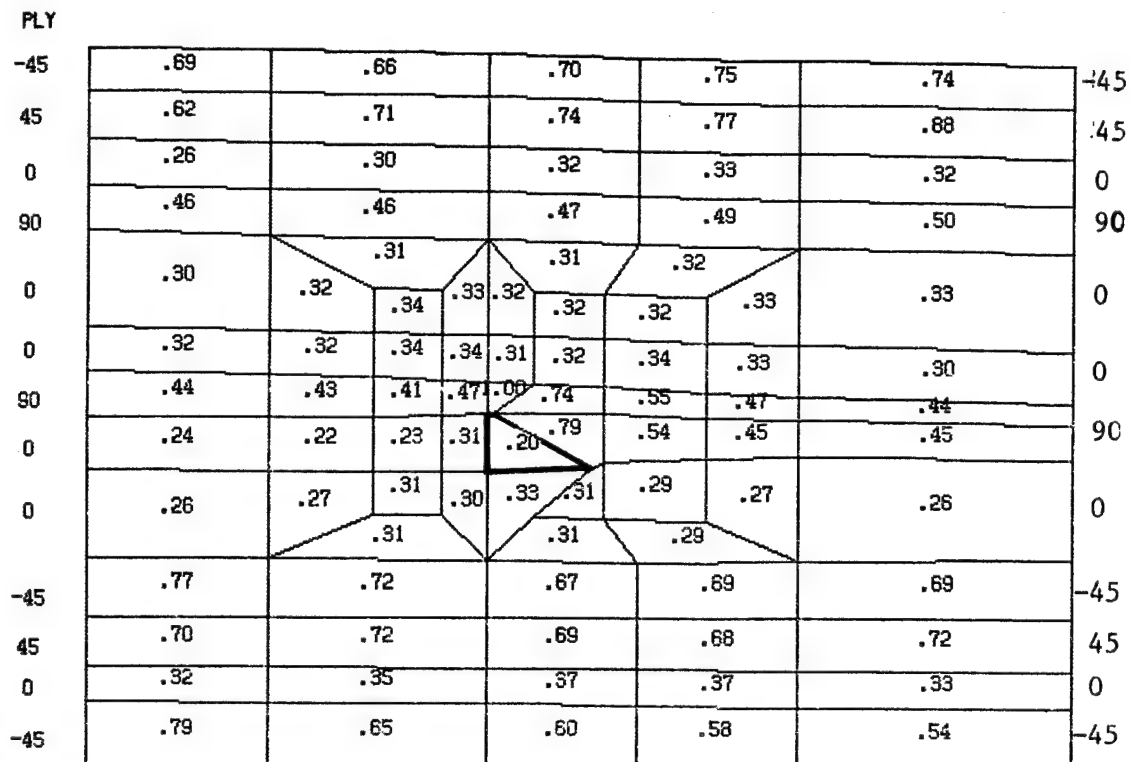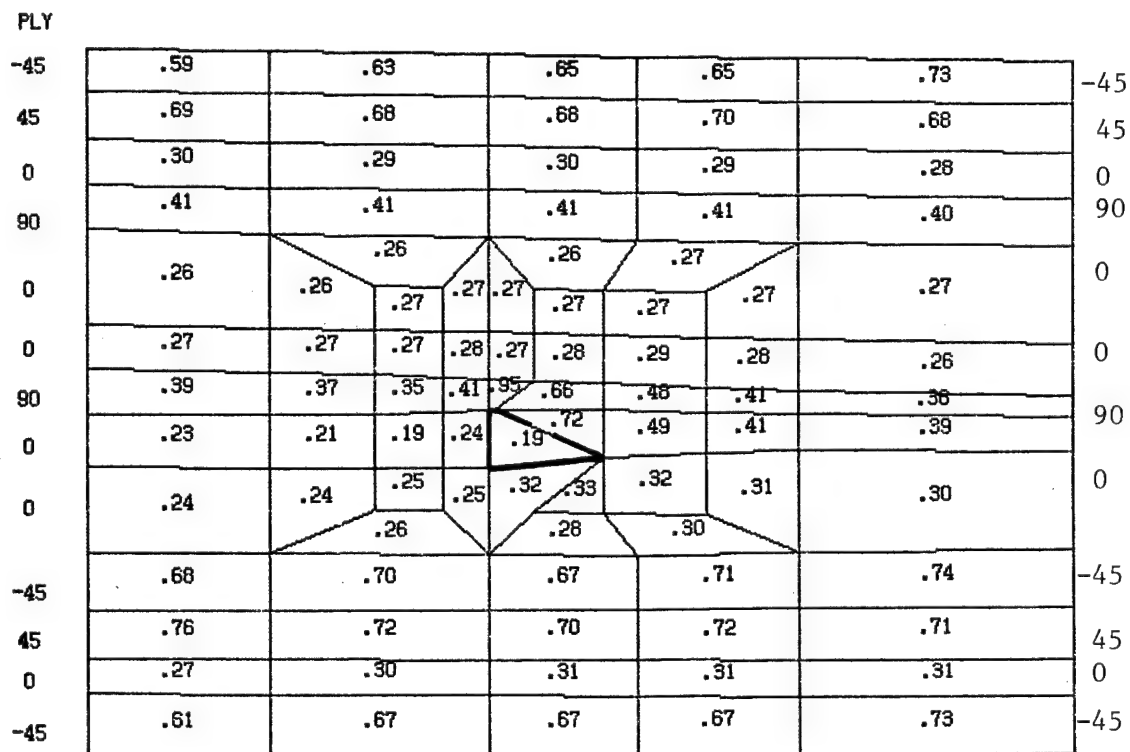
Figure 55. Normalized Values for σ_{eff} in Layer 3 for the 45° Drop-off Case, Small Resin Pocket, Under RTD Conditions, where $\bar{\sigma}_x = -38.0$ ksi.

89

Figure 56

PLY					
-45	-.65	-.63	-.67	-.62	-45
45	-.62	-.68	-.71	-.83	45
0	-.40	-.42	-.44	-.45	0
90	-.82	-.84	-.85	-.86	90
0	-.43	-.43	-.42	-.43	0
0	-.44	-.42	-.42	-.42	0
90	-.87	-.86	-.83	-.87	90
0	-.43	-.43	-.41	-.42	0

PLY										
0		.44		.42			.41			0
	-.45	-.45	-.44	-.42	-.42	-.42	-.41	-.40	-.41	-.40
0	-.49	-.46	-.43	-.41	-.37	-.37	-.38	-.39	-.39	-.40
-45	-.89	-.76	-.64	-.19	.17	.13	.14	.15	-.61	-.72	45
	-.73	-.70	-.59	-.64	-.59	-.57	-.56	-.61		
45		.65		-.62	-.60		-.41	-.40	-.40	0
0	-.46	-.45	-.43	-.41	-.41	-.40	-.40		
-45	-.74	-.56	-.53	-.54	-.53	-.50	-.44	-45

Figure 56. Normalized Values for σ_x in Layer 1 for the 45° Drop-off Case, Large Resin Pocket, Under RTD Conditions, where $\bar{\sigma}_x = -55.0$ ksi.

Figure 57

PLY					
-45	-.56	-.59	-.59	-.64	-45
45	-.62	-.63	-.63	-.61	45
0	-.44	-.43	-.42	-.40	0
90	-1.00	-1.00	-.98	-.99	90
0	-.43	-.43	-.43	-.43	0
0	-.44	-.43	-.42	-.42	0
90	-.99	-.98	-.94	-.97	90
0	-.43	-.43	-.42	-.43	0

PLY										
0		.44		.42			.42			0
	-.45	-.44	-.44	-.42	-.43	-.42	-.41	-.40	-.41	-.40
0	-.46	-.46	-.45	-.44	-.39	-.38	-.39	-.39	-.38	-.38
-45	-.67	-.72	-.69	-.20	.14	.12	.13	.14	-.49	-.51	45
	-.69	-.68	-.63	-.67	-.56	-.52	-.58	-.57		
45		.61		-.60	-.58		-.41	-.41	-.41	0
0	-.44	-.42	-.42	-.41	-.41	-.41	-.41		
-45	-.47	-.54	-.53	-.52	-.53	-.55	-.57	-45

Figure 57. Normalized Values for σ_x in Layer 3 for the 45° Drop-off Case, Large Resin Pocket, Under RTD Conditions, where $\bar{\sigma}_x = -55.0$ ksi.

-45	.76		.77		.81		.79	-45
45	.74		.82		.86		.97	45
0	.30		.34		.35		.34	0
90	.52		.52		.53		.53	90
0	.36		.36		.36		.36	0
0	.37		.36		.35		.34	0
90	.54		.53		.51		.51	90
0	.32		.32		.31		.31	0

.31   .31   .31

.31   .32   .31   .30   .30   .30   .29   .28   .28   .28   0

.35   .38   .40   .37   .31   .28   .27   .26   .28   .28   0

1.00   .90   .82   .18   .18   .18   .18   .20   -45

.84   .80   .74   .82   .74   .69   .67   .72   .75   .80   45

.79   .72

.37   .35   .34   .32   .32   .32   .31   0

.88   .77   .73   .71   .69   .63   .56   -45

Figure 58. Normalized Values for σ_{eff} in Layer 1 for the 45° Drop-off Case, Large Resin Pocket, Under RTD Conditions, where $\bar{\sigma}_x$ = -38.0 ksi.

-45	.70		.74		.74		.80	-45
45	.77		.76		.76		.72	45
0	.32		.31		.31		.29	0
90	.46		.46		.44		.43	90
0	.30		.30		.29		.29	0
0	.31		.30		.29		.29	0
90	.48		.47		.45		.46	90
0	.31		.30		.29		.30	0

.31   .30   .29

.31   .31   .31   .30   .30   .30   .29   .29   .28   .28   0

.33   .33   .35   .37   .35   .31   .30   .29   .28   .28   0

.90   .93   .94   .17   .13   .21   .20   .20   -45

.93   .88   .85   .95   .79   .69   .72   .72   .62   .63   45

.81   .82   .78

.33   .41   .45   .45   .44   .39   .35   0
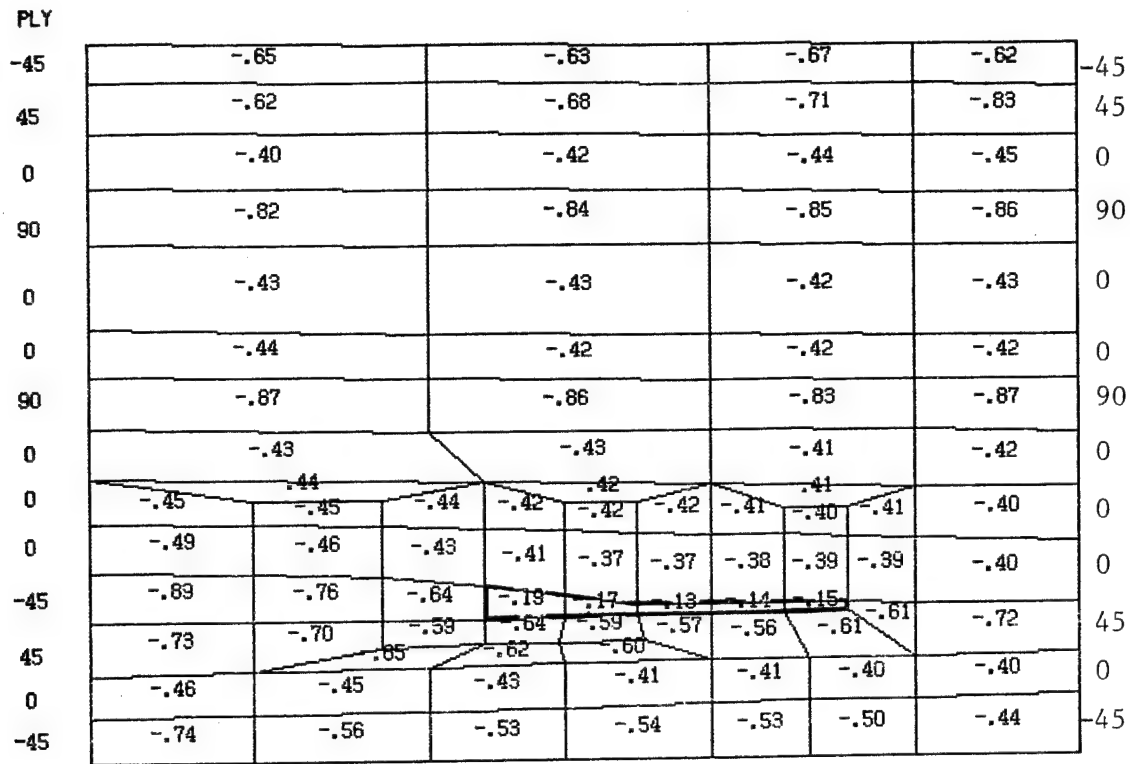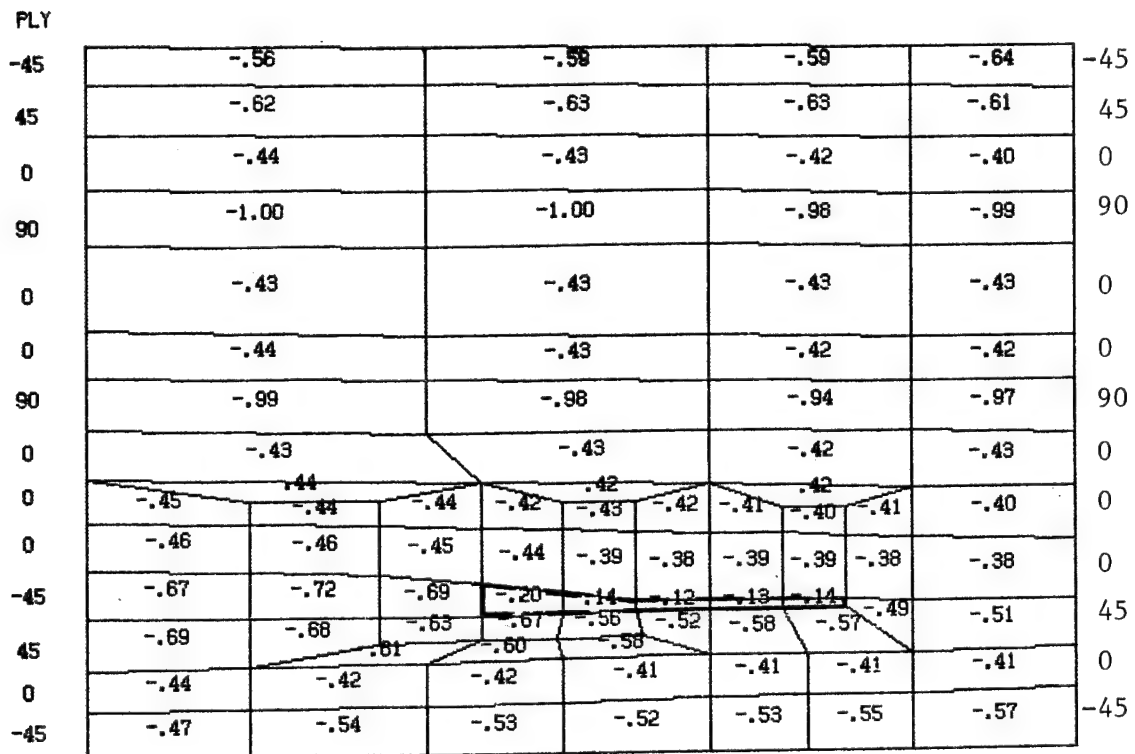
.66   .75   .74   .74   .76   .77   .87   -45

Figure 59. Normalized Values for σ_{eff} in Layer 3 for the 45° Drop-off Case, Large Resin Pocket, Under RTD Conditions, where $\bar{\sigma}_x$ = 38.0 ksi.
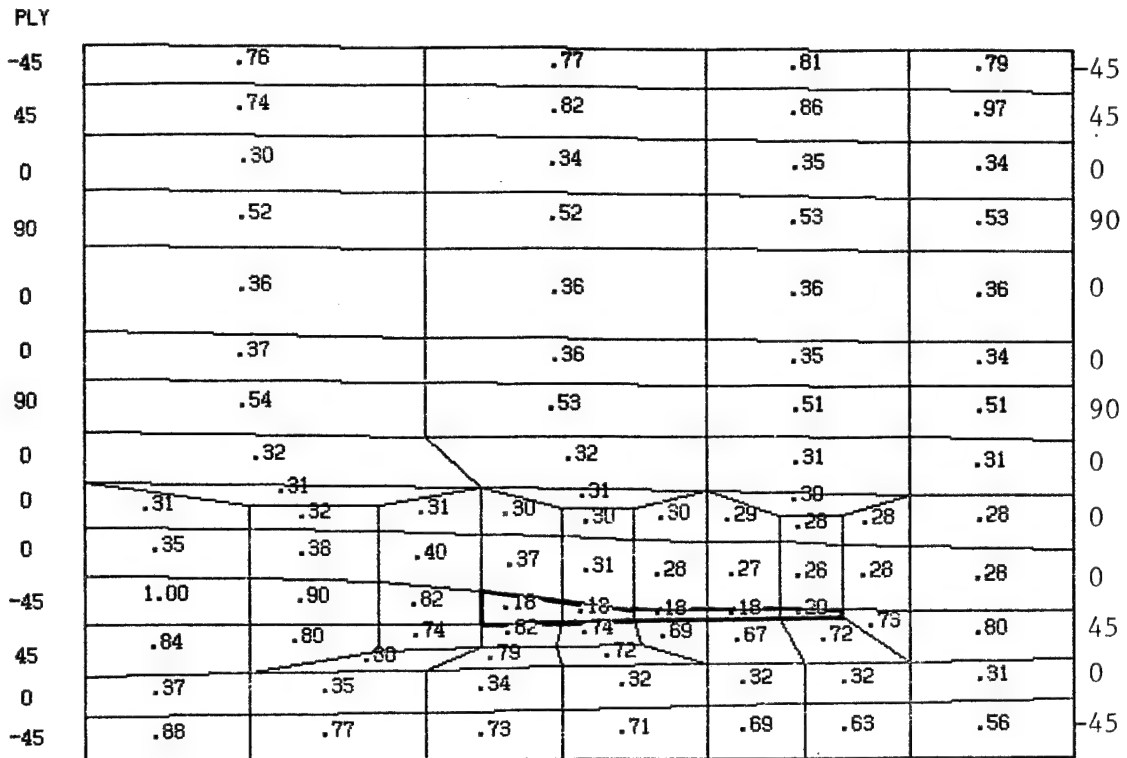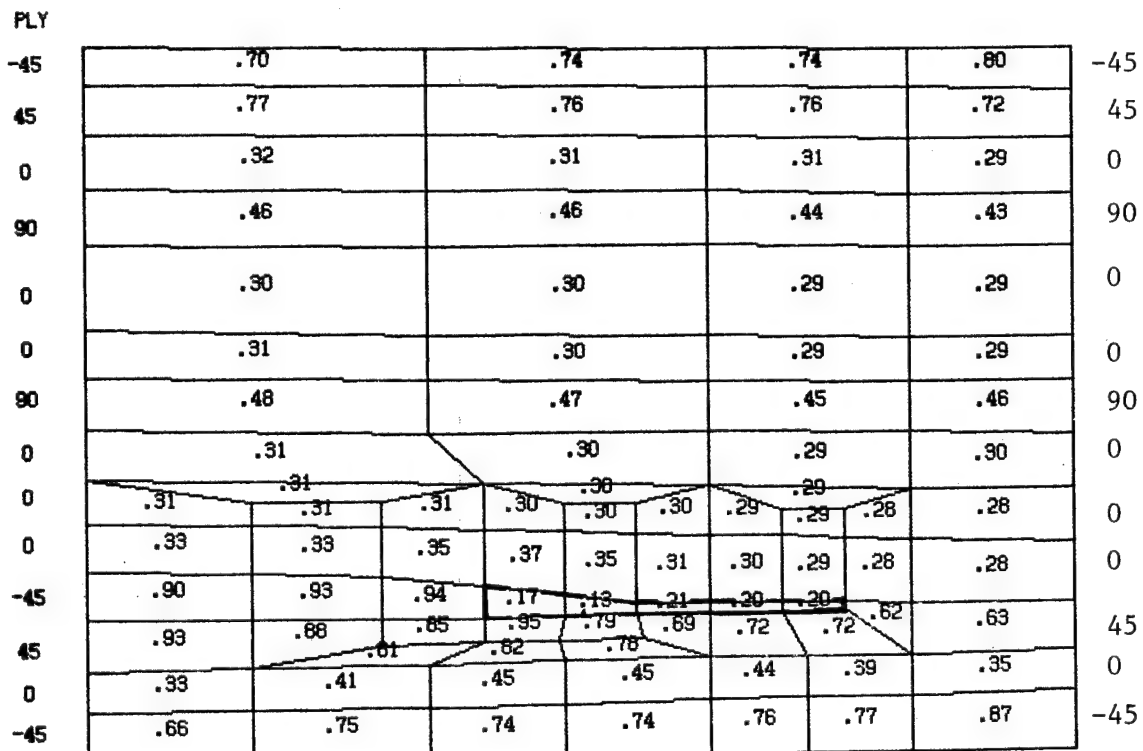
study [3]. In each load increment, temperature was increased uniformly throughout the laminate, in equal amounts of 29.6°F. Moisture content was increased in increments of 0%, 0.1%, 0.2%, 0.3%, and 0.4% for each load increment, respectively, to account for the fact that moisture is absorbed more quickly at higher temperatures. Material properties were allowed to vary with each load increment. At the end of the last increment, an average normal compressive stress was applied in the x-direction, high enough to produce a critical failed element, as in the room temperature, dry case.

Since the size of the resin pocket had no effect on the 45° drop-off case, and only a minor effect on the 0° drop-off case, results are presented for the small resin pocket cases only.

4.4.5.1 Plain Laminate

Figures 60 and 61 show normalized stresses for σ_x in Layers 1 and 3, respectively. As in the RTD case, the critical elements are in the 90° plies. In the present case, however, the 0° plies are loaded very minimally with respect to their ultimate values as compared to the RTD case. This is because the higher thermal and moisture expansion of the 90° plies make them carry a greater share of the load upon mechanical compression loading. Thus they become critical before the 0° plies have an opportunity to become more fully loaded. The failure stress was $\bar{\sigma}_x = -7.2$ ksi for the ETW case. The cause of failure is two-fold; adverse effects of hogrothermally-induced stresses before mechanical loading occurs, and reduction of material strengths themselves due to elevated temperature and moisture.

Results presented for the RTD case for stresses σ_y, σ_z, τ_{yz}, and τ_{xz} are not repeated here for the ETW case because 1) all of these stresses were small in the RTD case to begin with, and were presented then for a one-time comparison, and 2) they were made even smaller in this case, probably due to a leveling-out effect of the hygrothermal loads.

Results for the in-plane shear stress τ_{xy} are presented in Figures 62 and 63 for Layers 1 and 3 respectively. As expected, values are low for the 0° and 90° plies, and somewhat higher for the 45° plies. The value of 0.57 in the upper right element of the first layer made this element critical in effective stress.
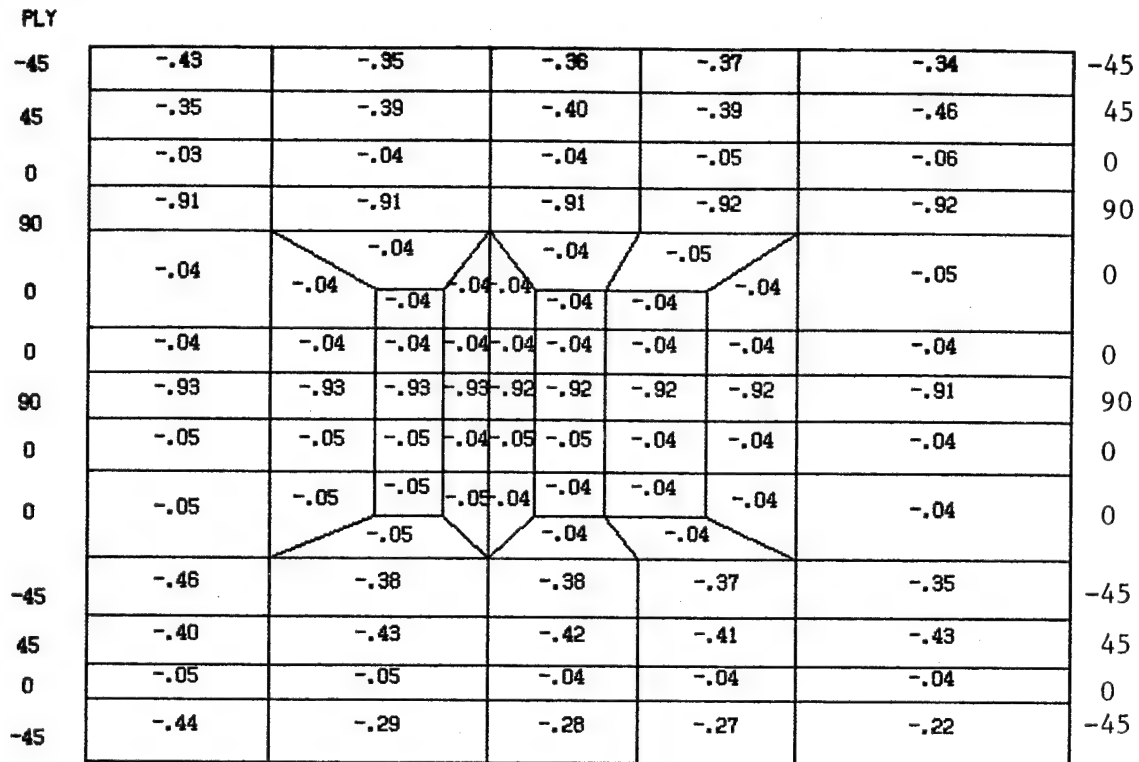
92

PLY

PLY (left)						PLY (right)
-45	-.43	-.35	-.36	-.37	-.34	-45
45	-.35	-.39	-.40	-.39	-.46	45
0	-.03	-.04	-.04	-.05	-.06	0
90	-.91	-.91	-.91	-.92	-.92	90
0	-.04	-.04 / -.04	-.04 / -.04 / -.04	-.05 / -.04 / -.04	-.05	0
0	-.04	-.04 / -.04	-.04 / -.04 / -.04	-.04 / -.04	-.04	0
90	-.93	-.93 / -.93	-.93 / -.92 / -.92	-.92 / -.92	-.91	90
0	-.05	-.05 / -.05	-.04 / -.05 / -.05	-.04 / -.04	-.04	0
0	-.05	-.05 / -.05	-.05 / -.04 / -.04	-.04 / -.04	-.04	0
-45	-.46	-.38	-.38	-.37	-.35	-45
45	-.40	-.43	-.42	-.41	-.43	45
0	-.05	-.05	-.04	-.04	-.04	0
-45	-.44	-.29	-.28	-.27	-.22	-45

Figure 60. Normalized Values for σ_x in Layer 1 for the No Drop-off Case, Under ETW Conditions, where $\bar{\sigma}_x$ = -7.2 ksi.

PLY

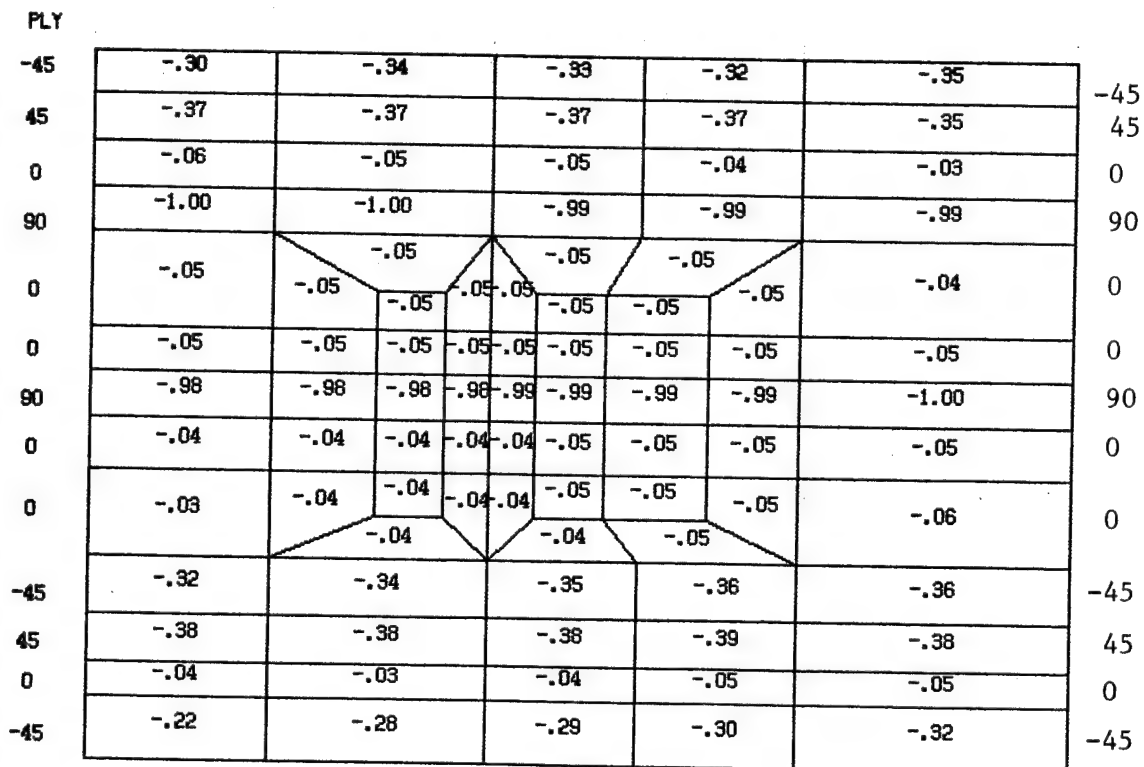| PLY (left)						PLY (right)
-45	-.30	-.34	-.33	-.32	-.35	-45
45	-.37	-.37	-.37	-.37	-.35	45
0	-.06	-.05	-.05	-.04	-.03	0
90	-1.00	-1.00	-.99	-.99	-.99	90
0	-.05	-.05 / -.05	-.05 / -.05 / -.05	-.05 / -.05	-.04	0
0	-.05	-.05 / -.05	-.05 / -.05 / -.05	-.05 / -.05	-.05	0
90	-.98	-.98 / -.98	-.98 / -.99 / -.99	-.99 / -.99	-1.00	90
0	-.04	-.04 / -.04	-.04 / -.04 / -.05	-.05 / -.05	-.05	0
0	-.03	-.04 / -.04	-.04 / -.04 / -.05	-.05 / -.05	-.06	0
-45	-.32	-.34	-.35	-.36	-.36	-45
45	-.38	-.38	-.38	-.39	-.38	45
0	-.04	-.03	-.04	-.05	-.05	0
-45	-.22	-.28	-.29	-.30	-.32	-45

Figure 61. Normalized Values for σ_x in Layer 3 for the No Drop-off Case, Under ETW Conditions, where $\bar{\sigma}_x$ = -7.2 ksi.
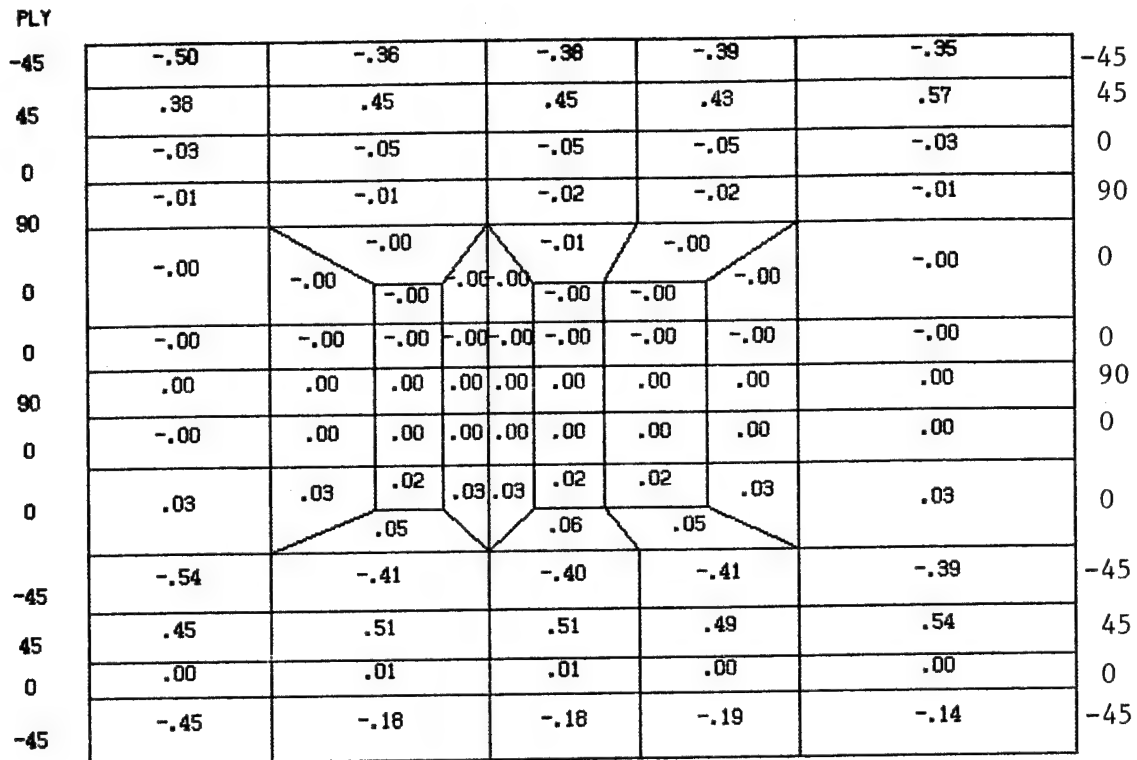
Figure 62. Normalized Values for τ_{xy} in Layer 1 for the No Drop-off Case, Under ETW Conditions, where $\bar{\sigma}_x = -7.2$ ksi.

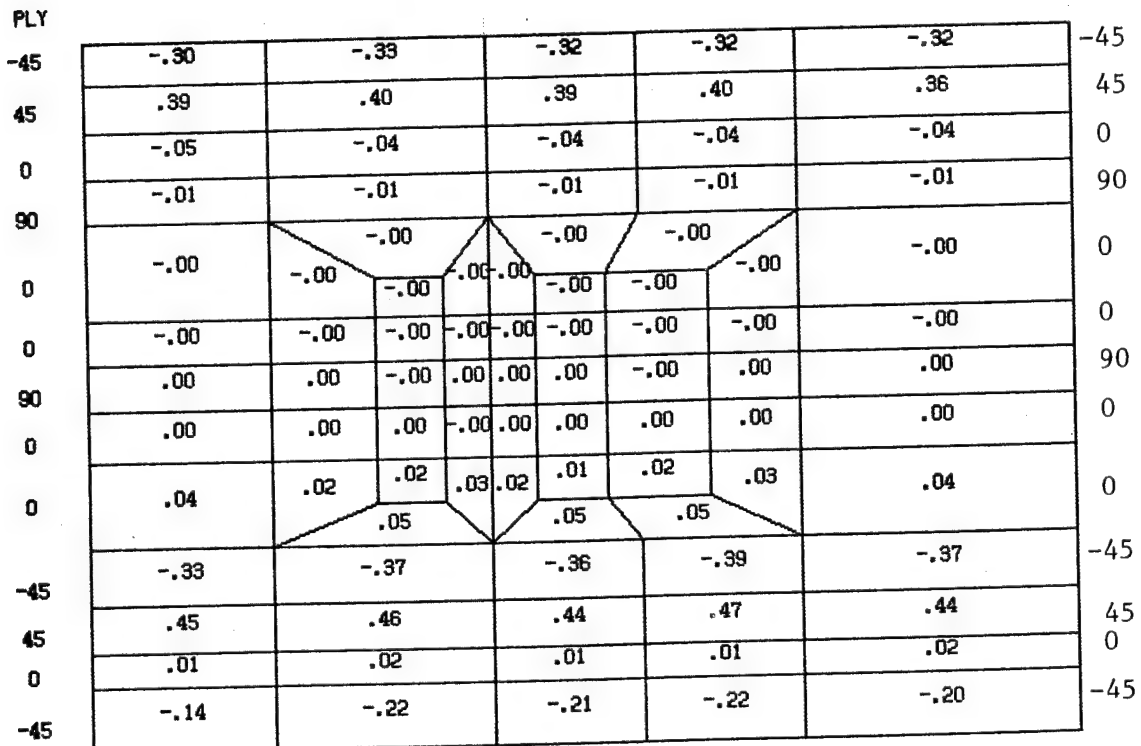| PLY						PLY
−45	−.50	−.36	−.38	−.39	−.35	−45
45	.38	.45	.45	.43	.57	45
0	−.03	−.05	−.05	−.05	−.03	0
90	−.01	−.01	−.02	−.02	−.01	90
0	−.00	−.00 / −.00	−.00 −.00 / −.00	−.01 / −.00 −.00	−.00 / −.00	0
0	−.00	−.00 −.00	−.00 −.00 −.00	−.00 −.00	−.00	0
90	.00	.00 .00	.00 .00 .00	.00 .00	.00	90
0	−.00	.00 .00	.00 .00 .00	.00 .00	.00	0
0	.03	.03 .02	.03 .03 .02 / .05 .06	.02 .03 / .05	.03	0
−45	−.54	−.41	−.40	−.41	−.39	−45
45	.45	.51	.51	.49	.54	45
0	.00	.01	.01	.00	.00	0
−45	−.45	−.18	−.18	−.19	−.14	−45

Figure 63. Normalized Values for τ_{xy} in Layer 3 for the No Drop-off Case, Under ETW Conditions, where $\bar{\sigma}_x = -7.2$ ksi.

PLY						PLY
−45	−.30	−.33	−.32	−.32	−.32	−45
45	.39	.40	.39	.40	.36	45
0	−.05	−.04	−.04	−.04	−.04	0
90	−.01	−.01	−.01	−.01	−.01	90
0	−.00	−.00 / −.00	−.00 −.00 / −.00	−.00 / −.00 −.00	−.00 / −.00	0
0	−.00	−.00 −.00	−.00 −.00 −.00	−.00 −.00	−.00	0
90	.00	.00 −.00	.00 .00 .00	−.00 .00	.00	90
0	.00	.00 .00	−.00 .00 .00	.00 .00	.00	0
0	.04	.02 .02	.03 .02 .01 / .05	.02 .03 / .05	.04	0
−45	−.33	−.37	−.36	−.39	−.37	−45
45	.45	.46	.44	.47	.44	45
0	.01	.02	.01	.01	.02	0
−45	−.14	−.22	−.21	−.22	−.20	−45

94

Normalized effective stresses for Layers 1 and 3 are shown in Figures 64 and 65, respectively. As already stated, the critical element occurs in the upper right 45° element of Layer 1, and results because of the combination of large σ_x and τ_{xy} acting there. Effective stresses for the 90° plies were not critical because of a beneficial σ_z stress (not shown) of about -0.06 acting on them. This value is small, but of the same sign as the critical σ_x stress, thus reducing the effective stress for these 90° plies and permiting a larger applied stress of $\overline{\sigma}_x$ = -14.5 ksi at failure.

Whichever failure criterion is used, however, the allowable applied load for first-element failure was considerably less for the ETW case than for the RTD case, as expected.

4.4.5.2 0° Drop-off Laminate

Figures 66 and 67 show results for normalized σ_x stress in Layers 1 and 3, respectively. As in the RTD case, the critical element is the 90° element immediately above the resin pocket in Layer 3. This time, however, all elements of that ply, especially after the drop-off, are near critical, which results because of the high thermal and moisture expansion of that ply, and the subsequent compression loading of it. The upper 90° ply experienced high values for the same reason. For this case, the failure load was $\overline{\sigma}_x$ = -5.5 ksi, only 25 percent lower than that for the plain laminate. The percentage reduction for the RTD case was 62 percent, indicating that hygrothermal effects influence first-element failure more than ply drop-off effects.

Results for normalized σ_z stresses are shown in Figures 68 and 69, for Layers 1 and 3, respectively. All values are small, as expected, except in the region of the resin pocket where they are higher due to the different expansion rate of the resin pocket itself as compared to that of the 90° elements surrounding it. The high negative value of -0.39 in the element above the resin pocket in Layer 3 greatly reduced the effective stress there, but the low value of -0.01 in the element to the right of the element above the resin pocket in Layer 1 could not reduce effective stress there, making this element critical in effective stress.

Results for effective stress are shown in Figures 70 and 71 for Layers 1 and 3, respectively. The critical element occurred in Layer 1, as already explained. The failure stress was $\overline{\sigma}_x$ = -12.6 ksi, which is much higher than
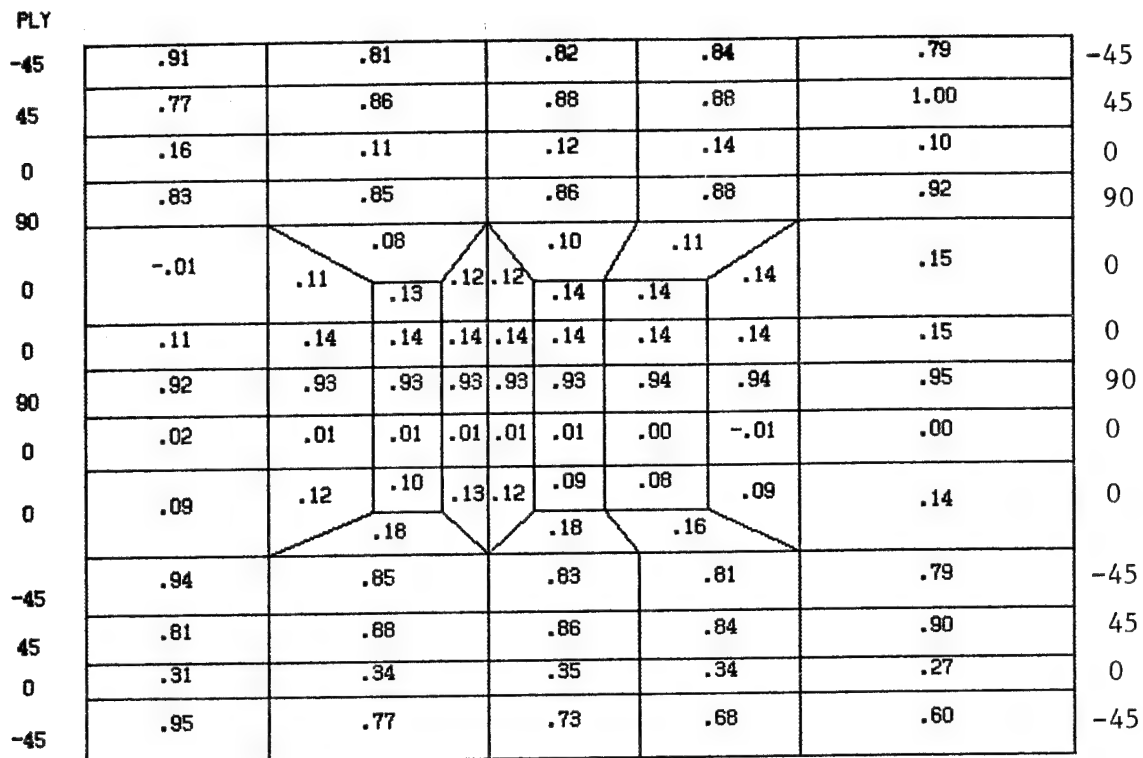
Figure 64:

PLY										PLY
-45	.91		.81		.82		.84		.79	-45
45	.77		.86		.88		.88		1.00	45
0	.16		.11		.12		.14		.10	0
90	.83		.85		.86		.88		.92	90
0	-.01	.11	.08 / .13	.12 / .12	.10	.14	.14	.11 / .14	.15	0
0	.11	.14	.14	.14 / .14	.14	.14	.14	.14	.15	0
90	.92	.93	.93	.93 / .93	.93	.94	.94		.95	90
0	.02	.01	.01	.01 / .01	.01	.00	-.01		.00	0
0	.09	.12	.10 / .18	.13 / .12	.09 / .18	.08 / .16		.09	.14	0
-45	.94		.85		.83		.81		.79	-45
45	.81		.88		.86		.84		.90	45
0	.31		.34		.35		.34		.27	0
-45	.95		.77		.73		.68		.60	-45

Figure 64. Normalized Values for σ_{eff} in Layer 1 for the No Drop-off Case, Under ETW Conditions, where $\bar{\sigma}_x = -14.5$ ksi.
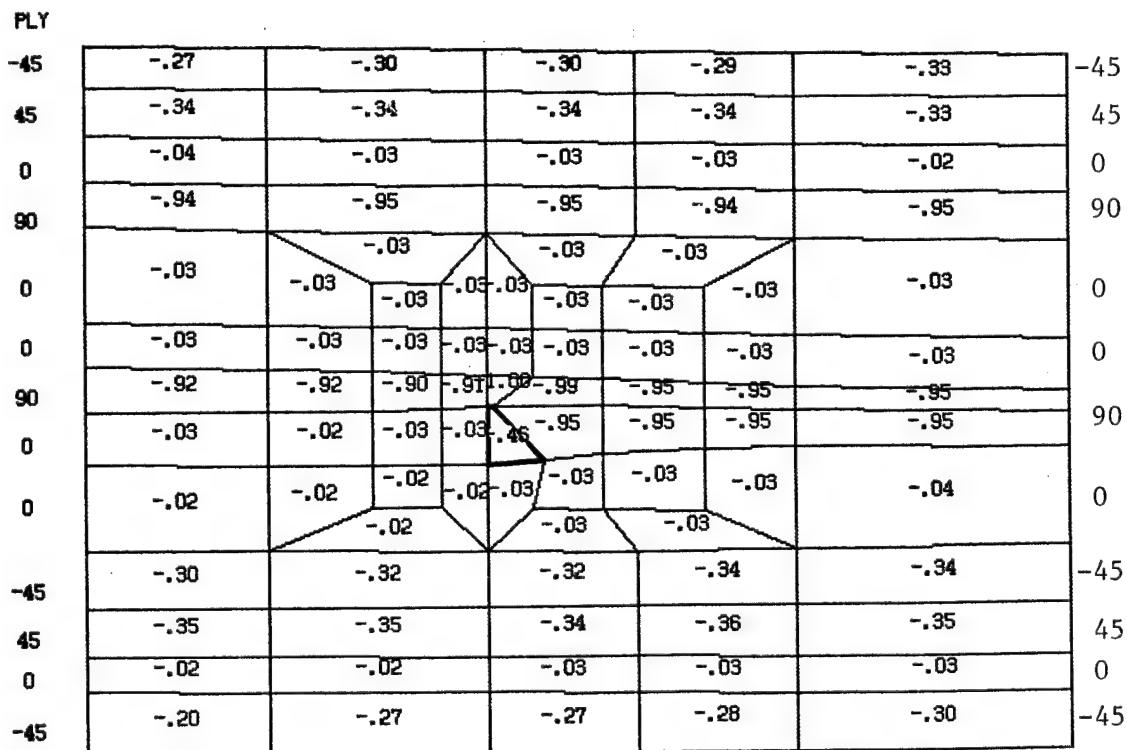
Figure 65:

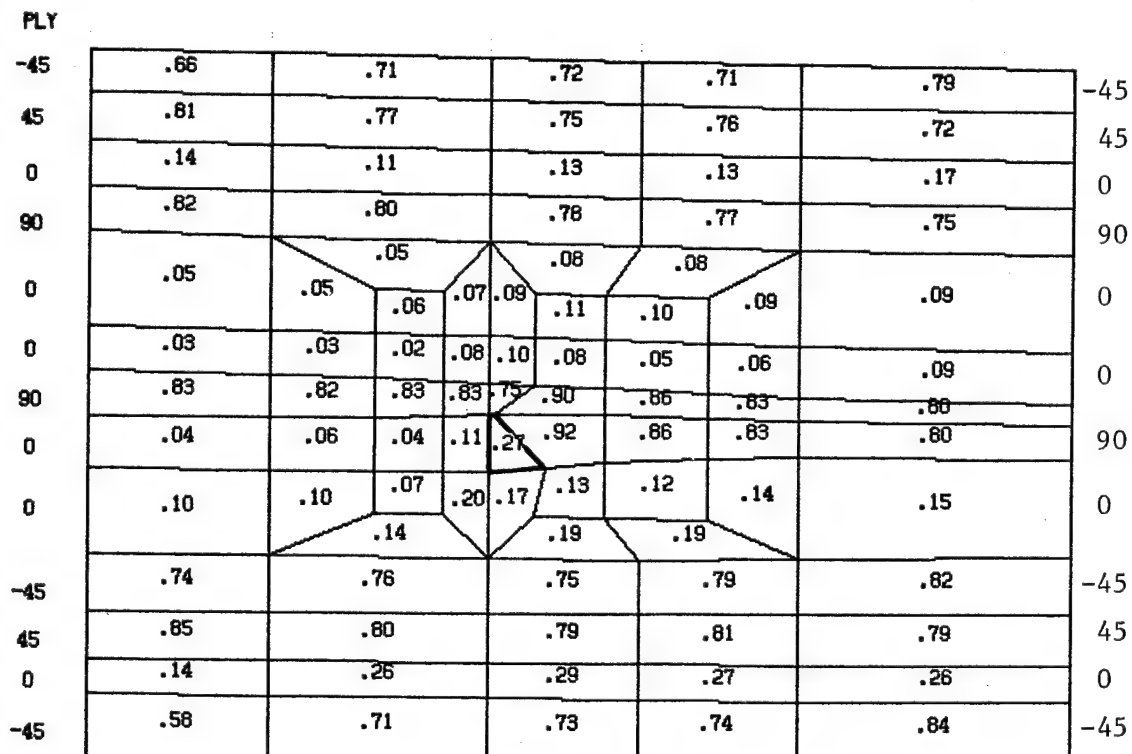| PLY										PLY
-45	.74		.79		.79		.76		.81	-45
45	.89		.83		.82		.81		.75	45
0	.16		.13		.14		.14		.17	0
90	.84		.83		.81		.79		.77	90
0	.06	.07	.07 / .09	.08 / .08	.07 / .09	.07 / .09		.09	.08	0
0	.04	.05	.05	.05 / .05	.05	.05	.06		.07	0
90	.87	.86	.86	.86 / .86	.86	.86	.85		.84	90
0	.04	.05	.06	.06 / .06	.07	.07	.07		.07	0
0	.12	.14	.14 / .18	.16 / .16	.14 / .20	.14 / .20		.16	.17	0
-45	.78		.80		.82		.85		.87	-45
45	.89		.84		.86		.88		.85	45
0	.17		.28		.31		.29		.27	0
-45	.60		.74		.79		.80		.91	-45
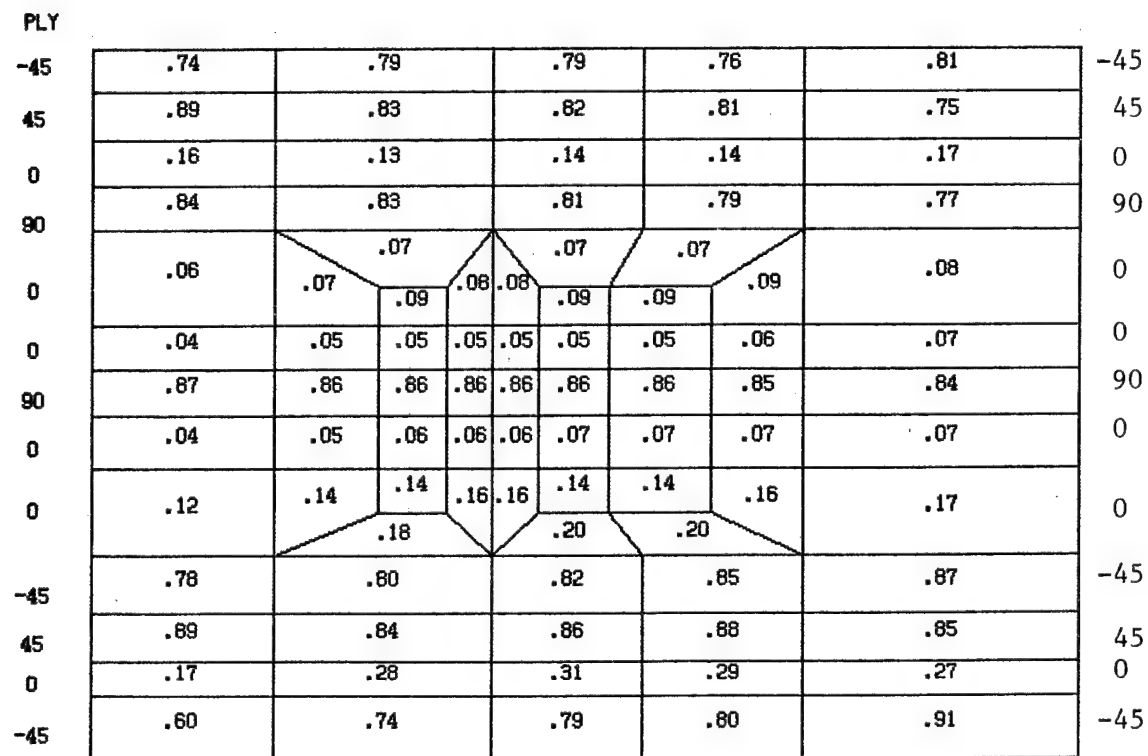
Figure 65. Normalized Values for σ_{eff} in Layer 3 for the No Drop-off case, Under ETW Conditions, where $\sigma_x = -14.5$ ksi.

PLY

-45	-.39	-.32	-.39	-.35	-.32	-45
45	-.32	-.36	-.37	-.36	-.43	45
0	-.01	-.02	-.03	-.03	-.04	0
90	-.86	-.86	-.87	-.88	-.88	90

(center region with resin pocket)

-.03 -.03 -.03
-.03   -.03 -.03-.03 -.03 -.03 -.03 -.03   0
-.03 -.03 -.03-.03-.03 -.03 -.03 -.03 -.03   0
-.88 -.87 -.85 -.85 -.91 -.93 -.88 -.88 -.87 90
-.03 -.03 -.03 -.03 .46 -.91 -.89 -.87 -.87   0
-.04 -.03 -.03-.03-.03 -.03 -.03 -.03 -.02   0
           -.03   -.03   -.02

-45	-.42	-.35	-.35	-.35	-.33	-45
45	-.37	-.39	-.38	-.37	-.40	45
0	-.03	-.03	-.03	-.02	-.02	0
-45	-.40	-.26	-.25	-.25	-.21	-45
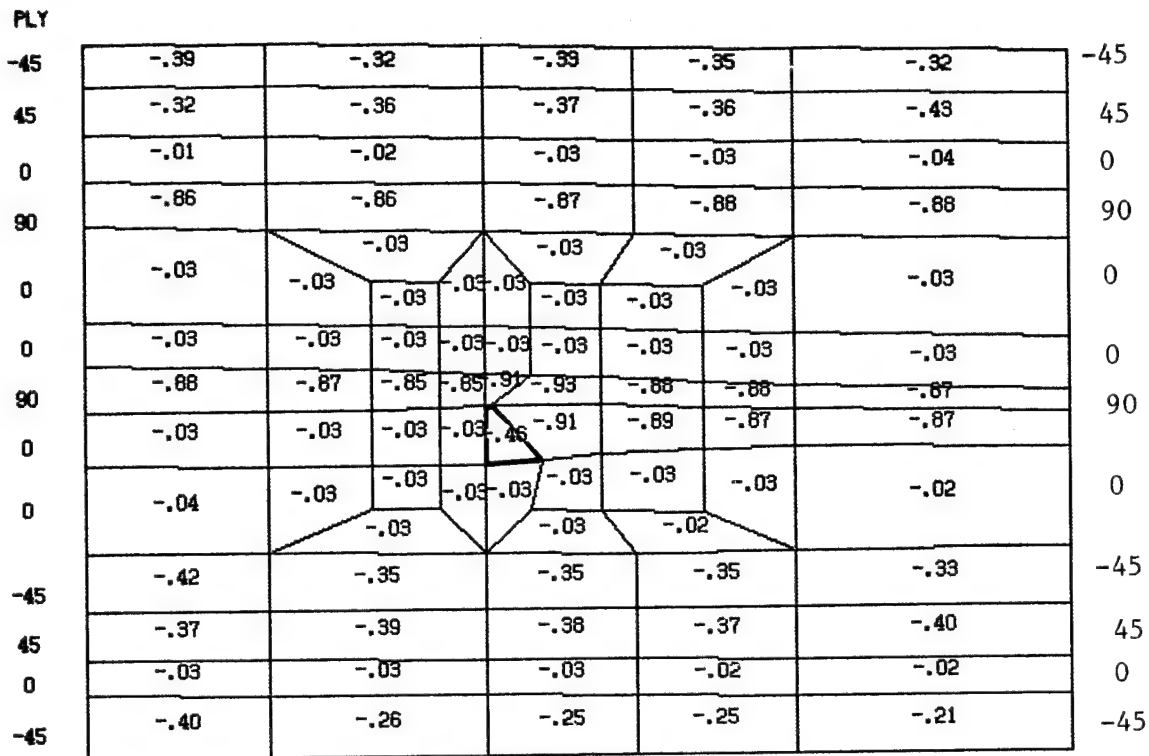
Figure 66. Normalized Values for σ_x in Layer 1 for the 0° Drop-off Case, Small Resin Pocket, Under ETW Conditions, where $\bar{\sigma}_x = -5.5$ ksi.

PLY

-45	-.27	-.30	-.30	-.29	-.33	-45
45	-.34	-.34	-.34	-.34	-.33	45
0	-.04	-.03	-.03	-.03	-.02	0
90	-.94	-.95	-.95	-.94	-.95	90

(center region with resin pocket)

-.03 -.03 -.03
-.03   -.03 -.03-.03 -.03 -.03 -.03 -.03   0
-.03 -.03 -.03 -.03-.03 -.03 -.03 -.03 -.03   0
-.92 -.92 -.90 -.91 -1.00 -.99 -.95 -.95 -.95 90
-.03 -.02 -.03 -.03 .46 -.95 -.95 -.95 -.95   0
-.02 -.02 -.02 -.02-.03 -.03 -.03 -.03 -.04   0
           -.02   -.03   -.03

-45	-.30	-.32	-.32	-.34	-.34	-45
45	-.35	-.35	-.34	-.36	-.35	45
0	-.02	-.02	-.03	-.03	-.03	0
-45	-.20	-.27	-.27	-.28	-.30	-45

Figure 67. Normalized Values for σ_x in Layer 3 for the 0° Drop-off Case, Small Resin Pocket, Under ETW Conditions, where $\bar{\sigma}_x = -5.5$ ksi.

97

PLY

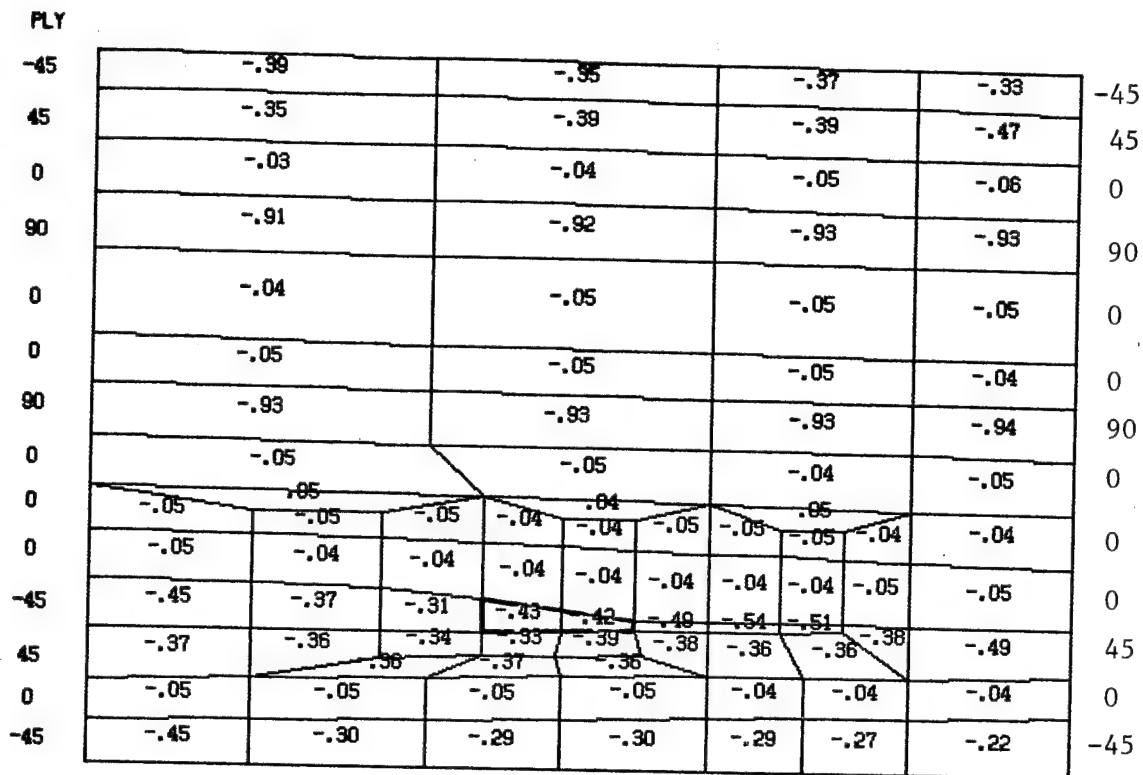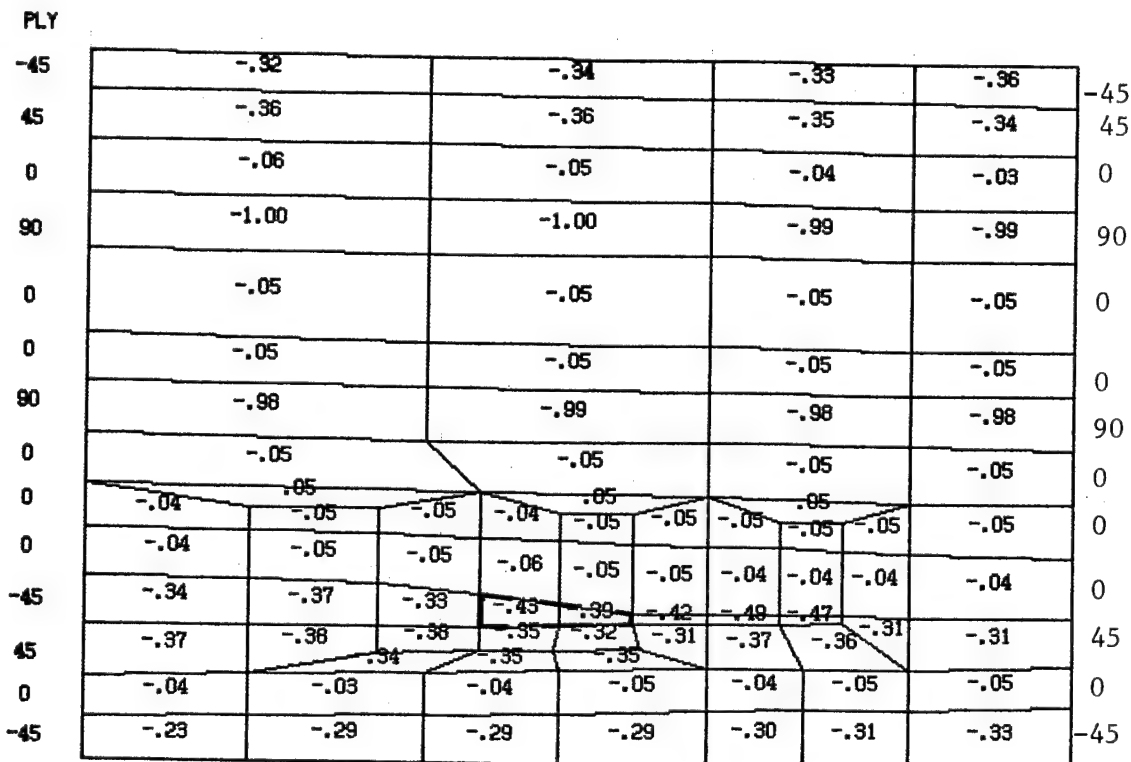| -45	-.02	-.00	-.01	-.01	.01	-45
45	-.03	.00	.00	.01	.05	45
0	-.01	.02	.02	.03	.06	0
90	.03	.04	.04	.05	.07	90
0	.05	.06 .08	.06 .05 .03 .04	.06 .03 .05	.06 .07	0
0	.05	.07 .09	.05 -.01 .02	.05 .06	.07	0
90	.04	.06 .11	.11 -.29 -.01	.05 .05	.06	90
0	.03	.05 .08	.33 .24 .04	.03 .04	.05	90
0	.01	.03 .08	-.01 -.05 -.01 .01	.01	.02 .03	0
			-.04	-.01		
-45	-.01	-.01	-.04	-.03	-.01	-45
45	-.06	-.03	-.05	-.04	-.00	45
0	-.05	-.03	-.05	-.05	-.01	0
-45	-.01	-.01	-.04	-.05	-.03	-45
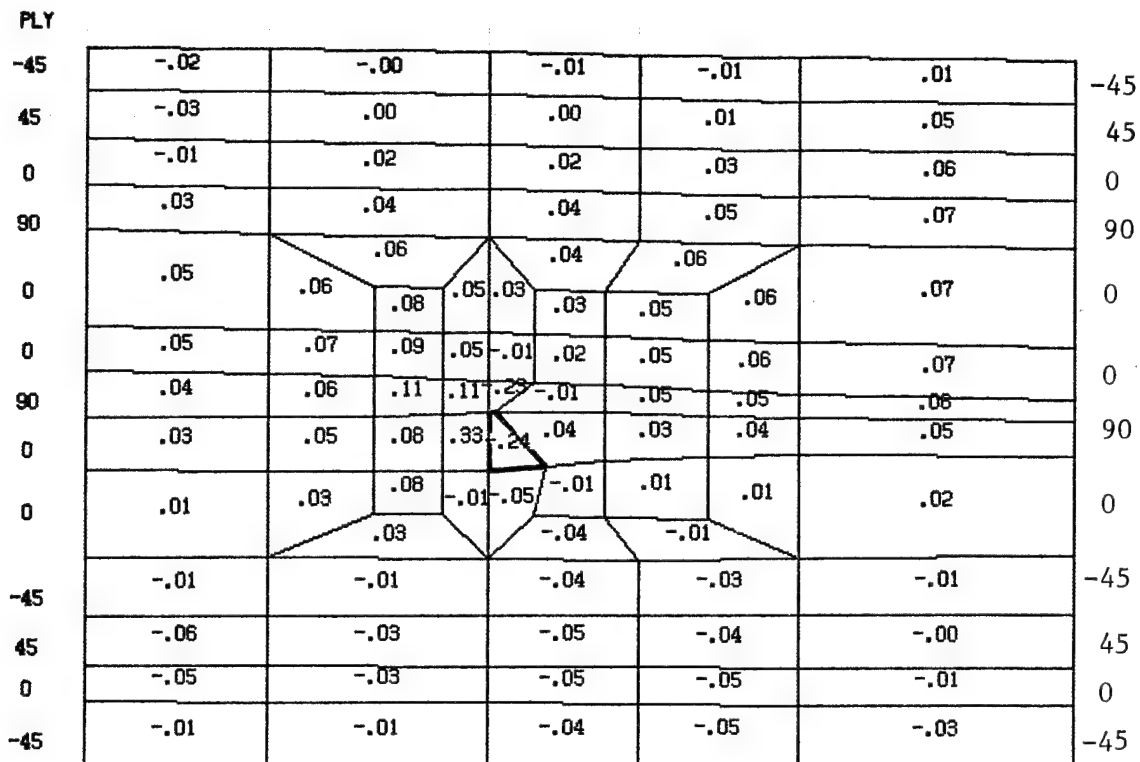
Figure 68. Normalized Values for σ_z in Layer 1 for the 0° Drop-off Case, Small Resin Pocket, Under ETW Conditions, where $\overline{\sigma}_x = -5.5$ ksi.

PLY

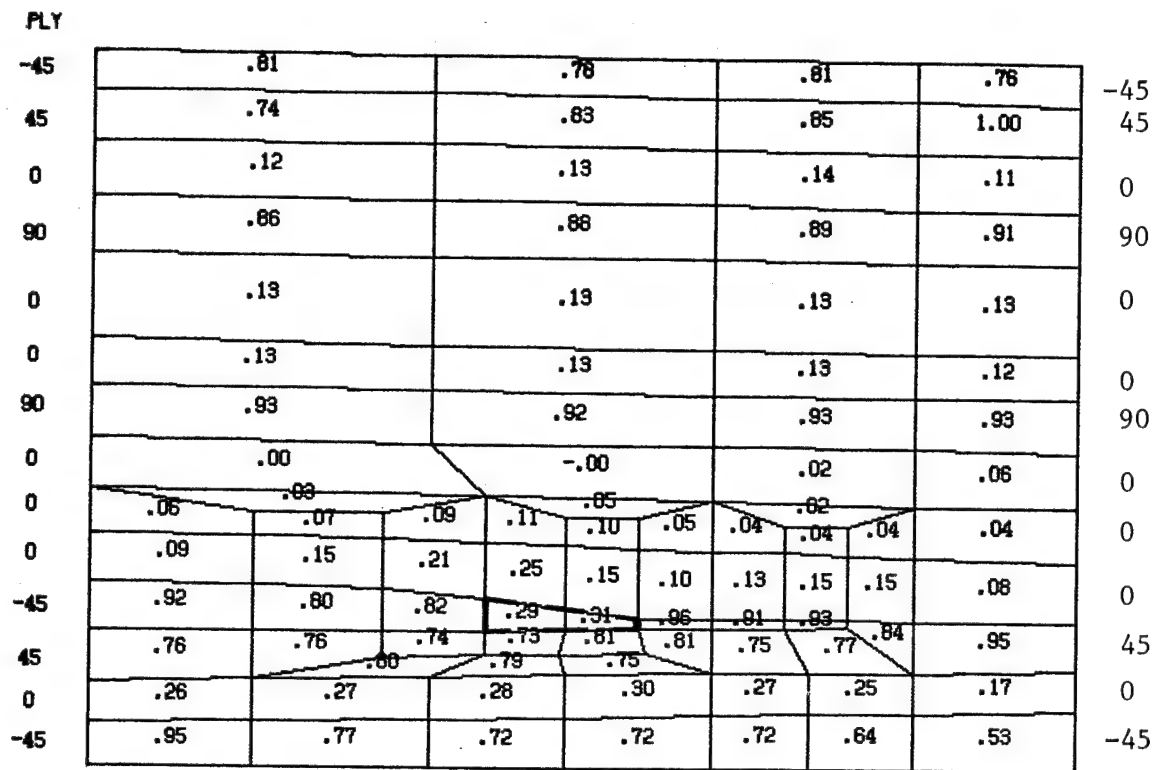| -45	.02	-.01	-.02	-.00	-.04	-45
45	.06	-.01	-.03	-.02	-.08	45
0	.02	-.04	-.06	-.06	-.12	0
90	-.04	-.07	-.09	-.10	-.12	90
0	-.05	-.05 -.05	-.06 -.06 .10 -.10	-.10 -.09 -.09	-.09 -.11	0
0	-.05	-.05 -.03	-.08 -.14 -.11	-.08 -.08	-.10	0
90	-.04	-.05 -.00	-.01 .39 -.13	-.07 -.08	-.09	90
0	-.03	-.03 -.01	.30 .24 -.05	-.07 -.07	-.09	0
0	-.01	-.01 .03	-.03 -.08 -.06	-.05 -.04	-.03	0
		.02	-.04	-.02		
-45	.04	.04	.02	.02	.03	-45
45	.10	.05	.03	.03	.01	45
0	.06	.03	.02	.01	.01	0
-45	-.02	-.01	-.01	-.00	.03	-45
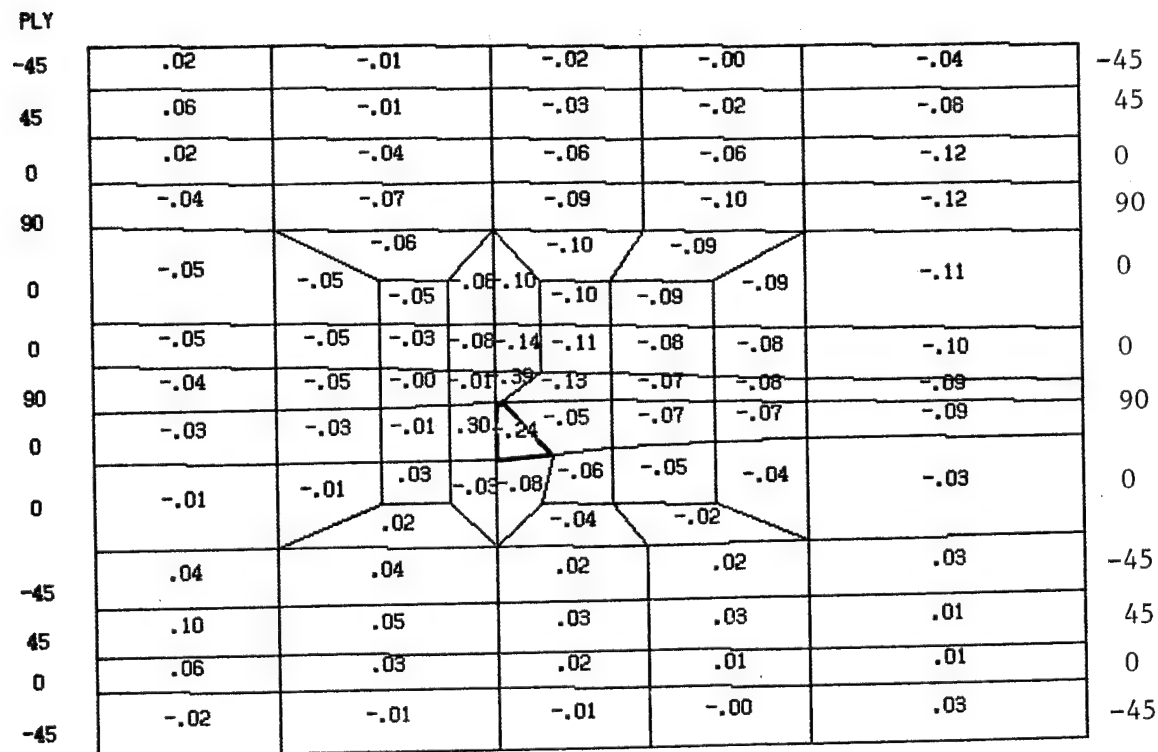
Figure 69. Normalized Values for σ_z in Layer 3 for the 0° Drop-off Case, Small Resin Pocket, Under ETW Conditions, where $\overline{\sigma}_x = -5.5$ ksi.

98

PLY

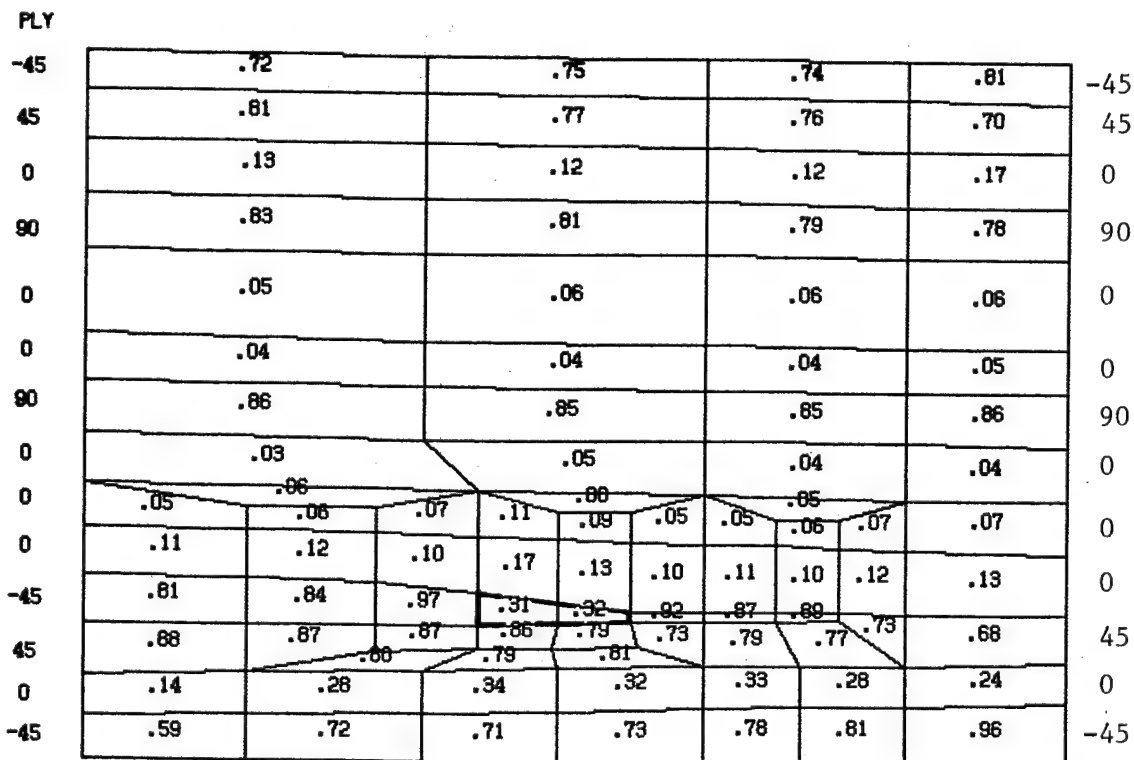| -45	.82	.74	.77	.81	.78	-45
45	.70	.80	.82	.84	.97	45
0	.15	.13	.15	.16	.10	0
90	.80	.82	.83	.84	.89	90
0	.06 .12	.10 .14	.11 .09 .12	.12 .12	.12 .13	0
0	.11 .12	.14	.10 -.01 .01	.09 .09	.11	0
90	.89 .89	.89	.91 .85 1.00	.95 .91	.91	0
0	.03 .04	.05	.17 .28 .99	.90 .87	.87	90
0	.09 .11	.08 .15	.09 .14 .07 .20	.04 .15 .05	.10	0
-45	.89	.80	.77	.76	.75	-45
45	.77	.82	.79	.77	.84	45
0	.28	.33	.35	.35	.27	0
-45	.91	.72	.67	.63	.56	-45
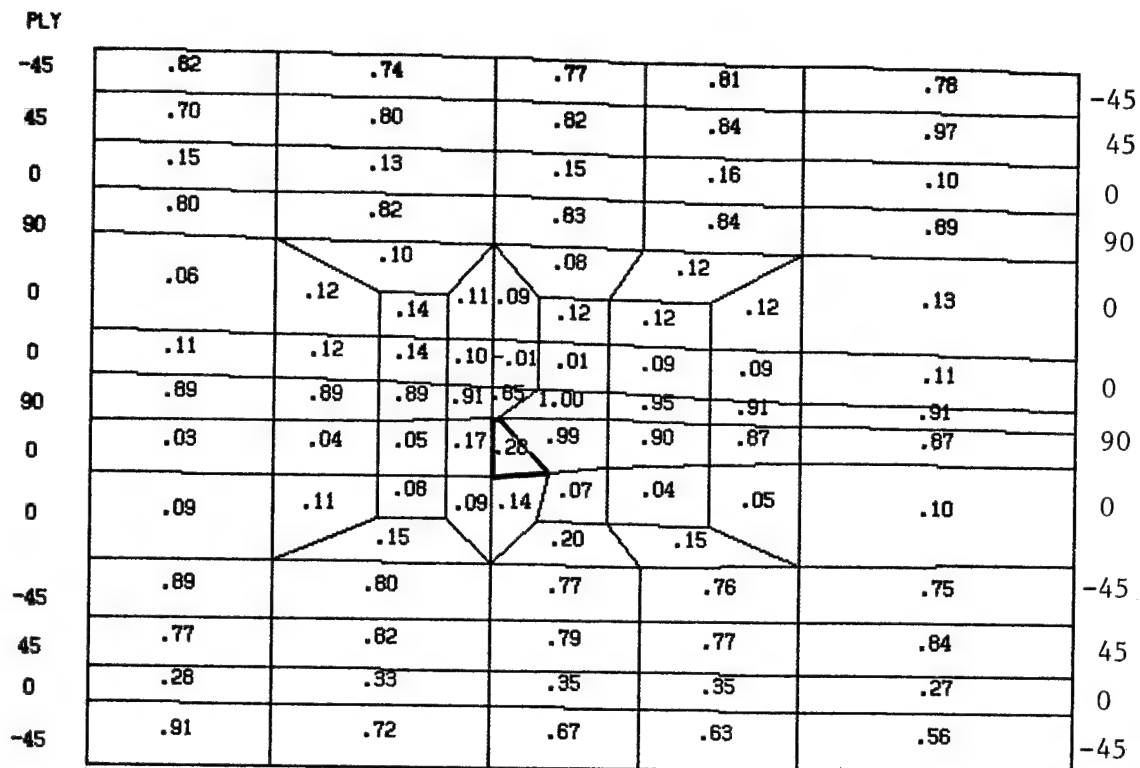
Figure 70. Normalized Values for σ_{eff} in Layer 1 for the 0°
Drop-off Case, Small Resin Pocket, Under ETW Conditions,
where $\bar{\sigma}_x$ = -12.6 ksi.

PLY

-45	.66	.71	.72	.71	.79	-45
45	.81	.77	.75	.76	.72	45
0	.14	.11	.13	.13	.17	0
90	.82	.80	.78	.77	.75	90
0	.05 .05	.05 .06	.07 .09 .11	.08 .10 .09	.09	0
0	.03 .03	.02	.08 .10 .08	.05 .06	.09	0
90	.83 .82	.83	.83 .75 .90	.86 .83	.80	0
0	.04 .06	.04	.11 .27 .92	.86 .83	.60	90
0	.10 .10	.07 .14	.20 .17 .13 .19	.12 .19 .14	.15	0
-45	.74	.76	.75	.79	.82	-45
45	.85	.80	.79	.81	.79	45
0	.14	.26	.29	.27	.26	0
-45	.58	.71	.73	.74	.84	-45

Figure 71. Normalized Values for σ_{eff} in Layer 3 for the 0°
Drop-off Case, Small Resin Pocket, Under ETW Conditions, where
$\bar{\sigma}_x$ = -12.6 ksi.

that for the maximum normal stress failure criterion case because of the beneficial subtracting effect of σ_x and σ_z stresses in the critical elements (the other stresses being negligible there). However, in-plane shear produced values as high as 0.97 for effective stress in the upper right element of the +45° ply of Layer 1. Thus, the detrimental effect of in-plane shear on effective stress is present even under conditions of hygrothermal loading.

Again, whichever failure criterion is used, the allowable applied stress is greatly reduced under ETW conditions compared to RTD conditions.

4.4.5.3 45° Drop-off Laminate

Results for normalized σ_x are shown in Figures 72 and 73 for Layers 1 and 3, respectively. As in the RTD case, the critical elements are in the 90° plies of the third layer. Again, these 90° plies expand more than the others in the x-direction. Therefore, they take more load when subjected to the applied compressive stress $\bar{\sigma}_x$, which in this case was -7.6 ksi at failure. The drop-off area is noncritical in both layers. Because of the drop-off, more load is shifted to the 0° ply above the dropped ply, and since 0° plies are more efficient load carriers, the allowable load on this laminate was increased over that of the plain laminate, as occurred in the RTD case as well.

In-plane shear stress τ_{xy} is shown in Figures 74 and 75. As always, values are low except in the 45° plies. The high values in the edge elements of the 45° plies caused values for effective stress there to be high as well.

Effective stress is shown in Figures 76 and 77. The critical element is the upper right element of the +45° ply in Layer 1. Elements in the lower lefthand corner for the 45° plies in Layer 1 have high values as well. No 90° elements were critical in effective stress because of a beneficial σ_z stress (not shown) acting on them. The failure stress was $\bar{\sigma}_x$ = -13.9 ksi, which is higher than that required to fail an element if the maximum normal stress failure criterion is used. Thus, the presence of hygrothermal loads, with their stress redistribution effect, produced results more favorable to the effective stress failure criterion than to the maximum normal stress failure criterion, which is the opposite of what occurred in the RTD case.

PLY

PLY					
-45	-.99	-.95	-.37	-.33	-45
45	-.35	-.39	-.39	-.47	45
0	-.03	-.04	-.05	-.06	0
90	-.91	-.92	-.93	-.93	90
0	-.04	-.05	-.05	-.05	0
0	-.05	-.05	-.05	-.04	0
90	-.93	-.93	-.93	-.94	90
0	-.05	-.05	-.04	-.05	0
0	-.05	.05	-.05 -.04	.04 -.05 -.05 .05 -.04	-.04	0
0	-.05	-.04 -.04	-.04 -.04 -.04	-.04 -.04 -.05	-.04	0
-45	-.45	-.37 -.31	-.43 .42 -.49 -.54 -.51		-.05	0
45	-.37	-.36 -.34	-.33 -.39 -.38 -.36 -.36 -.38	.56 -.37 -.36	-.49	45
0	-.05	-.05	-.05	-.05 -.04 -.04	-.04	0
-45	-.45	-.30	-.29	-.30 -.29 -.27	-.22	-45

Figure 72. Normalized Values for σ_x in Layer 1 for the 45° Drop-off Case, Small Resin Pocket, Under ETW Conditions, where $\bar{\sigma}_x$ = -7.6 ksi.

PLY

PLY					
-45	-.32	-.34	-.33	-.36	-45
45	-.36	-.36	-.35	-.34	45
0	-.06	-.05	-.04	-.03	0
90	-1.00	-1.00	-.99	-.99	90
0	-.05	-.05	-.05	-.05	0
0	-.05	-.05	-.05	-.05	0
90	-.98	-.99	-.98	-.98	90
0	-.05	-.05	-.05	-.05	0
0	-.04	.05	-.05 -.04	.05 -.05 -.05 .05 -.05	-.05	0
0	-.04	-.05 -.05	-.06 -.05 -.05	-.04 -.04 -.04	-.04	0
-45	-.34	-.37 -.33	-.43 .39 -.42 -.49 -.47		-.04	0
45	-.37	-.38 -.38	-.35 -.32 -.31 -.37 -.36 -.31	.34	-.31	45
0	-.04	-.03	-.04	-.05 -.04 -.05	-.05	0
-45	-.23	-.29	-.29	-.29 -.30 -.31	-.33	-45

Figure 73. Normalized Values for σ_x in Layer 3 for the 45° Drop-off Case, Small Resin Pocket, Under ETW Conditions, where $\bar{\sigma}_x$ = -7.6 ksi.

101

PLY

	-.45	-.36	-.39	-.33	-45
-45					
45	.39	.42	.42	.59	45
0	-.03	-.05	-.05	-.03	0
90	-.01	-.01	-.01	-.00	90
0	-.00	-.00	-.00	-.00	0
0	-.00	-.00	-.00	-.00	0
90	.00	-.00	-.00	-.00	90
0	.00	-.00	-.00	-.00	0

0	.00	.00	-.00	.00	.00	0
.00	.00	.00	-.00	-.00	-.00	-.00	-.00	-.00	-.00
0	.03	.03	.02	-.02	-.02	-.01	-.01	-.01	-.03	-.03	0
-45	-.56	-.42	-.34	-.02	.02	-.77	-.79	-.74	.36	.60	45
45	.41	.41	.36	.25	.34	.41	.37	.37			0
			.37	.36	.33					-.01	
0	.00	.01	.01	.01	.00	.00		-45
-45	-.49	-.20	-.19	-.21	-.22	-.20	-.12	

Figure 74. Normalized Values for τ_{xy} in Layer 1 for the 45°
Drop-off Case, Small Resin Pocket, Under ETW Conditions, where
$\bar{\sigma}_x = -7.6$ ksi.

PLY

	-.34	-.32	-.32	-.31	-45
-45					
45	.38	.38	.37	.32	45
0	-.04	-.04	-.04	-.04	0
90	-.01	-.01	-.01	-.01	90
0	-.00	-.00	-.00	-.00	0
0	.00	-.00	-.00	.00	0
90	.00	-.00	.00	.00	90
0	.00	-.00	-.00	-.00	0

0	.01	.01	.01	.00	-.01	0
.01	.01	.01	-.01	-.01	-.01	.00	-.00	.01	
0	.04	.03	.03	-.05	-.04	.00	-.00	-.00	-.05	-.05	0
-45	-.37	-.42	-.38	-.04	.04	-.60	-.68	-.68	.25	.25	45
45	.41	.44	.44	.24	.22	.34	.42	.39			0
			.38	.31	.33					.01	
0	-.00	.02	.01	.01	.02	.00		-45
-45	-.16	-.23	-.22	-.20	-.20	-.25	-.20	

Figure 75. Normalized Values for τ_{xy} in Layer 3 for the 45°
Drop-off Case, Small Resin Pocket, Under ETW Conditions, where
$\bar{\sigma}_x = -7.6$ ksi.

Figure 76 — Normalized Values for σ_{eff} in Layer 1

PLY labels (left) | values | (right)

PLY					PLY
-45	.81	.78	.81	.76	-45
45	.74	.83	.85	1.00	45
0	.12	.13	.14	.11	0
90	.86	.88	.89	.91	90
0	.13	.13	.13	.13	0
0	.13	.13	.13	.12	0
90	.93	.92	.93	.93	90
0	.00	-.00	.02	.06	0
0	.06 / .03 / .07 / .09	.11 / .05 / .10 / .05	.04 / .02 / .04 / .04	.04	0
0	.09 / .15 / .21	.25 / .15 / .10	.13 / .15 / .15	.08	0
-45	.92 / .80 / .82	.29 / .91 / .96	.91 / .93 / .84		0
45	.76 / .76 / .60 / .74	.73 / .79 / .81 / .75	.75 / .77 / .84	.95	45
0	.26 / .27	.28 / .30	.27 / .25	.17	0
-45	.95 / .77	.72 / .72	.72 / .64	.53	-45

Figure 76. Normalized Values for σ_{eff} in Layer 1 for the 45°
Drop-off Case, Small Resin Pocket, Under ETW Conditions, where
$\bar{\sigma}_x = -13.9$ ksi.

Figure 77 — Normalized Values for σ_{eff} in Layer 3

PLY					PLY
-45	.72	.75	.74	.81	-45
45	.81	.77	.76	.70	45
0	.13	.12	.12	.17	0
90	.83	.81	.79	.78	90
0	.05	.06	.06	.06	0
0	.04	.04	.04	.05	0
90	.86	.85	.85	.86	90
0	.03	.05	.04	.04	0
0	.05 / .06 / .07	.11 / .08 / .09 / .05	.05 / .06 / .07	.07	0
0	.11 / .12 / .10	.17 / .13 / .10	.11 / .10 / .12	.13	0
-45	.81 / .84 / .97	.31 / .32 / .92	.87 / .89 / .73	.68	0
45	.68 / .87 / .60 / .87	.86 / .79 / .81 / .73	.79 / .77		45
0	.14 / .28	.34 / .32	.33 / .28	.24	0
-45	.59 / .72	.71 / .73	.78 / .81	.96	-45

Figure 77. Normalized Values for σ_{eff} in Layer 3 for the 45°
Drop-off Case, Small Resin Pocket, Under ETW Conditions, where
$\bar{\sigma}_x = -13.9$ ksi.

4.4.6 Results for the Elevated Temperature, Dry (ETD) Case

As in the ETW case, a hygrothermal load was applied in five equal load increments to bring the temperature up to 218°F before the mechanical loading was applied. No moisture loads, of course, were applied since this was a moisture-free test case.

In the second-year study [3] Northrop tested only the plain laminate under ETD conditions, so results are presented here for that laminate only.

Figures 78 and 79 show the normalized σ_x stresses in Layers 1 and 3, respectively. The results are the same as for all other cases, i.e., the critical elements are in the 90° plies of Layer 3. The 0° plies took more load than in the ETW case (although still considerably less than in the RTD case), because in this case there is no moisture swelling; the easily swelled 90° plies were not called upon to take as much load as in the ETW case, allowing more applied load before they failed. The failure load was -12.4 ksi, considerably above the -7.2 ksi value for the ETW case.

As in the ETW case, small but negative values of σ_z in the 90° plies reduced the effective stresses in those plies, while the in-plane shear stress τ_{xy} in the 45° plies increased the effective stresses in these plies, making them critical. Figures 80 and 81 show the effective stress for Layers 1 and 3, respectively. The critical element is the same one as in the ETW and RTD cases, i.e., the upper right element of the +45° ply in Layer 1. High values occurred in all edge elements of the 45° plies, as in the ETW and RTD cases as well. The failure stress was $\bar{\sigma}_x = -17.2$ ksi, which is considerably higher than that under which failure occurs by the maximum normal stress failure criterion, for the same reason given in the discussion of the ETW case.

4.5 Comparison with Experimental Results and Conclusions

The experimental results given on Page 2.9 of the second-year report [3] present the applied stresses required to produce compressive failure of the whole laminate, but give no information about where the first failure occurs, and at what applied stress level. On the other hand, the present analytical results predict where first element failure occurs, and at what applied stress, but say nothing of how failure propagates, and at what stress ultimate failure occurs. Therefore, a direct comparison between experimental and analytical results cannot be made at this time. What can be done, though, is to show what percentage of the applied stress required
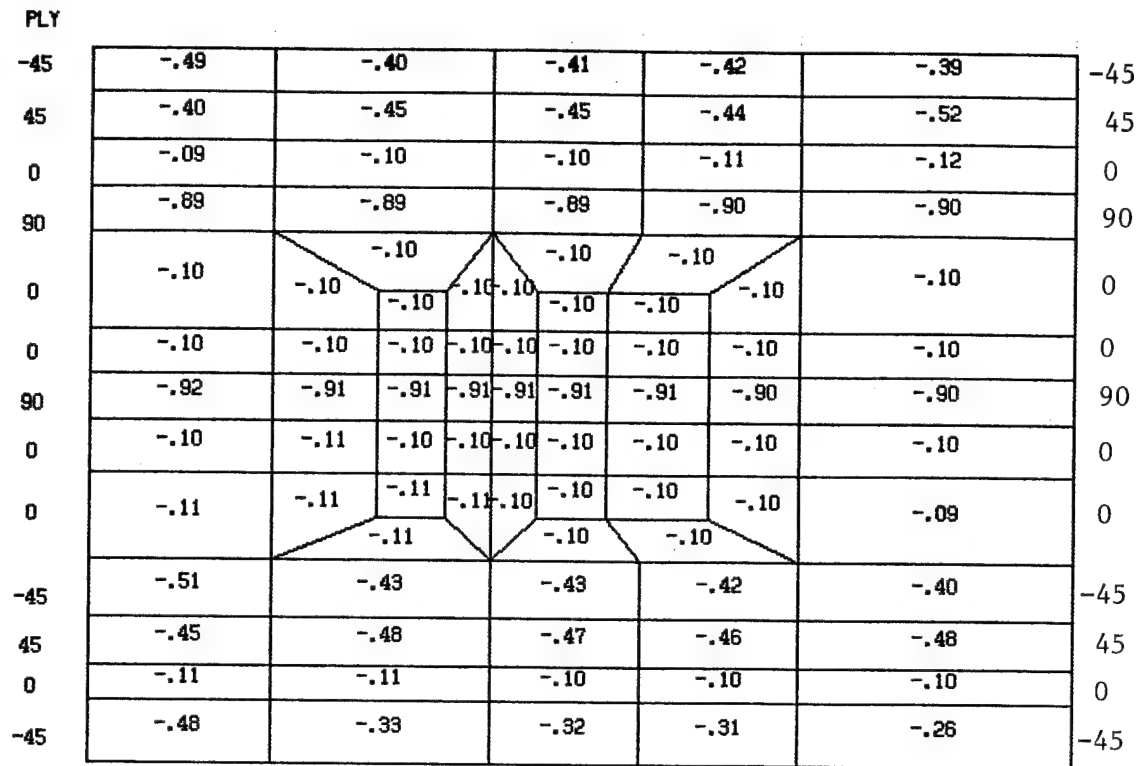
Figure 78. Normalized Values for σ_x in Layer 1 for the No Drop-off Case, Under ETD Conditions, where $\bar{\sigma}_x = -12.4$ ksi.

Figure 79. Normalized Values for σ_x in Layer 3 for the No Drop-off Case, Under ETD Conditions, where $\bar{\sigma}_x = -12.4$ ksi.

Figure 80. Normalized Values for σ_{eff} in Layer 1 for the No Drop-off Case, Under ETD Conditions, where $\bar{\sigma}_x = -17.2$ ksi.

Figure 81. Normalized Values for σ_{eff} on Layer 3 for the No Drop-off Case, Under ETD Conditions, where $\bar{\sigma}_x = -17.2$ ksi.

to produce ultimate failure based on experimental results is the applied stress required to produce first-element failure. Table 18 provides such a comparison, for both the maximum normal stress and effective stress failure criteria. Consistency is maintained for a given environmental condition for both criteria, except for the 0° ply drop-off, RTD condition, where the maximum normal stress criterion shows 19 percent, well below the other values of approximately 50 percent. In all cases, however, the RTD condition is most favorable and the ETW case is the least favorable, indicating that residual stresses due to hygrothermal loads are detrimental to both initial failure and gross failure for this material.

The experimental data [3] indicated that gross static failure was relatively insensitive to the presence of ply drop-offs, and more sensitive to the environmental condition. Since the analysis showed that nowhere were 0° plies critical, it seems logical that all plies except these 0° plies will fail first, no matter what the ply drop-off condition is. Therefore, gross failure would be a function of the strength of these 0° plies more so than of the presence of ply drop-offs. Since the strength of the 0 plies decreases with increasing temperature and/or moisture content gross failure should occur at a lower stress value for the ETD and ETW cases, as was shown to occur experimentally.

The first-year report [1] gave values for the compressive strength in the fiber direction of a unidirectional laminate under RTD, ETW and ETD conditions. If the assumed ultimate failure criterion is defined as failure occurring when all plies other than 0° plies have failed, and the 0° plies are all at their compressive strength limits, all that is needed is the percentage of 0° plies in a laminate. The predicted ultimate failure stress would be the ultimate strength of a 0° ply multiplied by the percentage of these plies in the laminate. Such predictions are given in Table 19, where the predicted values are then compared with the actual experimental values of the second-year report [3].

The percentage differences are all less than 20 percent, with most of them under 12 percent. Since the rule of mixtures failure criterion does not recognize any plies other than 0° plies, it is not surprising that predicted failure stresses are all below the actual ones, although not by much.

In summary, based upon what has been presented in this section, two conclusions seem valid. First, if not only gross failure but also local failure and its propagation is required, a three-dimensional finite element

TABLE 18. PERCENTAGE OF APPLIED LOAD PREDICTED TO PRODUCE FIRST-ELEMENT FAILURE RELATIVE TO THAT EXPERIMENTALLY DETERMINED TO PRODUCE TOTAL FAILURE

	Effective Stress Failure Criterion	Maximum Normal Stress Failure Criterion
Plain Laminate, RTD	37	50
0° Ply Drop-offs, RTD	30	19
45° Ply Drop-offs, RTD	36	51
Plain Laminate, ETD	19	14
Plain Laminate, ETW	19	9
0° Ply Drop-offs, ETW	17	7
45° Ply Drop-offs, ETW	16	9

TABLE 19. PREDICTED GROSS FAILURE BASED ON A RULE-OF-MIXTURES FAILURE
CRITERION OF 0° PLIES COMPARED TO EXPERIMENTAL DATA IN
REFERENCE [1].

Configuration	Environmental Conditions	Percent 0° Plies Beyond the Drop-off	Ultimate Strength of 0° Ply	Predicted Ultimate Strength of Laminate	Actual Ultimate Strength of Laminate	Percentage Difference
Plain Laminate	RTD	53.3	-175 ksi	-93.3 ksi	-105.0 ksi	11
0° Ply Drop-offs	RTD	50.0	-175 ksi	-87.5 ksi	-107.4 ksi	19
45° Ply Drop-offs	RTD	57.1	-175 ksi	-99.9 ksi	-107.1 ksi	7
Plain Laminate	ETD	53.3	-160 ksi	-85.3 ksi	- 89.1 ksi	4
Plain Laminate	ETW	53.3	-134 ksi	-71.4 ksi	- 75.9 ksi	6
0° Ply Drop-offs	ETW	50.0	-134 ksi	-67.0 ksi	- 75.1 ksi	11
45° Ply Drop-offs	ETW	57.1	-135 ksi	-76.5 ksi	- 89.4 ksi	14

analysis with crack propagation capability is needed. Second, if gross failure is all that is needed, and accuracy within 10 to 20 percent is sufficient, the simple rule of mixtures failure criterion can be used, and no elaborate analysis is needed.

SECTION 5

SUMMARY OF RESULTS, CONCLUSIONS AND RECOMMENDATIONS – POROSITY EFFECTS

5.1 SUMMARY OF RESULTS

An experimental program was conducted to quantify the effects of materials- and process-related defects on the integrity of AS/3501-6 graphite/epoxy laminates. Porosity (microvoids) and delaminations were identified as the defects to be studied, with the major emphasis on porosity effects. It was assumed that the presence of porosity or delamination would affect the mechanical response of laminates more under compression than tension. Consequently, static compression and compression fatigue tests were carried out to quantify the worst effects of porosity and delaminations. Test laminates included basic layups, like $[0]_{24T}$, $[90]_{24T}$ and $[\pm 45]_{6S}$, and a 30-ply $[(\pm 45)_5/0_{16}/90_4]_c$ layup. The 30-ply laminate had a layup similar to a highly loaded portion of the F/A-18A vertical stabilizer skin. Generated test data were compared with data on defect-free laminates with identical layups to quantify the effects of porosity and delaminations. The results of the program are listed below.

(1) The main materials- and processes-related defect to be studied was selected to be uniform porosity, measuring $3 \pm 2\%$ via chemical analysis and $4 \pm 2\%$ via SEM image analysis. This was induced by eliminating the debulking operation during layup, by using only vacuum pressure during heat-up and dwell, and by applying only a 15 psi pressure during final cure. Program test laminates met the established goal, and contained porosity levels ranging from 1.49% to 2.12% via chemical analysis, and from 2.31% to 3.06% via SEM image analysis. The quantification of porosity level differs with the technique employed (Ref. 2). The uniformity of the induced porosity was verified through ultrasonic C-scans and photomicrographic examination of selected laminate cross-sections.

111

(2) The induced porosity levels in test laminates were approximately twice the worst porosity measurement in F/A-18A vertical stabilizer skins thus far (Ref. 2).

(3) A secondary and limited study was also conducted on a non-porous laminate with a 0.5 in. long delamination imbedded at midplane. The 30-ply layup mentioned earlier was adopted for these tests.

(4) Static compression and compression fatigue (R = 10, ω=10 Hertz) tests were conducted on laminates with induced porosity and delamination defects. Reductions in the static compressive strengths and compression fatigue threshold strain levels, due to the induced defects in test laminates, were recorded. Comparisons between defective and defect-free laminate results were drawn based on chemical analysis porosity measurements that are lower than SEM image analysis measurements. Prior to making comparisons, differences in the fiber volume percentages between compared defective and defect-free laminates were appropriately accounted for.

5.2 CONCLUSIONS

(1) Static compression test data indicated significant (> 10%) reductions in the strength and failure strain values of test laminates due to the presence of induced defects (porosity and delamination). This was observed under all the considered environmental conditions, (RTD, RTW and 218FW). The combination of moisture and porosity induced very significant reductions in the proportional limit stresses and strains. Poissons' ratio and modulus of elasticity suffered negligible degradations despite the presence of defects and changes in environment.

(2) Based on the generated static compression test data, empirical relationships are proposed for quantifying the effect of porosity (% voids) on the static compression strength (σ^{ult}) of AS/3501-6 laminates:

112

Under RTD conditions,

$\% \Delta\sigma^{ult}$ = 6.5x % voids   for $0 < \%$ voids < 1.28

           = 8.4 + 35.09 x % voids   for   % voids > 1.28

Under RTW conditions,

$\% \Delta\sigma^{ult}$ = 4.58x % voids   for $0 < \%$ voids < 0.83

           = 3.8 + 18.52 x % voids   for % voids > 0.83

$\% \Delta\sigma^{ult}$ is the percentage reduction in the static compression strength, and % voids is measured via chemical analysis.

(3)   Constant amplitude, compression fatigue tests were conducted at R = 10 and ω = 10 Hertz, and the effects of induced porosity and delaminations were quantified through the computation of percentage reductions in the threshold strain levels. Very signficiant effects were observed in $[0]_{24T}$ (40%), $[90]_{24T}$ (29%) and $[\pm45]_{6S}$ (33%) specimens, due to induced porosity, under RTW conditions. RTD compression fatigue tests on porous $[(\pm45)_5/0_{16}/90_4]_c$ specimens exhibited a signifcant (16%) reduction in the threshold strain level, while RTW tests only measured a small (6%) effect. 218FW conditions caused the worst reduction (20%) in the threshold strain level of the porous 30-ply laminate. Imbedded delaminations in the non-porous 30-ply laminate caused no measurable degradation in the threshold strain level. This is possibly due to to its size and midplane location.

5.3   RECOMMENDATIONS

A set of basic laminates and a 30-ply laminate, representative of a highly loaded F/A-18A vertical stabilizer skin section, have been subjected to three phases of compression tests. In the initial program (Ref. 1) compression test data were generated for these laminates in a defect-free state. In the second program (Ref. 3) similar compression test data were generated on the same 30-ply laminate with two ply drop-off configurations. In this report, the effects of porosity and delamination on the compression

113

fatigue behavior of the 30-ply laminate were quantified. A logical contin-
uation of this study would be to address the combined effect of porosity
and ply drop-off on the compression fatigue behavior of the 30-ply laminate.
And, a representation of an F/A-18A vertical stabilizer skin attachment to
an aluminum spar should also be considered through the introduction of
fastener holes. Furthermore, open hole test data should be complemented
by data generated on specimens with a representative bolt-load to by-pass
load ratio. The recommended continuation study will help determine the
combined effect of porosity, ply drop-off and fastener holes on the static
compression and compression fatigue behavior of the referenced 30-ply
laminate. Static strength reductions and percentage degradations in the
compression fatigue ($R = 10$, $\omega = 10$ Hertz) threshold strain levels due to
porosity, ply drop-off, open fastener holes, and loaded holes have already
been estimated under situations where only one of the degradation-inducing
factors exists. In the recommended study, a combined degradation factor
will be measured, and the interaction among the various anomalies established.

SECTION 6

SUMMARY OF RESULTS, CONCLUSIONS AND RECOMMENDATIONS -
PLY DROP-OFF ANALYSIS

6.1 Summary of Results

The ply drop-off experimental data generated as part of the second-year
study [3] were used as the basis for the analytical results presented in
Section 4 of the present report. A recently developed [6] three-dimensional
finite element analysis (and the associated computer program) was utilized.

Since the present analysis represents one of the first practical
applications of this new analytical tool, a considerable amount of effort
was expended in obtaining suitable material properties input data, in
constructing finite element models, and in developing methods of inter-
preting the numerical results obtained. Actual photomicrographs were
taken and used to establish the various ply drop-off geometries.

There are practical limits to the size of the three-dimensional
finite element grid which can be utilized, associated with the size of
the computer available. The University of Wyoming has a CDC Cyber 730/760
Dual Processor Mainframe, a computer of reasonably large size. Thus, it
would be possible to use a finer finite element grid than that utilized
in the present exploratory work. The present three-layer grid array is
adequate to indicate trends, but is not sufficiently refined to fully
model free-edge stress effects.

Because of the preliminary nature of the present study, and the
limited amount of experimental data available for composite materials
in the inelastic range of response, no attempt was made to model inelastic
response, although the analysis is fully capable at the present time.
Curing residual stresses were also not included, although the analysis
has this capability.

In spite of these deliberate simplifications, the analysis predicted
a number of significant results. The ability to define the critical ply,
and the location around any specific ply drop-off geometry where failure
occurs, was demonstrated. The capability of modeling temperature- and/or
moisture-induced stress effects was demonstrated. In fact, it was shown
that these hygrothermal stress effects can be more significant than the
geometry-induced effects associated with ply drop-offs.

A scheme has been developed for presenting computer-generated data in a readily understandable format. This provides an immediate visual display of the variation of any one of the six different stress components or the effective stress value over the entire region around a ply drop-off.

The results of the present analytical study, although preliminary in the sense that it will now be practical to perform a much more rigorous analysis in any future work, correlated well with the conclusions derived from the corresponding experimental study [3]. That is, the various ply drop-off geometries do not significantly influence the composite laminate strength. Other influences, such as the hygrothermal environment and the presence of interlaminar stresses at the free edges of the laminate, are more significant. The present analysis permits the quantification of these effects, individually or in any combination. It has also been used to explain why certain apparent experimental anomalies were observed.

6.2 Conclusions

Ply drop-offs result in relatively minor reductions in the ultimate strength of the 0^0 ply-dominated laminate studied, although first-ply failure can occur at relatively low stress levels in the 45^0 and 90^0 plies. If the onset of off-axis ply cracking is not of major concern, a simple rule-of-mixtures relation can be used to predict ultimate strength.

The present analytical work concentrated on correlations with static test results. However, the fatigue data appear to follow similar trends [3]. Thus, ply drop-offs do not appear to be a strong influence on fatigue crack propagation either. The normal discontinuities induced at ply interfaces are almost as severe as the ply drop-off effects.

The present study has served the important function of providing a general analytical approach, however, applicable to any laminate configuration. It is likely that a lay-up configuration not dominated by unidirectional plies in the principal loading directions will be more sensitive to ply drop-offs and their relative locations within the laminate stack. The present analysis will handle such configurations with no modifications required.

6.3 Recommendations

Having established a general analysis methodology as part of the present study, it will be possible to extend this work to more complex

geometries. For example, the combined influences of ply drop-offs, loaded or unloaded holes, and manufacturing-induced defects such as porosity can be analyzed.

Since inelastic response in the form of local plastic deformations around holes and ply drop-offs will be of special interest in future investigations, this capability of the present analysis will be certain to be used. Correspondingly, it is recommended that a crack propagation capability be added to the present analysis, so that material response beyond first failure can be studied. The propagation and arresting of cracks in the vicinity of local discontinuities will be a particularly important analysis capability.

SECTION 7

REFERENCES

1. Grimes, G.C. and Adams, D.F., "Investigation of Compression Fatigue Properties of Advanced Composites", Northrop Technical Report. NOR 79-17, Contracts N00019-77-C-0518 and N00019-77-C-0519 with the Naval Air Systems Command, October 1979.

2. Knauss, J.F., and Black, G.T., "The Effect of Porosity on the F/A-18A Vertical Tail Skin," Northrop Report NOR 81-315, September 1981.

3. Grimes, G.C., Adams, D.F., and Dusablon, E.G., "The Effects of Discontinuities on Compression Fatigue Properties of Advanced Composites," Northrop Technical Report NOR 80-158, Contracts N00019-79-C-0275 and N00019-79-C-0276 with the Naval Air Systems Command, October 1980.

4. Ramkumar, R.L, "Fatigue Degradation in Compressively Loaded Composite Laminates," NASA Contractor Report 165681, April 1981.

5. Ramkumar, R.L., "Performance of a Quantitative Study of Instability – Related Delamination Growth," Ongoing Northrop Contract NAS1-16727 with NASA, Langley Research Center.

6. Monib, M.M. and Adams, D.F., "Three-Dimensional Elastoplastic Finite Element Analysis of Laminated Composites," Report UWME-DR-001-102-1, Department of Mechanical Engineering, University of Wyoming, Laramie, Wyoming, November 1980.

7. Hill, R., The Mathematical Theory of Plasticity, Oxford University Press, London, 1950.

8. Whitney, J.M., "Free-Edge Effects in the Characterization of Composite Materials," Analysis of the Test Methods for High Modulus Fibers and Composites, ASTM STP 521, American Society for Testing and Materials, Philadelphia, 1973.

APPENDIX A

SPECIFICATIONS

QUALITY CONTROL INSTRUCTION (Q.C.I.) AND

PROCESS INSTRUCTION (P.I.) SHEETS FOR

MATERIALS AND PROCESSES DEFECTS (M&P-D) LAMINATES

Definitions for these Instruction Sheets

QC	- Quality Control
M&P-D	- Materials and Processes Defects: specifications applicable to these research programs.
MMS	- McDonnell-Douglas Aircraft (MCAIR) Material Specification
PS	- Process Standard
IT-58	- Northrop Materials Test Specification
W	- weight
V	- volume
μ	- 10^{-6}, micro
NAI	- Northrop Material Specification
mil	- 0.001 inch
MMM-A-132	- Military specification on structural adhesives
T-Peel	- A cleavage-fracture peel test described in MMM-A-132
UP	- uniform porosity
DL	- delamination
NDI	- nondestructive inspection

PREPREG REQUIREMENTS FOR HERCULES AS/3501-6 GRAPHITE/EPOXY

Incoming graphite/epoxy prepreg shall conform to the requirements as set forth in MMS-549. In case of conflict between this document and MMS-549, the requirements of this document shall take precedence. Acceptance testing shall be performed at Northrop to verify these requirements and in accordance with MCATR P.S. 21332. In case of conflict, this document will take precedence.

TABLE A1. AS/3501-6 ACCEPTANCE REQUIREMENTS

PROPERTY	ACCEPTANCE REQUIREMENTS*		TEST METHOD
	TYPE I	TYPE II	
Nongraphite content (%W)	42 ± 3	35 ±3	P.S. 21332
Flow (%)	12 to 30	15 to 30	P.S. 21332
Volatile content, 250F (%W)	1.5 maximum	1.5 maximum	P.S. 21332
0° flexural strength, ksi	220 min avg	220 min avg	IT-58 Para. 3.14
Laminate fiber volume (%V)	62 ±3	62 ±3	IT-58 Para. 3.14
Laminate void content (%V)	1 maximum	1 maximum	IT-58 Para. 3.14
Laminate specific gravity	1.59 to 1.63	1.59 to 1.63	IT-58 Para. 3.15
Transverse tension (μ-in/in)	5,000 min avg 4,000 min individual	5,000 min avg 4,000 min individual	IT-58** IT-58**

Laminates to be cured per instructions in Process Instruction Sheet M&P–D No. 1.

Material that has been stored more than six months at $0°F$, or has been exposed to room temperature for more than a cumulative total of 40 hrs, must be retested prior to use.

*Based on a minimum of three determinations. Type I single ply; Type II double ply.

**Clip-on extensometer may be used for strain measurements.

QC Instruction Sheet No. 2

Physical and Mechanical Property Requirements for Program Laminates

The physical and mechanical properties of the QC test specimens from porous and non-porous laminates shall meet the requirements set forth in Table A2.

TABLE A2. PHYSICAL AND MECHANICAL PROPERTY REQUIREMENTS FOR PROGRAM LAMINATES

PROPERTY	ACCEPTABLE REQUIREMENTS		TEST METHODS
	POROUS	NON–POROUS	
Fiber Volume (%)	55+5	59+4	IT–58, para. 3.14
Void Content (%)	3+2	≤1	IT–58, para. 3.14
Specific gravity	1.45-.155	1.56-1.62	IT–58, para. 3.15
Transverse compression:			
a) $[90]_{nT}$	25 ksi	30 ksi	See Refs. 1, 3
b) $[\pm 45/0/90]_{nS}$	40 ksi	50 ksi	See Refs. 1, 3
Longitudinal compression strength minimum, individual:			
a) $[0]_{nT}$	110 ksi	120 ksi	See Refs. 1, 3
b) $[\pm 45/0/90]_{nS}$	90 ksi	94 ksi	See Refs. 1, 3
Transverse Tension: $[\pm 45/0/90]_{nS}$	25 ksi	30 ksi	ASTM D–3039

PROCESS INSTRUCTION SHEET NO. 1

SOLID LAMINATE ASSEMBLIES

I. Process Specification P.S. 14240 (MCAIR)

P.S. 14240 specification applies. However, in case of conflict with this document (PIS - ID/CF-1), the latter takes precedence.

II. Layup of Graphite Prepreg

1. Cut, layup, and debulk books of material as necessary.

2. Over a clean caul plate covered with nonporous Armalon, layup the graphite prepreg books precut to the size, stacking order, and number of plies as specified in the appropriate drawing or specification. Use cork, coreprene, or silicone rubber dams around circumference.

3. A ply of porous Armalon shall be placed over the graphite prepreg followed by plies of 120 glass bleeder cloth. A ratio of one ply of 120 glass cloth to the required amount of graphite shall be used.

4. One ply of nonporous Armalon shall be placed on top of the last ply of 120 glass bleeder cloth.

5. Wrap the assembly with a minimum of three layers of Osnaburg cloth.

6. Vacuum bag the entire assembly.

III. Cure Cycles

a. For Laminates A, B, and C

1. Apply full vacuum (24-inch to 28-inch Hg) to the bagged assembly and apply 15±2 psig autoclave pressure.

2. Heat to 240±10°F at a heat-up rate of 3°F/min to 6°F/min, hold at 240°F for 60 to 70 minutes.

3. Holding autoclave pressure at 15 psig, vent bag and raise temperature to 350°F at 1° to 6°F/min.

4. Hold at 350°F for two hours (120 ±10 minutes).

5. Cool the assembly to 150°F or less under pressure.

6. Release the pressure and then remove assembly from autoclave.

7. Postcure the assembly at 350°F for a minimum of 8 hours in an air-circulating oven.

b. For Laminate D

1. Apply full vacuum (24-inch to 28-inch Hg) to the bagged assembly and apply 85 ±5 psig autoclave pressure.

2. Heat to 240 ±10 F at a heatup rate of 3 F/min to 6 F/min, hold at 240 F for 60 to 70 minutes.

3. Increase autoclave pressure to 100 psig and vent vacuum bag, raise temperature to 350 F at a rate of 1 F /min to 6 F/min.

4. Hold at 350 F for two hours (120 ±10 minutes).

5. Cool the assembly to 150 F or less under pressure.

6. Release the pressure and then remove assembly from autoclave.

7. Postcure the assembly at 350 F for a minimum of 8 hours in an air-circulating oven.

IV. Nondestructive Inspection

The laminate assemblies shall be submitted to the inspection facility (in-house or subcontract service) for nondestructive inspection. NDI will consist of ultrasonic C-scan inspection and radiographic inspection on laminates A, B and C, and C-scan inspection only, on laminate D.

V. Destructive Inspection

1. Trim the assembly to final dimensions and cut QC specimens as specified in appropriate drawing, fabrication work order, or specifications.

2. QC test specimens shall meet the minimum requirements set forth in QC Instruction Sheet No. 2.

VI. Fabrication of 1581/5208 Fiberglass Tabs

1. Over a clean caul plate covered with nonporous Armalon, layup the required size laminate of 1581/5208 fiberglass cloth prepreg, as specified. One peel ply shall be placed on top of the last ply of fiberglass prepreg.

2. One ply of porous Armalon shall be placed on top of the peel ply. One ply of nonporous Armalon shall be placed on top of the porous Armalon.

3. Wrap the assembly with at least two-ply Osnaburg cloth.

4. Vacuum bag the entire assembly.

5. Cure the assembly for 90 ±10 minutes at 350 ±10°F using 35 ± psi autoclave pressure plus full vacuum (approximately 50 psi total).

6. Heatup rate to 350°F is to be 3°F/min to 6°F/min.

7. Fiberglass tabs shall be cut from the fiberglass laminate to the dimensions specified.

VII.   Secondary Bonding of 1581/5208 Fiberglass Tabs

1. The fiberglass tabs shall be bonded to the assembly using Metalbond 329, AF-143, FM-123, of AF-126 as required by the appropriate Fabrication work order, drawing, or specification.

2. The bonding cycle for Metalbond 329 on AF-143 shall be 350 ±10°F for 60 to 70 minutes using 50 ±5 psi per NAI 1370. Heatup rate from RT to 225°F shall be 3°F/min to 6°F/min. The bonding cycle for FM-123 or AF-126 shall be between 250°F and 275°F for 90 to 100 minutes using 35 ±5 psi. Heatup rate from RT to 225°F shall be 3°F/min to 6°F/min. From 225°F to 350°F the heat-up rate will be 1°F to 6°F.

VIII.   Machining of Test Specimens

Test specimens shall be sectioned from the assembly as specified in the appropriate drawings and specifications.

Prepared by *Edmond G. Dusablon*
Approved by *Glenn C. Grinier*

APPENDIX B

DRAWINGS AND PHOTOMICROGRAPHS

FABRICATION DRAWINGS FOR PROGRAM TEST LAMINATES.

DRAWINGS FOR TEST SPECIMEN CONFIGURATIONS AND
TEST FIXTURE DETAILS.

PHOTOMICROGRAPHS OF LONGITUDINAL (L) AND
TRANSVERSE (T) CROSS-SECTIONS OF SPECIMENS
FROM PROGRAM LAMINATES.
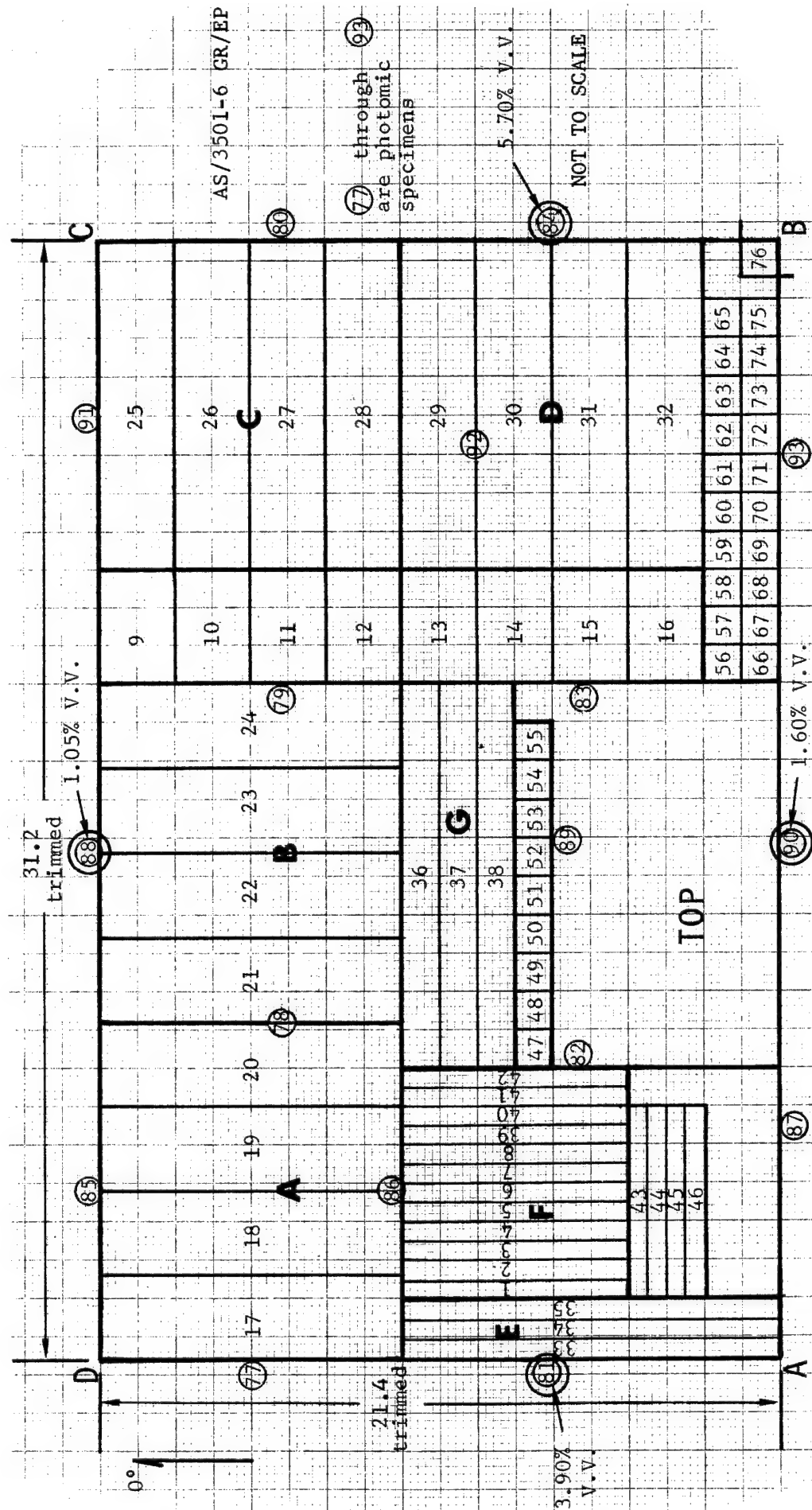
Figure B1. Uniform Porosity Laminate A, $[0]_{24T}$, Specimen Cutting Diagram.

127
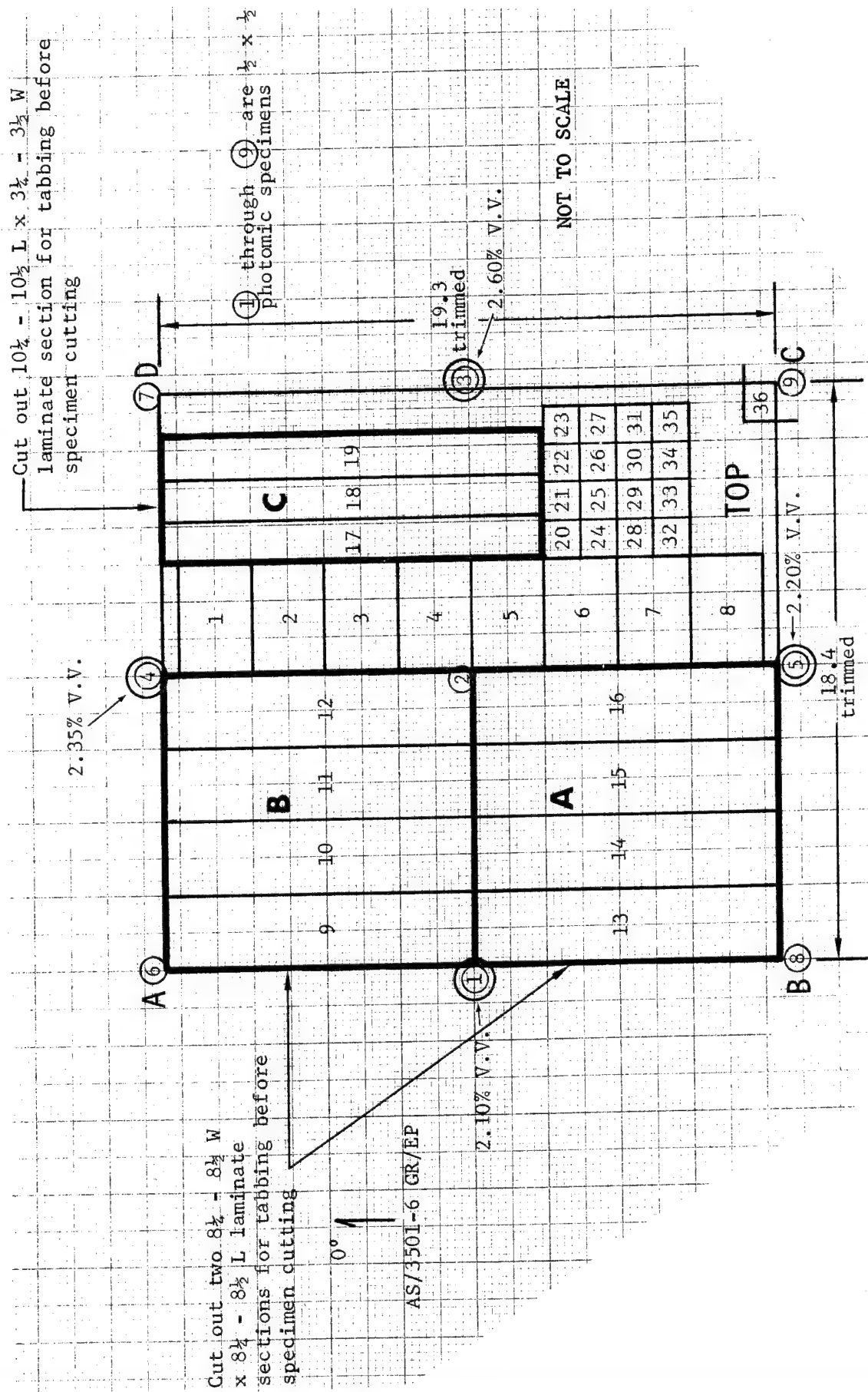
Figure B2. Uniform Porosity Laminate B, $[\pm45]_{6s}$, Specimen Cutting Diagram.

Figure B3. Uniform Porosity Laminate C, $[(\pm45)_5/0_{16}/90_4]_c$, Specimen Cutting Diagram.

129

Built in delamination between 15th and 16th ply, 3 places.

① through ⑮ are ½ x ½ photomic specimens

0°

AS/3501-6 GR/EP

NOT TO SCALE

< 0.10% V.V.

< 0.10% V.V.

0% V.V.

26 trimmed

< 0.05% V.V.

16 trimmed

TOP

Cut out two 8¼ - 8½ L x 8¼ x 8½ L laminate sections for tabbing before specimen cutting.

Cut out 3¼ - 3½ L x 10¼ - 10½ W laminate section for tabbing before specimen cutting

A 1, 2, 3, 4, 5, 6, 7, 8

B 9, 10, 11, 12, 13, 14, 15

C 13, 14, 15

16 17 18 19 20 21 22 23 24 31 32
25 26
27 28
29 30

A ① ⑩ ⑫ ④ ⑭ B ⑦
D ③ ⑥ ⑮ C ⑨
② ⑪ ⑬ ⑧

Figure B4. DL Laminate D, [(±45)₅/0₁₆/90₄]c, Specimen Cutting Diagram.

130
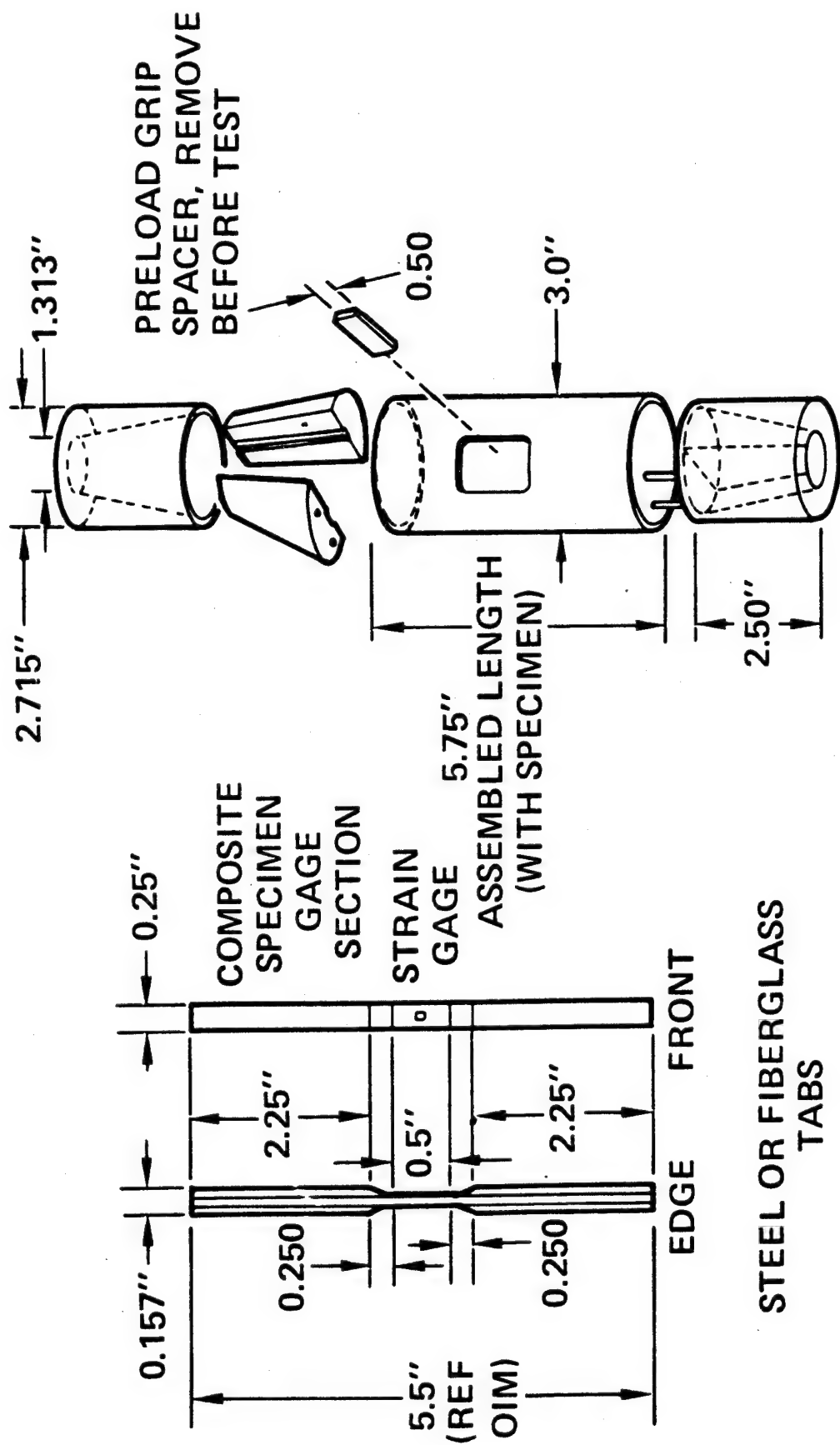
Figure B5. Standard Compression Test Method (Celanese, Reference ASTM D-3410)

131
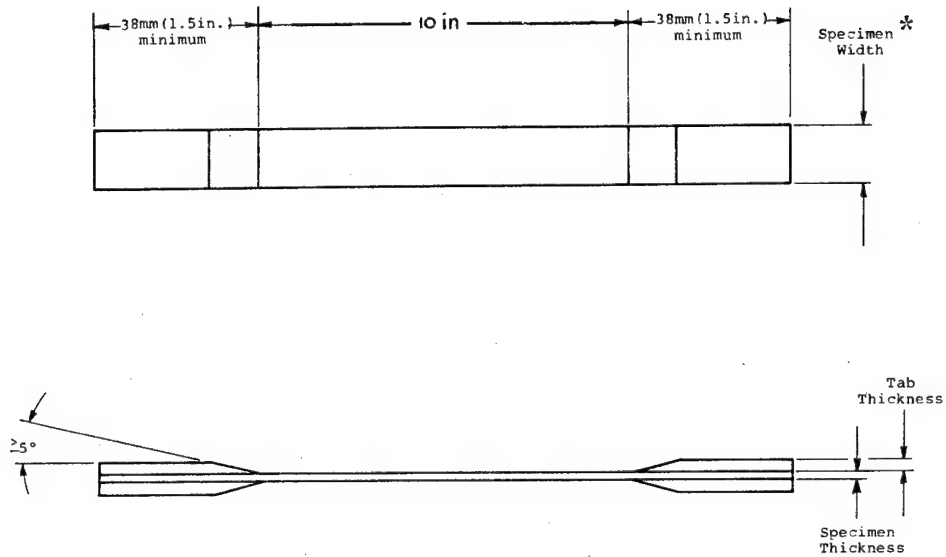
NOTE—Bond laminate tabs on two sides and at both ends. Tabs are applied to the end of the test composite with a suitable adhesive. Each tab is a minimum of 38 mm (1.5 in.) long by the width of the laminate and a thickness of approximately 1.5 to 4 times the thickness of the test composite.

*Specimen width = 1/2" for static longitudinal tension
 Specimen width = 1 " for static transverse tension

Figure B6.   Static Longitudinal and Transverse Tension Specimen.
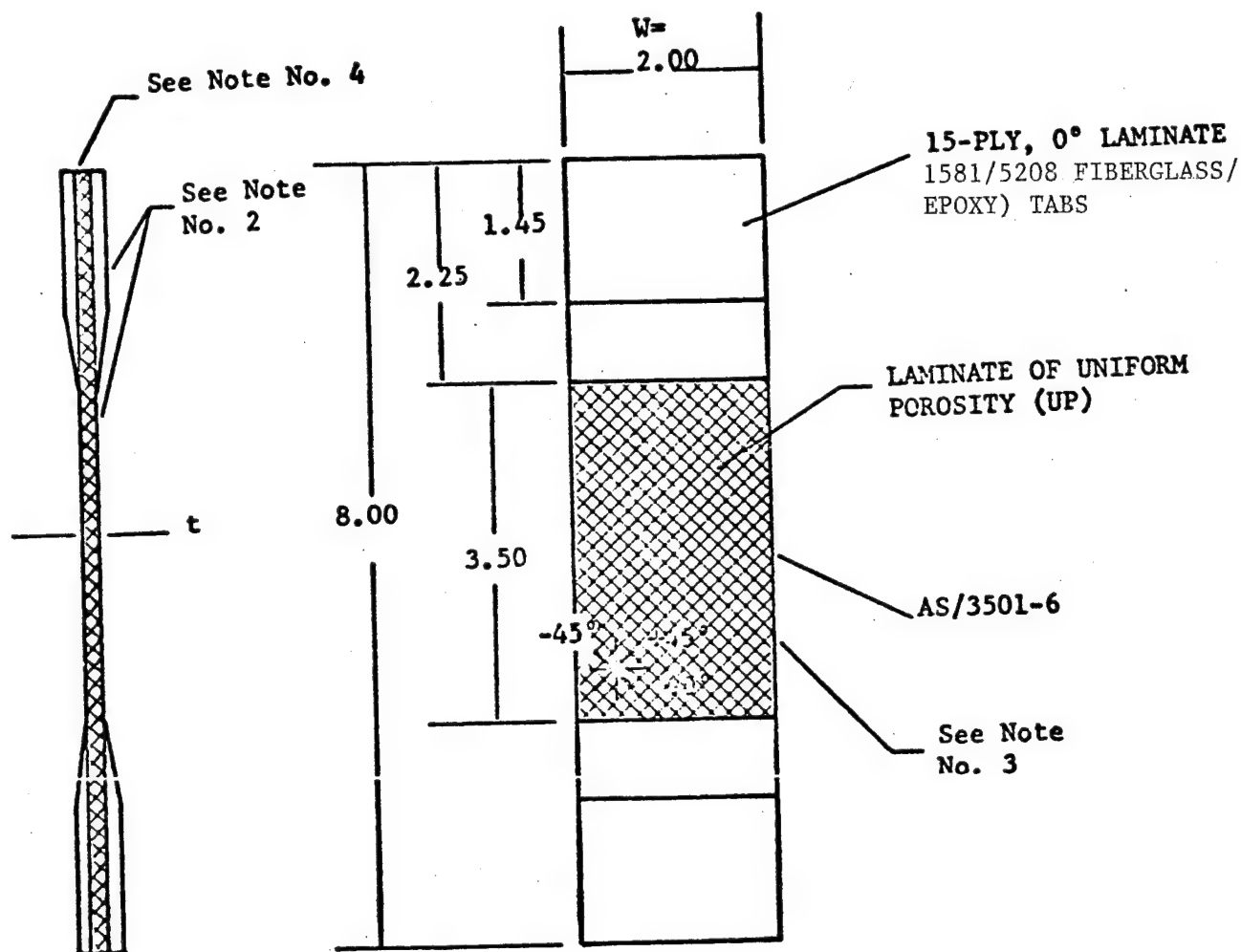
1. BOND 1581/5208 TABS WITH APPROPRIATE ADHESIVE.

2. SPECIMEN THICKNESS SHALL NOT VARY MORE THAN ±0.005 INCH FROM NOMINAL.

3. SPECIMEN LONGITUDINAL EDGE SHALL BE PARALLEL TO 0.005 INCH.

4. TOP AND BOTTOM SURFACES SHALL BE FLAT AND PARALLEL TO 0.001 INCH.

Figure B7. Atmur Test Specimen-Uniform Porosity Laminate
Fatigue and Residual Strength.

All dimensions in inches (1 in. = 25.4 mm)

Section A-A
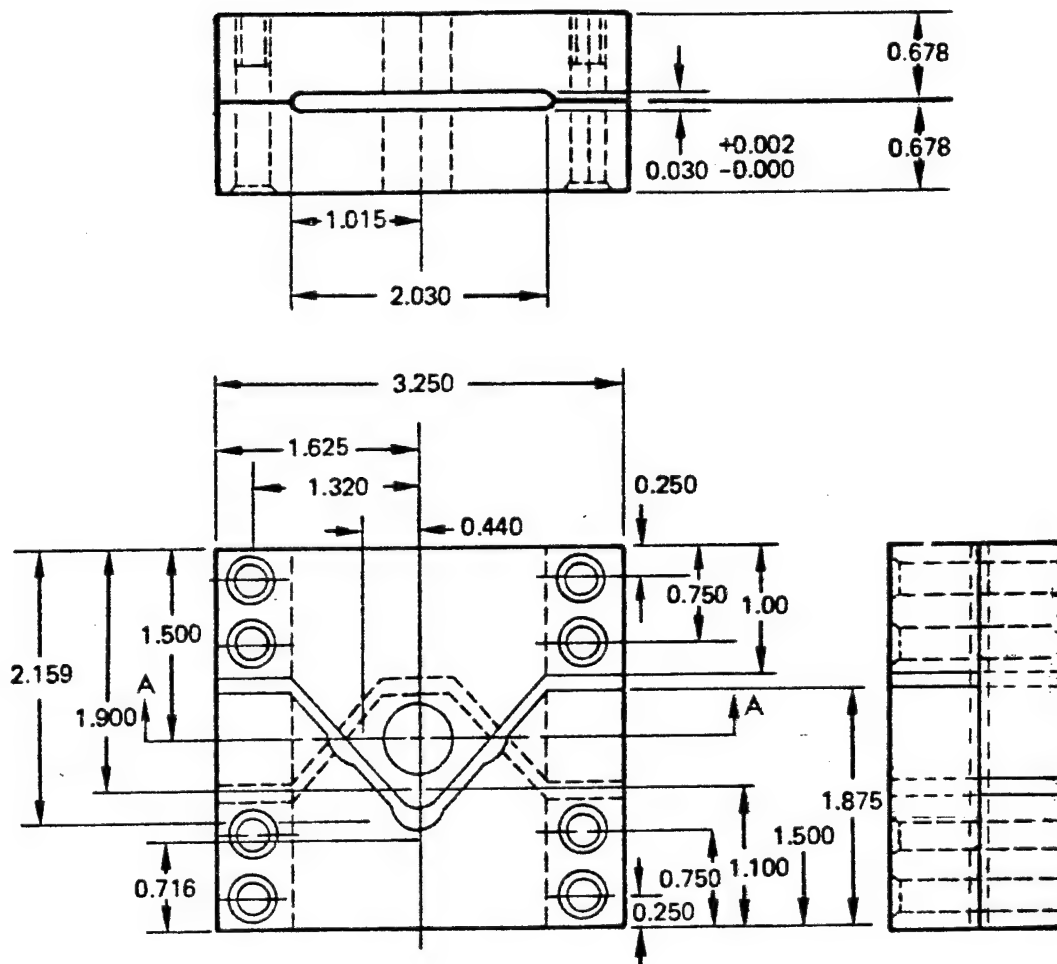
Figure B8.   Static Compression Test Fixture
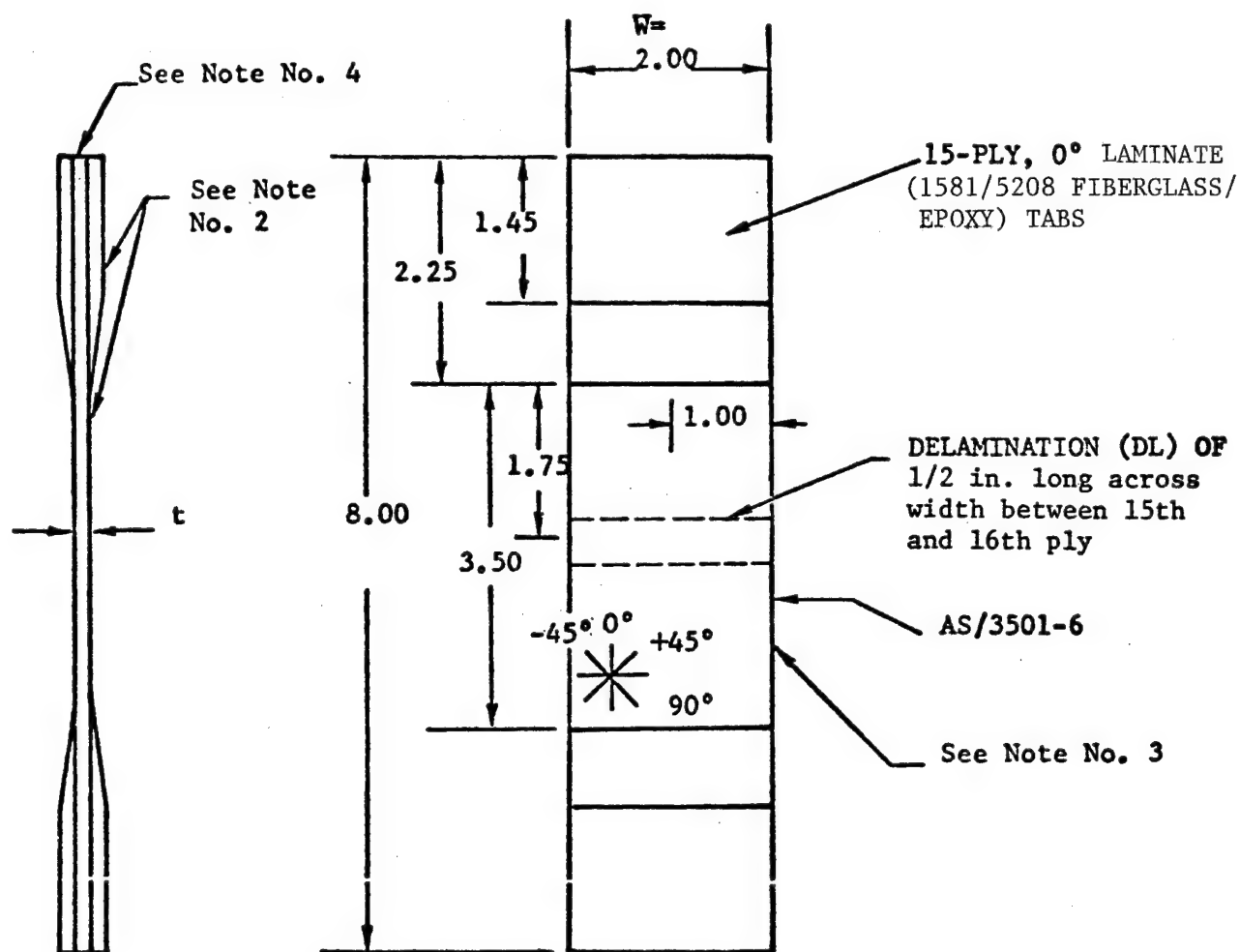
1. BOND 1581/5208 TABS WITH APPROPRIATE ADHESIVE.

2. SPECIMEN THICKNESS SHALL NOT VARY MORE THAN ±0.005 INCH FROM NOMINAL.

3. SPECIMEN LONGITUDINAL EDGES SHALL BE PARALLEL TO 0.005 INCH.

4. TOP AND BOTTOM SURFACES SHALL BE FLAT AND PARALLEL TO 0.001 INCH.

Figure B9. Atmur Test Specimen-Laminate With Delamination
Fatigue and Residual Strength

135
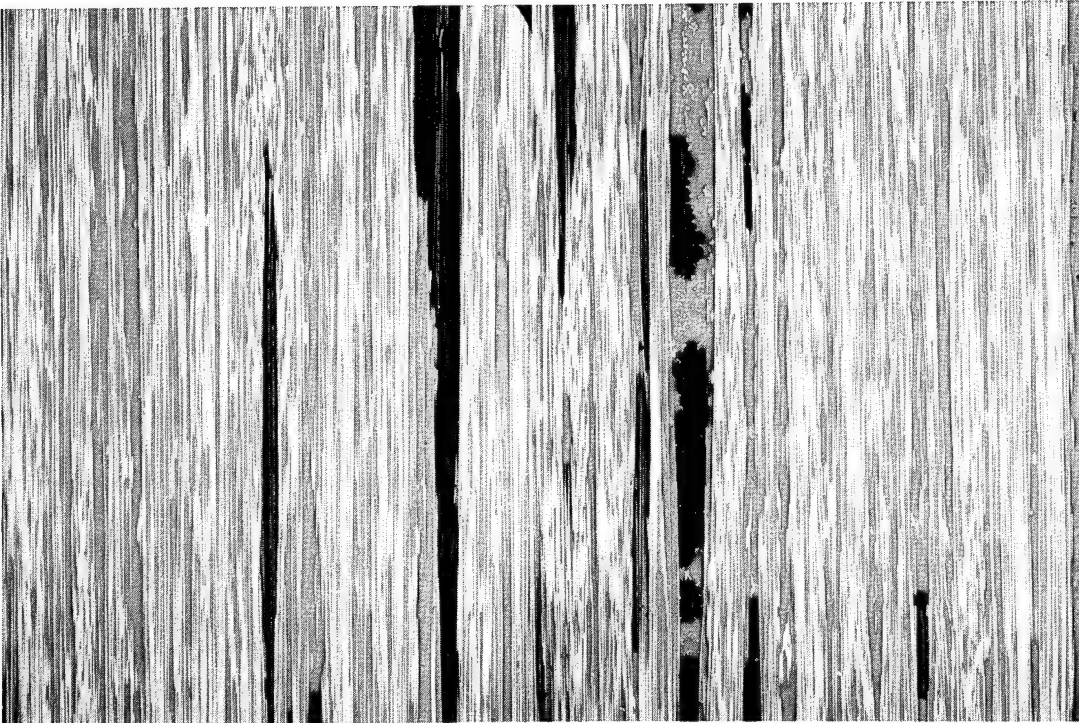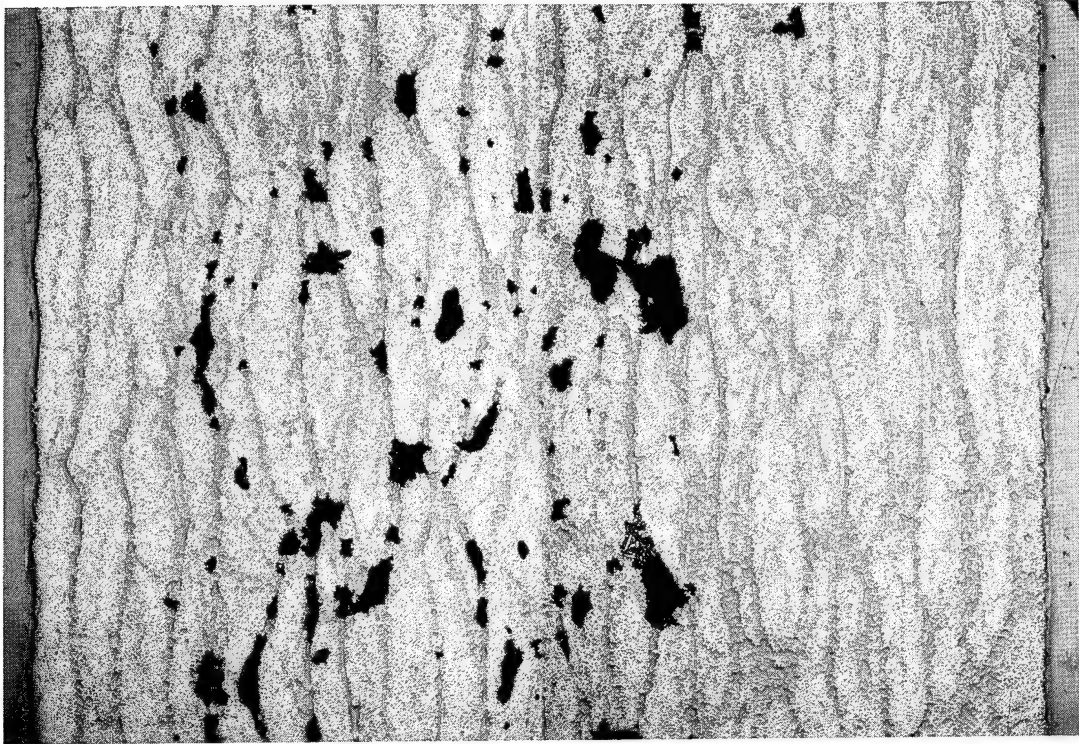
Specimen A-84T

Specimen A-84L

Figure B10. Specimen A-84 (ACL-4464); 50x Photomicrograph (reduced to ~70% of original size) of L and T Cross-Sections – I.A.V.V. = 5.7%.
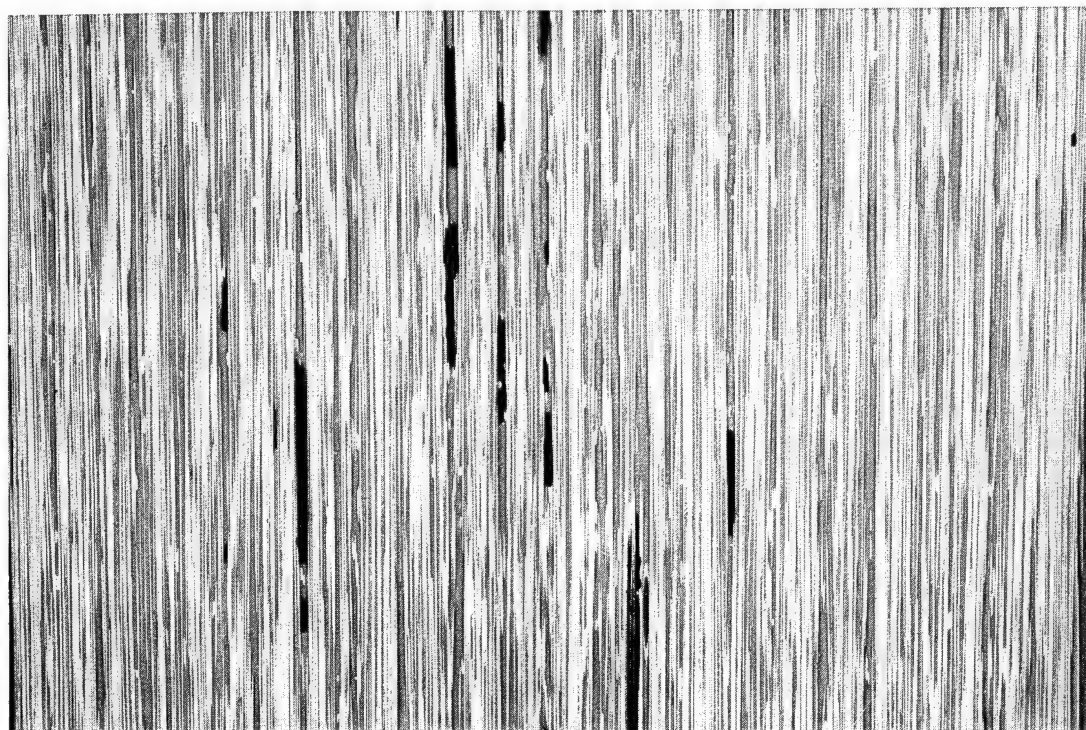
Specimen A-88L
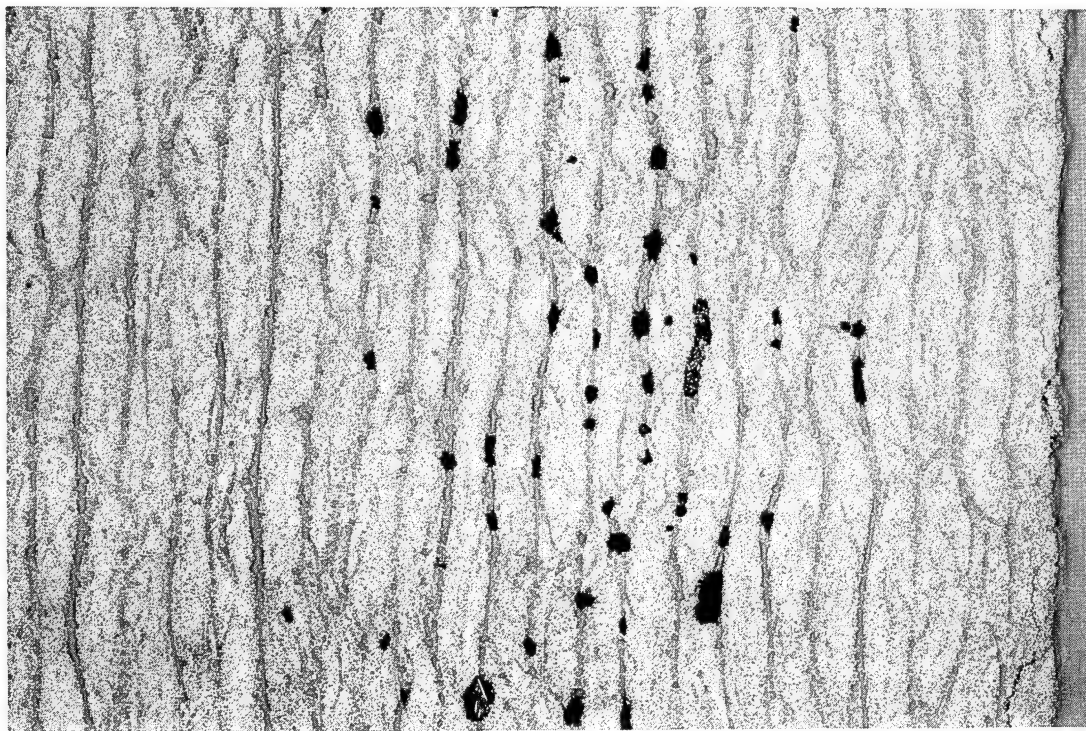
Specimen A-88T

Figure B11. Specimen A-88 (ACL-4464); 50x Photomicrograph (reduced to ~70% of original size) of L and T Cross-Sections - I.A.V.V. = 1.05%.
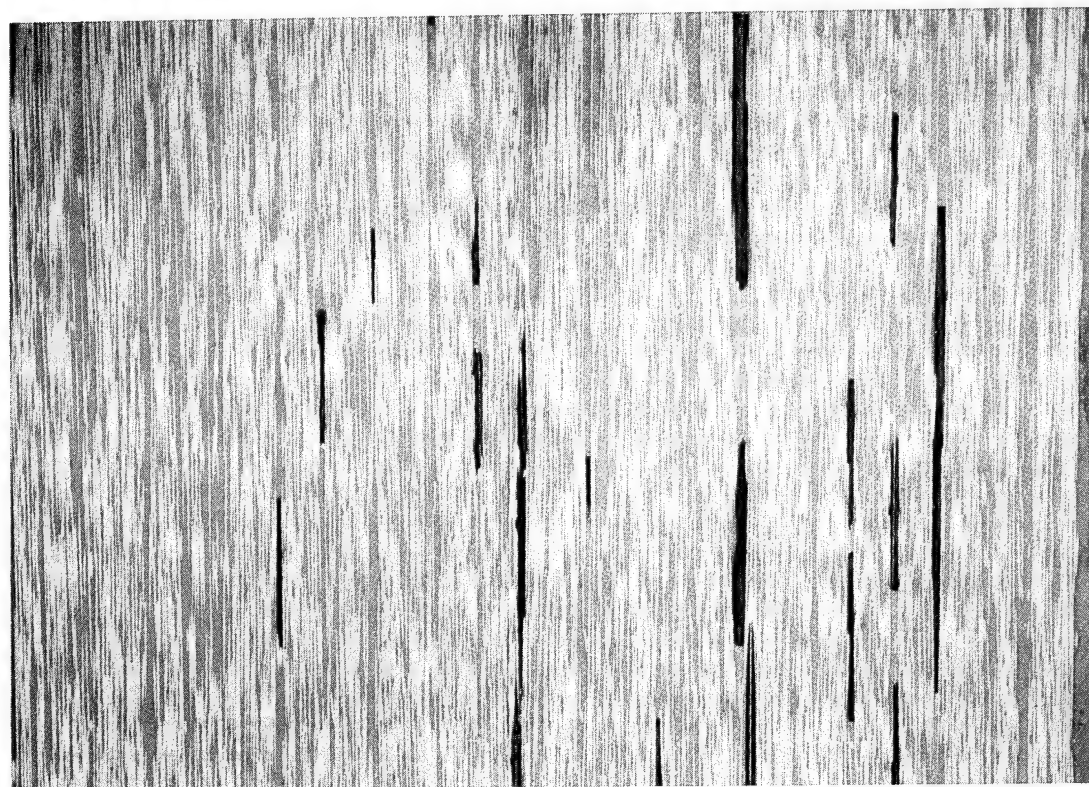
Specimen A-90T
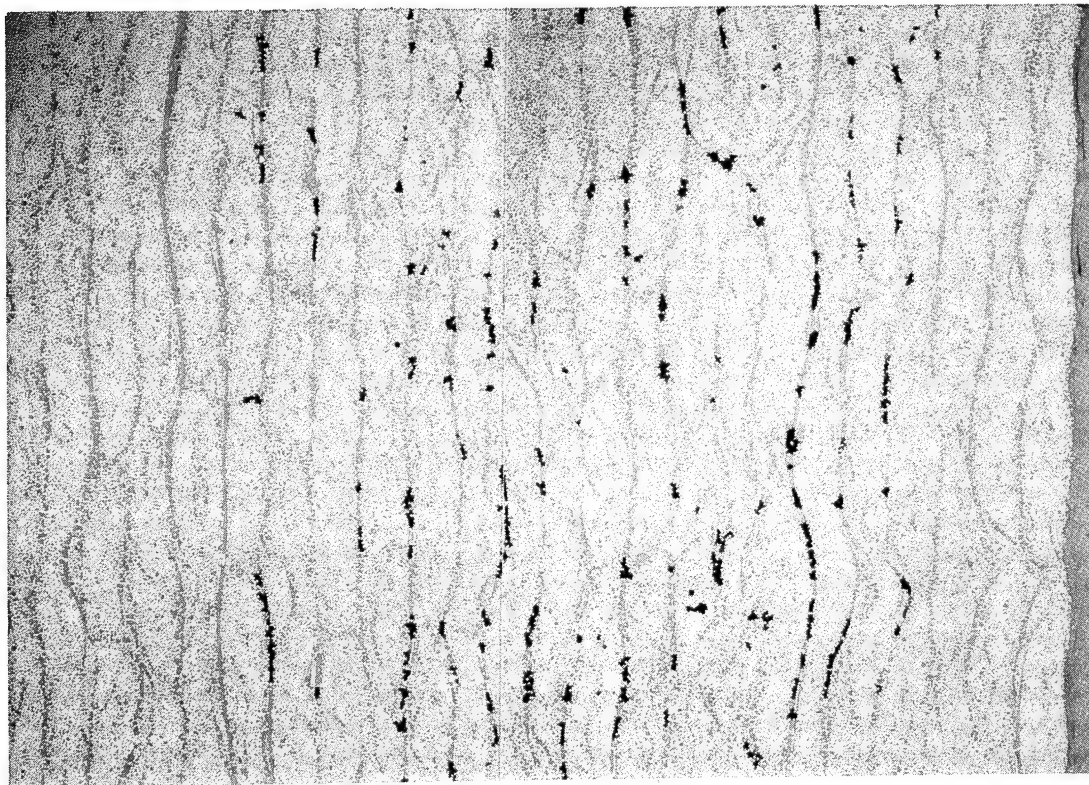
Specimen A-90L

Figure B12. Specimen A-90 (ACL-4464);50x Photomicrograph (reduced to ~75% of original size) of L and T Cross-Sections - I.A.V.V. = 1.60%.

138
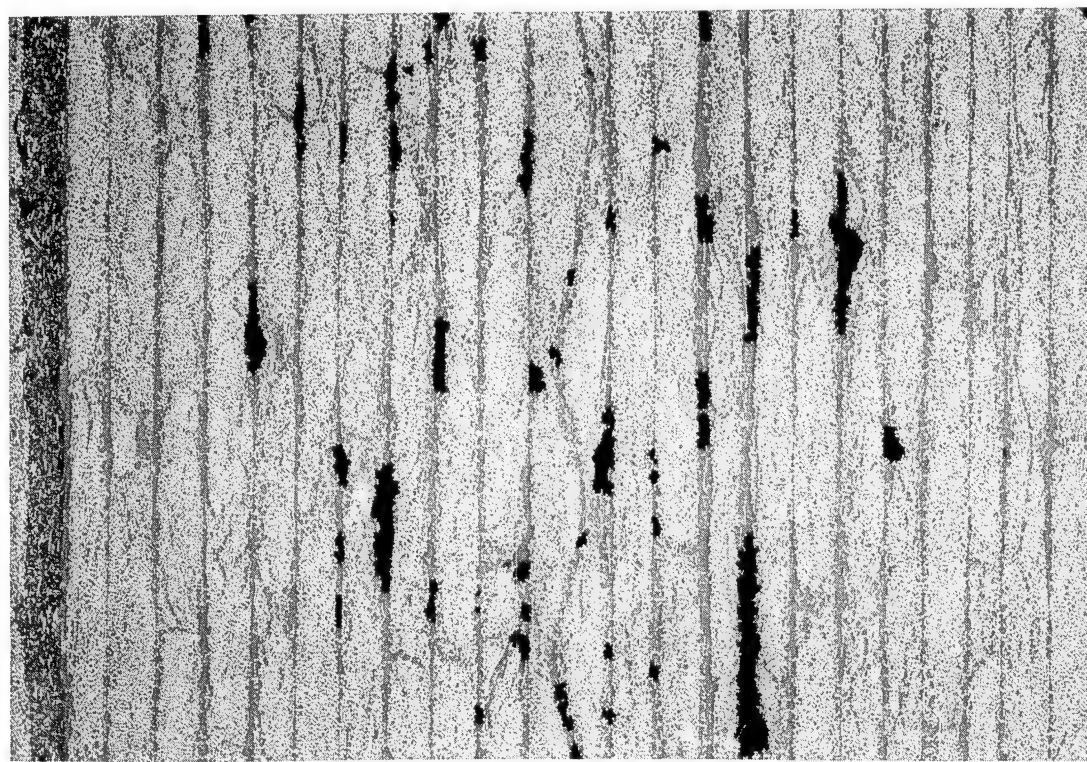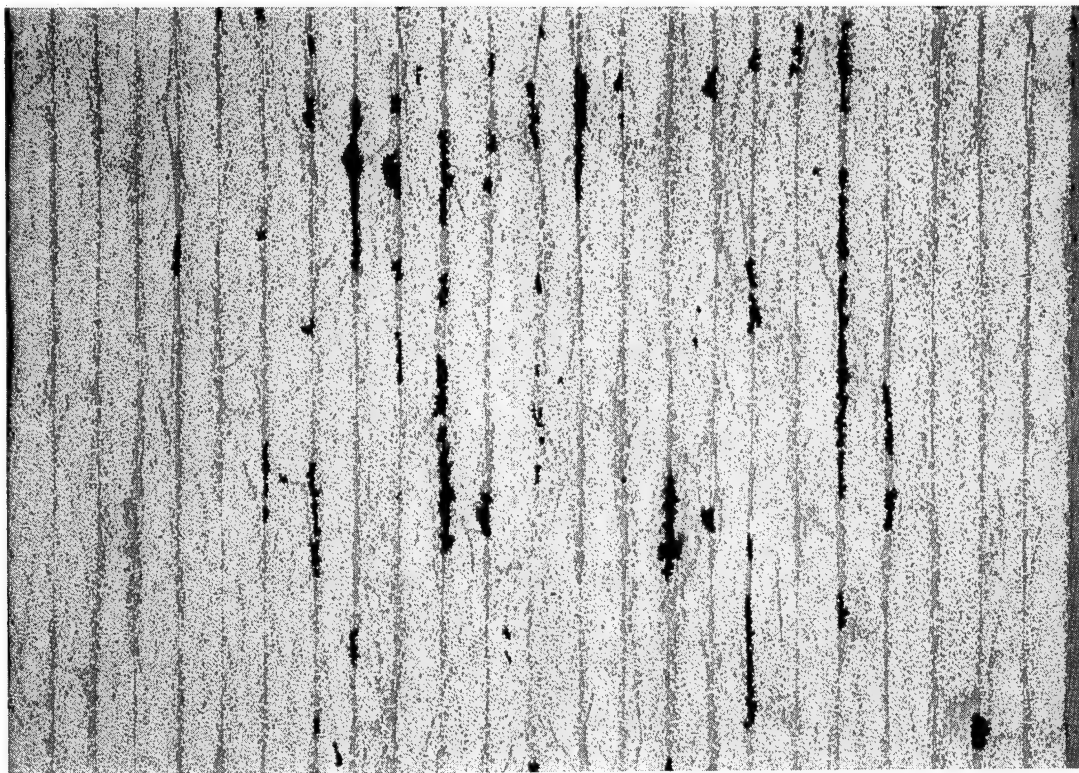
Specimen B-1T

Specimen B-1L

Figure B13. Specimen B-1 (ACL-4465); 50x Photomicrograph (reduced to ~75% of original size) of L and T Cross-Sections - I.A.V.V. = 2.10.
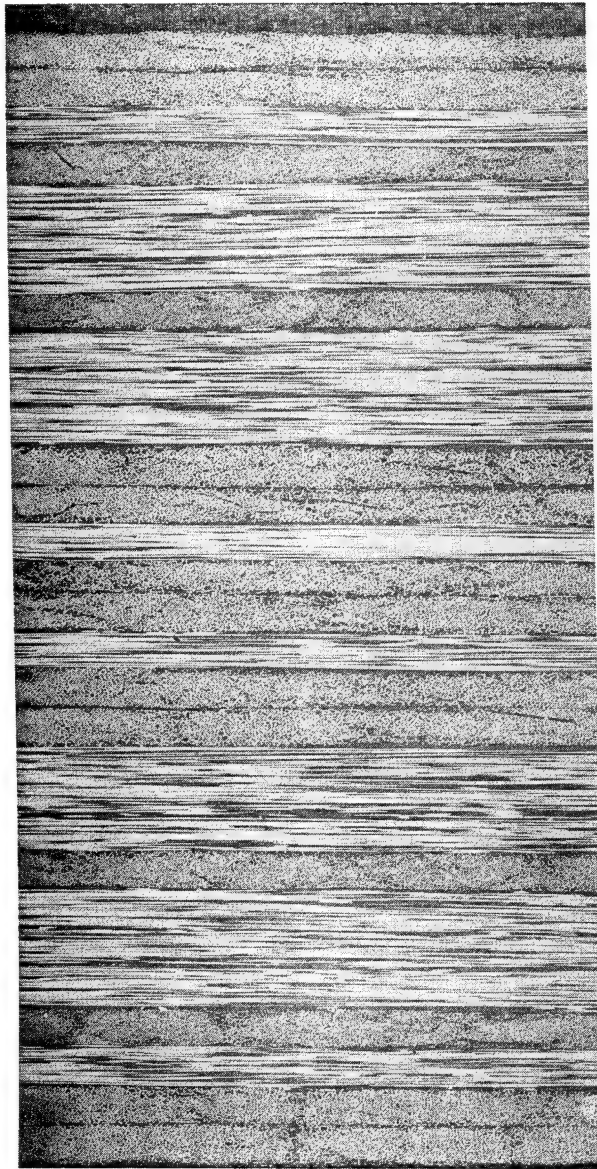
139
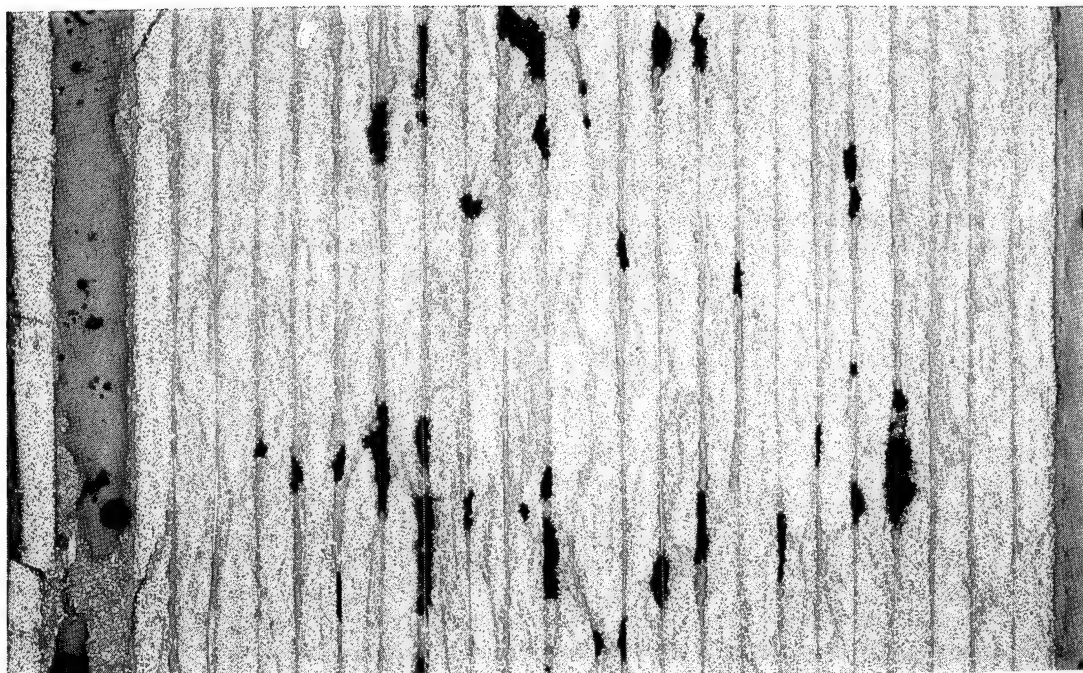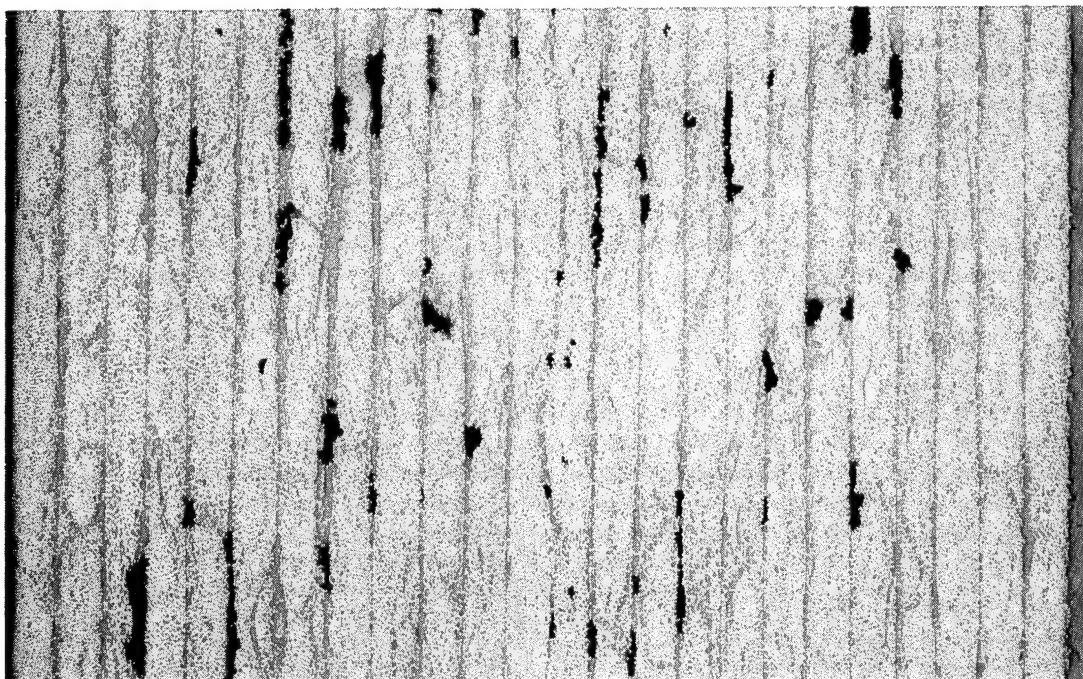
Specimen B-3T

Specimen B-3L

Figure B14. Specimen B-3 (ACL-4465); 50x Photomicrograph (reduced to~70% of original size) of L and T Cross-Sections - I.A.V.V. = 2.60%.
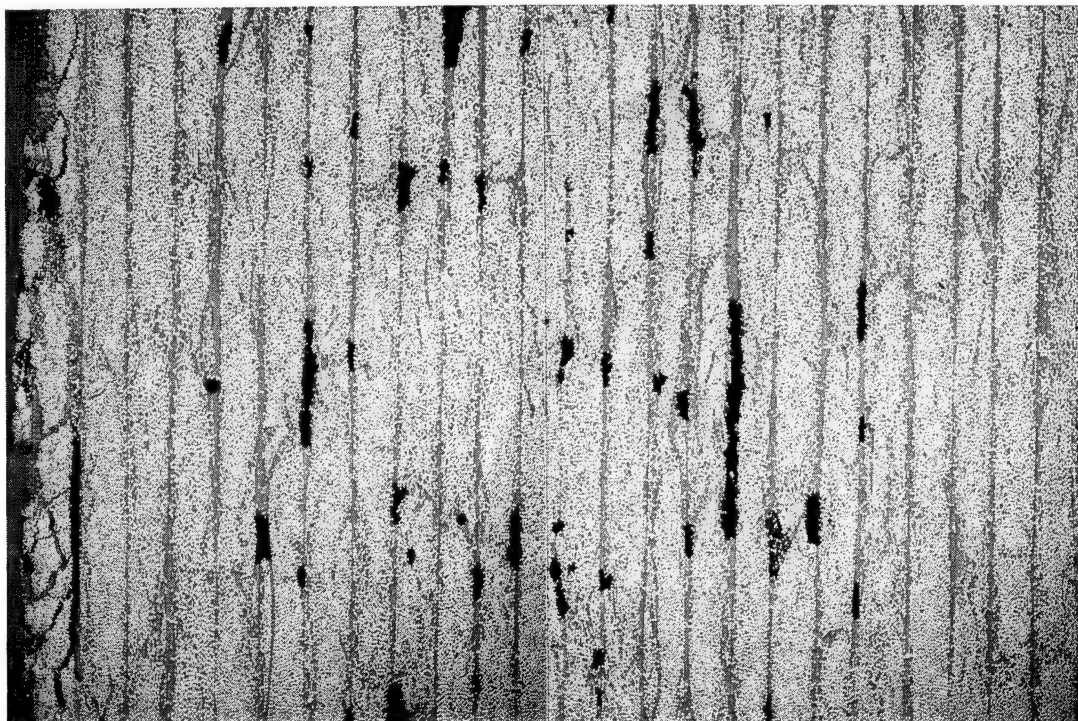
Specimen B-4T
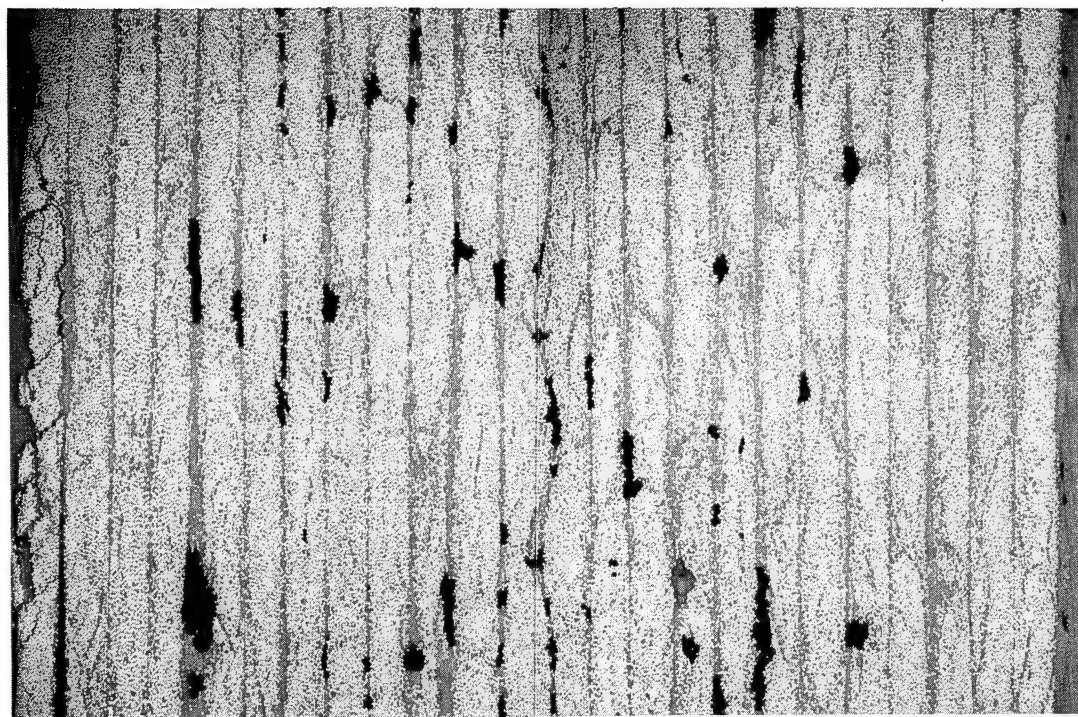
Specimen B-4L

Figure B15. Specimen B-4 (ACL-4465); 50x Photomicrograph (reduced to ~70% of original size) of L and T Cross-Sections - I.A.V.V. = 2.35%.

141
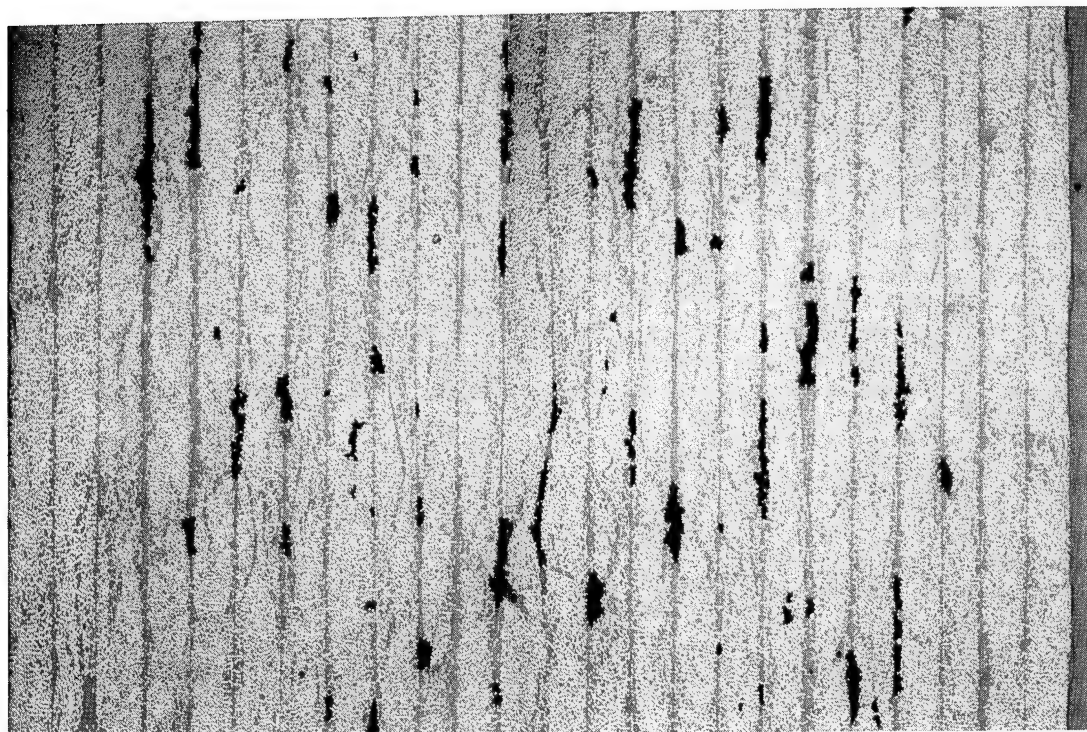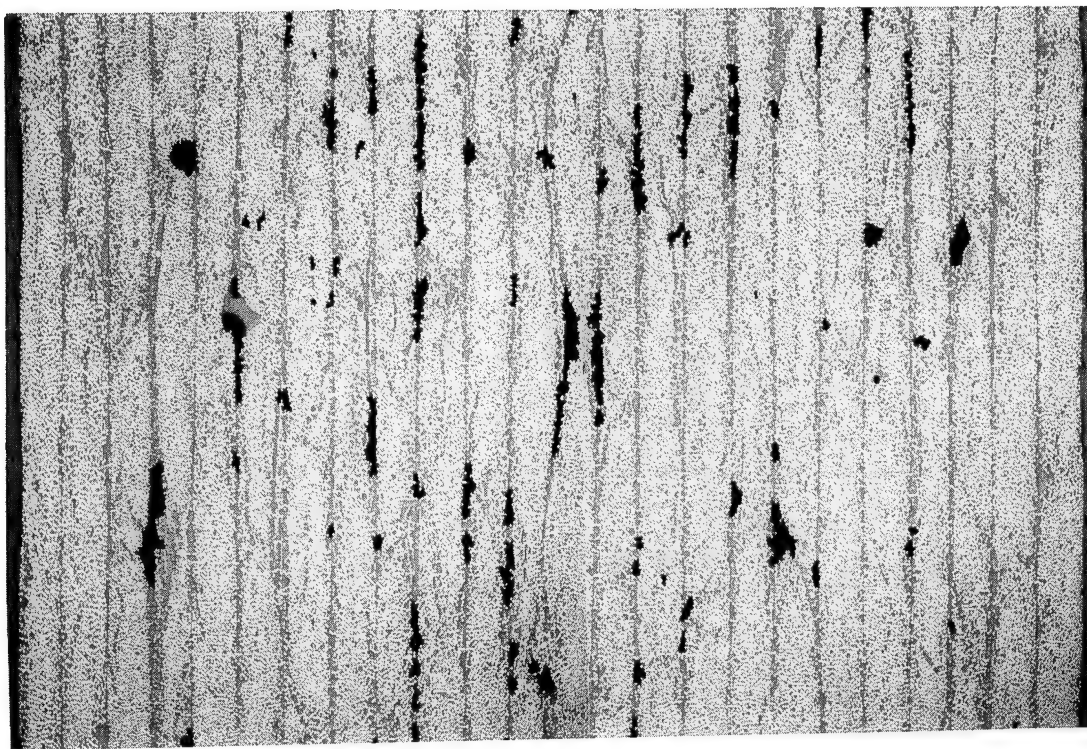
Specimen B-5T

Specimen B-5L

Figure B16. Specimen B-5 (ACL-4465); 50x Photomicrograph (reduced to ~70% of original size) of L and T Cross-Sections - I.A.V.V. = 2.20%.
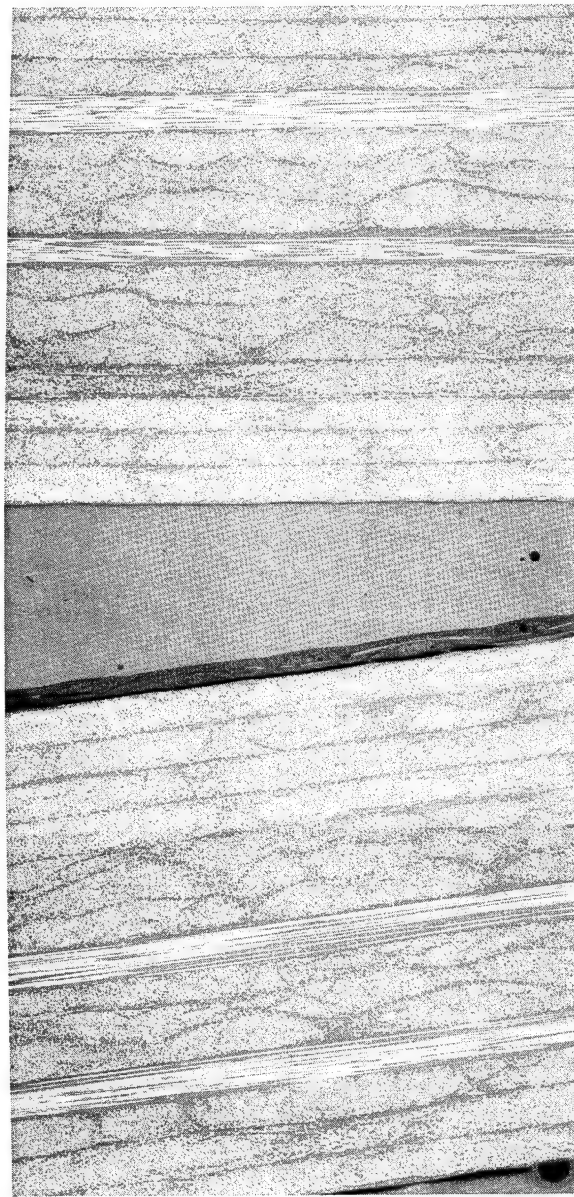
142
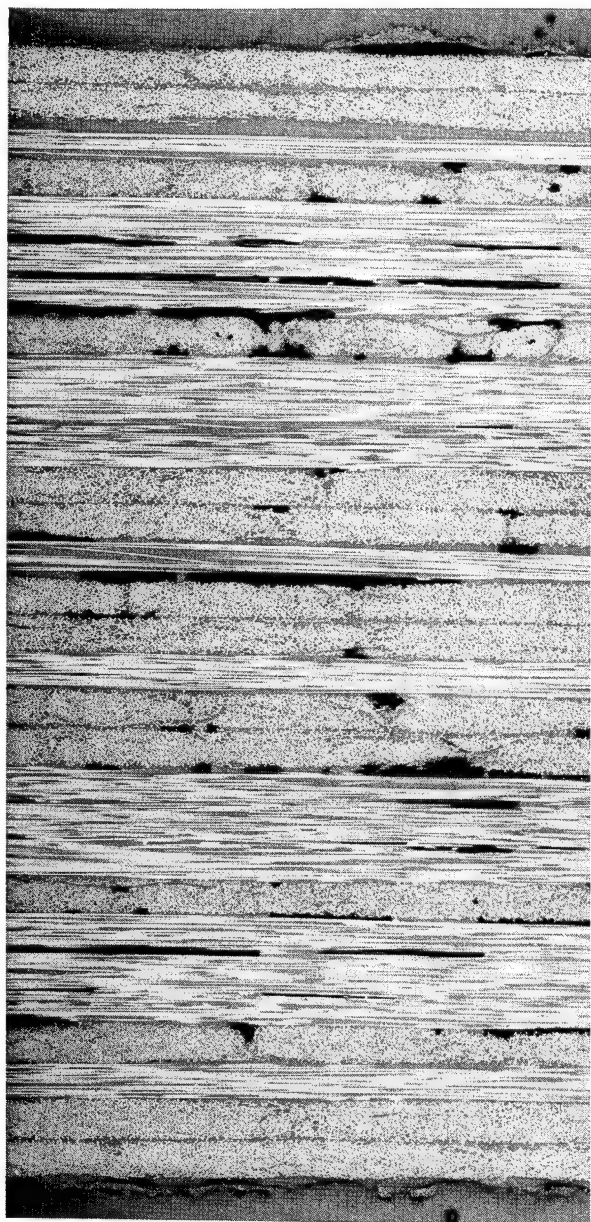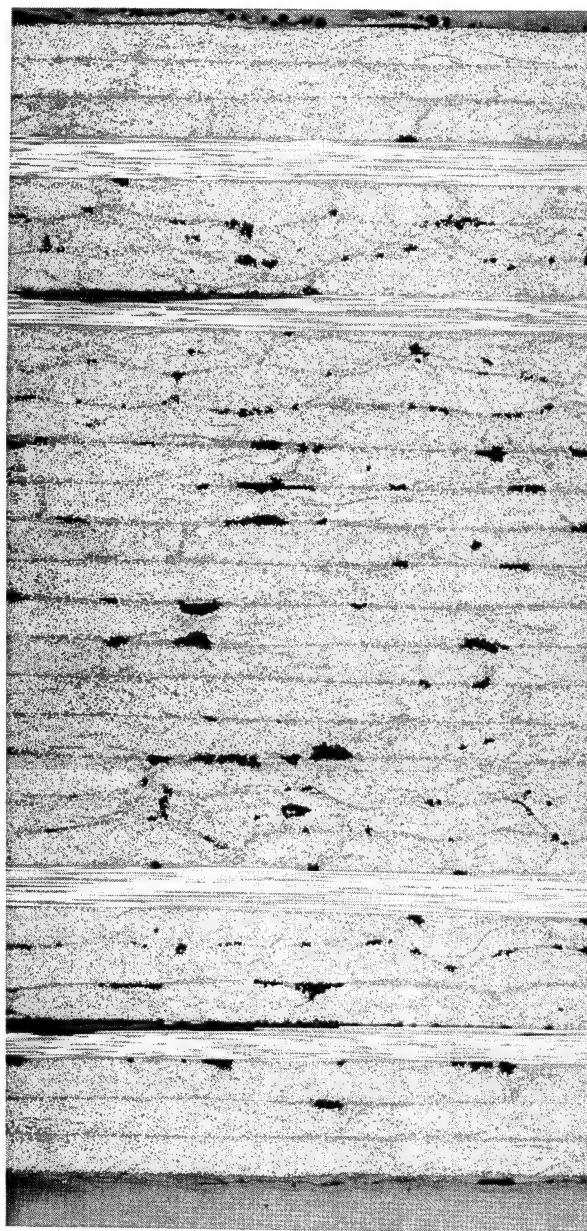
Specimen C-2L   Specimen C-2T

Figure B17.   Specimen C-2 (ACL-4466); 50x Photomicrograph (reduced to
              ~70% of original size) of L and T Cross-Sections – I.A.V.V.=
              3.35%.
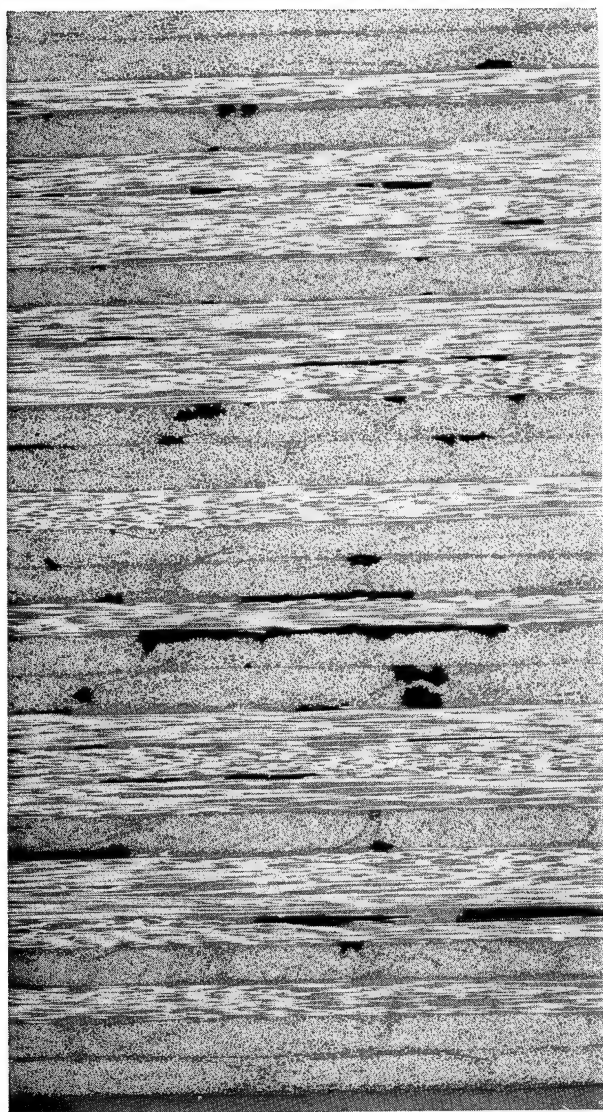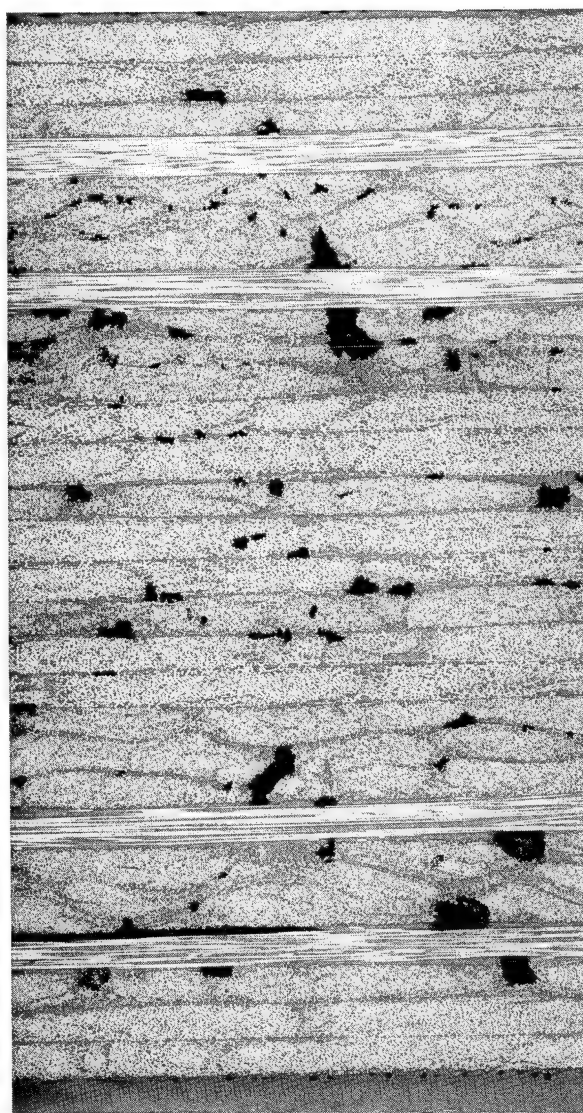
Specimen C-4L   Specimen C-4T

Figure B18.   Specimen C-4 (ACL-4466); 50x Photomicrograph (reduced to
              ~70% of original size) of L and T Cross-Sections-I.A.V.V. =
              2.70%.
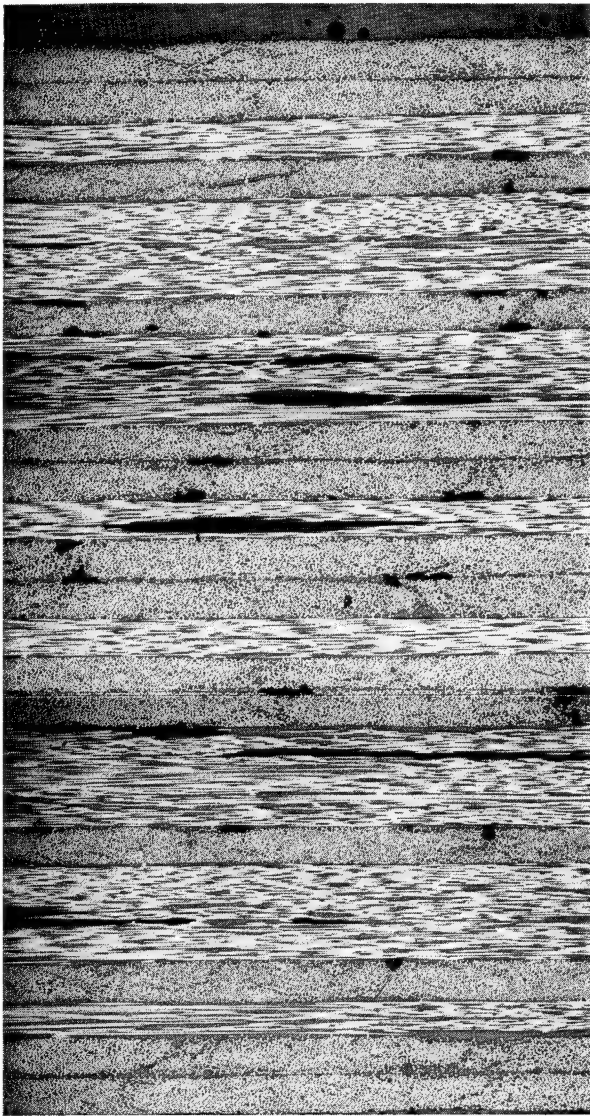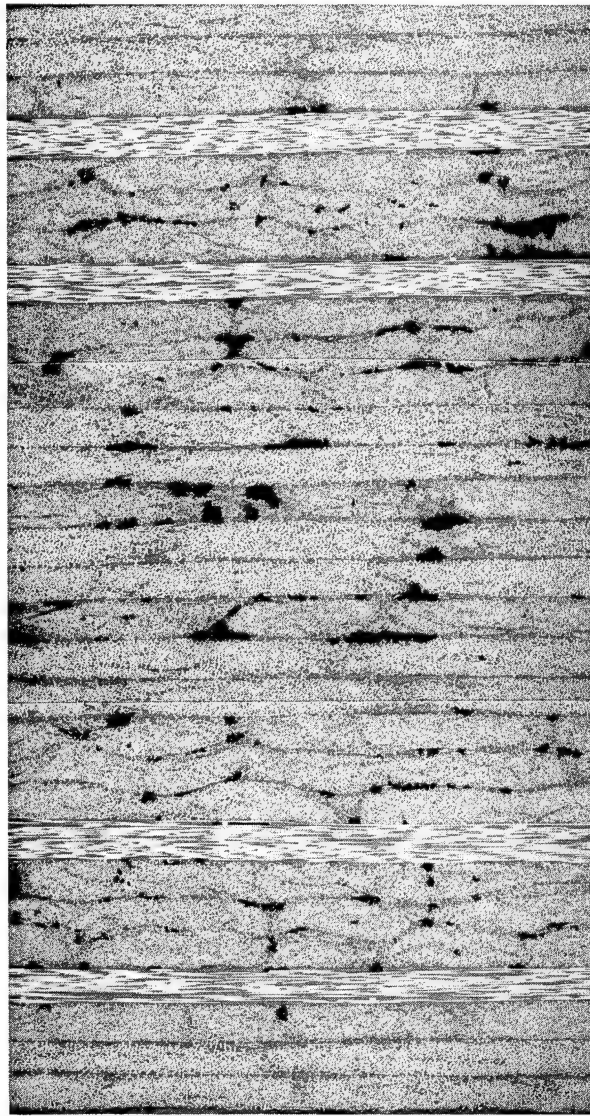
Specimen C-7L   Specimen C-7T

Figure B19.   Specimen C-7 (ACL-4466); 50x Photomicrograph (reduced to 70% of
                original size) of L and T Cross-Sections - I.A.V.V. = 3.20%.
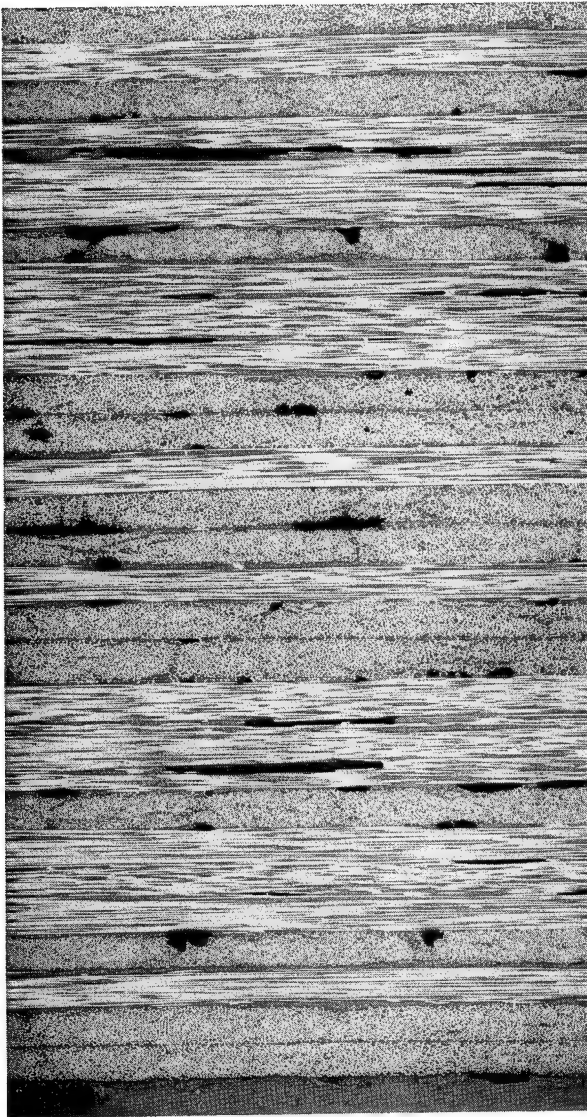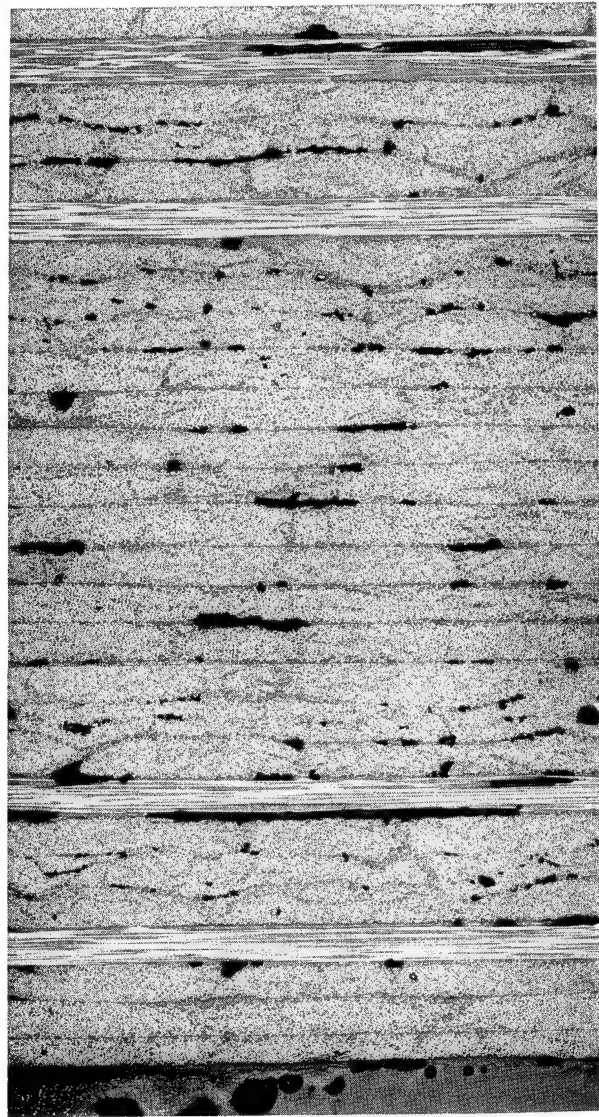
Specimen C-9L   Specimen C-9T

Figure B20.   Specimen C-9 (ACL-4466); 50x Photomicrographs (reduced to 70%
               of original size) of L and T Cross-Sections - I.A.V.V. =
               2.95%.
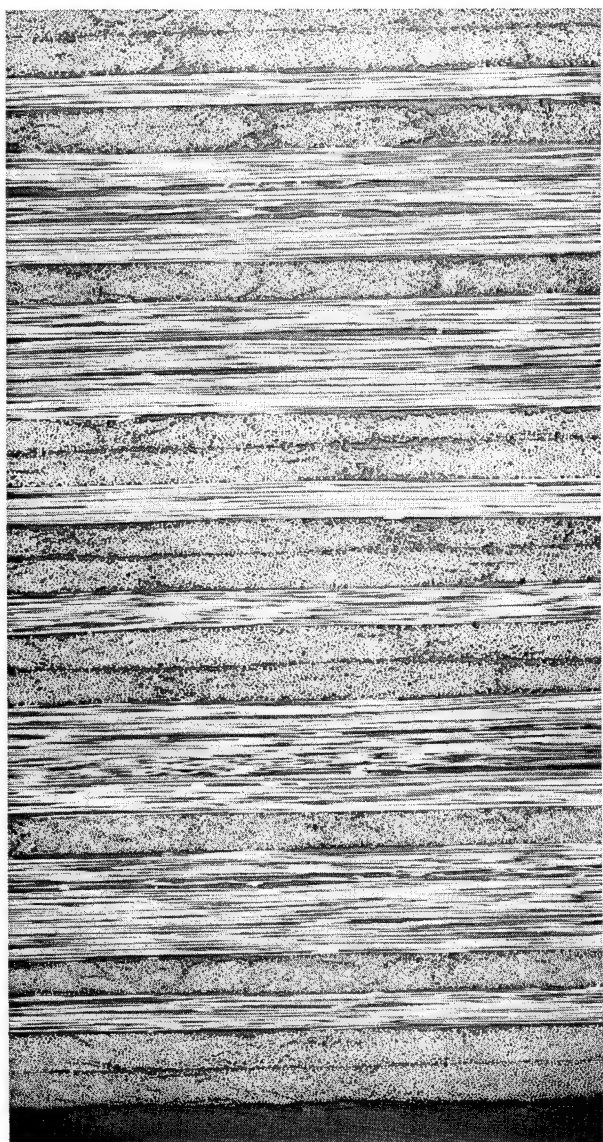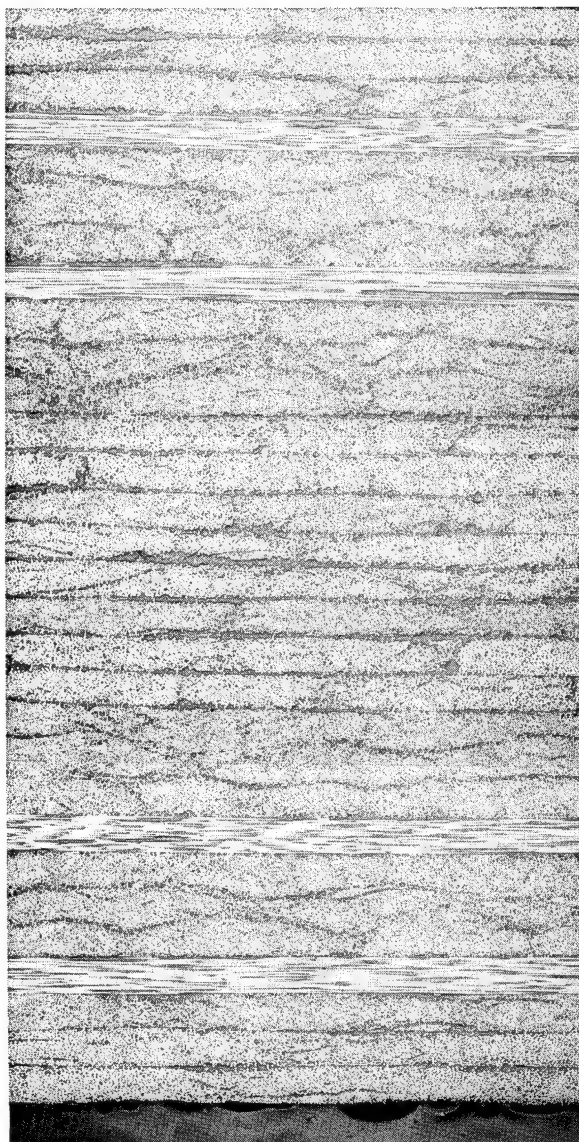
Specimen D-2L   Specimen D-2T

Figure B21.   Specimen D-2 (ACL-4472); 50x Photomicrograph (reduced to ~70%
              of original size) of L and T Cross-Sections - I.A.V.V. < 0.10%.
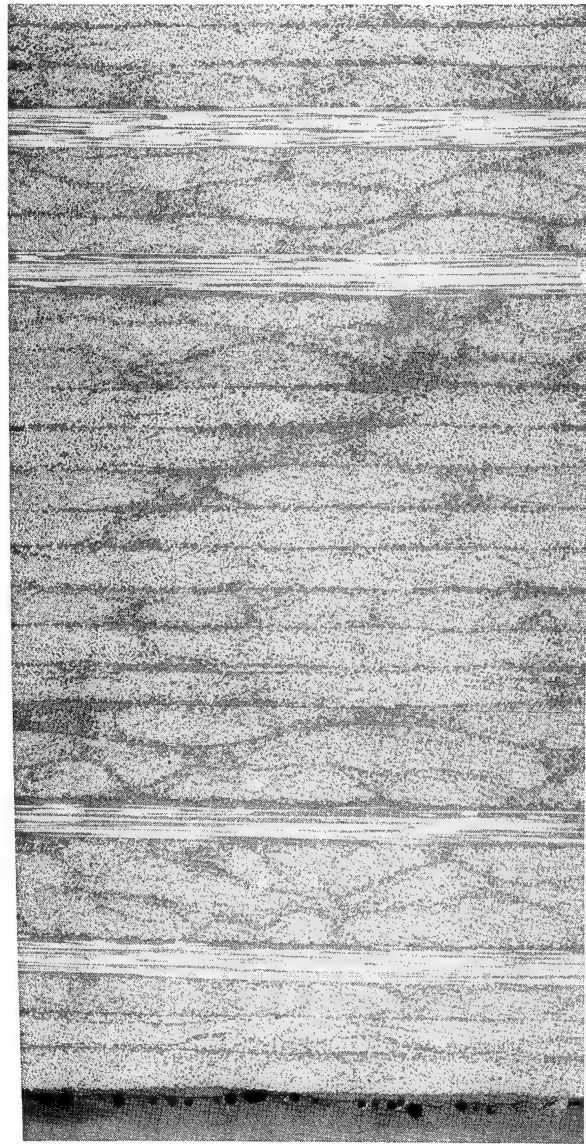
Specimen D-6L   Specimen D-6T

Figure B22.   Specimen D-6 (ACL-4472); 50x Photomicrographs (reduced to ~70% of original size) of the L and T Cross-Sections - I.A.V.V. = 0%.

Specimen D-8L

Figure B23. Specimen D-8 (ACL-4472); 50x Photomicrograph (reduced
to 70% of original size) of L Cross-Section - I.A.V.V.
< 0.05%.

Specimen D-10L   Specimen D-10T

Figure B24.   Specimen D-10 (ACL-4472);50x Photomicrograph (reduced to 70%
              of orignial size) of L and T Cross-Sections - I.A.V.V. < 0.10%.

TEST REPORT #: 3871MAL—R681-2   2 June 1981

REFERENCE: MTWO 8437 (MAL 481-29)

SUBMITTED BY: G. Grimes

REPORT BY: *S. L. Feenstra*   S. L. Feenstra

                      M. H. Ransick   M. H. Ransick

CONCURRENCE: *R. T. Kessler*   R. T. Kessler

SUBJECT:

     Photomicrographs of M & P Defect Specimens

PROCEDURE:

     Sixteen specimens were cut and mounted in the longitudinal and transverse direction. They were then polished and photographed at 50X. A montage was then made of the 50X photos for each specimen.

     After completion of the photomicrographs, image analyses to determine the void content of each specimen were performed.

RESULTS:

     As seen in the attached montages, a large amount of voids were present in A-81, A-84, A-88, A-90, B-1, B-3, B-4, B-5, C-2, C-4, C-7, and C-9. Although specimen D-10 did not contain any voids, it did contain a ply of something other than graphite/epoxy in the center of the laminate.

     All of the B specimens did not exhibit an apparent longitudinal or transverse direction. This indicated the orientation of the laminates was +45 degrees.

     Some of the specimens were wider in one direction than in the other. This appeared to be caused by the specimen being cut too close to the edge of the laminate where the dimensions are irregular.

The following is a listing of the void content as determined by image analysis.

Spec.#		% Voids	Spec.#		% Voids
A-81	T	4.6	C-2	T	3.1
A-81	L	3.2	C-2	L	3.6
A-84	T	5.8	C-4	T	3.1
A-84	L	5.6	C-4	L	2.3·
A-88	T	1.3	C-7	T	3.0
A-88	L	0.8	C-7	L	3.4
A-90	T	1.3	C-9	T	3.8
A-90	L	1.9	C-9	L	2.1
B-1	T	2.1	D-2	T	<.1
B-1	L	2.1	D-2	L	<.1
B-3	T	2.6	D-6	T	0
B-3	L	2.6	D-6	L	0
B-4	T	2.5	D-8	T	<.1
B-4	L	2.2	D-8	L	0
B-5	T	2.3	D-10	T	<.1
B-5	L	2.1	D-10	L	<.1

Mount numbers for the specimens are as follows:

Spec.#	Mount #	Spec.#	Mount #
A-81	81-0182-7-2	C-2	81-0190-7-2
A-84	81-0183-7-2	C-4	81-0191-7-2
A-88	81-0184-7-2	C-7	81-0192-7-2
A-90	81-0185-7-2	C-9	81-0193-7-2
B-1	81-0186-7-2	D-2	81-0194-7-2
B-3	81-0187-7-2	D-6	81-0195-7-2
B-4	81-0188-7-2	D-8	81-0196-7-2
B-5	81-0189-7-2	D-10	81-0197-7-2

APPENDIX C

PHOTOGRAPHS OF FAILED TEST SPECIMENS
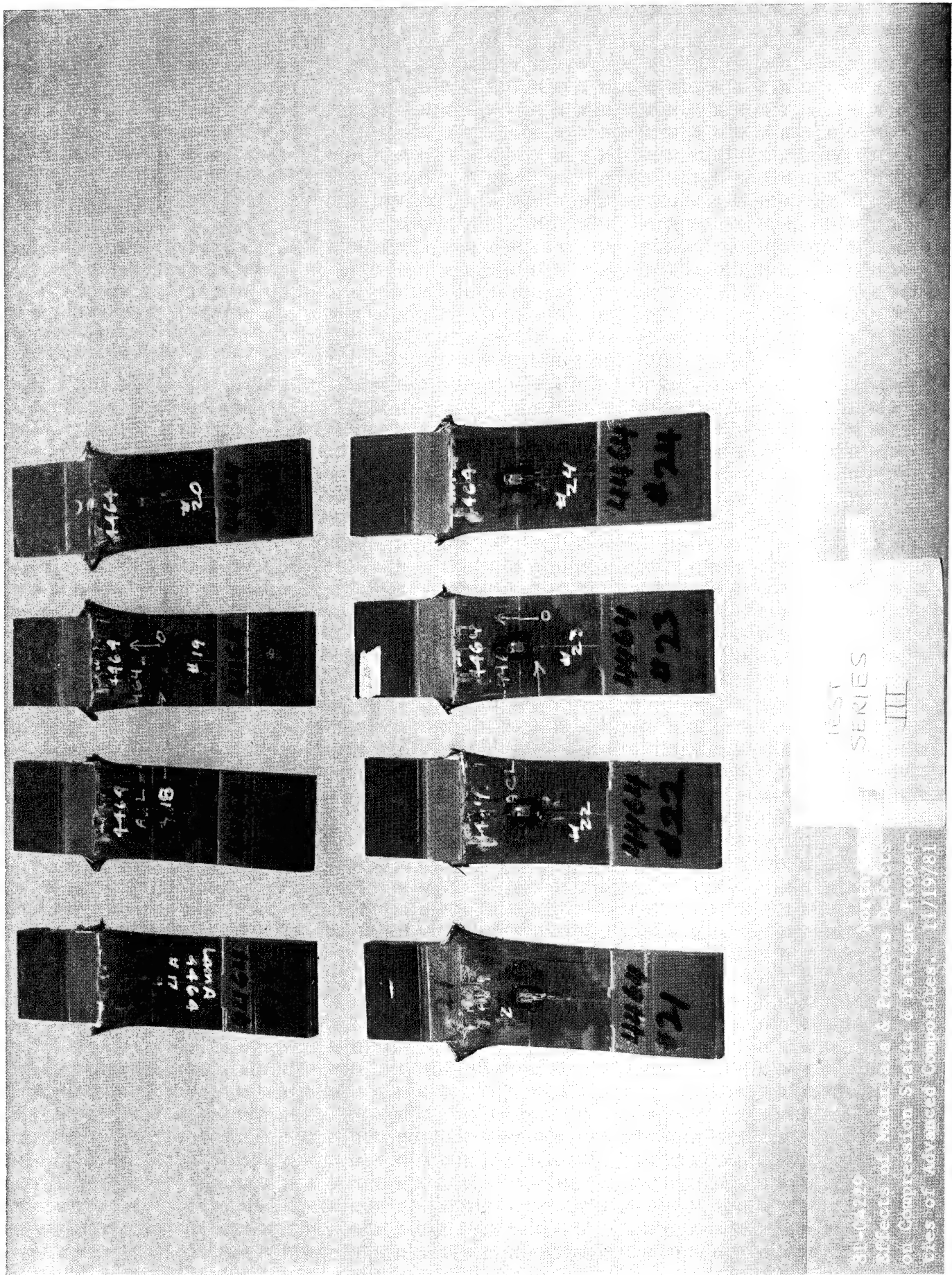
Figure C1. Failed Specimens From Test Series III
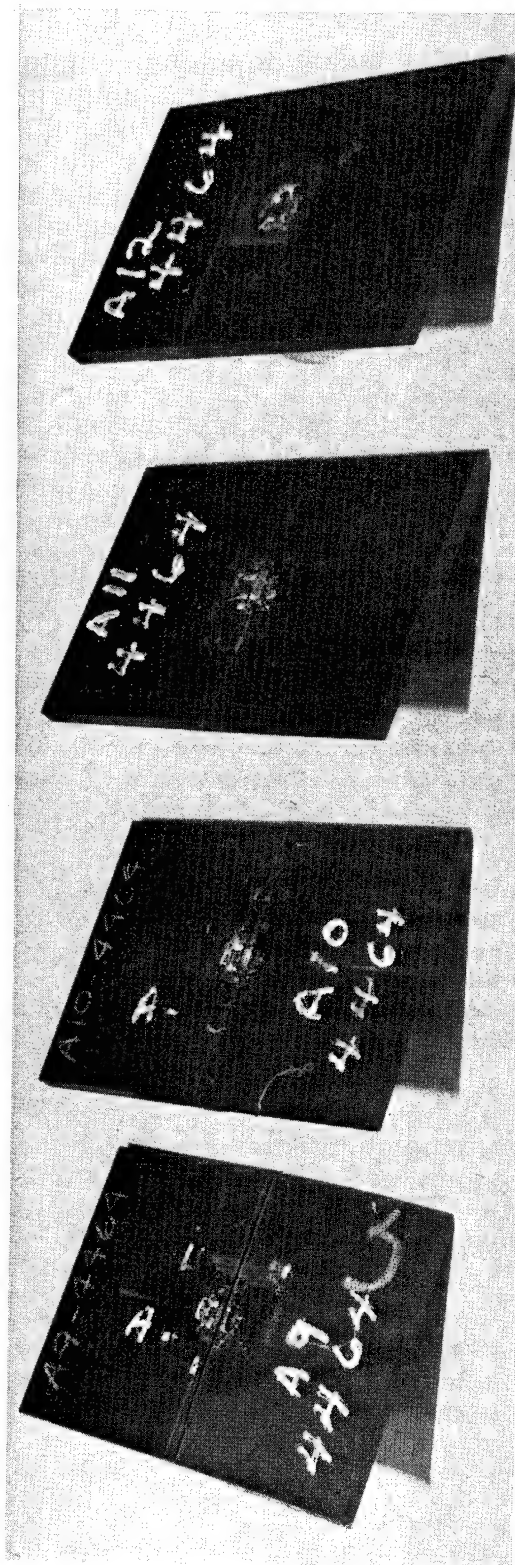
Figure C2. Failed Specimens From Test Series IV

155

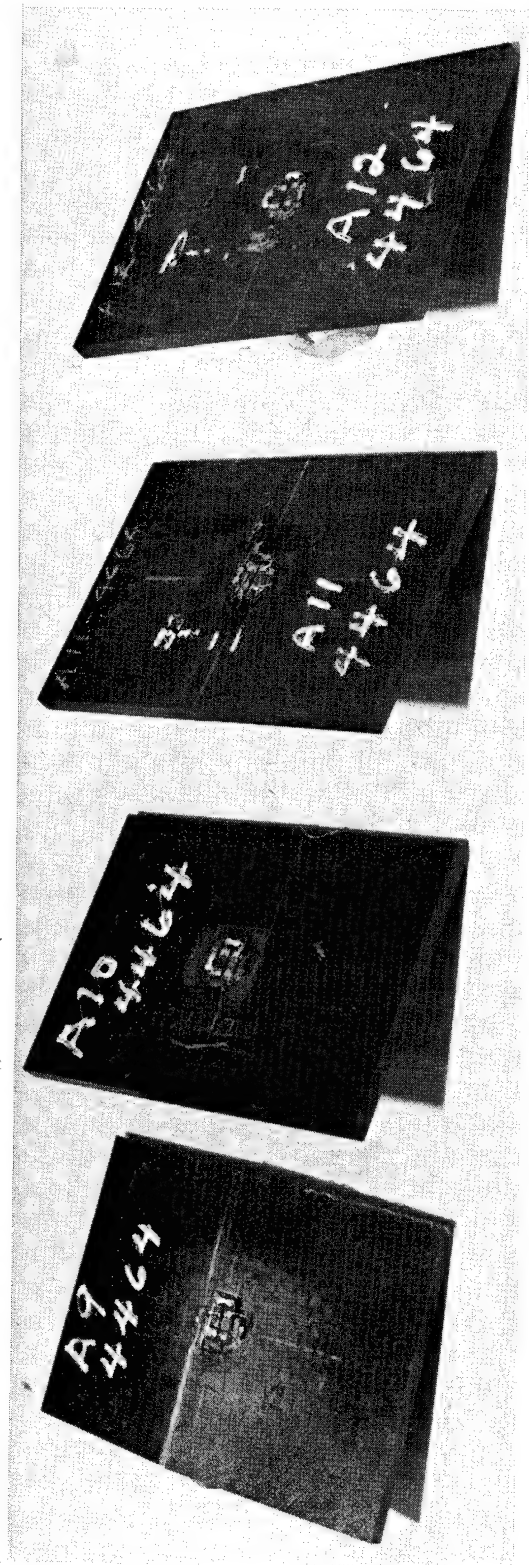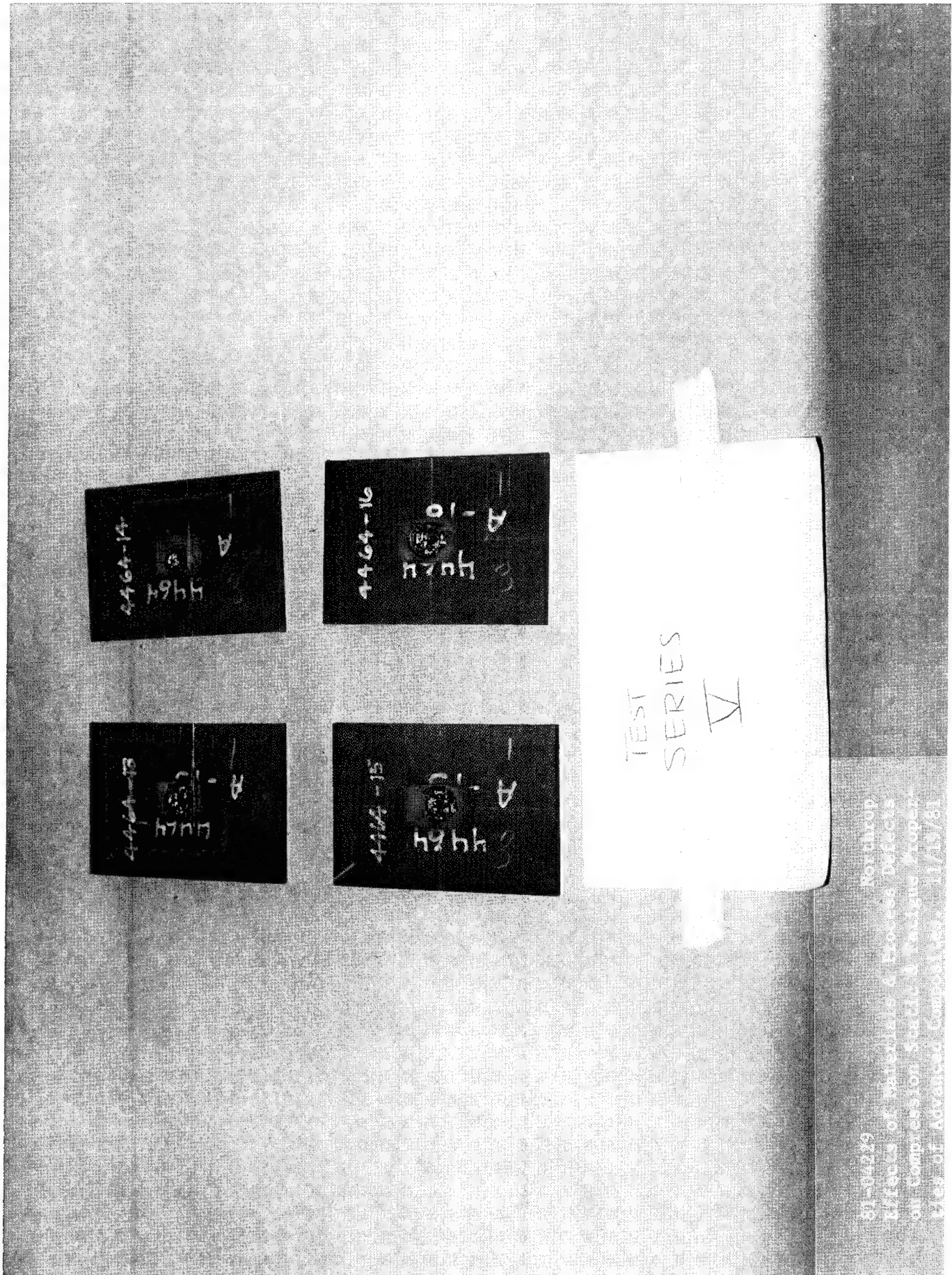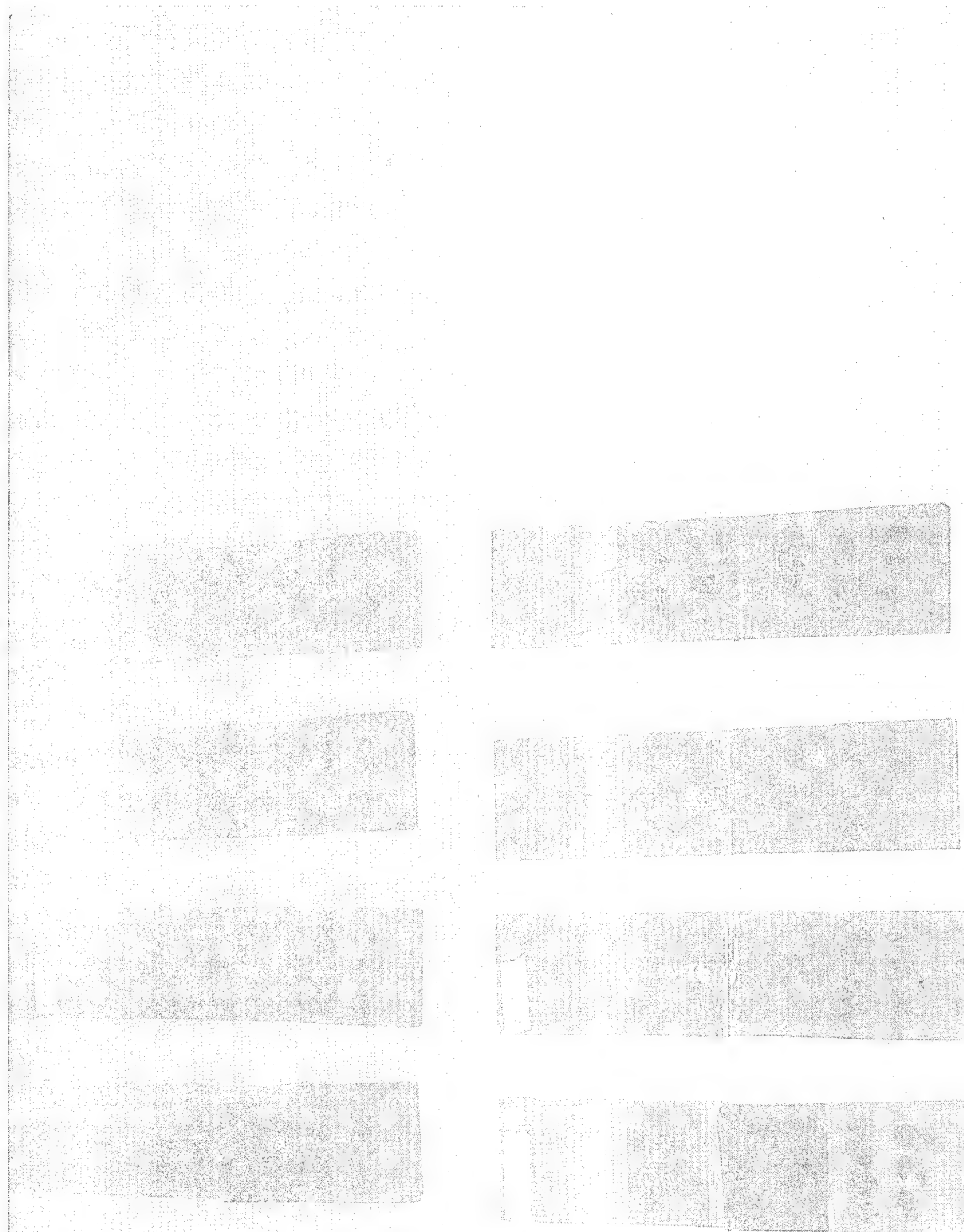Figure C3. Failed Specimens From Test Series V
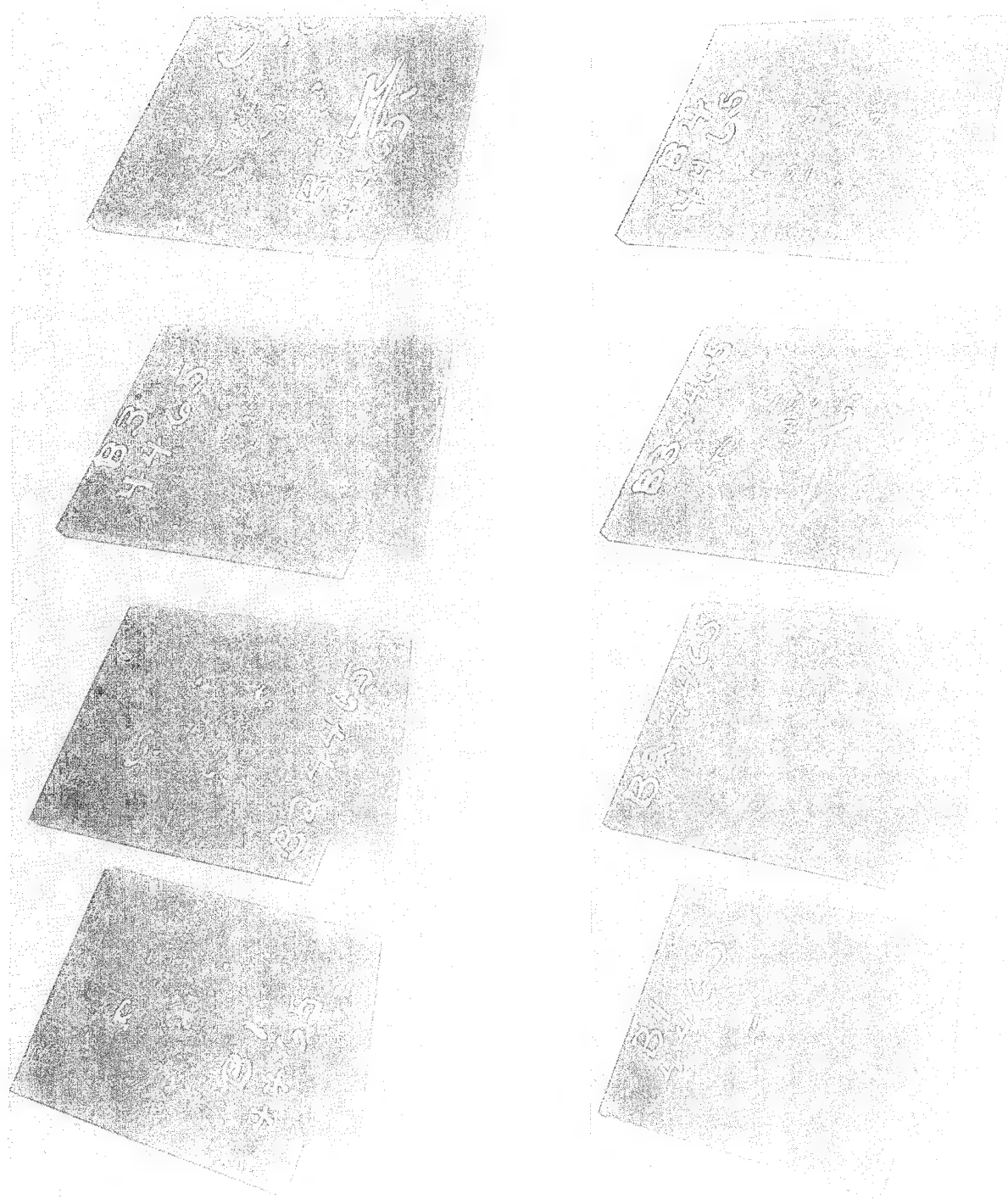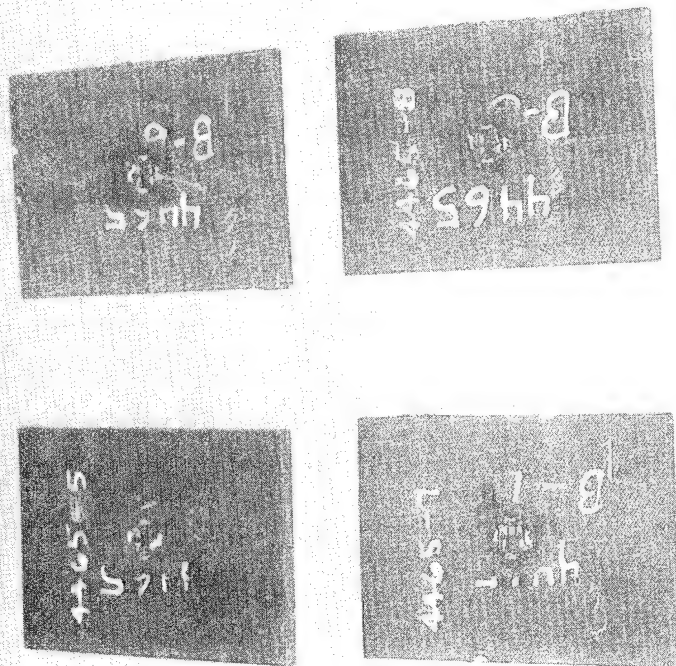
156

Figure C4. Failed Specimens From Test Series VI

Figure C5. Failed Specimens From Test Series VII

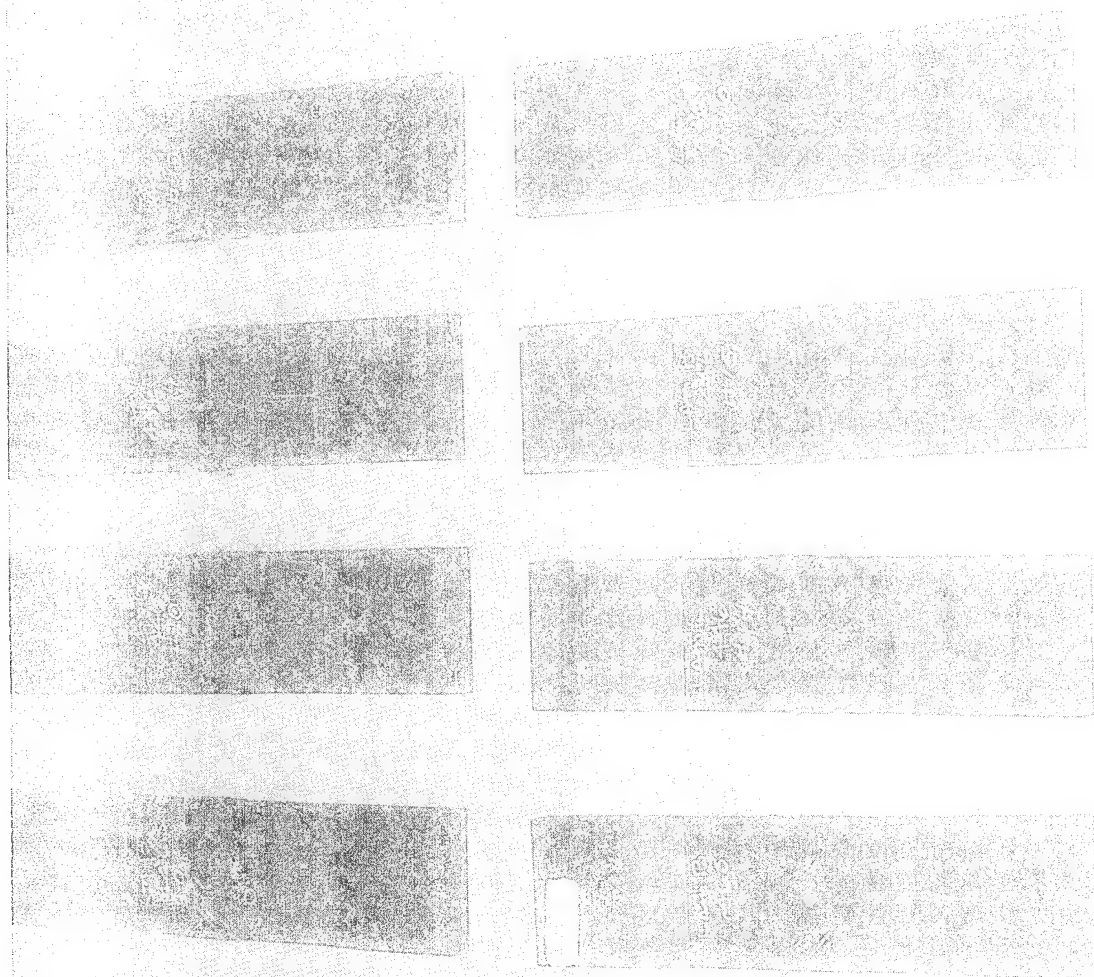Figure C6. Failed Specimens From Test Series VIII

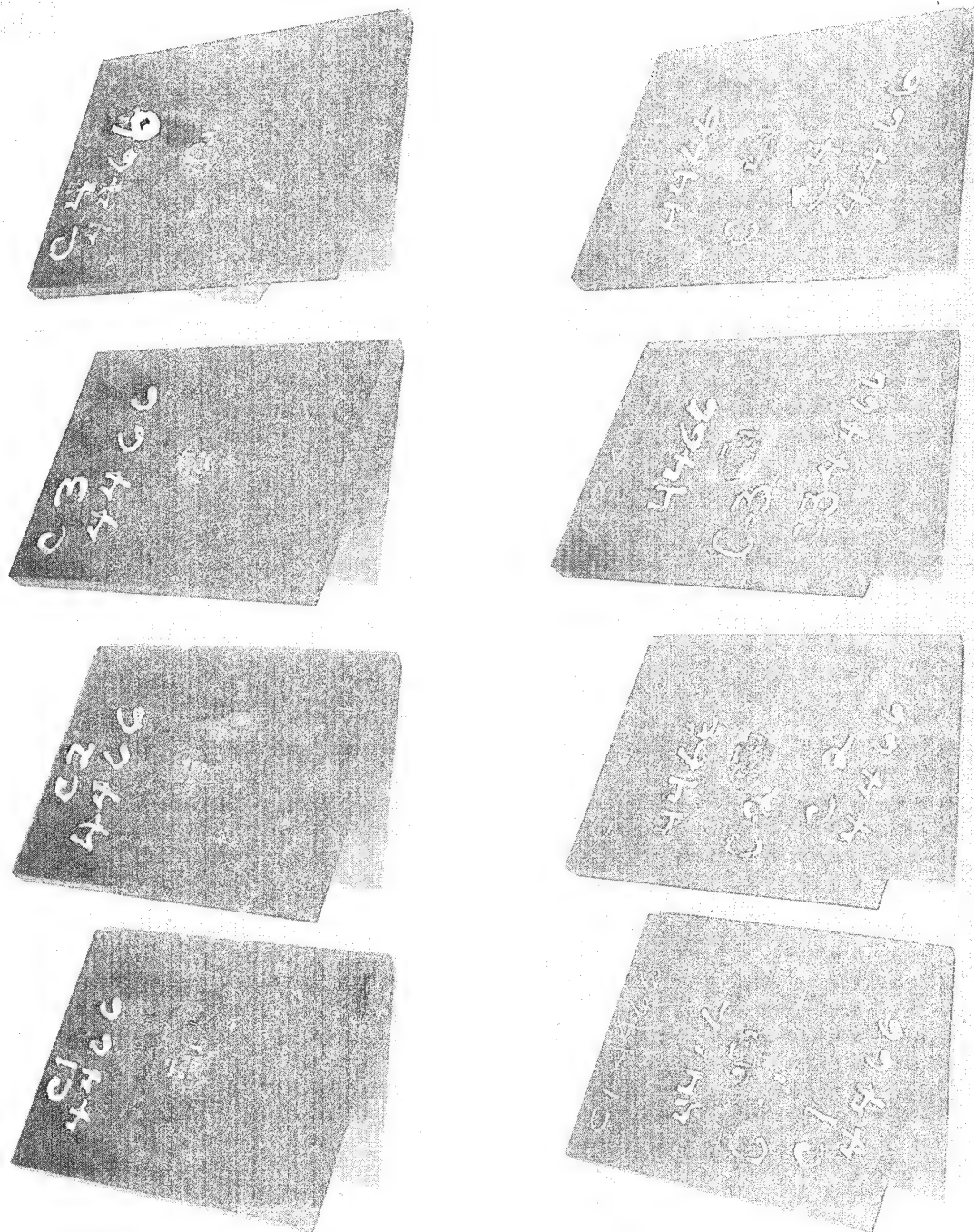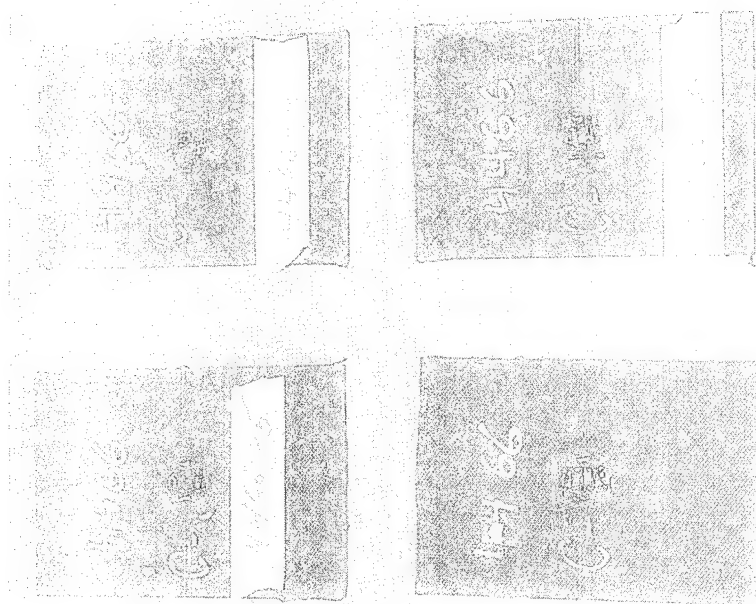Figure C7. Failed Specimens From Test Series IX

Figure C8. Failed Specimens From Test Series X
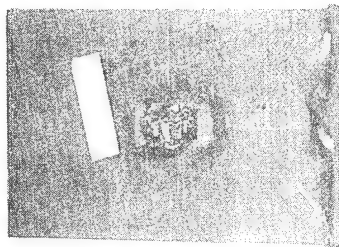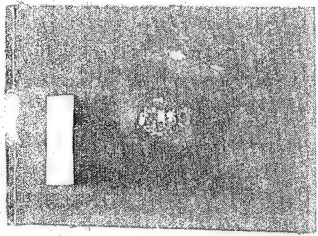
Figure C9. Failed Specimens From Test Series XI

Figure C10. Failed Specimens From Test Series XII

Figure C11.   Failed Specimens From Test Series XIII

164

Figure C12. Failed Specimens From Test Series XIV
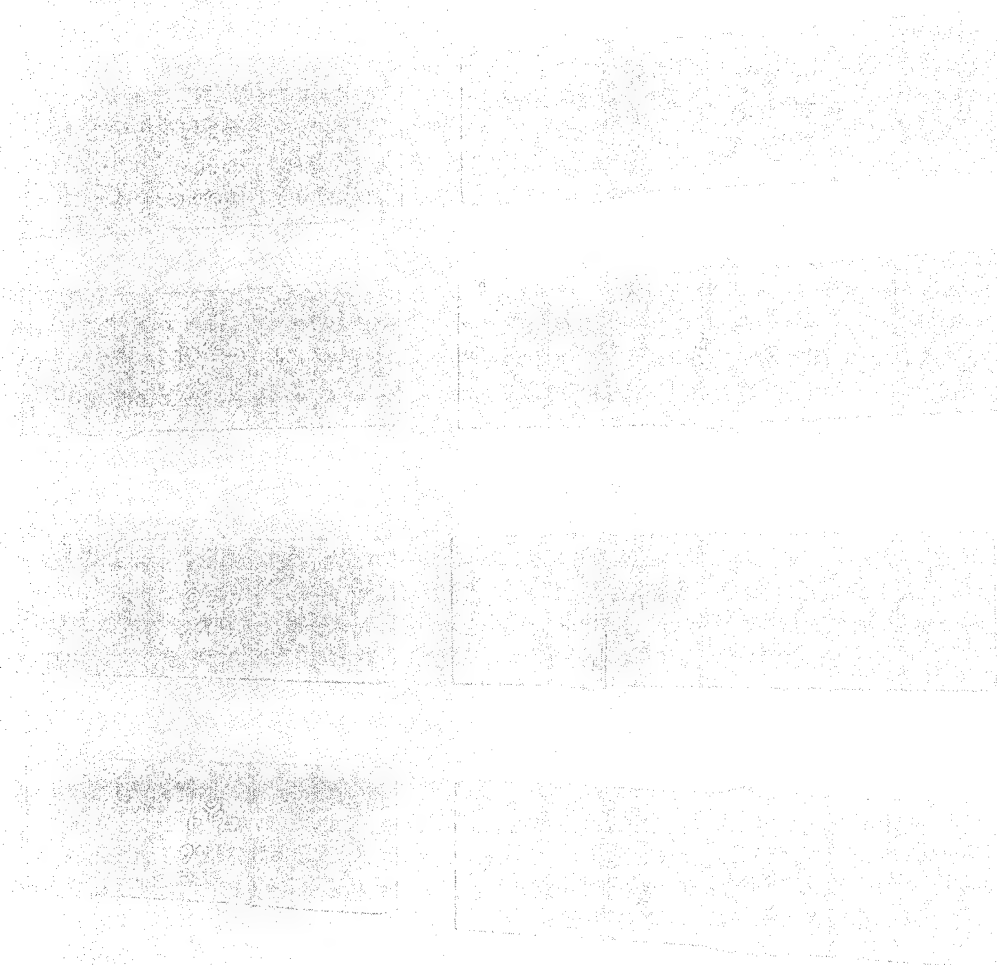
Figure C13. Failed Specimens From Test Series XV

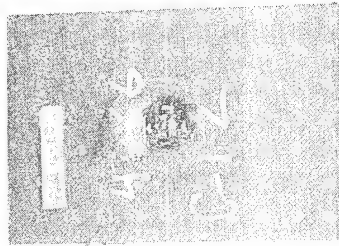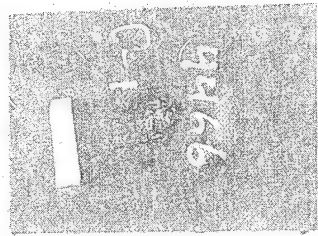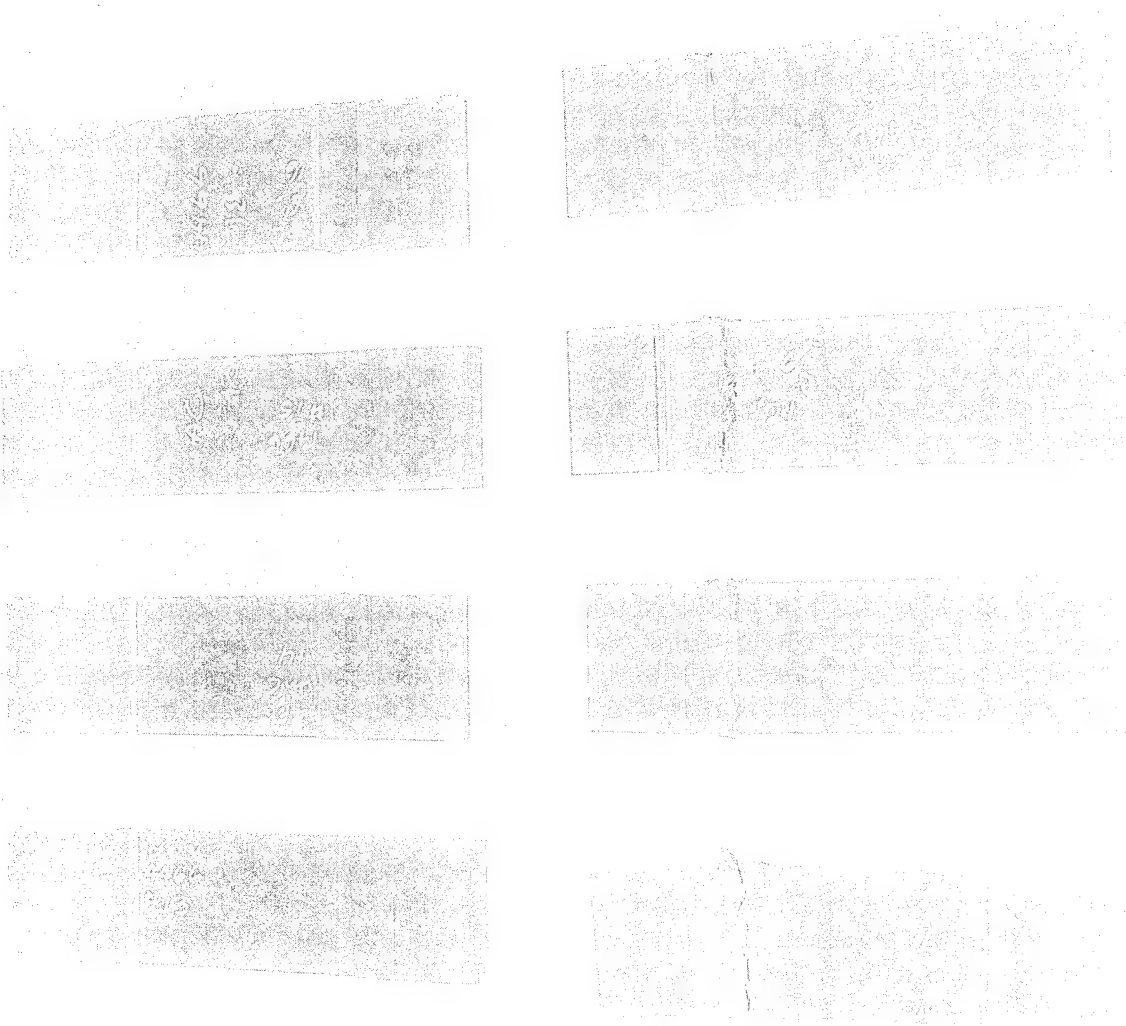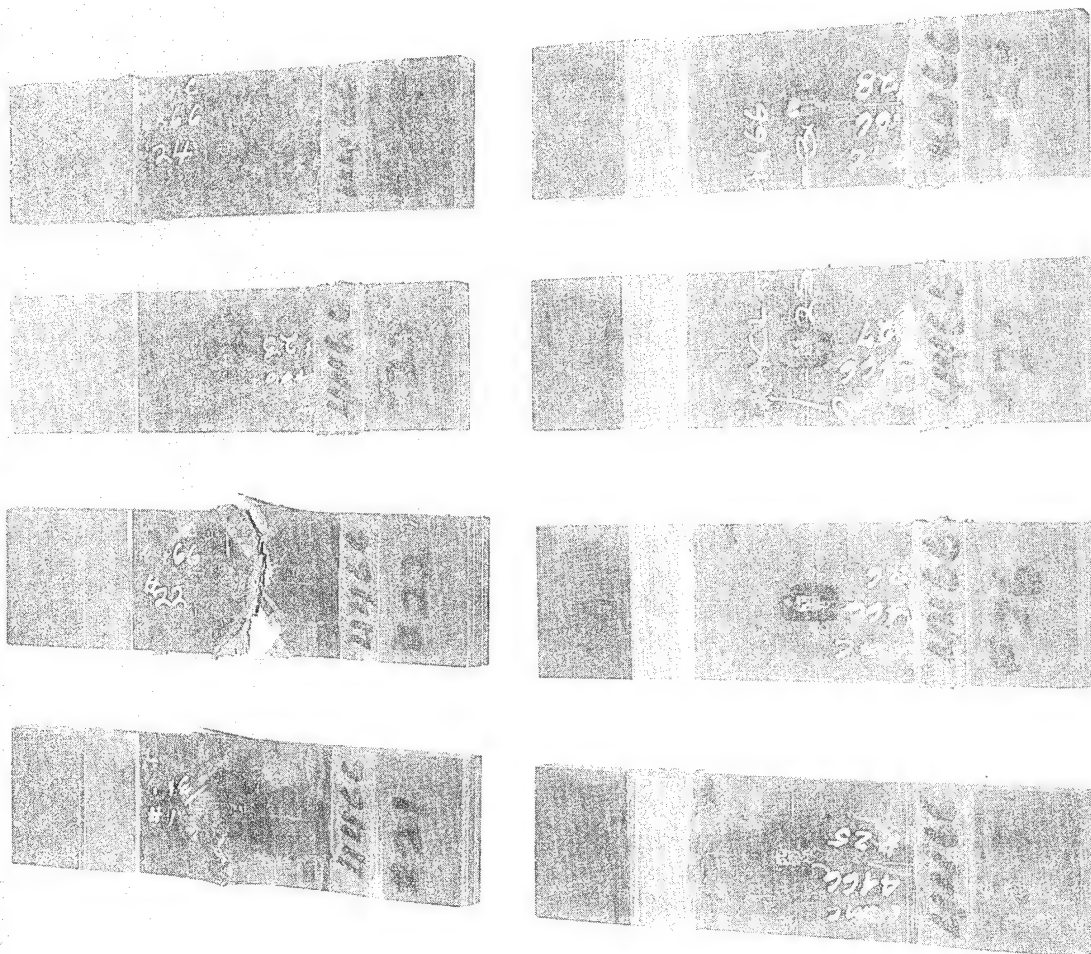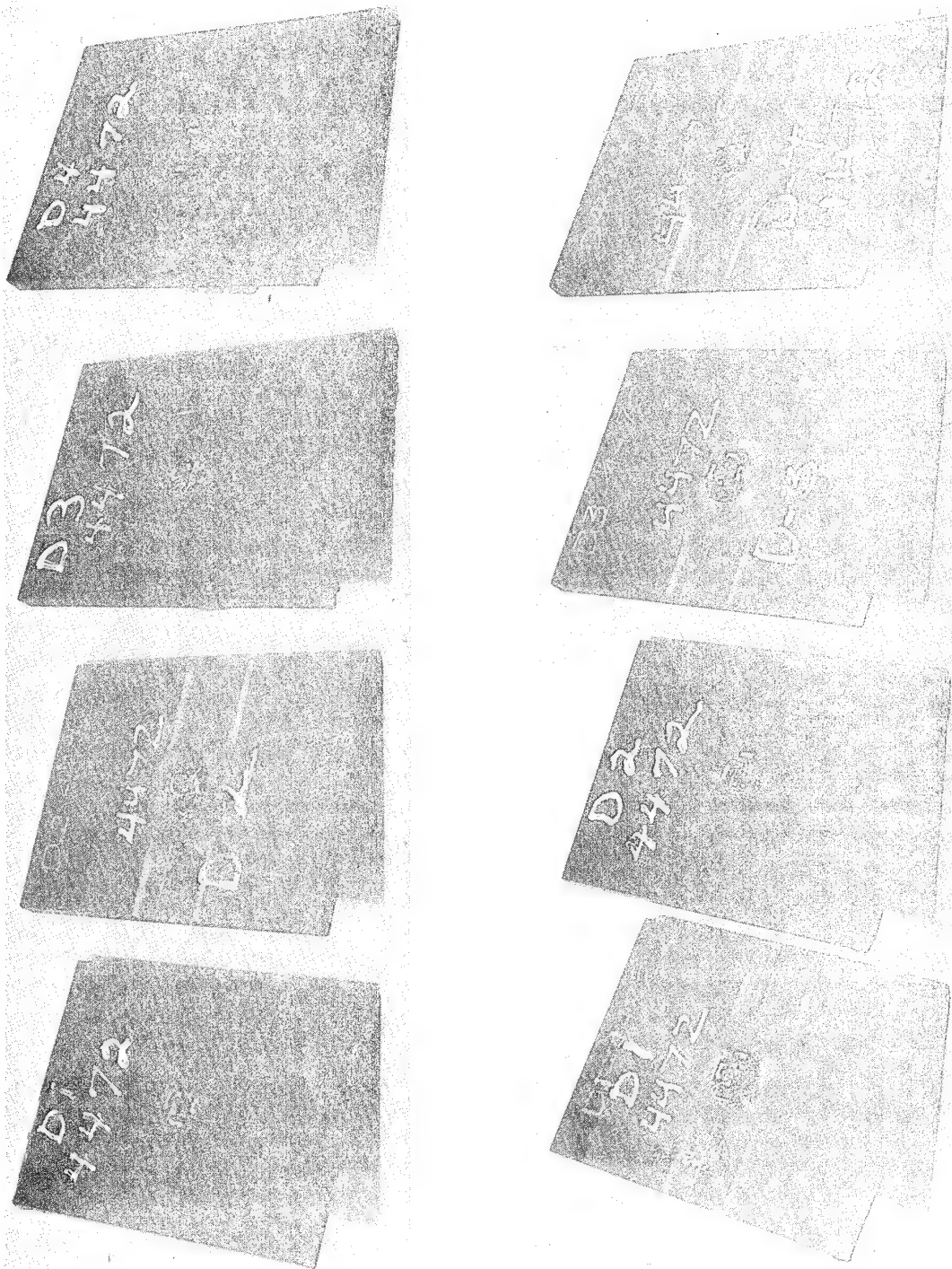Figure C14. Failed Specimens From Test Series XVI

Figure C15. Failed Specimens From Test Series XVII

DISTRIBUTION LIST

No. of Copies

Naval Air Systems Command Attn: Code-5304C Washington, D.C. 20361	8
Office of Naval Research (Code 472) Washington, DC 20350	1
Office of Naval Research, Boston 495 Summer St. Attn: Dr. L. H. Peebles Boston, MA 02210	1
Naval Research Laboratory Codes 6306 and 6120 Washington, DC 20350	2
Naval Surface Weapons Center Code R-31 White Oak, Silver Spring, MD 20910	1
Naval Air Propulsion Test Center ATTN: J. Glatz Trenton, NJ 08628	1
Commander U.S. Naval Weapons Center China Lake, CA 92555	1
Naval Ship R&D Center ATTN: Mr. M. Krenzke, Code 727 Washington, DC	1
Naval Sea Systems Command Navy Dept. Codes 05R and 05D23 Washington, DC 20360	2

Commander
Naval Air Development Center
ATTN: Aero Materials Laboratory
      Aero Structures Division
      Radomes Section
Warminster, PA 18974
	3

DISTRIBUTION LIST (Cont'd)

Air Force Materials Laboratory.   4
ATTN: Codes LC (1 copy)
             LN ("   ")
             LTF ("   ")
             LAE ("   ")
Wright-Patterson AFB, OH 45433

Air Force Flight Dynamics Laboratory   1
ATTN: Code FDTC
Wright-Patterson AFB, OH 45433

U.S. Applied Technology Laboratory   1
U.S. Army Development Laboratories (AVRADCOM)
ATTN: DAVDL-ATL-ATS
Fort Eustis, VA 23604

Director   1
Plastics Technical Evaluation Center
Picatinny Arsenal
Dover, NJ 07801

Department of the Army   1
Army Materials & Mechanics Research Center
Watertown, MA 02172

NASA   1
Langley Research Center
Hampton, VA

NASA Headquarters   1
Code RV-2 (Mr. N. Mayer)
600 Independence Ave., SW
Washington, DC 20546

AVCO Corporation   1
Applied Technology Division
Lowell, MA 01851

Bell Aerospace Co.   1
ATTN: Mr. F. M. Anthony
Buffalo, NY 14240

The Boeing Company   1
Aerospace Division
P. O. Box 3707
Seattle, WA 98124

Boeing-Vertol Co.   1
P. O. Box 16858
ATTN: Dept. 1951
Philadelphia, PA 19142

No. of Copies

Brunswick Corporation   1
Technical Products Division
325 Brunswick Lane
Marion, VA 24354

Celanese Research Company   1
Box 1000
ATTN: Mr. R. J. Leal
Summit, NJ 07901

Defense Ceramic Information Center   1
Battelle Memorial Institute
505 King Ave
Columbus, OH 43201

E. I. DuPont de Nemours & Co.   1
Textile Fibers Dept
Wilmington, DE 19898

Ewald Associates, Inc.   1
105 Skyline Drive
Morristown, NJ 07960

Fiber Materials Inc.   1
ATTN. Mr. J. Herrick
Biddeford Industrial Park
Biddeford, ME

General Dynamics   1
Convair Aerospace Division
ATTN: Tech Library
P. O. Box 748
Ft. Worth, TX 76101

General Dynamics   1
Convair Division
ATTN: Mr. W. Scheck; Dept 572-10
P. O. Box 1128
San Diego, CA 92138

General Electric   1
R&D Center
ATTN: Mr. W. Hillig
Box 8
Schnectady, NY 12301

General Electric Company   1
Valley Forge Space Center
Philadelphia, PA 19101

DISTRIBUTION LIST (Cont'd)

	No. of Copies
B. F. Goodrich Aerospace & Defense Products 500 South Main St Akron, OH 44318	1
Graftex Division EXXON Industries 2917 Highwoods Blvd Raleigh, NC 27604	1
Great Lakes Research Corporation P. O. Box 1031 Elizabethton, TN	1
Grumman Aerospace Corp ATTN: Mr. G. Lubin Bethpage, LI, NY 11714	1
Hercules Incorporated ATTN: Mr. E. G. Crossland Magna, UT 84044	1
HITCO 1600 W. 135th St Gardena, CA 90406	1
Illinois Institute of Technology Research Center ATTN: Dr. K. Hofer 10 West 35th St Chicago, IL 60616	1
Lockheed California Co. ATTN: Mr. J. H. Wooley Box 551 Burbank, CA 91520	1
Lockheed-Georgia, Co ATTN: Mr. L. E. Meade Marietta, GA 30063	1
Lockheed Missiles & Space Co. ATTN: Mr. H. H. Armstrong, Dept 62-60 Sunnyvale, CA 94088	1
Material Sciences Corporation 1777 Walton Road Blue Bell, PA 19422	1

DISTRIBUTION LIST (Cont'd)

	No. of Copies
McDonnell Douglas Corp McDonnell Aircraft Co. ATTN: Mr. J. Juergens P. O. Box 516 St. Louis, MO 63166	1
McDonnell-Douglas Corp Douglas Aircraft Co ATTN: Mr. R. J. Palmer 3855 Lakewood Blvd Long Beach, CA 90801	1
Monsanto Research Corp 1515 Nicholas Road Dayton, OH 45407	1
North American Aviation Columbus Division 4300 E. Fifth Ave Columbos, OH 43216	1
Northrop Corp One Northrop Avenue ATTN: Mr. G. Grimes, Mail Code 3852-82 Hawthorne, CA 90250	1
Philco-Ford Corp Aeronutronic Division Ford Road Newport Beach, CA 92663	1
Rockwell International Corp ATTN: Mr. C. R. Rousseau 12214 Lakewood Blvd Downey, CA 90241	1
Stanford Research Institute ATTN: Mr. M. Maximovich 333 Ravenswood Ave, Bldg 102B Marlo Park, CA 94025	1
TRW, Inc Systems Group One Space Park, Bldg. 01; Rm 2171 Redondo Beach, CA 90278	1
TRW, Inc 23555 Euclid Ave Cleveland, OH 44117	1

DISTRIBUTION LIST (Cont'd)

	No. of Copies
Union Carbide Corporation Chemicals & Plastics One River Road Bound Brook, NJ	1
Union Carbide Corporation Carbon Products Division P. O. Box 6116 Cleveland, OH 44101	1
United Aircraft Corporation United Aircraft Research Laboratories E. Hartford, CT 06108	1
United Aircraft Corporation Pratt & Whitney Aircraft Division East Hartford, CT 06108	1
United Aircraft Corporation Hamilton-Standard Division ATTN: Mr. T. Zajac Windsor Locks, CT	1
United Aircraft Corporation Sikorsky Aircraft Division ATTN: Mr. J. Ray Stratford, CT 06602	1
University of California Lawrence Livermore Laboratory ATTN: Mr. T. T. Chiao P. O. Box 808 Livermore, c A 94550	1
University of Maryland ATTN: Dr. W. J. Bailey College Park, MD 20742	1
University of Wyoming Mechanical Engineering Dept ATTN: Dr. D. F. Adams Laramee, WY 82071	12
Westinghouse R&D Center ATTN: Mr. Z. Sanjana 1310 Beulah Road Churchill Boro Pittsburgh, PA 15235	1

DISTRIBUTION LIST (Cont'd)

No. of Copies

Robert A. Signorelli   1
Mail Stop 106-1
NASA Lewis Research Center
Cleveland, Ohio 44135

Dr. Ingr. Dr. Schutz   1
Laboratorium for Betriebsfestigkeit
61 Darmstadt-Neu Kranichstien
Bartningstrasse 47, Germany

Dr. C. C. Chamis, Mat'ls & Struct. Div.   1
NASA Lewis Research Center
Cleveland, Ohio 44135

Joe Noyes   1
Compositek Engineering Corp.
6925-1 Aragon Circle
Buena Park, CA 90620

Dr. Satish Kulkarni   1
2864 Aptos Way
San Ramon, CA 94583

K. N. Lauraitis, Dept. 74-71/204/2   1
Lockheed California Company
Burbank, CA 91508

Dr. G. C. Sih, Packard Lab. #19   1
Lehigh University
Institute of Fracture & Solid Mechanics
Bethlehem, PA 18015

LTV Aerospace Corp.   1
Attn: O. E. Dhonau
P. O. Box 5003
Dallas, Texas 75222

Rockwell International   1
Attn: Dr. L. M. Lackman
L. A. International Airport
Los Angeles, CA 90009

Air Force Flight Dynamics Lab.   1
Attn: Dr. G. P. Sendeckji/FBE
Wright-Patterson AFB, Ohio 45433

DISTRIBUTION LIST (Cont'd)

No. of Copies

Air Force Materials Lab   1
Attn: Dr. J. M. Whitney/MBM
Wright-Patterson AFB, Ohio 45433

Southwest Research Institute   1
Attn: Dr. L. R. Calcote
Box 28510
San Antonio, Texas 78284

Vought Corporation   1
Advanced Technology Center, Inc.
Attn: J. W. Renton
P. O. Box 6144
Dallas, Texas 75222

Hughes Helicopter   1
Attn: Chief Librarian
Centinela & Teale Sts.
Culver City, CA 90230

Bell Helicopter   1
Attn: S. C. Aker
Fort Worth, Texas 76101